Application of Membrane Technologies in Water Purification

Junjie Shen

Submitted for the degree of Doctor of Philosophy

Heriot-Watt University

School of Engineering and Physical Sciences

Institute of Chemical Sciences

Edinburgh, United Kingdom

May 2016

Abstract

The world is facing a serious water crisis due to rapid population growth, industrialization and climate change. Water purification using membrane technologies provides a promising solution to address this problem. This thesis investigated the feasibility of membrane technologies in a wide range of applications covering drinking water purification and wastewater treatment. Target contaminants included fluoride, natural organic matter (NOM), emerging contaminants bisphenol A (BPA) and cimetidine, and the waterborne parasite *Cryptosporidium*. The first part of the thesis explored the solute-solute interactions of fluoride and humic substances (HS) in order to understand the behaviour of fluoride in natural water and during membrane filtration processes. It is shown that, at low *pH* and high ionic strength, fluoride ions are temporarily trapped inside the structure of HS aggregates. The second part of the thesis examined the feasibility of nanofiltration (NF) and reverse osmosis (RO) in treating challenging natural waters in Tanzania containing high fluoride and NOM concentrations, with the aim to increase the availability of drinking water sources. Fluoride retention was found to be dependent on ionic strength and recovery, which was predominantly due to a solution-diffusion mechanism. NOM retention was independent of water matrices but was governed by a size exclusion mechanism. NOM was observed to have a positive impact on fluoride removal. The third part of this work evaluated the on-site performance of a pilot-scale renewable energy powered membrane system in remote areas under varying solar conditions. While the technology is well established, the adaptation to remote areas is far from achieved. The system used in this study reliably produced high-quality drinking water despite of solar fluctuations. This area requires further work in terms of integration, technology adaptation and operation and maintenance schemes. The last part of the thesis reported the development of a series of novel photocatalytic polymers and tested their capabilities in removing wastewater contaminants. The photoactive polymers were highly capable of degrading BPA and cimetidine, as well as inactivating *Cryptosporidium*. These are very promising materials for simultaneous decontamination and disinfection of wastewater. The results obtained from this thesis provide new insights into solute-solute interactions, solute transport mechanisms, decentralized membrane system and novel membrane materials, which are hoped to contribute to advancements in current membrane technologies.

Acknowledgements

Foremost, I would like to express my deepest gratitude to my two academic supervisors, Dr Valeria Arrighi and Professor Martin McCoustra, for your invaluable guidance and support throughout my PhD. Valeria, you have always encouraged me to find my own path but also provided wise advice when I felt lost. Your philosophy of never forcing but suggesting suits me perfectly. You have managed to fire fight my worries, concerns and anxieties, and helped me develop confidence in both myself and my work. Martin, when I desperately needed a new supervisor to save my PhD, you came on board and connected me with Valeria. Your deep insights and prompt feedback have benefitted me greatly. Both of you have been steady hands to steer me through to the end.

My PhD studentship was provided by Energy Technology Partnership (ETP) with Drinking Water Quality Regulator for Scotland (DWQR) being the industrial sponsor. I would like to thank my industrial supervisor, Matthew Bower, from DWQR. Thank you for your unswerving support for me no matter I was in Tanzania, in China or in Edinburgh. Your insights into the water industry are inspiring to me. I have had a great time with your team at the membrane workshop.

Professor Andrea Schäfer and Professor Bryce Richards (Karlsruhe Institute of Technology, Germany) were my supervisors during the field trip in Tanzania. Your vision, knowledge and experience have contributed to the success of the field trip. I particularly appreciate your scientific input on my PhD, such as designing research projects and commenting on papers. I also appreciate your investment into my personal development, such as encouraging me to climb Mt. Kilimanjaro and attend the Oxford Leadership Academy.

My four-year PhD journey started from Edinburgh in July 2012. Just four months later I found myself on the plane flying to Tanzania and the planned three-month field trip turned to be as long as one and a half years! The long stay in Tanzania is a formative experience for me, which has changed the way I view my life and the world. I have learned to appreciate my abundance in every aspect, and to embrace the good days and the bad ones. I would like to say Asante Sana (thank you in Swahili) to several people who have made my life in Tanzania enjoyable. Professor Felix Mtalo (University of Dar es Salam,

ACADEMIC REGISTRY
Research Thesis Submission

Name*:*	Junjie Shen		
School/PGI:	School of Engineering and Physical Science		
Version: *(i.e. First, Resubmission, Final)*	Final	Degree Sought (Award **and** Subject area)	PhD Chemistry

Declaration

In accordance with the appropriate regulations I hereby submit my thesis and I declare that:

1) the thesis embodies the results of my own work and has been composed by myself
2) where appropriate, I have made acknowledgement of the work of others and have made reference to work carried out in collaboration with other persons
3) the thesis is the correct version of the thesis for submission and is the same version as any electronic versions submitted*.
4) my thesis for the award referred to, deposited in the Heriot-Watt University Library, should be made available for loan or photocopying and be available via the Institutional Repository, subject to such conditions as the Librarian may require
5) I understand that as a student of the University I am required to abide by the Regulations of the University and to conform to its discipline.

* *Please note that it is the responsibility of the candidate to ensure that the correct version of the thesis is submitted.*

Signature of Candidate*:*		Date:	

Submission

Submitted By *(name in capitals):*	JUNJIE SHEN
Signature of Individual Submitting:	
Date Submitted:	

For Completion in the Student Service Centre (SSC)

Received in the SSC by *(name in capitals):*			
Method of Submission *(Handed in to SSC; posted through internal/external mail):*			
E-thesis Submitted **(mandatory for final theses)**			
Signature:		Date:	

Contents

List of figures

xi

List of tables

List of abbreviations

In alphabetical order:

ABT	4,4-(benzo[c][1,2,5]thiadiazole-4,7-diyl)dianiline
AFM	Atomic force microscopy
AHA	Aldrich humic acid
BBT	4,7-bis(4,4,5,5-tetramethyl-1,3,2-dioxaborolan-2-yl)benzo[c][1,2,5]thiadiazole
BPA	Bisphenol A
CA	Cellulose acetate
CDTA	Trans-1,2-diaminocyclohexane-N,N,N',N'-tetraacetic acid monohydrate
CHN	Carbon, hydrogen and nitrogen
CNTs	Carbon nanotubes
DBPs	Disinfection by-products
DI	Deionised
DLCA	Diffusion-limited colloid aggregation
DLS	Dynamic light scattering
DLVO	The Derjaguin, Landau, Verwey and Overbeek theory
DOC	Dissolved organic carbon
DWQR	Drinking Water Quality Regulator for Scotland
EC	Electrical conductivity
EDCs	Endocrine disrupting compounds
EM	Electrophoretic mobility
ESI-MS	Electrospray ionization mass spectrometry
ETP	Energy Technology Partnership
FA	Fulvic acid
FFA	Furfuryl alcohol
FT-IR	Fourier transform infrared
GPC	Gel permeation chromatography
HBSS	Hanks Buffered Salt Solution
HPLC	High performance liquid chromatography
HS	Humic substances
HWU	Heriot-Watt University

IC	Inorganic carbon
ICP-MS	Inductively coupled plasma-mass spectrometry
ICP-OES	Inductively coupled plasma-optical emission spectrometry
ICR	Inorganic carbon remover
ISE	Ion selective electrode
KHP	Potassium hydrogen phthalate
KIT	Karlsruhe Institute of Technology
LC-OCD	Liquid chromatography-organic carbon detection
LDE	Laser Doppler electrophoresis
LMW	Low molecular weight
MF	Microfiltration
MPD	m-phenylendiamine
MWCO	Molecular weight cut-off
NDRS	Ngurdoto Defluoridation Research Station
NF	Nanofiltration
NM-AIST	Nelson Mandela African Institution of Science and Technology
NMR	Nuclear magnetic resonance
NNHS	Ngare Nanyuki humic substances
NOM	Natural organic matter
NPOC	Non-purgeable organic carbon
PA	Polyamide
PA-ABT (x%)	ABT incorporated polyamide
PAHA	Purified Aldrich humic acid
PBS	Phosphate-buffered saline
PCPs	Personal care products
Pd(PPh3)4	Tetrakis(triphenylphosphine)palladium
PDT	Photodynamic therapy
PES	Polyethersulfone
PMR	Photocatalytic membrane reactors
PSU	Polysulfone
PV	Photovoltaic
PVDF	Polyvinylidene fluoride
RE-membrane	Renewable energy powered membrane
RLCA	Reaction-limited colloid aggregation
RO	Reverse osmosis

ROS	Reactive oxidative species
ROSI	Reverse osmosis solar installation
SAS	Solar array simulator
SEC	Specific energy consumption
SEM	Scanning electron microscopy
SRHA	Suwannee River humic acid
SUVA	Specific UV absorbance
TC	Total carbon
TDS	Total dissolved solids
TEM	Transmission electron microscope
TFC	Thin film composite
THF	Tetrahydrofuran
THMs	Trihalomethanes
TISAB	Total ionic strength adjustment buffer
TMC	Trimesoylchloride
TMP	Transmembrane pressure
TOC	Total organic carbon
UDSM	University of Dar es Salaam
UF	Ultrafiltration
USEPA	United States Environmental Protection Agency
UV/Vis	Ultraviolet-visible
WHO	World Health Organization

Publications

Accepted:

Shen, J. and Schäfer, A.I., *Removal of fluoride and uranium by nanofiltration and reverse osmosis: A review.* Chemosphere, 117, 679–691 (2014)

Shen, J. and Schäfer, A.I., *Factors affecting fluoride and natural organic matter (NOM) removal from natural waters in Tanzania by nanofiltration/reverse osmosis.* Science of the Total Environment, 527–528, 520–529 (2015)

Shen, J., Mkongo, G., Abbt-Braun, G., Ceppi, S.L., Richards, B.S., and Schäfer, A.I., *Renewable energy powered membrane technology: Fluoride removal in a rural community in northern Tanzania.* Separation and Purification Technology, 149, 349–361 (2015)

Shen, J., Steinbach, R., Tobin, J., Nakata, M.M., Bower, M., McCoustra, M.R.S., Bridle, H., Arrighi, V., and Vilela, F., *Photoactive and metal-free polyamide-based polymers for water and wastewater treatment under visible light irradiation.* Applied Catalysis B: Environmental, 193, 226–233 (2016)

Submitted:

Shen, J., Gagliardi, S., McCoustra, M.R.S., and Arrighi, V., *Effect of humic substances aggregation on the determination of fluoride in water using an ion selective electrode.* Submitted to Chemosphere, 2015

Shen, J., Richards, B.S., and Schäfer A.I., *Renewable energy powered membrane technology: Case study of St. Dorcas borehole in Tanzania demonstrating fluoride removal via nanofiltration/reverse osmosis.* Submitted to Separation and Purification Technology, 2016

Chapter 1: Introduction

1.1   Motivation

Water is the defining resource of the 21st Century. According to a recent report from the World Health Organization (WHO), 748 million people lack access to safe drinking water and 2.5 billion people suffer from unacceptable sanitary conditions [1]. Millions of people, mostly children, die every year from water-related diseases, such as malaria, cholera and typhoid. Inability to meet the basic survival needs for safe drinking water is leading to increasing regional conflicts [2, 3].

Many factors contribute to the water crisis. Population growth, industrialization and urbanization not only increase water demands but also give rise to water pollution. Climate change causes frequent hydrological extremes, such as droughts in some areas and floods in others, affecting the availability and quality of fresh water [2]. The developing regions are the most affected by water crisis, because of their rapidly growing population and inadequate water infrastructure. The future situation may likely get worse if nothing is done.

Water purification is the key to addressing the global water crisis. Novel approaches are needed to purify water in a cost-effective and environmentally-friendly manner. Membrane technologies have distinct advantages in water purification, such as high separation efficiency, compact modular construction and easy maintenance [4]. This thesis studied the removal of several typical water contaminants by membrane filtration and related processes. The aim is to contribute to the understanding of membrane processes, with the motivation to provide safe drinking water to developing regions using sustainable membrane technologies.

1.2   Target contaminants

The Safe Drinking Water Act defines the term "contaminant" as meaning any physical, chemical, biological, or radiological substance or matter in water [5]. Physical contaminants affect the physical appearance of water. Examples are sediments and

organic material from soil erosion. Chemical contaminants include inorganic and organic compounds. They can be either naturally occurring or man-made. Examples are arsenic, fluoride, mercury (inorganic) and dioxin, pesticides, pharmaceuticals (organic). Biological contaminants are microorganisms, such as bacteria, viruses, protozoan, and parasites. Radiological contaminants are chemical elements with radioactivity, such as radium and uranium. This thesis covered chemical, physical and biological contaminants, with an emphasis on the inorganic contaminant fluoride.

1.2.1 Fluoride

Fluoride (F^-), as the anion of fluorine, is widely detected in drinking water sources all over the world [6]. The occurrence of fluoride in natural waters is closely linked to the local geology. The chemical element fluorine is abundant in the Earth's crust (625 mg kg^{-1}) as a result of volcanic activity and fumarolic gases [7]. Fluorides are naturally released into water by the dissolution of fluoride-containing rocks and soils. The dissolution process is affected by various factors including rock chemistry, groundwater age, residence time, well depth and conditions of the pathways [8]. Fluoride concentration in water is strongly controlled by the solubility of minerals, especially calcium fluorite (CaF_2) which has the lowest solubility of 15 mg L^{-1} at 18 °C [9]. Therefore high fluoride concentrations are associated with minerals with low calcium contents, or high alkaline and carbonous conditions where sodium instead of calcium dominates the water composition [10]. One typical example arises in the East African Rift Valley. The fluoride concentration in local soda lakes is up to 2170 mg L^{-1} and in groundwater is as high as 330 mg L^{-1} [11, 12]. Other areas that are severely affected by fluoride include regions within Middle East, Argentina, the United States, India, and China [10].

In addition to natural dissolution of minerals, industrial operations, such as metallurgical industries, fertilizer plants, and semi-conductor production, generate effluents with high fluoride content [13, 14]. These effluents are often highly acidic. For example, wastewater from a fertilizer plant has a *pH* of 2 and fluoride concentration of 1225 mg L^{-1} [15]. The presence of hydrofluoric acid (HF) at acidic *pH* makes such effluent extremely aggressive towards the environment.

Fluoride has been recognized to have either beneficial or detrimental effect on human health, depending on the concentration and the uptake duration [12]. Small amounts of fluoride can be beneficial to the teeth, preventing dental caries among children [7]. However, chronic ingestion of fluoride at high doses leads to a wide variety of adverse effects. Dental fluorosis and crippling skeletal fluorosis are the first adverse effects that fluoride can have on the body, which are manifested by mottled teeth in mild cases, brittle bones and neurological complications in severe cases [7, 12, 16]. Some researches indicated that chronic exposure to fluoride is further associated with decreased birth rates, increased rates of kidney stones formation, impaired thyroid function, and lower intelligence in children [17, 18]. In light of the complex effects of fluoride on human health, WHO recommended a guideline value of 1.5 mg L^{-1} as a level below which the detrimental effect should be minimal [12].

1.2.2 *Natural organic matter and humic substances*

As the product of plant and biological decay, Natural organic matter (NOM) is ubiquitous in the natural aquatic environment. There are two major NOM sources in natural water: (1) the leaching of surrounding soils (pedogenic origin) and (2) the metabolic activities of microorganisms (aquagenic origin) [19, 20]. Some researchers suggested that pedogenic NOM is more hydrophobic and has higher aromatic contents than aquagenic NOM [20, 21]. The composition of NOM varies spatially and temporally, depending on geological location, environmental conditions, and seasonal weather [22]. Previous studies using liquid chromatography-organic carbon detection (LC-OCD) showed that NOM can be characterized into five fractions, namely biopolymers (polysaccharides, proteins and colloidal organics) (> 20,000 Da), humic substances (HS) (approximately 1000 Da), building blocks (300–500 Da), low molecular weight (LMW) acids (< 350 Da) and LMW neutrals (< 350 Da) [21, 23, 24].

HS represent a ubiquitous and active fraction of NOM [25]. It was reported that HS account for 60–70% of total organic carbon (TOC) in soils and 60–90% of dissolved organic carbon (DOC) in natural water [26]. This study used HS as a representative of NOM. The nature of HS was discussed in details in Chapter 1.3.

1.2.3 *Emerging contaminants*

Many chemicals that have not previously been considered as contaminants are detected in the aquatic environment. These chemicals are known as "contaminants of emerging concern" or simply "emerging contaminants", because there is concern that they may have an impact on human health and the environment [27]. Some emerging contaminants may demonstrate acute toxicity while others may interfere with the function of hormones in the body, resulting in a variety of health effects at very low levels of exposure [27]. Pharmaceuticals, endocrine disrupting compounds (EDCs), personal care products (PCPs), and pesticides are among the prime examples of emerging contaminants. In the UK, for example, approximately 70 types of pharmaceuticals have been detected in natural waters, which are mainly from the discharge of treated wastewater [28].

In this study, bisphenol A (BPA) and cimetidine were selected as two representative emerging contaminants [28]. BPA is widely used as a monomer for making polycarbonate plastic and epoxy resins. As a well-known example of EDCs, BPA exhibits hormone-disrupting properties and has been shown to cause negative health effects in animal studies [29]. Cimetidine is a pharmaceutical compound used in the treatment of heartburn and peptic ulcers. It poses an environmental threat due to its physiological effect on humans [30].

1.2.4 *Pathogenic microorganisms*

Waterborne diseases caused by pathogenic microorganisms, such as bacteria, viruses and parasites, are the most common and widespread health risk associated with drinking water [31]. This study used *Cryptosporidium* as a typical pathogenic microorganism. *Cryptosporidium* is a protozoan parasite that causes the diarrheal disease cryptosporidiosis. Cryptosporidiosis can last up to three weeks in relatively healthy patients but can also be fatal for immunosuppressed individuals (such as people infected with HIV) [32]. The dormant (inactive) form of *Cryptosporidium* is called an oocyst. Oocysts are excreted in the feces of an infected host and are widespread in surface bodies of water. Each oocyst consists of four sporozoites housed within a thick wall and can survive for months under a wide range of environmental conditions [33]. *Cryptosporidium* oocysts are highly resistant towards traditional disinfectants chlorine

and chloramines, which makes it tougher to kill than most disease-causing pathogens [34, 35].

1.3   Solute-solute interactions

HS function in aquatic systems as a major complexing component and a natural buffer because the molecules have abundant carboxylic and phenolic functional groups [36]. The interactions of HS with many environmental contaminants, including heavy metals and pesticides, have been extensively reported [37-41]. However, the effect of HS on fluoride remains poorly understood.

1.3.1   Nature of fluoride

The speciation of fluoride is *pH* dependent with the equilibrium constant of hydrofluoric acid being $pK_a = 3.2$ [42] with negative fluoride ions dominating at *pH* values above the *pKa*. Fluoride forms complexes with a number of cations due to charge attraction. **Table 1.1** summarises common fluoride species in water and their physicochemical properties [9]. The solubility of fluoride species varies significantly, among which calcium, magnesium and strontium fluorides are very insoluble. In addition, the fluoride ion has the same charge and nearly the same ionic radius as the hydroxyl (OH^-) ion. Therefore fluoride ions may replace hydroxide in mineral structures under acid conditions through ion exchange [12]. This explains why some common mineral species of low solubility contain fluoride.

Table 1.1: Physicochemical properties of common fluoride species [9]

Fluoride species	Molecular weight	Solubility in water (g L^{-1})	Melting point (°C)	Boiling point (°C)
NaF	42	43 (25 °C)	993	1704
KF	58	923 (18 °C)	857	1503
NH$_4$F	37	1000 (0 °C)	-	-
CaF$_2$	78	0.015 (18 °C)	1418	2500
MgF$_2$	62	0.087 (18 °C)	1248	2260
SrF$_2$	126	0.117 (18 °C)	1190	2460
AlF$_3$	84	5.59 (25 °C)	1260	-

1.3.2 Nature of HS

It is well known that HS are abundant of carboxylic and phenolic functional groups [36]. But the structures of HS are ill-defined due to their high heterogeneity and variability. An early but still popular view is that HS are macromolecules which coil under either high ionic strength or low *pH* but form linear chains under either low ionic strength or high *pH* [43-47]. The macromolecular nature of HS has been recently challenged, since a few spectroscopic, microscopic, and soft desorption ionization studies were not consistent with it [48]. Piccolo [49] suggested that, humic substances are not polymeric in nature but consist of supramolecular associations of heterogeneous and relatively small molecules. This model suggests that HS molecules are held together by weak forces such as hydrophobic interactions (van der Waals, π–π, and CH–π interactions) and hydrogen bonds [49, 50]. The presence of supramolecular associations of HS has been experimentally observed *via* analytical techniques such as gel permeation chromatography (GPC), size exclusion chromatography, nuclear magnetic resonance (NMR), electrospray ionization mass spectrometry (ESI-MS), transmission electron microscope (TEM) and atomic force microscopy (AFM) [50-55].

Despite this ongoing debate on molecular structure, it is well accepted that HS have colloidal character [56, 57]. The dispersion and aggregation of HS colloids in water can be interpreted using the Derjaguin, Landau, Verwey and Overbeek (DLVO) theory which assumes that the interaction forces between colloidal particles are a superposition of van der Waals and electrostatic (double layer) forces [58, 59]. Based on the DLVO theory, two regimes of colloid aggregation have been identified, namely diffusion-limited colloid aggregation (DLCA) and reaction-limited colloid aggregation (RLCA) [60]. DLCA occurs when there is negligible repulsive force between the colloidal particles and the aggregation rate depends only on the diffusion of the particles; RLCA occurs when there is a substantial repulsive force between particles and the particles have to cross an energy barrier created by the double layer interactions [60, 61]. However, many non-DLVO interactions, such as hydrogen bonding and hydrophobic interactions, may also affect the stability of HS colloids [62]. Van Oss [63] developed an extended DLVO (XDLVO) theory which accounts for hydrophobic interactions that are not considered in the classical DLVO theory. The XDLVO theory is widely used to describe the stability of colloidal particles in water, such as the aggregation of silica particles [64]. In addition, HS colloids in water can possess high negative charges due to the deprotonation of carboxylic and

phenolic groups [36, 65], but the negative charges can be altered by the screening effect of cations. Therefore, the degree of HS aggregation is expected to vary significantly under different environmental conditions.

1.3.3   *Possibility of fluoride-HS interactions*

In general, dissolved ions interact with HS in three manners: electrostatic attraction, site binding and territorial binding [66]. Electrostatic attraction is a primary mechanism for cationic species because most HS groups are negatively charged at neutral and alkaline *pH*. For anions such as fluoride the electrostatic effect is repulsive in nature.

Site binding is a strong, site-specific binding that involves hydrogen bonding or chemical bond formation. Fluoride is a very good proton acceptor due to its high negative charge density, so it can form hydrogen bonds with proton donors. Moreover, fluoride prefers to interact with single and strong donor, especially hydroxyl and amino groups [67]. In aqueous environment fluoride is easily surrounded by water molecules *via* hydration. The chemical process is that water molecules break the hydrogen bonds to their nearest neighbour and compete for the lone pairs of electrons in fluoride. Due to the very short lifetime of hydrogen bonding in aqueous solution, multiple hydrogen bonds are unlikely to exist simultaneously. Therefore it is assumed that the hydration shell of an anion is maintained by a single hydrogen bond which frequently occurs between the anion and different water molecules [68]. Given that the only hydrogen bonding site is occupied by the surrounding water, fluoride ions can hardly bond to other compounds unless they are dehydrated. Previous studies reported that in the membrane filtration process, highly hydrated ions may detach from their hydration layers [69], making it possible to form new hydrogen bonds with other compounds (*e.g.* polymers in the membrane). However, the formation of new hydrogen bonding during fluoride dehydration is still unconfirmed.

On the other hand, the probability of encountering stronger proton donors is not small, especially in a solution containing organic matter. In general, HS contain a wide range of carboxylic acid and alcohol functional groups which can act as proton donors. Kovács and Varga [67] reported that LMW alcohols can form even stronger hydrogen bonding with halide anions than water molecules. Given that the stronger donor dominates such interaction in competitive situations, it is in theory possible that specific groups in HS can

substitute water molecules in complex formation with fluoride. However, the attraction of the proton-donating groups can be significantly weakened by the hydration shell, and as consequence the chance of interacting with fluoride ions is reduced. Interestingly, it is the strong hydrogen bonding capacity of fluoride that entraps it into the "water cage". In the case of fluoride-HS interactions, hydrogen bonding is an unlikely mechanism. Weak binding that may be thought of as "territorial binding", is widely present between ions and organic molecules [70]. The concept of territorial binding was introduced by Manning [71] as part of the polyelectrolyte binding theory. At the condition where there are intervening water molecules around the ions, the interaction (attraction or repulsion) between the ions and certain functional groups of organic molecules is sufficiently weakened, and dominated by the overlapping electric fields of many spatially-distributed functional groups [71]. As a result, the ions will be trapped in the structure but without being bound to any particular site. One can imagine the ion as a lion in a cage: the lion is more or less free to wander but cannot escape until the cage (electric field) is opened. Hayes *et al*. [72] found that fluoride had a *pH*-dependent adsorption to humic acid and they attributed this to territorial binding. At *pH* 5, the amount of fluoride bound to humic acid was as high as 90%, and it decreased to 25% at higher *pH* due to increased charged repulsion and reduced size of humic acid [72]. The dominant functional groups that cause territorial binding are carboxylic groups, which are ubiquitous in almost all HS molecules [73]. Previous studies reported that the contribution of carboxylic groups on territorial binding is related to their proximity to each other or to other functional groups, especially hydroxyl groups [73]. However, due to the complexity of the structural arrangement of these groups (*e.g.* aliphatic or aromatic), the charge distribution around a molecule is likely to be extremely variable, making it difficult to predict the possible occurrence of territorial binding in the molecules.

Various studies on adsorbents for fluoride removal may have implications for understanding the potential interaction between fluoride and HS. Ion exchange is widely accepted as a major mechanism for fluoride adsorption. Sivasamy *et al*. [74] suggested that fluoride adsorb to coal-based sorbents by replacing the hydroxyl ions from the surface functional groups. Abe *et al*. [75] also investigated the adsorption of fluoride ions onto bone char (which is composed of calcium phosphate and calcium carbonate), and demonstrated that the phosphate ions in bone char were exchanged by fluoride ions. The sorption process can also be accompanied by the swelling of adsorbents in water which

enlarges their internal structure. Both ion exchange and adsorbent swelling can explain the reversible aspect of the fluoride sorption while the irreversible aspect may be attributed to some tighter fluoride binding such as specific anion-cation interaction or hydrogen bonding [76]. HS is usually abundant in hydroxyl groups, indicating a potentially feasibility for ion exchange. It is worth exploring whether similar sorption behaviours (especially ion exchange) occur between fluoride and HS.

Based on the above analysis, fluoride itself is difficult to bind to HS due to its negative charge and hydration shell. Cations are then studied as a key role in the fluoride-HS interactions as they have a good affinity for both fluoride and HS. The multiple functional groups associated with HS can initially bind cations and then attract fluoride ions *via* cation-anion interaction. Lund *et al*. [77] investigated the binding of fluoride to a hydrophobic macromolecule using molecular dynamics simulations. The results showed that fluoride, as a strongly hydrated ion, can bind to the metal ion loaded macromolecule because specific cation-anion interactions overcome the charge repulsion. In this case the cations may act as a bridge combining fluoride and HS.

On the other hand, extensive research has been carried out on the interactions of fluoride with free metal ions in aqueous phase. With the highest electronegativity, fluoride ions have a very strong affinity to multivalent metal elements and the solubility of the corresponding metal fluoride tends to decrease as the valence of the metal ion increases. Chemical precipitation has been widely used as another effective method for removing fluoride. Tokunaga *et al*. [78] studied the role of calcium and aluminium ions in fluoride removal and concluded that these two metal ions precipitate fluoride by different mechanisms. Specifically, calcium and fluoride can form insoluble CaF_2 *via* a stoichiometric reaction in the *pH* range of 4 to 10, while aluminium and fluoride can co-precipitate along with the formation of $Al(OH)_3$ precipitate in the narrow *pH* range of 6 to 8 [78]. It is noteworthy that fluoride concentration plays a key role in precipitation. At a concentration of 1 mg L^{-1}, fluoride was not observed to interact with any cation except aluminium [79]. But once the concentration exceeds certain level, F^- can even displace CO_3^{2-} from calcium carbonate ($CaCO_3$) and form the more insoluble compound, calcium fluoride (CaF_2) [80]. Considering that HS in natural waters tend to attract colloidal and suspended particles such as $Al(OH)_3$ and $CaCO_3$ which are capable of binding fluoride, it is possible for HS to bind fluoride through these inorganics. In fact

Farrah *et al*. [80] reported that the inorganic components (especially Al species) in humic acids were the main contributors for fluoride adsorption.

1.4   Membrane technologies

1.4.1   *Principles*

In general, a membrane is a selective barrier between two phases. The permeation process takes place when a driving force is introduced to the system [81]. The driving force across the membrane is generally a difference in chemical potential due to a pressure or concentration gradient. Depending on membrane porosity and the trans-membrane gradient involved, a number of different types of membrane processes exist including reverse osmosis (RO), nanofiltration (NF), ultrafiltration (UF), and microfiltration (MF) (**Figure 1.1**).

UF and MF have various applications in wastewater treatment and drinking water pretreatment [4, 82]. UF and MF are well recognised as porous membranes. MF membranes have larger pore sizes (0.1–5 µm) and can reject particles and bacteria. UF membranes have smaller pore sizes (0.01–0.1 µm) than MF and can filter macromolecules and viruses [4].

RO is commonly used for desalination of brackish water or seawater for drinking purposes [82]. RO membranes are generally made of dense materials with non-porous structure. These membranes can near-completely remove all monovalent and multivalent ions.

NF, which is defined as an interface process between UF and RO, can separate multivalent ions from monovalent ions. Therefore NF is often used to soften hard water [83]. It is somewhat arbitrary to claim that NF membranes are either porous or non-porous, because the openness of NF lies in the spectrum between discrete pores (UF/MF) and dense materials (RO) [84, 85]. Some polymeric NF membranes are non-porous cross-linked network structures, while inorganic NF membranes contain discrete pores with sizes ranging from 0.5 to 2 nm [86].
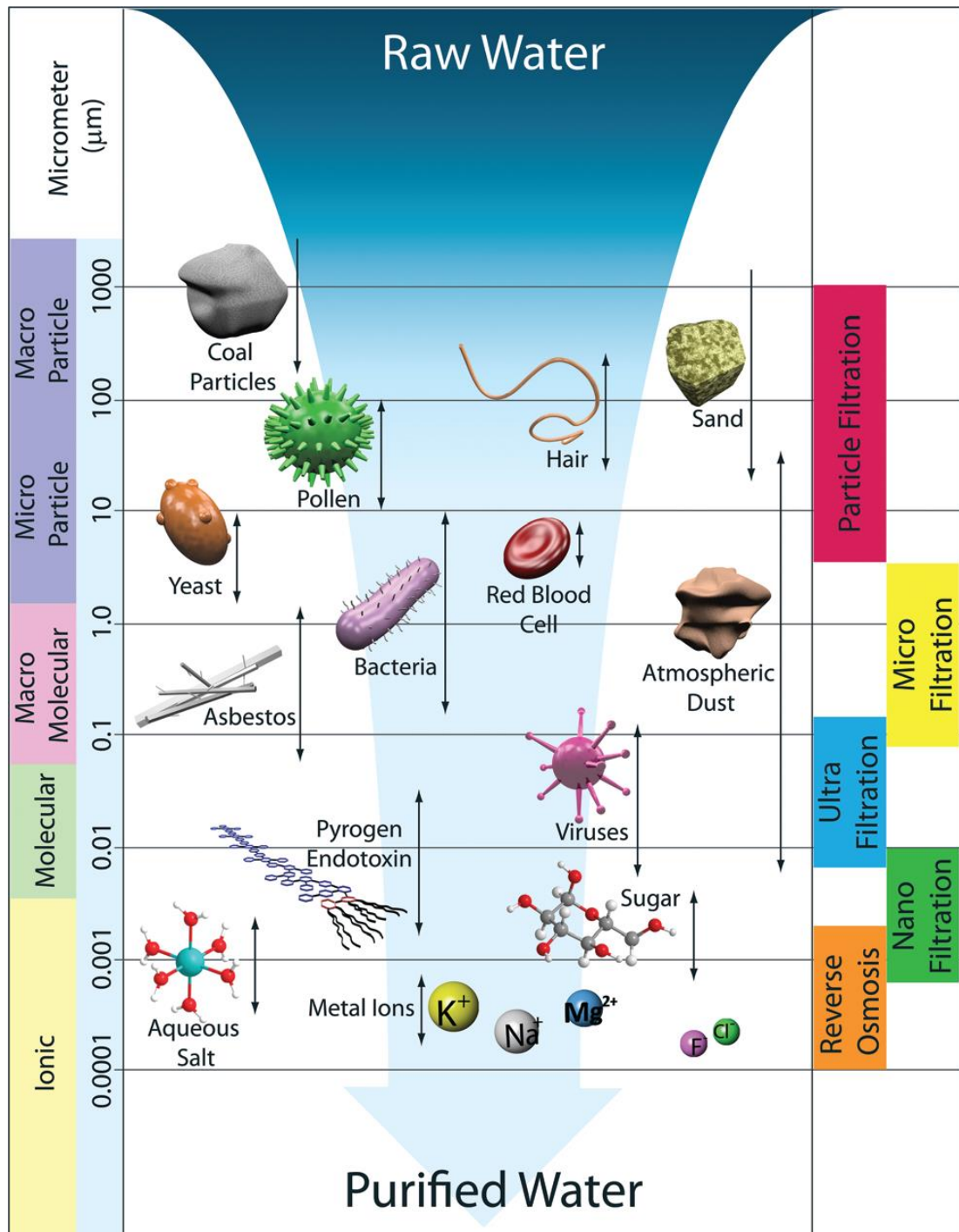
Figure 1.1: Schematic of membrane filtration spectrum [4]

For non-porous membranes, the transport mechanism is best described by the solution-diffusion model, wherein solutes dissolve in the dense material and then diffuse through statistically distributed free volume areas down a concentration gradient [85]. The solute transport rate and selectivity depends on interactions between solute and membrane materials. For porous membranes, solutes transfer through membrane pores following a pressure gradient. The transport rate and selectivity are primarily dominated by convective flow and sieving or size exclusion, combined with other mechanisms such as

charge repulsion or sorption. As NF operates in the transition region between RO and UF, its transport mechanism is recognized to be complex and combines characteristics of both non-porous and porous membranes [84].

1.4.2 Membrane materials

The performance of a membrane is largely dependent on the physical and chemical properties of the material. Both inorganic and organic materials can be made into membranes. Most commercially available membrane materials are synthetic polymers, such as polyvinylidene fluoride (PVDF), cellulose acetate (CA), polysulfone (PSU), polyethersulfone (PES), polyamide (PA). For example, PSU and PES are often used for UF and as supporting layers for NF and RO membranes [87]. These materials generally exhibit good mechanical strength and water permeability. However, a main disadvantage of polymeric membranes is their high fouling tendency due to their inherent hydrophobicity [88]. Fouling issues (biofouling, inorganic scaling, organic, and colloidal fouling) lead to shortened lifetime of the membrane and higher operation and maintenance cost. In addition, many polymeric materials suffer from poor chemical/thermal stability and low oxidation resistance [4].

Compared to organic membranes, inorganic membranes exhibit greater thermal/chemical stability, as well as higher fouling resistance [4]. Typical materials for inorganic membranes include ceramics (*e.g.* TiO_2, Al_2O_3, ZnO, SiO_2) and their composites (*e.g.* TiO_2-SiO_2) [89, 90], graphene-based materials [91] and carbon nanotubes (CNTs) [92]. Ceramic membranes containing TiO_2 or its composites have recently gained considerable attention because they have both separation and photocatalytic functions. The most extensively studied applications of these photocatalytic membranes are disinfection and decomposition of wastewater [4]. However, large-scale applications of inorganic membranes are still rare, mainly due to cost issues [4].

More recent attention has focused on the development of hybrid membrane materials which may overcome limitations of both inorganic and organic membranes. A common approach is to introduce inorganic materials into a polymeric matrix system. A diversity of fabrication methods have been developed to achieve incorporation, such as blending, interfacial polymerization, layer-by-layer deposition, surface grafting, self-assembly of

nanoparticles, and phase inversion methods [4, 93]. For example, Balta *et al*. [94] incorporated the inexpensive ZnO nanoparticles into PES matrix using phase inversion. The PES/ZnO composite membrane showed improved permeability, mechanical strength and more importantly, excellent antifouling properties. Hybrid materials are the current trends in this field, expected to lead to the development of next-generation membranes. Recent research focuses on the development of novel functional materials (both inorganic and organic) and improvement of synthesis methods [4].

1.4.3 Filtration processes

Depending on the direction of the feed flow towards the membrane surface, filtration systems can be classified into two modes, namely dead-end filtration and cross-flow filtration (shown in **Figure 1.2**).
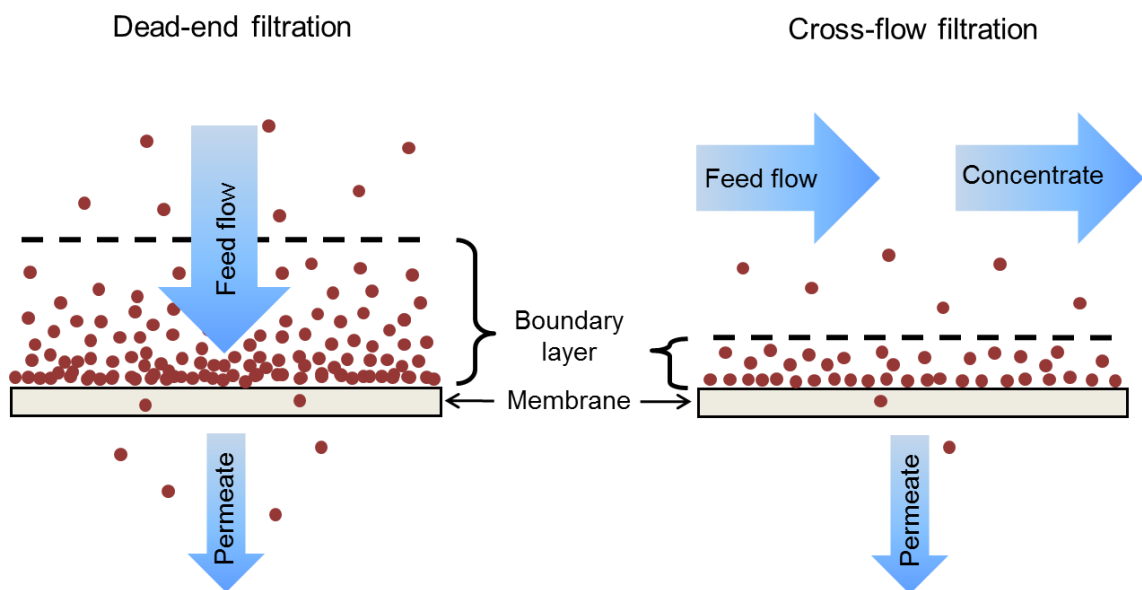
Figure 1.2: Schematic of dead-end filtration and cross-flow filtration

In a dead-end filtration mode, the direction of feed flow is perpendicular to the membrane surface. While water is forced to pass through to the membrane, the retained particles rapidly accumulate on the membrane surface, forming what is called a boundary layer. In a cross-flow filtration mode, on the other hand, the feed flow is tangential to the membrane surface and particles that cannot pass through the membrane are carried away by the concentrate flow. The cross-flow velocity creates a shear force that reduces the development of a boundary layer. This process is referred to as "cross-flow" because the

direction of the feed and concentrate flows is perpendicular to the direction of the permeate flow, while the pressure gradient is still across the membrane.

1.4.4 Renewable energy powered membrane systems

Membrane systems are widely used for large-scale applications, such as central seawater desalination at coastal sites. However, there are many remote locations that are away from central water supply and grid electrical connections. The inhabitants of remote places with no clean water sources have to depend on long distance transport of water, or even collect water from a distance by themselves. The later situation is very common in sub-Saharan Africa, where women and girls are responsible for finding and collecting water for their families [95].

The development of renewable energy powered membrane (RE-membrane) systems has provided a sustainable water supply solution for remote areas [96]. The integration of renewable energy with membrane technology has many benefits. Firstly, utilization of locally available renewable resources resolves the needs for installing traditional electricity infrastructure. Secondly, RE-membrane systems allow autonomous operation with minimum requirement for manpower. Furthermore, both renewable energy equipment and membrane units are modular in nature, thus enabling the system to be scaled based on local conditions and demands [95].

The main renewable energy sources used for RE-membrane systems are solar photovoltaic (PV), solar thermal, wind and geothermal energy. PV and wind are mostly used for RO desalination, while thermal energy is paired with distillation desalination [82]. Over the last two decades, RE-membrane systems powered by PV or wind energy have been successfully implemented in remote communities in both developed and developing regions, such as in Australia [97], Saudi Arabia [98], Spain [99], and Namibia [95].

In general, the total costs of RE-membrane systems are higher than grid-powered systems, mainly because the former are smaller in size and extra capital investment is required for renewable energy equipment [82]. However, Schäfer *et al.* [95] found that the general estimated costs for decentralized RE-membrane systems are within the range of untreated

water costs in developing countries (*e.g.* water tankers or vendors). The biggest challenge to apply RE-membrane technology in a remote location may not be the lack of financial resources, but rather sustainability issues such as lack of system maintenance personnel and unavailability of service networks [95]. Therefore, innovative approaches to increase the sustainability of RE-membrane technology are required for remote areas worldwide.

1.5   Removal of fluoride by NF/RO

Removal of fluoride by NF/RO from water has been reported to be successful. Dolar *et al.* [14] showed that fluoride rejections with RO membranes were higher than 96%, with tight NF membranes higher than 90% and with loose NF membranes higher than 50%. On the other hand, Lhassani *et al.* [100] and Pontie *et al.* [101] reported that the advantage of NF compared to RO is that NF rejects fluoride selectively from other halide ions. Pontie *et al.* [102] further compared the performances of NF and RO membranes and indicated that NF reduces partially the total salinity and removes fluoride to meet WHO guideline for feed concentrations up to 15 mg L^{-1} with lower energy consumption than RO. Previous studies indicate that fluoride retention varies significantly with membrane types, inviting a thorough investigation on the retention mechanisms (influenced by operating conditions and water chemistry) for better understanding and predicting NF/RO performance.

1.5.1   Solution-diffusion

The solution-diffusion model is the most widely used transport model for permeation in a non-porous membrane [85]. Solution-diffusion is basically a three-step process (**Figure 1.3**A): (1) the solute leaves the solvent by dissolving in the membrane, (2) the solute diffuses through the membrane driven by a concentration gradient, and (3) it enters again in the solvent phase that permeates through the membrane. Step 1 and 3 are very fast relative to step 2, so diffusion through the membrane is the rate-limiting step in mass transfer. The diffusive flux ($J_{\text{diffusive}}$, mol s^{-1} m^{-2}) follows the general form of Fick's first law as:

$$J_{diffusive} = -D\frac{dc}{dx} \tag{1}$$

where dc/dx is the concentration gradient across the membrane (mol m^{-4}) and D is the diffusion coefficient of the solute in the membrane (m^2 s^{-1}). In a closed system (*e.g.* a dead-end filtration cell), feed solution concentration increases continuously, leading to an increasing concentration gradient across the membrane. As a result, the diffusion rate of ions is increased, allowing more ions to permeate the membrane [103].
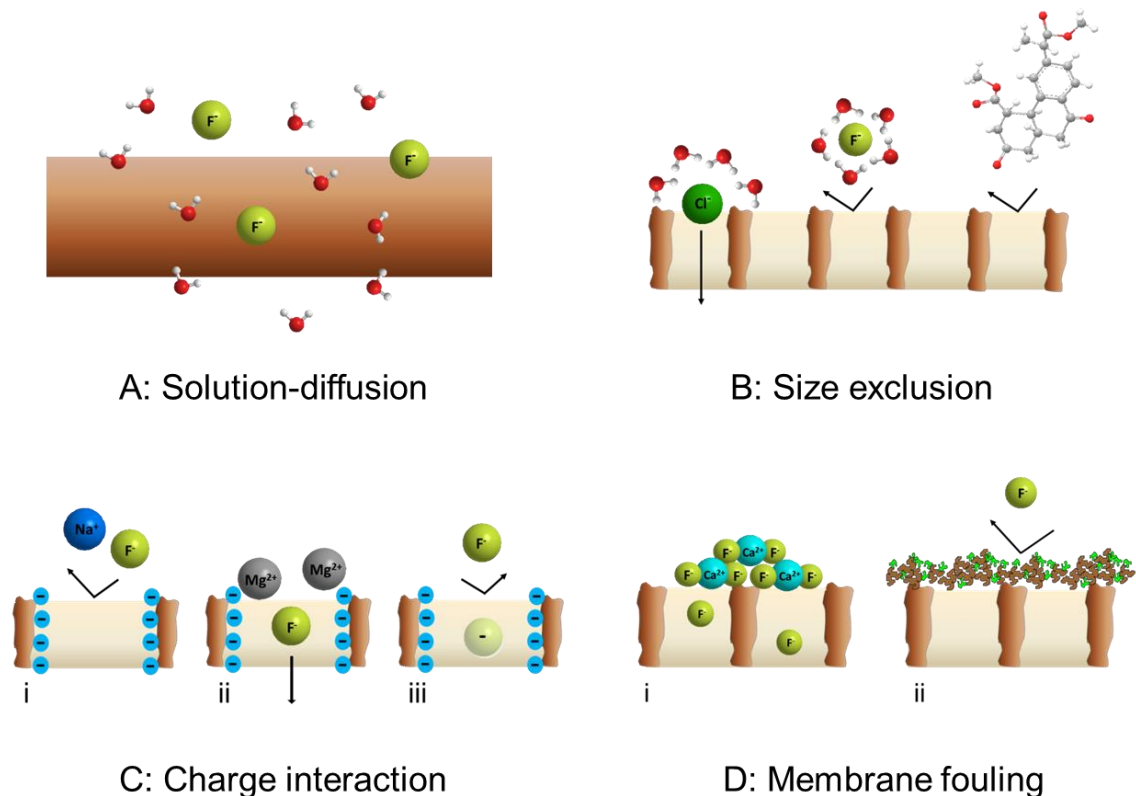
Figure 1.3: Schematic of fluoride retention mechanisms in NF/RO

The diffusion rate is also influenced by the solubility limit of the solute within the polymer matrix. Selective fluoride retention from other solutes is attributed to the high solubility of fluoride in water, which makes it difficult to dissolve in the membrane. Hydration plays a key role because fluoride ions need to be detached from its hydration shell to diffuse through the membrane. On the contrary, other ions such as nitrate and boron are less hydrated and are less retained by the membrane [104]. Moreover, fluoride retention was proven to be unaffected by pressure, indicating that the passage of this ion is mainly due to diffusion [100].

1.5.2   *Size exclusion*

Size exclusion is widely regarded as the basic mechanism of porous pressure driven membrane filtration processes [105]. In a size exclusion model, any solute larger than the pore size of the membrane is retained. In NF this is complicated because the sub-nanometer pore size of the membrane is not constant. Most membranes are characterised by a pore size distribution rather than a specific pore size which complicates size evaluations. Several authors have investigated the pore sizes of some commercial NF membranes and found that the approximate effective pore radius is between 0.4 and 1.5 nm with the majority in the range of 0.4 to 0.8 nm [86, 106, 107]. This is obviously very dependent on membrane materials and structures.

Generally, small solutes have non-spherical and often flexible shapes. For the sake of simplification, the size exclusion model assumes that solutes are spheroids and the membrane pores are uniform cylindrical capillaries. The Stokes radius r_s (m) is defined as the effective size of a theoretical solid sphere that diffuses at the same speed as the target ion. This parameter is commonly used to describe the effective ion size [108, 109] and it is calculated from

$$r_s = \frac{k_B T}{6\pi\eta D} \qquad\qquad (2)$$

where k_B is the Boltzmann constant (J mol^{-1} K^{-1}), η is viscosity (kg m^{-1} s^{-1}), T is temperature (K) and D is the solute diffusion coefficient (m^2 s^{-1}). Ions with smaller Stokes radius have a higher mobility and *vice versa*.

The fluoride ion has a small Stokes radius of 0.13 nm [110]. However, in water, the dissolved fluoride ions are surrounded by water molecules and thus form larger entities [69]. As a result the effective size needs to account for both ionic size and hydration layers. Christl *et al*. [41] concluded that the hydrated radius is determined by the charge density and the crystal radius of the central ion. Having higher charge density, the smaller ions hold the water molecules more strongly. Richards *et al*. [111] determined the hydrated radii of several monovalent anions using molecular dynamics simulations. They found that fluoride ions have a hydrated radius of 0.34 nm and chloride ions have a hydrated radius of 0.38 nm. Although hydrated chloride is still larger than hydrated

fluoride, chloride is more weakly hydrated and its hydration shell can be detached more easily [69]. Therefore, chlorides can pass through the membrane more readily than fluorides, as can be seen from **Figure 1.3**B [103]. Knowledge on hydration and dehydration of small ions shed light in understanding the higher retention of fluoride compared with other anions [112].

1.5.3   Charge interaction

Charge interaction refers to the repulsion or attraction between a charged solute and a charged membrane. This mechanism reveals its importance especially when the size of the charged solute is smaller than the membrane pore size [103].

Solute charge varies with chemical speciation, which depends on the specific water chemistry, including *pH*, ionic strength, temperature, and available ligands [113]. As mentioned earlier, negative F^- exist above *pH* 3.2.

Membrane charge is determined by the ionisable functional groups on the surface [114, 115]. The isoelectric points of most NF membranes usually fall in the range of *pH* 3−6 so they are negatively charged at neutral and alkaline *pH* [116]. Due to the dissociation of functional groups, charge repulsion between the polymer chains increases and forces the membrane pores to 'open up' [117]. At the isoelectric point, membrane functional groups are uncharged and hence the pores are believed to be smallest. However, some researchers reached opposite conclusions and argued that the absence of repulsion forces actually contributes to the expansion of membrane pores [118]. The point of contention is how charge repulsion between polymers affects the membrane pore size. More studies on the distribution of various functional groups in the membrane structure need to be carried out before a further conclusion can be drawn. Richards *et al*. [104] studied the permeate flux of a number of NF/RO membranes as a function of *pH*. Surprisingly, the results showed that flux (permeability) is independent of *pH* for most membranes, indicating that the influence of membrane charge on pore size may indeed be overstated.

Once the electrostatic properties of the solute and the membrane are determined, the charge interactions can be understood. **Figure 1.3**C highlights the effects of charge interactions on the behaviour of fluoride in NF/RO. The first ruling principle is Donnan

equilibrium as shown in **Figrue 1.3**C (i) [119, 120]. In this mechanism charges on the membrane functional groups (such as COO⁻ groups) prevents F⁻ co-ions from entering the membrane phase while attracting counter-ions. Meanwhile, an equivalent number of low charge counter-ions (Na^+ in this case) are retained to satisfy the electro-neutrality condition. This leads to the retention of the ion-pair NaF as a whole. In the case of various ion-pairs, the effect of charge becomes even more complex. Mulder *et al*. [86] reviewed the retention of Na_2SO_4, NaCl and $CaCl_2$ by a negative membrane and a positive membrane. For the negative membrane, the retention of Na_2SO_4 was highest and that of $CaCl_2$ the lowest. For the positive membrane, the reversed order was observed with the highest retention for $CaCl_2$ while Na_2SO_4 had the lowest retention. It was concluded that in salt mixtures the retention of single-charged co-ions decreased drastically whereas the retention of multiple-charged co-ions hardly changed [86]. Furthermore, the monovalent co-ions may even be negatively rejected, depending on the concentration ratio between single-charged and multiple-charged co-ions in the electrolyte solution [86, 121].

The second principle is charge shielding, which refers to the shielding effect of counter-ions on membrane surface charge [122]. Teixeira *et al*. [120] found that calcium ions screened the ionized sites of a polyamide membrane so remarkably that zeta-potentials switched from negative to positive as the calcium concentration increased and the isoelectric point of the membrane was consequently modified. As shown in **Figure 1.3**C (ii), the negatively charged fluoride should be highly rejected by the membrane, but an increase in divalent cation (*e.g.* Mg^{2+}) concentration shields the membrane charge and thus allows anions to pass through. Charge shielding is tightly associated with the valence of counter-ions, wherein higher counter-ion valence leads to lower retention due to more effective charge shielding [123]. However, the shielding effect appears to be more effective for monovalent ions than divalent ions since the retention of divalent anions remains high despite the occurrence of charge shielding [124].

Dielectric exclusion is a further established non-sieving mechanism in NF [125-128]. Dielectric exclusion occurs when an ion interacts with the bound electrical charges induced by the ion, at the interface between media of different dielectric constants. In this case the interface is between the membrane matrix and the solvent [128]. Due to the fact that the dielectric constant of the aqueous solution is significantly higher than that of the polymeric matrix, the polarization charges have the same sign as the ions in the

aqueous solution. Consequently, the interaction always causes a repulsive effect on the ion [127]. The magnitude of the repulsive force can be described by the concept of 'image force' as illustrated in **Figure 1.3**C (iii): the interaction between a charged ion and a polarized interface is formally equivalent to the interaction with a fictitious image charge located at the other side of the interface (inside the membrane matrix) at the same distance from the interface as the real charge [128]. Yaroshchuk [125] has provided a comprehensive review of this exclusion mechanism and concluded that this interaction is dependent on the ion valance, the ratio of dielectric constants of the two media, and the pore geometry of the membrane. Dielectric exclusion is expected to be relevant to the high rejection of multivalent counter-ions by the uncharged membranes, for which Donnan exclusion is negligible [127]. However, the role of dielectric exclusion in the retention of fluoride has not been sufficiently characterised, which provides fertile areas for future research.

1.5.4   Influence of operating parameters

Operating parameters such as pressure, crossflow velocity and recovery significantly affect NF/RO performance. They may determine the dominant mechanisms by affecting the properties of the membrane and conditions at the membrane surface [103]. Previous studies revealed that retention of fluoride generally increased with applied pressure (**Figure 1.4**). Although the contribution of diffusion remains constant with pressure, the increase in water flux surpasses the increase in convective transport of fluoride, and therefore the retention increases. However, as the pressure increases, concentration polarization in the boundary layer increases and hence solute diffusion increases [129]. Concentration polarization leads to increased osmotic pressure and thus decreased flux. This further leads to an increased risk of membrane fouling. For crossflow NF/RO, the predominant operation mode, crossflow velocity has a significant effect on concentration polarization and the ensuing permeate flux decline in addition to pressure [130]. For example, Koyuncu and Topacik [131] observed that increased crossflow velocity resulted in higher rejection of NaCl, which was attributed to less concentration polarization under high crossflow conditions.
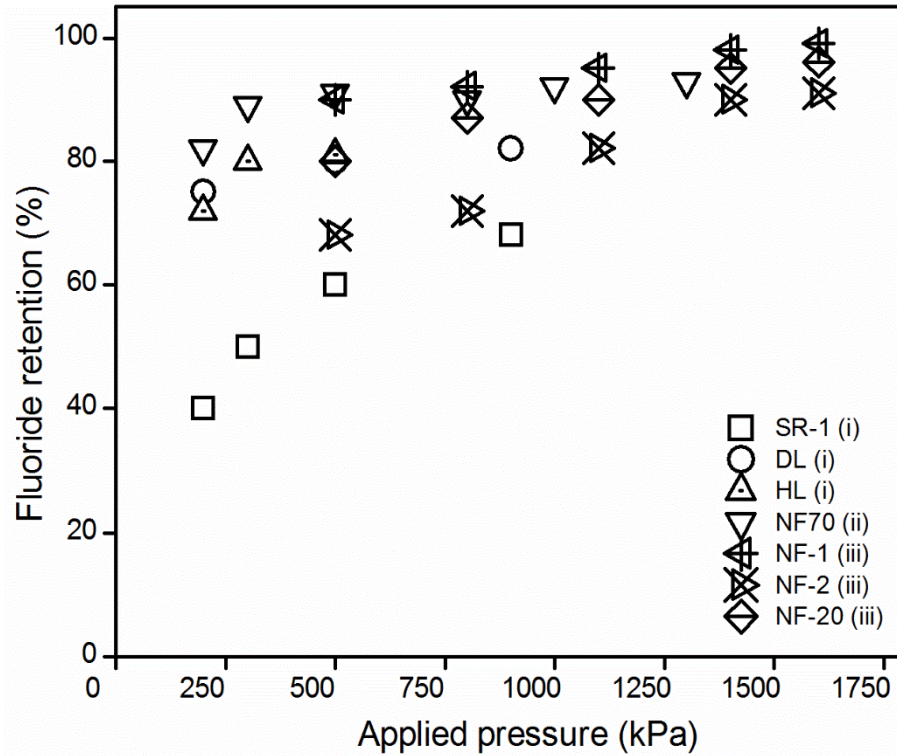
Figure 1.4: Effect of applied pressure on fluoride retention by different NF/RO membranes (data adapted from i [132], ii [100], iii [133])

Table 1.2: Characterization of the membranes used in the literatures (data from [100, 104, 132-134])

Type	Manufacture	MWCO (Da)	Pore radius (nm)	NaCl retention (%)	Permeability (L hr^{-1} m^{-2} bar^{-1})
BW30	Dow	98	0.32	99.8	4.4
NF70	Dow	180	–	–	–
NF90	Dow	100	0.34	83.7	9.7
NF270	Dow	180	0.38	42.4	16.2
NF-1	Sepro	–	0.53	90.0	11.2
NF-2	Sepro	300–400	0.57	50.0	13.3
NF-20	Sepro	–	0.54	35.0	12.2
TFC-S	Koch	200	0.34	86.8	5.8
SR-1	Koch	167	0.38	40.8	5.7
TR60	Toray	400	–	–	–
DL	Osmonics	150–300	0.58	58.0	7.2
HL	Osmonics	150–300	0.41	88.0	9.0

1.5.5   Influence of water chemistry

The impact of concentration on fluoride retention is closely linked to diffusion since the concentration gradient is the driving force for diffusive flux. High fluoride concentration

at the boundary layer increases solution-diffusion and hence the permeate concentration. Some previous studies show a descending trend of fluoride retention with increasing initial fluoride concentration while some show an ascending trend (**Figure 1.5**). Such difference is believed to be related to membrane characteristics which may affect the transport mechanisms of fluoride.
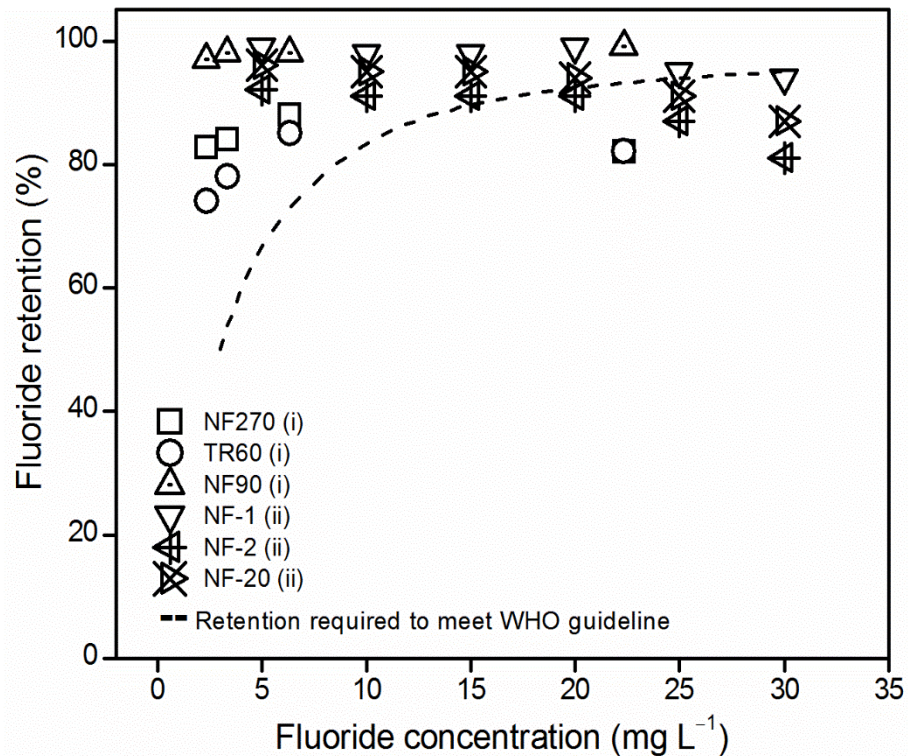
Figure 1.5: Effect of concentration on fluoride retention by different NF/RO membranes (data adapted from i [134], ii [133])

Solution *pH* is a very important parameter in NF/RO, because it affects not only solute speciation but also membrane characteristics [118]. Therefore, *pH* can impact both solvent permeability and solute retention mechanisms, especially the size exclusion and charge repulsion. The influence of *pH* on fluoride retention is shown in **Figure 1.6**. The uncharged HF is deprotonated at its acid dissociation constant (*pKa* = 3.2), and hence charge repulsion becomes significant. A change in fluoride species also affects hydration state and consequently hydrated radius, thus impacting retention when size exclusion is important [104].
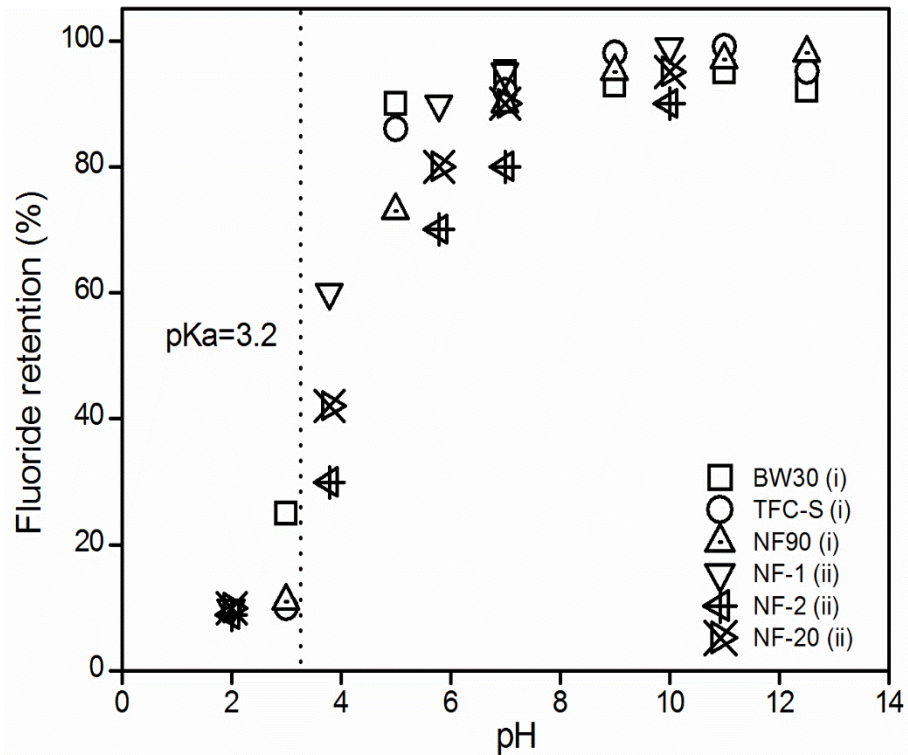
Figure 1.6: Effect of *pH* on fluoride retention by different NF/RO membranes (data adapted from i [104], ii [133])

The strength of electrostatic interaction between ions and the membrane varies according to solution *pH*, with minimal interaction occurring around the isoelectric point of the membrane surface. This can be seen in **Figure 1.6** where fluoride retention increases with increasing membrane charge. Besides, *pH* may affect the openness of the membrane by controlling the dissociation of the functional groups on the membrane surface though the effect is not universal for all membranes [117, 118]. Bellona and Drewes [135] found that an increasing *pH* can only increase the rejection of negatively charged organic solutes to a certain level before the effect of increased surface electronegativity is offset by the increased membrane pore size. Richards *et al*. [104] reported a similar phenomenon on fluoride retention but explained it using the hydration theory as they found the pore size of the membrane was not affected by *pH*.

1.5.6   *Influence of membrane fouling*

Apart from the above-mentioned mechanisms, membrane fouling in NF/RO plays a noteworthy role on fluoride retention. Fouling can be categorized into four types: biofouling, colloidal fouling, inorganic scaling and organic fouling [136]. In this chapter, only the latter two will be discussed because fluoride and NOM, as the two target

contaminants in this study, can cause inorganic scaling and organic fouling, respectively [103].

Inorganic scaling occurs when the concentration of inorganic ions at the membrane surface exceeds the solubility limit. One of the most common scalants is Ca^{2+} [136]. Ca^{2+} forms sparingly soluble salts such as $CaCO_3$, CaF_2 and $CaSO_4$, and precipitates on the membrane surface to cause membrane scaling (**Figure 1.3**D (i)). Tu *et al*. [137] observed decreased retention of boron by $CaSO_4$ fouled membrane due to cake-enhanced concentration polarization mechanism. Such fouling may further screen the negative charge of the membrane surface, and consequently reduce the retention of negative solutes. Inorganic scaling might decrease fluoride retention in the same way, but the mechanism would be more complicated as fluoride may precipitate in the filtration process.

Organic fouling exhibits a variety of characteristics due to the complex interactions between chemical functional groups of organic foulants and those of the polymeric membrane layer [136, 138]. It has been revealed that pore blocking is the predominant fouling mechanism during the first stages, while the later stages are governed by cake-enhanced mechanism [139]. Several previous studies found that organic fouling can significantly increase or decrease ion retention [136, 137, 140]. The formation of a denser and more negative fouling layer increases size and charge exclusion (**Figure 1.3**D (ii)), whereas cake-enhanced concentration polarization reduces retention.

Both inorganic and organic fouling can be avoided by early enough membrane cleaning. Sehn [141] reported the anti-fouling strategies of a large scale RO plant in Finland. The plant employed regular flushing and preventive cleaning to control the risk of membrane fouling. After more than three years of operation, the salt and fluoride rejections were still the same as in the beginning.

1.6   Removal of NOM by NF/RO

NOM is another important contaminant in drinking water treatment as it leads to undesirable colour, taste and odor, and reacts with common disinfectants to produce a variety of toxic disinfection by-products (DBPs) including trihalomethanes (THMs)

[142]. Large NOM compounds like polysaccharides and humic substances can be effectively retained by NF/RO, during which size exclusion, charge repulsion, and hydrophobic interactions are well-known removal mechanisms [143, 144]. But LMW fractions are likely to permeate the membranes (especially the NF membranes), and thus produce the problem of bacterial regrowth in the drinking water distribution system [145]. Besides, NOM may cause severe membrane fouling and hence reduce system productivity and lifetime [138]. Both reversible and irreversible fouling mechanisms have been discussed in numerous studies [146, 147]. NOM characterization, solution chemistry, membrane properties and operational conditions have been reported to influence the fouling mechanisms to different extents [148]. Overall, NOM reduces the acceptability of water and increases the risk of forming DBPs [142]. As a result, removal of NOM is of crucial importance for membrane processes.

As discussed in Chapter 1.3, NOM has the potential to interact with fluoride ions *via* territorial interaction. If fluoride ions can be trapped in the NOM structure, the retention of fluoride by NF/RO is estimated to be heavily affected. Most NOM cannot penetrate tight NF/RO membranes due to size exclusion, so the fluoride ions bound to NOM will also be rejected by the membrane. Unfortunately there are no experimental data or observations convincing the effect of fluoride-NOM interactions on membrane. If NOM can immobilize freely dissolved fluoride ions, membrane filtration can become a very attractive option for removing fluoride and NOM at the same time.

1.7 Photosensitization processes

Photocatalysis is defined as acceleration of a chemical reaction or its initiation under light (ultraviolet, visible, or infrared radiation) in the presence of a catalyst [149]. This definition includes photosensitization, a process where a molecule (the photosensitizer) absorbs light and transfers the energy to another molecule (the target molecule) and then the target molecule undergoes chemical alteration [150]. Photosensitization reactions are widely used in the fields of photochemistry and photobiology, particularly in fine chemical synthesis, wastewater treatment, and photodynamic therapy (PDT).

1.7.1   *Photosensitizer and singlet oxygen*

In quantum mechanics, most stable molecules have singlet ground states because they have complete electron shells without unpaired electrons. Molecular oxygen (O_2) is an exception: it has triplet ground state because the molecule has two unpaired electrons [151]. Singlet or triplet state can form when the electron is excited to a higher energy level [152]. In an excited singlet state, the spin of the excited electron is paired with that of the ground state electron. In an excited triplet state, the spin of the promoted electron is parallel to that of the ground state electron.

A Jablonski diagram (**Figure 1.7**) illustrates the transformation of the photosensitizer from the singlet ground state to the triplet excited state [150, 153]. When absorbing light at a specific wavelength, the photosensitizer is excited from the ground state to the singlet excited state. Because the singlet excited state has a very short lifetime (10^{-15} s), it is unlikely that the molecule can react with another molecule *via* either electron or energy transfer [154]. There are several pathways for a molecule to dissipate the energy received from light. The first pathway is internal conversion, where the electron transfers from a high electronic state to a lower electronic state that has the same spin. The second pathway is intersystem crossing. This is where the electron changes spin and thus the molecule undergoes a transition from singlet excited state to triplet excited state. Because the transition from triplet state to singlet state is forbidden, the triplet excited state has a much longer lifetime (10^{-8} to 10^{-3} s) than the singlet excited state [154]. Therefore the molecule in the triplet excited state is more likely to be involved in energy transfer reactions. The last pathway a molecule may take is to emit a photon. Emission of a photon between two electronic states with the same spin is called fluorescence, and emission between a triplet excited state and a singlet ground state is called phosphorescence [154] (**Figure 1.7**).
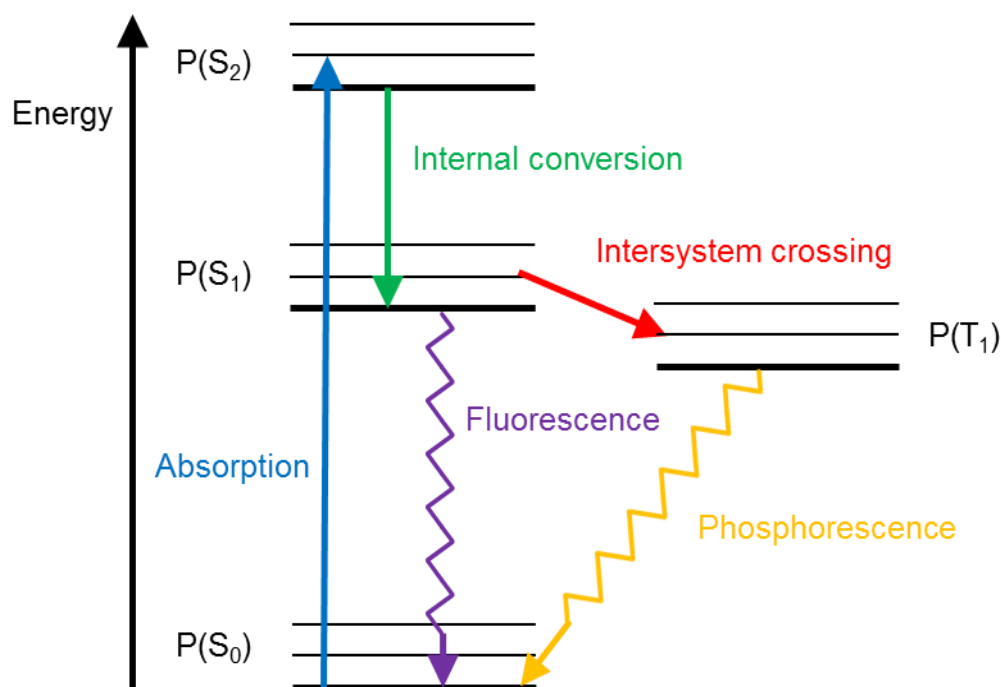
Figure 1.7: Jablonski diagram depicting electronic transitions following the absorption of light by a photosensitizer (P: Photosensitizer; S_0: singlet ground state; S_1 and S_2: singlet excited state; T_1: triplet excited state)

Once in the triplet excited state, the photosensitizer can undergo two types of photochemical reactions. In the Type I reaction, the photosensitizer reacts directly with the target molecule to generate active radicals. These radicals can further react with oxygen to form reactive oxidative species (ROS) such as the superoxide radical. In the Type II reaction, the excited photosensitizer transfer excess energy to triplet ground state oxygen ($^3O_2$) to produce singlet excited state oxygen, *i.e.* singlet oxygen ($^1O_2$). $^1O_2$ then reacts with the target molecule to generate oxidized products [150]. The occurrence of Type I and Type II reactions depends on the type of photosensitizer as well as the amount of the target molecule and oxygen. The Type II reaction is favored over the Type I reaction when the concentration of the target molecule is low and the concentration of oxygen is high. This work focused on Type II reaction which produces $^1O_2$.

The $^1O_2$ generating ability of a photosensitizer is measured by its quantum yield (Φ_Δ). The quantum yield of $^1O_2$ production is defined as the number of moles of the generated $^1O_2$ molecules divided by the number of photons absorbed by the photosensitizer [155]. The methods used to determine the quantum yield of $^1O_2$ production include (1) direct measurement of luminescence intensity; (2) photothermal methods, such as steady-state

photocalorimetric technique, time dependent thermal lensing, and laser induced photoacoustics; and (3) indirect measurement based on photo-oxidation reactions, such as measuring the change in absorbance or oxygen consumption [150, 156].

1.7.2   *Water treatment using singlet oxygen*

Photosensitized water treatment by $^1O_2$ has in recent years gained increasing interest as it involves three environmentally friendly components, namely the photosensitizer, a light source, and molecular oxygen. Common visible light active photosensitizers include organic dyes (*e.g.* Rose Bengal and Methylene Blue), fullerenes, porphyrins, phthalocyanines and transition metal complexes [157-164].

$^1O_2$ is a selective oxidant which readily oxidizes unsaturated double bonds, phenols, sulfides, amines and other electron-donor compounds due to its electrophilic nature [150]. $^1O_2$ is also highly cytotoxic and is thus capable of killing cells and microorganisms [165, 166]. With regard to water and wastewater treatment, $^1O_2$ becomes particularly attractive because it can carry out dual function of decontamination and disinfection [167]. Unlike conventional technologies which in most cases merely separate contaminants from water, $^1O_2$ can convert organic contaminants into biodegradable compounds as well as kill bacteria, fungi, and viruses [150, 168, 169]. Meanwhile, $^1O_2$ is much more selective towards organic compounds compared to hydroxyl radicals (OH·) and other ROS [170]. The selectivity of $^1O_2$ enhances its oxidation capacity when target pollutants are present in complex wastewater matrices with background constituents (*e.g.* NOM). Recent research showed that $^1O_2$ was more efficient than non-selective OH· in removal of some pharmaceuticals in real wastewater effluents [168].

1.7.3   *Limitations*

Although photosensitized $^1O_2$ has numerous advantages, there are a few limitations. (1) Many organic photosensitizers incorporate diverse metal species with visible light harvesting capacity [171-174]. These organic-metal complexes tend to be expensive, toxic and unsustainable [175]; (2) the vast majority of photosensitizers work in homogeneous conditions. When employing a homogeneous photosensitizer in water its separation and recovery becomes a severe problem and there is an increased risk of

leakage of the photosensitizer which may lead to environmental pollution [176]; (3) some photosensitizers suffer from photobleaching, which refers to the degradation of the photosensitizer *via* long exposure to light and/or to the generated $^1O_2$ [150]. Photobleaching significantly reduces the quantum yield and the lifetime of the photosensitizer. It is therefore desirable to develop heterogeneous and metal-free photosensitizers, which are photostable towards light and $^1O_2$.

1.8   Thesis overview

This thesis investigated the application of membrane technologies in drinking water purification and wastewater treatment. The thesis is organized in seven chapters. An overview of the thesis structure is given in **Figure 1.8**.

Chapter 1 introduced the target contaminants (fluoride, HS, emerging contaminants and *Cryptosporidium*) and their physicochemical characteristics, and reviewed the current progress in removing these contaminants by membrane technologies. Part of review presented in this chapter has contributed to a review paper: **Shen, J.** and Schäfer, A.I., *Removal of fluoride and uranium by nanofiltration and reverse osmosis: A review.* Chemosphere, 117, 679–691 (2014).

Chapter 2 described the chemicals and membranes used as well as the experimental and analytical equipment. Experimental procedures specific to an individual chapter are described in the relevant chapter.

The body of this thesis consists of four experimental chapters. Chapter 3 investigated the effect of HS on the fate and behaviour of fluoride in solution. The role of water chemistry parameters such as *pH* and ionic strength in fluoride-HS interaction was studied. Chapter 4 presented the results of bench-scale NF/RO experiments treating a wide range of natural water samples that were collected in Tanzania. Factors affecting fluoride and NOM removal by NF/RO were discussed. The work presented in this chapter has contributed to a publication: **Shen, J.** and Schäfer, A.I., *Factors affecting fluoride and natural organic matter (NOM) removal from natural waters in Tanzania by nanofiltration/reverse osmosis.* Science of the Total Environment, 527–528, 520–529 (2015).

Knowledge on solute-solute interactions obtained from Chapter 3 contributed to a better understanding of fluoride and NOM removal mechanisms. Some challenging but promising drinking water sources were identified in Chapter 4, and were further tested in pilot-scale experiments in Chapter 5.

Chapter 5 demonstrated the field performance of a pilot-scale RE-membrane system with specific regard to fluctuating energy. The feasibility and sustainability of RE-membrane system for supplying drinking water in remote areas were discussed. Some part of work reported in this chapter has contributed to a publication: **Shen, J.**, Mkongo, G., Abbt-Braun, G., Ceppi, S.L., Richards, B.S., and Schäfer, A.I., *Renewable energy powered membrane technology: Fluoride removal in a rural community in northern Tanzania.* Separation and Purification Technology, 149, 349–361 (2015).

Chapter 6 extended the research area from drinking water to wastewater. A novel type of photocatalytic polymer was developed and tested in terms of decomposition of emerging contaminants and disinfection of *Cryptosporidium.* The possible configurations of photocatalytic membrane reactors were also discussed. The work presented in this chapter has contributed to a publication: **Shen, J.**, Steinbach, R., Tobin, J., Nakata, M.M., Bower, M., McCoustra, M.R.S., Bridle, H., Arrighi, V., and Vilela, F., *Photoactive and metal-free polyamide-based polymers for water and wastewater treatment under visible light irradiation.* Applied Catalysis B: Environmental, 193, 226–233 (2016).

Chapter 7 concluded a summary of results obtained along with suggestions for future research.

Appendix 1 assessed the impact of fluoride in drinking water on human health based on a visit to some fluoride-affected villages in Tanzania. Prevalence and severity of endemic fluorosis in these remote villages highlighted the need for developing sustainable water purification technology. Appendix 2 included the complete results of water quality data for 166 Tanzanian water samples.
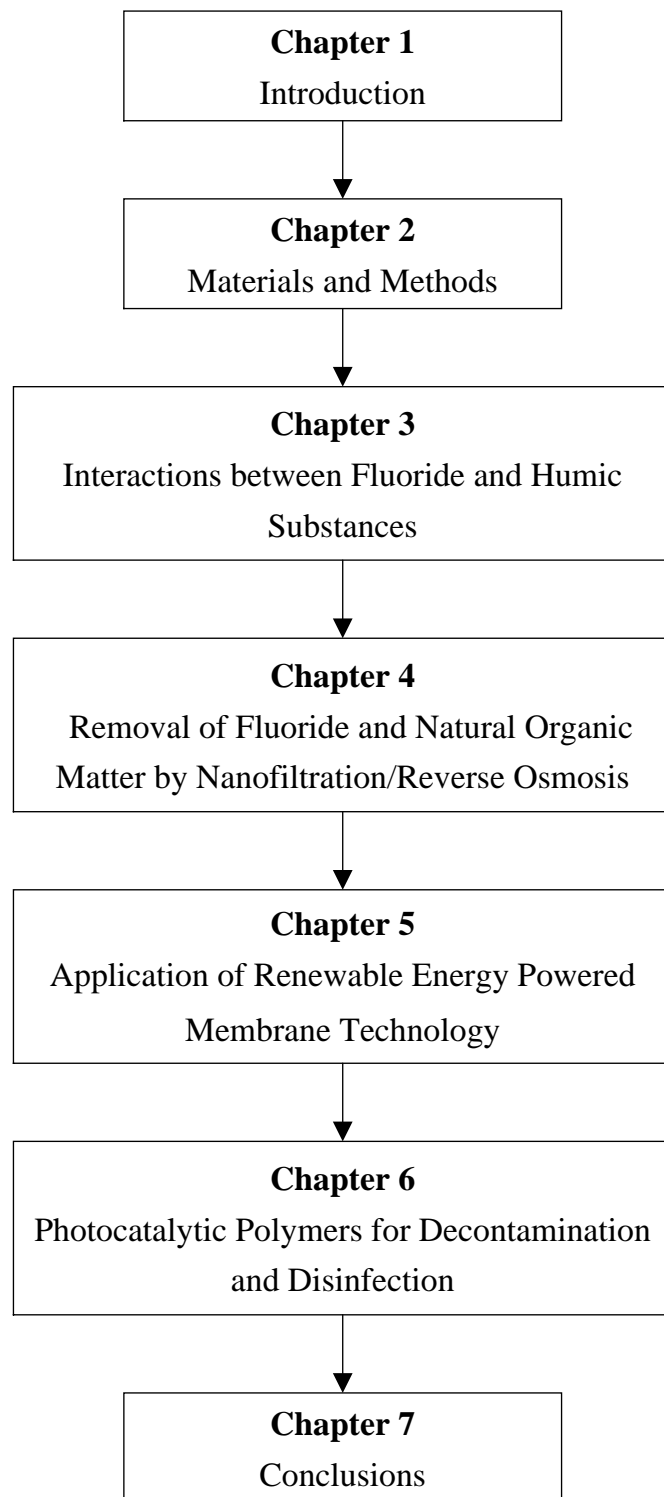
Figure 1.8: Overview of thesis structure

Chapter 2: Materials and Methods

2.1 Chemicals

2.1.1 Chemicals used in Chapter 3

Water used was deionised (DI) water (ELGA PURELAB Option-Q, USA). Aldrich humic acid (AHA) was provided by Sigma-Aldrich, Suwannee River humic acid (SRHA) was provided by the International Humic Substances Society. It should be pointed out that the classical definitions of HA, fulvic acid (FA) and humin are only operational on the basis of certain isolation/fractionation procedures, and do not indicate the existence of three distinct HS species [48]. In this study, HS refers to the generic term, regardless of the isolation method. Analytical grade sodium fluoride, sodium hydroxide, sodium chloride, hydrochloride acid, glacial acetic acid and IR grade potassium bromide were from Sigma-Aldrich. Analytical grade trans-1,2-diaminocyclohexane-N,N,N',N'-tetraacetic acid monohydrate (CDTA) was purchased from Fisher Scientific.

The major limitation of AHA as a model NOM is its high percentage of impurities (*e.g.* silicate) [177]. Therefore AHA was purified using the following procedure: 10 g AHA was dissolved in 0.1 M NaOH solution containing 0.2 g of NaF per gram of AHA. NaF was employed to reduce its ash content by dissolving silicate impurities under acid conditions [178]. AHA was precipitated by adding 5 M HCl until $pH = 1$ and the solution was stirred for 24 hr. The solution was centrifuged at 10000 rpm for 1 hr and the residue extensively washed with 1 M HCl. The residue was re-suspended with 0.1 M NaOH solution at pH 9 for 24 hr, and filtered with Whatman grade 1 filters. The suspension was adjusted to pH 2 with 1 M HCl for 24 hr, and centrifuged at 10000 rpm for 1 hr. The final residue was freeze-dried and stored in a glass container. The resulting purified AHA was denoted as PAHA.

In addition to synthetic solutions, a natural water sample containing high levels of fluoride and NOM was tested in this study. The sampling site was in a brown river in Ngare Nanyuki, Arusha, Tanzania (GPS coordinate S03°10.931'E036°51.677'). The natural water sample was collected in a plastic container and airfreighted to Scotland within three days after collection. Once arrived, the water was stored at 4 °C in darkness.

A series of synthetic solutions containing fluoride and HS were prepared using commercial HS. 1 g L^{-1} fluoride stock solution and 1 M NaCl stock solution were prepared by dissolving 2.21 g NaF and 5.85 g NaCl into 1 L DI water, respectively. 1 g L^{-1} HS stock solution was made by adding 1 g HS into 1 L DI water. The HS stock was adjusted to *pH* 9 to dissolve all particles. Samples with different *pH*, ionic strength, fluoride and HS concentrations were prepared by mixing the stock solutions, and adjusted to the required *pH* by 0.1 M NaOH or 0.1 M HCl solutions.

As for the natural water sample NNHS, the *pH* was adjusted by adding either 0.1 M NaOH or 0.1 M HCl, and its ionic strength was controlled by addition of appropriate amounts of solid NaCl. The concentrations of fluoride and HS in NNHS were left unchanged.

2.1.2   *Chemicals used in Chapter 4 and Chapter 5*

Water used was Mt Meru bottled water. This water is local surface water treated by reverse osmosis, ozonation, UV treatment. It was selected due to its superior chemical quality compared to all other available waters (*pH* = 7.2, EC < 18 μS cm^{-1}, TOC < 0.01 mg L^{-1}, fluoride < 0.01 mg L^{-1}). Suprapur nitric acid (65 %) and ICP multi-element standard solution VI was purchased from Merck. Other chemicals used were the same as mentioned above.

2.1.3   *Chemicals used in Chapter 6*

Distilled water was used throughout. 4-bromoaniline, 4,7-bis(4,4,5,5-tetramethyl-1,3,2-dioxaborolan-2-yl)benzo[c][1,2,5]thiadiazole (BBT), palladium chloride, triphenylphosphine, hydrazine hydrate, potassium carbonate, trimesoylchloride (TMC), m-phenylendiamine (MPD), α-terpinene, furfuryl alcohol (FFA), bisphenol A (BPA), and cimetidine were obtained from Sigma-Aldrich. Tetrahydrofuran (THF), hexane, and chloroform were purchased from Fisher Scientific. All of the chemicals were of analytical grade and used as received. *Cryptosporidium parvum* oocysts were purchased for Waterborne Inc. lot 24-15 shed on 23rd October 2015. The *Cryptosporidium* experiments were completed within 3 weeks of the shedding date.

The Pd(0) catalyst was prepared using palladium chloride. Briefly, 350 mg (2 mmol) palladium chloride and 2.62 g (10 mmol) triphenylphosphine were dissolved in 25 mL of anhydrous dimethyl sulfoxide. The mixture was stirred and heated to 140−160 °C under nitrogen until an orange solution was formed and stirring continued for 15 min thereafter. 0.39 mL (8 mmol) hydrazine hydrate was added quickly into the orange solution and the solution was left to cool to room temperature. During this time, yellow/green crystals were formed and were then filtered through a sintered glass adaptor under nitrogen. The crystals were washed with dry methanol and dry diethyl ether, left to dry under nitrogen and stored at −10 °C. The Pd(0) catalyst was then employed in the synthesis of the photosensitizer monomer.

The photosensitizer monomer used for making polymers is an aminophenyl-substituted benzothidiazole derivative, and is abbreviated as ABT. ABT was synthesised as follow: 378 mg (2.2 mmol) 4-bromoaniline, 388 mg (1.0 mmol) BBT, and 58 mg (0.05 mmol) Pd(0) catalyst were added to a 2 neck flask and mixed under a nitrogen atmosphere. The mixture was then dissolved in dry 40 mL THF. 415 mg (3.0 mmol) potassium carbonate was dissolved in 5 mL deionized water in a separate flask and degassed with nitrogen for 10 min. This aqueous solution was then added to the organic solution. The mixture was heated to 70 °C and stirred for 16 hr under nitrogen. The reaction mixture was then allowed to cool to room temperature and diluted with 100 mL methylene chloride. This was washed with deionized water and saturated sodium chloride. The organic phase was dried over magnesium sulfate and filtered. The solvent was removed under reduced pressure. Purification was performed *via* silica gel column chromatography (Ethyl acetate/Hexane 2:1) to yield 181 mg (57%) as a red solid.

2.2   Membranes

2.2.1   *Flat sheets*

Six commercial flat sheet membranes were used in the study. The BW30 and BW30-LE are two commonly used brackish water RO membranes while the NF90, NF270, TFC-SR2 and TFC-SR3 are NF membranes. The BW30, BW30-LE, NF90, and NF270 membranes were provided by Dow Filmtec. The TFC-SR2 and TFC-SR3 membranes were provided by Koch Membrane Systems. All these membranes are thin film

composite (TFC) membranes with a polyamide-based active layer [179-181]. The characteristics of the membranes are summarized in **Table 2.1**.

Table 2.1: Characterization of the selected membranes (data adapted from [182, 183])

Type	MWCO (Da)	Pore radius (nm)	NaCl Ret[a] (%)	Permeability (L hr^{-1} m^{-2} bar^{-1})	ZP[b] (mV)	Contact angle (°)
BW30	98	0.32	99.8	4.4	−12	40.3 ± 1.1
BW30-LE	98	NA	99.5	5.8	−35[c]	NA
NF90	100	0.34	83.7	9.7	−26	47.9 ± 1.7
NF270	180	0.38	42.4	16.2	−14	29.1 ± 1.6
TFC-SR2	460	0.52	22.7	14.1	−16	61.5 ± 2.6
TFC-SR3	167	0.38	40.8	5.7	−20	48.5 ± 1.4

Abbreviation: Ret is Retention; ZP is zeta potential.

[a] 0.1 M NaCl, at 10 bar; [b] at *pH* 8, in 20 mM NaCl and 1 mM NaHCO$_3$; [c] at *pH* 8, in 1 mM KCl

The molecular weight cut-off (MWCO) and pore radius are particularly important because they imply the size of solutes which can be sterically retained by the membrane. As **Table 2.1** shows, there is a trade-off between solute retention and pure water permeability. Membranes with larger MWCO/pore sizes have lower salt retention and higher permeability, and *vice versa*.

Zeta potential is the indicator of membrane surface charge which affects the charge repulsion mechanisms. The membrane zeta potential was calculated from the streaming potential which was measured using an electrokinetic analyzer (EKA, Anton Paar KG, Austria) [183]. At *pH* 8 all the membranes are negatively charged (note the Tanzanian samples are generally alkaline). Since the *pH* and ionic strength of real water samples are quite different from those at zeta potential measurement, the zeta potential values of different membranes should be considered relative to each other.

Contact angle represents the hydrophilicity/hydrophobicity of a membrane. Hydrophilic membranes have more interaction with water and hence form smaller contact angle. High hydrophilicity contributes to high permeability due to the diffusive transport of water (*e.g.* NF270 in **Table 2.1**).

2.2.2 *Spiral wound modules*

Flat sheets can be fabricated into spiral wound module or plate-and-frame module. The schematic of a spiral wound module is shown in **Figure 2.1**. The module consists of flat sheet membranes, feed spacers, permeate spacers, and a permeate tube. The feed water travels through feed spacers tangentially across the length of the module. The permeate then passes across the membrane into permeate spacers where it is conducted spirally to the permeate tube. The feed, on the other hand, becomes concentrated at the end of the module. The spiral wound module has a few advantages compared to the plate-and-frame module, such as high packing density and easy cleaning through backwash.
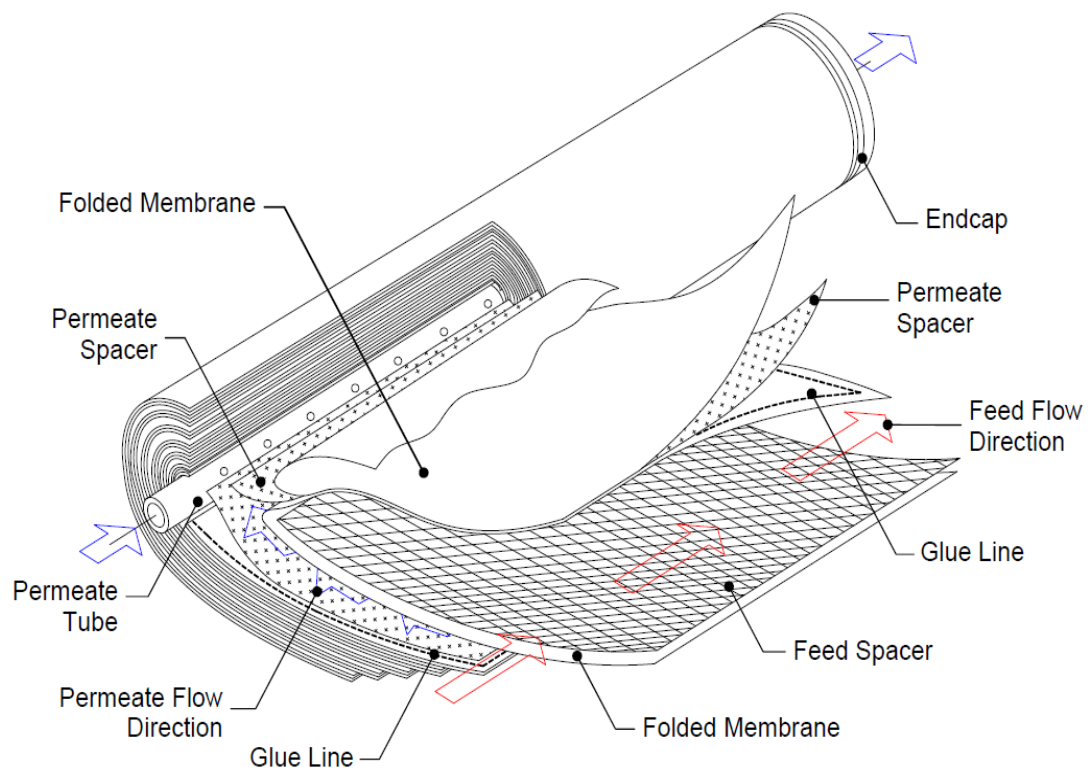
Figure 2.1: Schematic of a spiral wound membrane module [184]

Four spiral wound membrane modules were used in this study, namely BW30, BW30-LE, NF90, and NF270 (Dow Filmtec). They are all in the size of 4040, which means that the module diameter is 4 inch and the module length is 40 inch. Membrane specifications were provided by the manufacturer (**Table 2.2**)

Table 2.2: Spiral wound membrane specifications from the manufacturer [185-187]

Module	Active area (m^2)	Permeate flux (L hr^{-1} m^{-2})	Retention (%)	Test condition
BW30	7.2	52.7	99.5	2000 mg L^{-1} NaCl at 15.5 bar, 15% recovery, 25 °C
BW30-LE	7.2	55.0	99.0	2000 mg L^{-1} NaCl at 10.3 bar, 15% recovery, 25 °C
NF90	7.6	41.7	>97.0	2000 mg L^{-1} MgSO$_4$ at 4.8 bar, 15% recovery, 25 °C
NF270	7.6	52.1	>97.0	2000 mg L^{-1} MgSO$_4$ at 4.8 bar, 15% recovery, 25 °C

2.3 Experimental equipment

2.3.1 Stirred cell

In Chapter 4, a stainless steel stirred cell was used for bench-scale experiments (schematic shown in **Figure 2.2**). The cell was firstly developed by Neale [188]. The volume of the cell is 990 mL and the internal diameter is 70 mm. A membrane is placed on the base of the cell with a surface area of 38.48 cm^2. In order to reduce boundary layer, the cell contains a magnetic stirrer assembly (Millipore, UK) operated at 300 rpm using a magnetic stirrer plate (SM1, Stuart Instrument, UK). The cell was pressurized with compressed medical air (TOL, Tanzania) with a maximum pressure of 10 bar. Internal pressure and temperature were measured by a pressure transducer (PX219-30V85G5V, Omega Engineering, UK) and a thermocouple (TJ2-CPSS-M60U-250-SB, Omega Engineering, UK). Permeate mass was measured by an electronic balance (Adventurer Pro 2102, Ohaus, Switzerland). All the data were collected by a laptop with a data acquisition module (DAQ-54, Omega Engineering, UK).
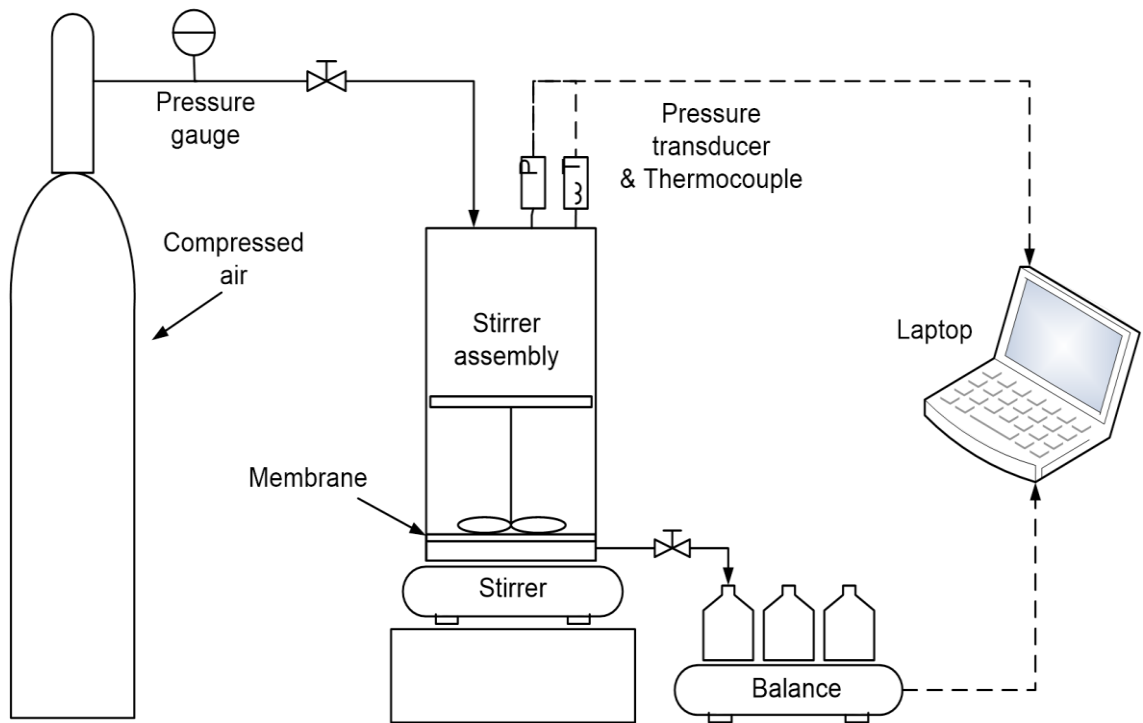
Figure 2.2: Schematic of the dead-end stainless steel stirred cell

Figure 2.3: Photo of the stainless steel stirred cells at UDSM

2.3.2 RE-membrane system

In Chapter 5, a reverse osmosis solar installation (ROSI) was used for pilot-scale experiments. ROSI has been extensively described in previous publications [189-191]. The ROSI system consisted of two stages: the pretreatment stage with an UF membrane is followed by a NF/RO stage. The UF pretreatment stage was designed to remove particles, viruses and bacteria while the NF/RO stage removes salts and trace contaminants. The submerged ultrafiltration was a GE Water ZeeWeed 500 module with a membrane surface area of 31.6 m^2. The NF/RO pressure vessel held one interchangeable 4040 membrane module. A progressive cavity pump (Mono-Pumps, Australia) drew feed water through the UF and then into the NF/RO at pressures up to 12 bar.

A schematic of the ROSI system is shown in **Figure 2.4**. It can operate in two modes, namely batch and continuous modes. In batch mode, the permeate and concentrate were continuously recycled to the feed tank; in continuous mode, the feed tank was continuously filled with water from the source while the permeate was collected in the product tank and the concentrate was discharged.
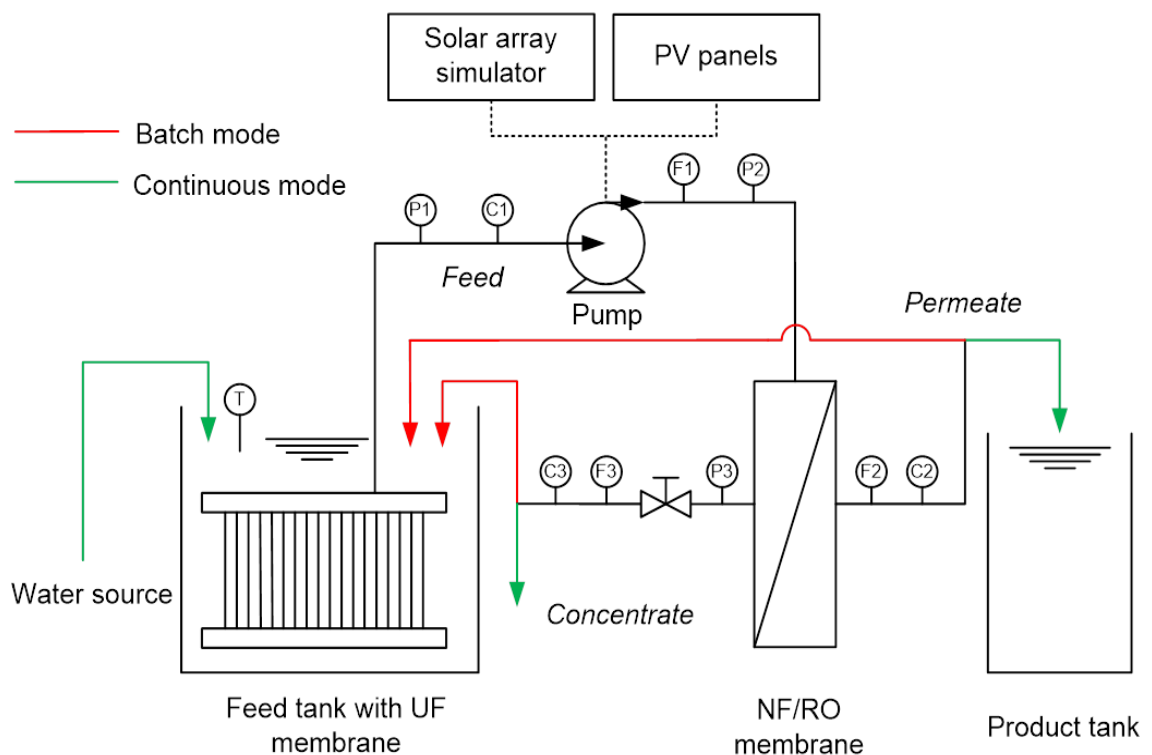
Figure 2.4: Schematic of ROSI in bath and continuous modes, sensors are marked as P (pressure), F (flow), C (EC) and T (temperature).

The system was equipped with a number of sensors to monitor operating parameters under transient operation. Pressure was measured after the UF module, before and after the NF/RO module using Bürkert 8323 pressure transducers (P1, P2, and P3 in **Figure 2.4**). Flow sensors (Omega FTB9512 for F1 and F3, Omega FTB9510 for F2) were installed on the feed, permeate and concentrate lines. They were all equipped with Omega FLSC-62A signal conditioners for 4–20 mA output [192]. EC sensors (Georg Fischer Signet3-2822 for C1 and C3, Georg Fischer Signet 3-2821 for C2) were equipped with Georg Fischer 2850 transmitters with 4–20 mA output. Temperature in the feed tank was measured by Omega KTSS thermocouple. Pump voltage and current were measured directly from the pump. Uncertainty of measurement is ± 1%. All outputs were recorded with a datalogger (DataTaker DT500) at 2s intervals and displayed instantaneously on a laptop running LabVIEW 8.0 (National Instruments).

The system can be powered by solar energy *via* PV panels. Four 24 V_{DC} PV panels (BP Solar, BP3150S) were mounted on a single axis solar tracker (Mono-Pumps) which was guided by a global positioning system and thus followed the path of the sun from east to west during the day. More controlled tests were conducted in the field at Ngurdoto Defluoridation Research Station (NDRS), where power was controlled using a solar array simulator (SAS) (Agilent Technologies E4350B-J02). The operation of SAS power was controlled by the LabVIEW 8.0 interface.

Figure 2.5: Photo of ROSI installed at Ngare Nanyuki, Tanzania

Preventative membrane cleaning is a necessary part of regular maintenance and can suppress membrane fouling and restore membrane performance. The cleaning strategies for the UF and NF/RO modules are different and they should be disconnected before cleaning. The UF module is made of PVDF and thus resistant to chlorine. Its cleaning procedure is as follow:

(1) Fill the feed tank with NDRS tap water.

(2) Add 1 L household bleach (3.85% NaClO) in the tank.

(3) Turn on the air bubbler to ensure homogenous mixing. Leave the system for 1 hr.

(4) Drain the tank and refill it with tap water.

(5) Add 20 g sodium metabisulfite in the tank to eliminate residue chlorine. Keep bubbling for 30 min.

(6) Drain the tank and refill it with tap water.

The NF/RO membranes are made of polyamide and thus vulnerable to chlorine. They can be cleaned by a two-step procedure including alkaline wash and acid wash. The alkaline wash aims to remove organic fouling and biofouling, while the acid wash removes inorganic precipitates such as calcium and iron. For regular use, 100 L of NaOH

solution (*pH* 11) and 100 L of HCl solution (*pH* 3) were prepared using RO permeate and stored in sealed plastic containers in dark. The cleaning procedure is as follow:

(1) Connect the feed tubing to a microfilter to ensure no particles enter the NF/RO module.

(2) Immerse the microfilter in the alkaline tank. Start the pump with 90 W input power. Make sure there is no permeate. Recycle the concentrate to the alkaline tank.

(3) Turn off the pump. Allow the membrane to soak in the cleaning solution for 1 hr.

(4) Rinse the microfilter and transfer it to a tank filled with RO permeate. Start the pump to flush out the foulants through the concentrate tubing and discard them into sewage.

(5) Transfer the microfilter to the acid tank. Repeat Step 2.

(6) Repeat Step 3.

(7) Repeat Step 4.

(8) Disconnect the feed tubing from the microfilter.

2.3.3 Flow reactor

In Chapter 6, a flow reactor (E-series, Vapourtec) was used for conducting continuous-flow reactions between the photocatalytic materials and the contaminants. Its schematic and photo are shown in **Figure 2.6** and **Figure 2.7**, respectively.

In general there are two ways to perform a chemical reaction. The first way is batch mode, *i.e.* the reaction takes place in a beaker or a flask. The second way is continuous-flow mode, *i.e.* the reagents are pumped through a tube and the reaction takes place inside the tube. Please note the different definitions of batch and continuous modes in filtration processes and in chemical reactions. The batch mode is suitable for small-scale reaction. But as the reaction scale goes up, it becomes increasingly difficult to control the experimental conditions, such as heating/cooling and light irradiation. Besides, performing large-scale reaction with hazardous reagents can be dangerous.

A flow reactor can overcome these problems. The continuous-flow reaction can be easily scaled up *via* increasing the reaction time rather than increasing the size of the flask. The reagents can be quickly heated or cooled inside the tube because of the high surface area

to volume ratio. It is also easier to stop a continuous-flow reaction since the amount of reagents in the tube at any one time is much smaller than in the flask. In the particular case of photocatalysis, light can more thoroughly penetrate through the tube than through bulk solution in the flask, leading to higher photocatalysis efficiency [193].
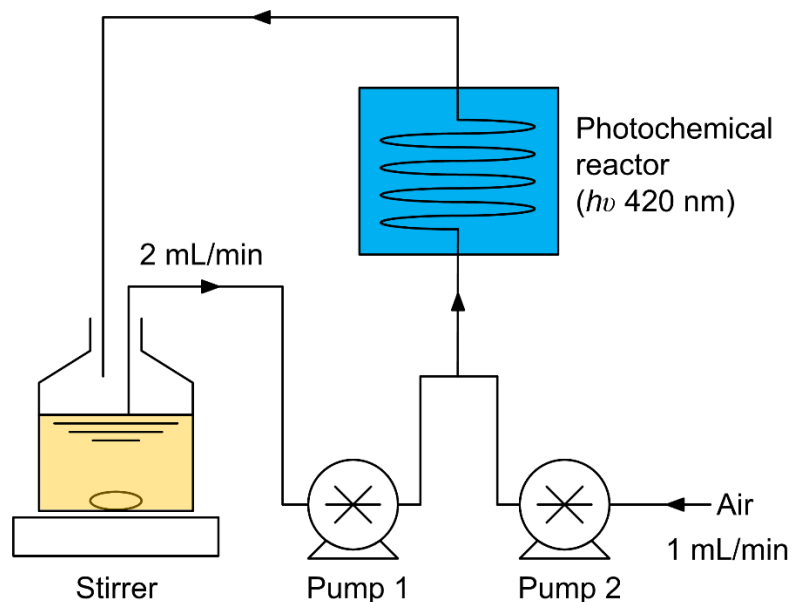
Figure 2.6: Schematic representation of the Vapourtec E-series flow reactor

The flow reactor used in Chapter 6 consisted of three main parts: a touchscreen interface, two peristaltic pumps, and a photochemical reactor (UV-150, Vapourtec). All control of the flow reactor was done *via* the touchscreen interface. Parameters including temperature, pressure, and flow rate were displayed on the interface. 20 mL solution and air were pumped into the system by two pumps. The flow rates of solution and air were fixed at 2 mL min^{-1} and 1 mL min^{-1}, respectively. The two streams were brought together using a T-piece before entering the photochemical reactor. The photochemical reactor was equipped with a LED lamp of 420 nm wavelength. The reactor was maintained at room temperature without heating or cooling, with negligible heating observed from the LED module. Sample aliquots of 1 mL were collected at constant time intervals for further analysis.
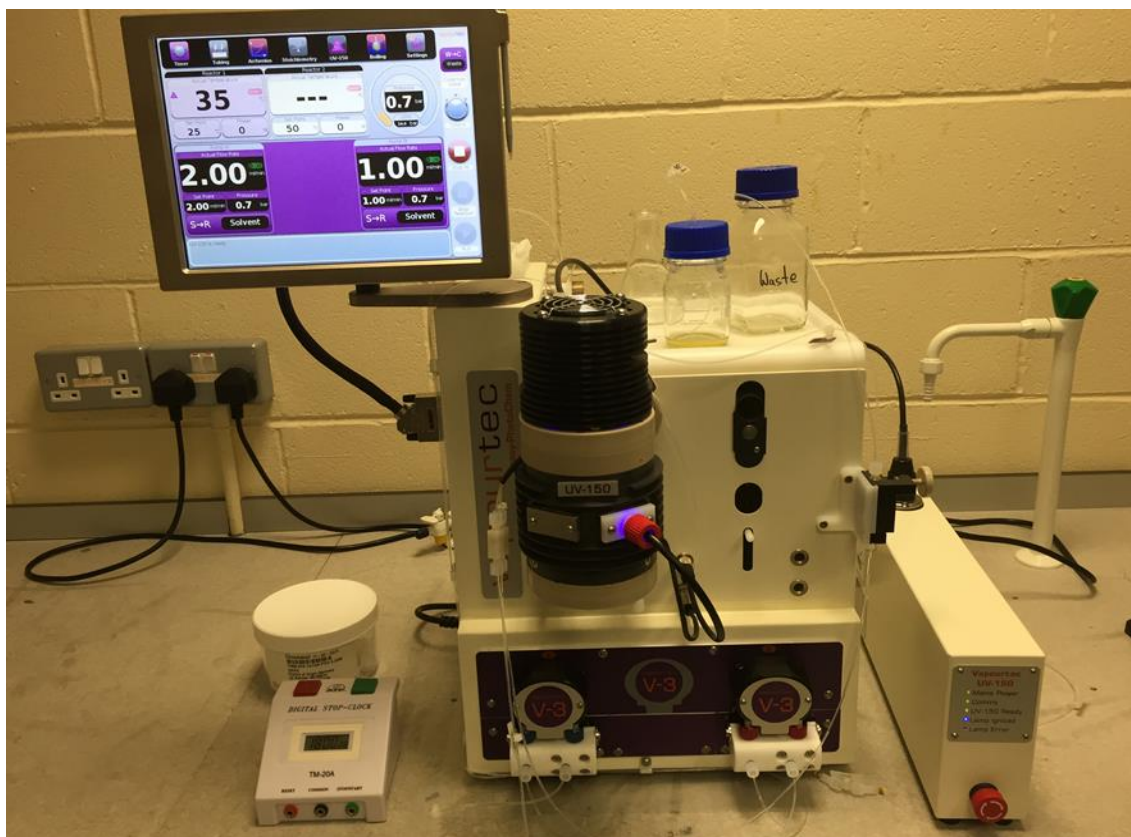
Figure 2.7: Photo of the flow reactor at HWU

2.4 Analytical methods

2.4.1 *Error analysis*

Uncertainty (δ) of directly-measured parameters (*e.g.* solute concentration, water flow and pressure) were taken to be the standard deviation of multiple measurements ($n \geq 5$). Uncertainty of indirectly-measured parameters (*e.g.* solute retention) was calculated using the error propagation equations:

If

$$f = f(a,\ b) \tag{3}$$

Then

$$\delta_f = \sqrt{\left(\frac{\partial f}{\partial a}\right)^2 (\delta a)^2 + \left(\frac{\partial f}{\partial b}\right)^2 (\delta b)^2} \tag{4}$$

where δ_f represents the uncertainty of the function f, δa and δb represent the uncertainty of variables a, b. $\frac{\partial f}{\partial a}$ and $\frac{\partial f}{\partial b}$ denote the partial derivatives of f with respect to the variables.

2.4.2   pH meter

The *pH* is a measure of acidity or basicity of a solution. By definition, it is the negative logarithm of the activity of hydrogen ion [194]. Solutions with a *pH* value lower than 7 are acidic and solutions with a *pH* value higher than 7 are basic. To measure the *pH* of a solution, two electrodes are needed, one is called the measuring electrode and the other is reference electrode. When submersed in solution, the measuring electrode (such as glass membrane electrode that is sensitive to hydrogen ion) determines the potential between a known liquid inside the electrode and an unknown liquid outside while the reference electrode maintains a constant potential and completes the electrical circuit. Modern *pH* meters usually have a combination electrode, which contains both the reference electrode and the measuring electrode in one body.

In Chapter 3 and 6, *pH* was measured by a combination *pH* electrode (InLab Science Pro) connected to a *pH* meter (FiveEasy, Mettler Toledo, Switzerland). In Chapter 4 and 5, *pH* was measured by a combination *pH* electrode connected to a *pH*/conductivity multimeter (WTW Multi 340i, Germany). The *pH* meters were calibrated with standard *pH* buffer solutions (*pH* 4, *pH* 7, and *pH* 9 at 25 °C) before use. Uncertainty of measurement is ± 1%.

2.4.3   Electrical conductivity meter

Electrical conductivity (EC) means the passage of an electrical current through a solution, which is proportional to the concentration of dissolved solids in the solution. EC is measured using a meter and a probe. The probe consists of two metal electrodes spaced on centimetre apart, thus the unit of EC is Siemens per cm, *e.g.* mS cm^{-1} or μS cm^{-1}. A constant voltage is applied between the two electrodes so that an electrical current flows through the solution. The current is then measured by the probe.

In Chapter 3, EC was measured by Peerless Autoanalyzer System at Scottish Water. In Chapter 4 and 5, EC was measured by WTW Multi 340i *pH*/conductivity multimeter with a conductivity electrode. The meter was calibrated with a standard EC solution (1413 μS cm^{-1} at 25 °C) before use. Uncertainty of measurement is $\pm$ 1%.

EC is often used for the estimation of total dissolved solids (TDS). The rule of thumb to convert EC (μS cm^{-1}) to TDS (mg L^{-1}) is to multiply the EC reading by a conversion factor. For the sodium chloride solution, the conversion factor is 0.51; for the sodium bicarbonate solution, the conversion factor is 0.97 [195]. Given the natural water quality in Tanzania, an intermediate value of 0.8 was used as the conversion factor.

2.4.4 *Fluoride ion selective electrode*

Various analytical methods are used for determining fluoride in water, including fluoride specific ion selective electrode (ISE) [196-198], ion chromatography [199], inductively coupled plasma-mass spectrometry (ICP-MS) [200], and spectrophotometry [201, 202]. The ISE method is the most widely used due to its simplicity and sensitivity [203]. This method utilizes a fluoride selective membrane (typically a lanthanum fluoride crystal) to measure the electrode potential which responds to fluoride activity in the solution. Fluoride activity is then related to the concentration of fluoride ions by the activity coefficient which is dependent on the total ionic strength of the solution [197].

The fluoride ISE method is affected by numerous interferences which may have different effects on the measurement. Major interferences include (1) polyvalent cations (*e.g.* Al^{3+}, Fe^{3+}, Ca^{2+}) and hydrogen ions (H^+) which readily form complexes with fluoride lowering the ISE response; (2) hydroxide ions (OH^-) which are of similar size to fluoride and consequently increase the ISE response; (3) total ionic strength and (4) temperature [197, 204, 205]. In order to eliminate interferences, a total ionic strength adjustment buffer (TISAB) solution is typically added into the samples. The TISAB solution contains three components: (1) a *pH* buffer (*e.g.* acetic acid-sodium acetate) to adjust the *pH* to an optimum value of 5.0–5.5; (2) a metal ion complexing reagent (*e.g.* CDTA or citric acid) to prevent fluoride from interacting with metal ions; and (3) a background electrolyte (*e.g.* NaCl or $NaNO_3$) which maintains constant ionic strength [204]. In addition, the samples and standards must be all measured at the same temperature.

In Chapter 3, fluoride concentration in the solutions was measured by a combined fluoride ISE connected to a *pH*/ion meter (SevenCompact *pH*/Ion S220, Mettler Toledo, Switzerland). In Chapter 4 and 5, fluoride concentration was determined by a fluoride ISE in conjunction with an Ag/AgCl reference electrode connected to a *pH* meter (826 *pH* Mobile Meter, Metrohm, UK). Both fluoride meters were calibrated using standard fluoride solutions. The TISAB solution used for the measurements consisted of 5.7% (by volume) glacial acetic acid, 4 g L^{-1} CDTA, 58 g L^{-1} NaCl and was adjusted to *pH* 5.0–5.5 by using 5 M NaOH. 5 mL sample was mixed with 5 mL TISAB solution before measurement. Every sample was measured three times and uncertainty of measurement is ± 1%.

2.4.5   Turbidity meter

Turbidity is the cloudiness of water caused by suspended particles that diminish the penetration of light [31]. Suspended particles can be inorganic (*e.g.* silica and lime), organic (NOM) or microorganisms (phytoplankton). A turbidity meter emits a known intensity of light through a sample and measures the scattered light by suspended particles. The results are shown in nephelometric turbidity units (NTU).

In Chapter 3, turbidity was measured by Peerless Autoanalyzer System at Scottish Water. In Chapter 4 and 5, turbidity was measured by a turbidity meter (TN 100, Eutech, USA). The turbidity meter was calibrated by a series of calibration standards (0.02, 20, 100, and 800 NTU). Uncertainty of measurement is ± 1%.

2.4.6   Total organic carbon analyzer

TOC in water comes from NOM as well as synthetic sources. Inorganic carbon (IC) in water includes carbonate, bicarbonate, and dissolved carbon dioxide (CO_2). Total carbon (TC) refers to all the carbon including TOC and IC. DOC refers to organic carbon remaining in the solution after filtration, typically using a 0.45 µm filter. There are two types of TOC measurement methods, one is the direct method and the other is the differential method [206]. In a direct method, the sample is firstly acidified to convert IC to CO_2 and subsequently purged or degassed to remove CO_2. Then TOC in the sample

can be determined. Because purging also removes purgeable organic carbon such as benzene, toluene and chloroform, TOC measured in this method is more accurately called non-purgeable organic carbon (NPOC). In the differential method, both TC and IC are determined separately and then TOC is calculated by subtracting IC from TC. TOC measured in this method may not be accurate when IC is close to TC (*i.e.* IC is much higher than TOC).

In Chapter 3, DOC was measured by Formacs HT combustion TOC analyzer (Skalar Analytical, The Netherlands) at Scottish Water. The sample was filtered through 0.45 µm cellulose acetate filter before DOC measurement. In Chapter 4 and 5, TOC, DOC and IC of water samples were measured by Sievers 900 Portable TOC analyzer (GE Analytical Instruments, USA) (**Figure 2.8**). This TOC analyzer worked primarily in the differential method. However, an inorganic carbon remover (ICR) unit was utilized when the water sample had extremely high IC. The schematic of the TOC analyzer is shown in **Figure 2.9**. A sample is introduced into the analyzed from either the autosampler or the vial port. 6 M phosphoric acid (H_3PO_4) is injected to the sample to reduce the *pH* to 2. If the ICR unit is turned on, the acidified sample then goes through the ICR where IC is removed by vacuum degasification. The sample is then mixed with 15% ammonium persulfate (($NH_4)_2S_2O_8$) for later oxidation of TC.

After that the sample is split into two streams. One stream is processed for TC measurement, and the other is for IC measurement. The TC stream enters an oxidation reactor where the sample is exposed to UV light. OH· radicals are formed by the photolysis of water and persulfate under UV irradiation. The produced OH· can completely oxidize TC into CO_2. Meanwhile the IC stream enters a delay coil which is designed to ensure that the TC and IC streams simultaneously reach the next module, where CO_2 is measured using a selective membrane-based conductometric detection technique [207]. Briefly, CO_2 passes through a gas-permeable membrane while other oxidation by-products are rejected by the membrane. CO_2 then react with water to form hydrogen and bicarbonate ions. The conductivity of hydrogen and bicarbonate ions is measured in the conductivity cell with temperature correction, and converted to CO_2 concentration. An ion exchange resin is used to remove bicarbonate ions after the conductivity measurement. After the CO_2 from the TC and IC streams are measured, the concentrations of TC and IC are known and TOC is calculated as the difference.

Uncertainty of measurement is $\pm$ 5% for TC and IC, and $\pm$ 7% for TOC. The detection limit for TOC is approximately 0.05 ppm.

Given that many natural water samples contained high IC (details see Chapter 4), each sample (even the NF/RO permeate samples) was analysed twice by the TOC analyzer, the first time with the ICR unit on for measuring TOC and the second time with the ICR unit off for measuring IC. Samples with extremely high IC or TOC concentrations were diluted with RO permeate before measurement. Concentration of bicarbonate and carbonate were calculated by Visual MINTEQ 3.0 software (KTH, Sweden) based on Bjerrum plot equations for carbonate system [208].

The TOC analyzer was calibrated at the factory and required recalibration only once per year. A regular verification of the calibration was performed every month. TOC calibration standards were potassium hydrogen phthalate (KHP) solutions (0.1, 1, 5, 10, 20 ppm) while IC calibration standards were Na_2CO_3 solutions (1, 5, 10, 20, 50, 100 ppm).

Figure 2.8: Photo of the TOC analyzer with the autosampler on its left side and the ICR unit on its right side
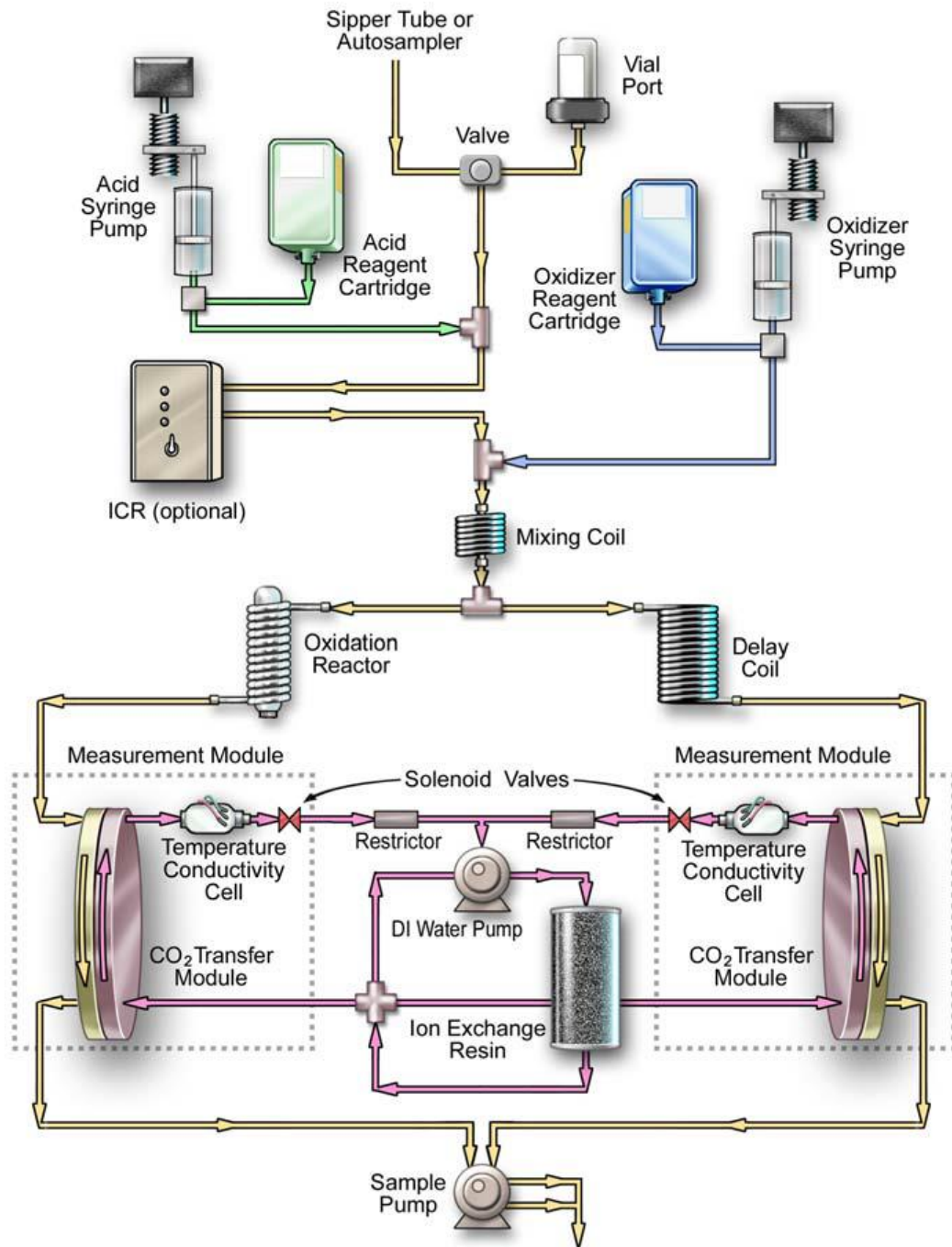
Figure 2.9: Schematic of the TOC analyzer with autosampler [207]

2.4.7 *Dynamic light scattering analyzer*

Dynamic light scattering (DLS) measures Brownian motion and relates the velocity of Brownian motion to the size of the particles [209]. The Z-average (intensity weighted) diameter (d) was calculated through the Stokes-Einstein equation assuming spherical particles [210]:

50

$$d = \frac{k_B T}{3\pi\eta D} \tag{5}$$

where k_B is the Boltzmann constant, T the temperature, η the viscosity and D the Z-average translation diffusion coefficient measured by DLS. The Z-average size is inadequate to describe the polymodal distribution of HS, because small particles can be hidden by larger particles [211]. Therefore, in this study, Z-average diameters were only used for comparative purposes.

The HS particle size was determined using a Zetasizer Nano ZS with a 633 nm He-Ne laser (Malvern Instrument, UK). It is necessary to use a red laser because HS can display fluorescence when excited by lower laser wavelengths [212]. All measurements were taken at 173 degree backscatter detection angle. Samples were kept in a disposable folded capillary cell during measurement (DTS 1070, Malvern Instrument, UK). The machine was calibrated with a particle size standard (polystyrene). For each sample, three replicate measurements were performed, each consisting of 15 runs.

The zeta potential (ζ) of HS was determined by the same Zetasizer Nano ZS instrument using laser Doppler electrophoresis (LDE) technique. The ζ data were calculated from the electrophoretic mobility (EM) using the Henry equation [213]:

$$EM = \frac{2\varepsilon\zeta}{3\eta} f(Ka) \tag{6}$$

where ε is the dielectric constant and $f(Ka)$ represents Henry's function. A value of 1.5 was used for $f(Ka)$ (Smoluchowski approximation) [214]. The instrument was checked by a zeta potential transfer standard with the zeta potential of -42 ± 4.2 mV. For each sample, three replicate measurements were performed and each measurement consisted of 100 runs.

2.4.8 *Ultraviolet-visible spectrophotometer*

When a molecule is exposed to ultraviolet or visible light having energy that matches a possible electronic transition, the molecule absorbs the light energy and one of its

51

electrons is promoted to a higher energy orbital. The degree of absorption at a certain wavelength is recorded by the Ultraviolet-visible (UV/Vis) spectrometer. Absorption can be presented as transmittance or absorbance spectrum. Molecules that absorb light strongly in the UV/Vis region are called chromophores.

In Chapter 4 and 5, UV absorbance of water samples was measured at 254 nm wavelength by UV-2800 spectrometer (UNICO, USA), with Mt Meru bottled water used as the blank. The sample was filtered through 0.45 µm cellulose acetate filter before UV measurements. Specific UV absorbance (SUVA) was calculated by dividing the UV absorbance at 254 nm by the DOC concentration. In Chapter 3 and 6, UV/Vis absorption spectra of both solutions and solids were obtained by Lambda 25 spectrometer (PerkinElmer, USA). A reflectance spectroscopy accessory (**Figure 2.10**) was used for measuring solid samples.

Figure 2.10: Photo of the reflectance spectroscopy accessory

2.4.9   *Fourier transform infrared spectrometer*

Fourier transform infrared (FT-IR) spectroscopy is a well-established technique to identify the presence of certain functional groups in a molecule [215]. While interaction

with UV/Vis light causes molecules to undergo electronic transitions, the lower energy infrared light causes molecules to undergo vibrational transitions. An IR spectrum shows the absorbance (or transmittance) peaks that correspond to the frequencies of vibrations. FT-IR obtains an IR spectrum by first collecting an interferogram of a sample using an interferometer, and then converting the raw data into the actual spectrum with a Fourier transform (a mathematical process).

In Chapter 3, the FT-IR spectra of HS samples were measured by Nicolet iS5 FT-IR spectrometer (Thermo Scientific, USA) coupled with iD1 transmission accessory. Pellets for FT-IR analysis were assembled from 10 mg of HS and 1000 mg of KBr. In Chapter 6, the FT-IR spectra of photocatalytic materials were measured using the same spectrometer but coupled with iD7 attenuated total reflectance (ATR) accessory. Each FT-IR spectrum had 128 scans with $2\,cm^{-1}$ resolution. Baseline correction was performed using the Omnic software.

2.4.10 Elemental analyzer

The carbon, hydrogen and nitrogen (CHN) contents in inorganic and organic compounds can be determined by combustion analysis, where a weighted sample is burned in pure oxygen under high temperature. The oxidized forms of these elements (CO_2, H_2O, NO or NO_2) are measured by a thermal conductivity detector in a succession of steps.

In Chapter 3, the CHN contents of HS were determined by elemental analyzer (CEC440, Control Equipment Corporation, UK). The oxygen level was determined as the difference from 100% on an ash-free and moisture-free basis. The ash content was determined by heating 30 mg of HS in an alumina crucible at 600 °C within a chamber furnace (Lenton, UK).

2.4.11 Inductively coupled plasma optical emission spectrometer

Inductively coupled plasma optical emission spectrometry (ICP-OES) is an analytical technique for the detection of trace-level elements [216]. The plasma is generated by the ionization of argon gas in an intense magnetic field. Samples are introduced into the plasma and the atoms of component elements become excited. When the excited atoms

return to ground state, emission rays are released and measured by OES. The type of element is identified by their characteristic emission rays (wavelength specific). The amount of each element is quantified by the ray's intensity.

In Chapter 3, sulfate and metal elements were measured by Optima 8300 ICP-OES (PerkinElmer, USA) at Scottish Water. In Chapter 4 and 5, metal and non-metallic elements were measured by Vista-PRO CCD Simultaneous ICP-OES (Varian, The Netherlands) at Karlsruhe Institute of Technology (KIT). The aqueous samples were filtered prior to analysis by using 0.45 µm membrane filers (cellulose acetate, 25 mm syringe filters) and acidified with HNO_3. Samples were diluted with water (Milli-Q, Millipore, Merck, Germany) according to the calibration range set for the different elements. The calibration was verified using ICP multi-element standard solution VI. Calibration was set from 10 to 2000 µg L^{-1} for B, Fe and Sr, from 20 to 5000 µg L^{-1} for Ca, K, Na, and Si, from 5 to 2000 µg L^{-1} for Mg, and from 5 to 1000 µg L^{-1} for Al and Zn. Uncertainty of measurement is ± 2% for each element.

2.4.12 Ion chromatography

Ion chromatography, as a form of liquid chromatography, measures concentrations of different ions based on their affinity to the ion exchanger [217]. When a sample solution is introduced into a sample loop, a buffered aqueous solution (the mobile phase) carries the sample from the loop to the column (the stationary phase) that contains resin or gel matrix with charged functional groups. The target ions (anions or cations) are retained by the oppositely-charged stationary phase, but can be eluted by increasing the concentration of another similarly-charged ion in the mobile phase. Different ion species have different retention times. The concentrations of eluted ions can be obtained by measuring conductivity or UV/Vis absorbance.

In Chapter 4 and 5, anions including chloride, sulfate, and nitrate were analyzed using an ion chromatograph equipped with a suppressor detection unit (IC 790, Metrohm, Germany). The mobile phase was 1 mM $NaHCO_3$ + 3.2 mM Na_2CO_3. Calibration was set to 0.1 to 10 mg L^{-1} or to 10 to 100 mg L^{-1} according to the need of the sample. Uncertainty of measurement is ± 2% for each anion.

2.4.13 High performance liquid chromatography

High performance liquid chromatography (HPLC) is a chromatographic technique used to separate, identify and quantify different components in a sample mixture. HPLC is distinguished from the traditional LC mainly because its operational pressures are significantly higher (50–350 bar). At high pressure, solvent containing the sample is forced through a column that is packed with a stationary phase composed of adsorbent materials [218]. Each component in the sample has different affinities towards the stationary phase. The stronger the affinity is, the slower the component travels through the column. A detector (*e.g.* UV/Vis, fluorescence, or photodiode array) detects each component eluting from the column and generates a signal proportional to the amount of the corresponding component.

In Chapter 6, quantitative analysis of FFA, BPA and cimetidine was performed using Shimadzu LC-20AD HPLC equipped with a C-18 column and SPD-20A UV/Vis detector. The mobile phase for FFA and cimetidine was 40% aqueous methanol, and that for BPA was 40% aqueous acetonitrile. For all target compounds, the analysis was carried out at a flow rate of 0.85 mL min^{-1} and a detection wavelength of 230 nm. Uncertainty of measurement is ± 2% for each compound.

2.4.14 Nuclear magnetic resonance spectrometer

Nuclear magnetic resonance (NMR) spectroscopy is an analytical technique used for determining molecular structure. Nuclear magnetic resonance is a property of the nucleus of an atom. All nuclei are charged and many nuclei have spin (such as nucleus of ^{1}H and ^{13}C). A charged and spinning nucleus generates a magnetic field. When an external magnetic field is applied, the nucleus aligns itself either with the field (lower energy) or against the field (higher energy). If radio waves are applied, nuclei in the lower energy absorb the energy and jump to the higher energy state. Then the nuclei relax back to the lower energy state while emitting electromagnetic signals. These signals can be detected and converted into the peaks in an NMR spectrum. The process that the nuclei flip back and forth between lower and higher energy states is called resonance [219].

In a molecule, nuclei that are not in the same structural situations do not experience the same external magnetic field because electrons around the nucleus shield them from the

field. Shielded and deshielded nuclei require different amounts of energy to bring them into resonance, which results in different peaks in the spectrum. As a result, information about the structure of the molecule can be derived from the NMR spectrum.

In Chapter 6, ^{1}H NMR spectra at 300.1 MHz and ^{13}C NMR spectra at 75.5 MHz were recorded on a Bruker AV-III300 spectrometer. The photosensitizer monomer was dissolved in $CDCl_3$ for ^{1}H NMR and ^{13}C NMR analysis. Solid-state ^{13}C NMR spectra of polymer at 100.6MHz were recorded at ambient temperature on a Bruker AVIII400 spectrometer equipped with a CPMAS probe.

2.4.15 Excystation assay

The excystation assay that determines the impact of photocatalytic polymers upon viability of *Cryptosporidium* was established by Robertson and Gjerde [220]. Briefly, samples were suspended in Hanks Buffered Salt Solution (HBSS) with 1% (w/v) trypsin and incubated at 37 °C for 1 hr. Samples were then centrifuged and the supernatant was discarded before 2.2% (w/v) sodium bicarbonate and 1% (w/v) sodium deoxycholate were added and samples were again incubated at 37 °C for 40 min. Viability of *Cryptosporidium* was assessed by counting the number of oocysts, sporozoites and number of empty shells by phase contrast microscopy, expressing the number of empty shells divided by number of oocysts and empty shells as a percentage and thus, a measure of excystation of the parasites.

Chapter 3: Interactions between Fluoride and Humic Substances

3.1   Introduction

Interactions between fluoride and HS in solution are important for understanding the behaviour and fate of fluoride in the environment and in the membrane filtration process. In Chapter 1, the nature of fluoride and HS was reviewed. It was concluded that the existing forms of fluoride and HS are heavily affected by water chemistry. Briefly, fluoride exists as hydrated and negatively charged ion in neutral and alkaline solutions, and transfers to uncharged hydrofluoric acid in acidic solution. HS are abundant of carboxylic and phenolic groups which dissociate at different *pH* values. In Chapter 1 several possible mechanisms accounting for fluoride-HS interactions were also discussed. Given its negative charge and hydration, the fluoride ion is unlikely to undergo chemical reaction or hydrogen bonding with HS. However, a previous study proposed a "territorial binding" concept where fluoride ions are physically trapped in the HS structure without undergoing chemical reaction or hydrogen bonding [72]. Unfortunately no other studies investigated "territorial binding" or reported similar phenomena.

The aim of the work presented in this first experimental chapter was to determine whether HS had a territorial effect on fluoride and if it had, what was the nature of such effect. Three assumptions were made in order to quantify such effect. Firstly, this territorial effect isolated a portion of fluoride from the bulk solution. In this context, the fluoride concentration measured in the bulk solution should vary. Secondly, this effect was considered to be temporary and reversible. Therefore, the occurrence of territorial effects could be represented by the variation of fluoride concentration. Thirdly, the degree of territorial effect was dependent on the configuration of HS structure. A large HS structure with enclosed configuration was expected to be favourable to this effect.

Based on the above assumptions, the approach of this chapter was to measure the variation of fluoride concentrations in the presence of HS. A fluoride ISE was used for measuring fluoride concentration due to its simplicity and accuracy. Parameters such as HS type, solution *pH*, and ionic strength were changed in order to create conditions for different HS structures. Dynamic light scattering (DLS) and laser Doppler electrophoresis (LDE) techniques were applied to characterize the size and charge properties of HS, respectively.

3.2   Experimental summary

This study did not attempt to extract HS from the natural water sample because the extraction and isolation procedures would greatly modify the properties of HS and may cause loss of certain fractions. In reporting measurements on natural water we took the view that HS should be kept in its natural state. HS from this natural water sample was denoted as NNHS (NN was short for Ngare Nanyuki). Overall, we studied HS samples from three different sources:

1.   Extracted HS from soil (AHA and PAHA)
2.   Extracted HS from an American river (SRHA)
3.   Unextracted HS from a Tanzanian river (NNHS)

By comparing results from these representative HS samples, we would gain a good overview on the behaviour of HS and the associated effects on fluoride.

Specific compositions of synthetic and natural solutions were listed in **Table 3.1**. For the *pH* experiments, the solution *pH* was adjusted to as low as *pH* 2. Although the *pH* of natural water is far from this value, some fluoride wastewater effluents can be highly acidic [15]. As a result, concentrations of fluoride and HS were measured over such a wide *pH* range.

Table 3.1: Summary of the compositions of synthetic and natural solutions for fluoride and HS measurement

Variable	Unit	Range	Condition	HS type
pH	–	2–12	Ionic strength: 20 or 100 mM F^-: 2 or 100 mg L^{-1} HS: 250 mg L^{-1}	AHA, PAHA, SRHA, NNHS
Ionic strength	mM	0–500	*pH*: 3 or 7 F^-: 2 or 100 mg L^{-1} HS: 250 mg L^{-1}	AHA, PAHA, SRHA, NNHS
Fluoride	mg L^{-1}	1–200	*pH*: 7 Ionic strength: 20 mM HS: 250 mg L^{-1}	AHA, PAHA
HS	mg L^{-1}	50–1000	*pH*: 7 Ionic strength: 20 mM F^-: 100 mg L^{-1}	AHA, PAHA

Once prepared, every solution was stirred at 350 rpm and room temperature for 24 hr. DLS and LDE measurements were conducted after 24 hr. Fluoride concentration was measured four times: (1) immediately after the solution was prepared; (2) after for 24 hr; (3) after 24 hr and then centrifuged at 10000 rpm for 1 hr; (4) after 24 hr and then filtered with 1 µm PTFE filter (Sartorius Stedim Biotech, Germany).

3.3 Characterization of HS and natural water

The commercial HS samples AHA, PAHA and SRHA were characterized by FT-IR and elemental analysis. FT-IR spectra are presented in **Figure 3.1**. Common absorbance bands for the three HS samples were observed at 3400 cm^{-1} (O−H stretching of carboxyl, phenol and alcohol), 2922 and 2880 cm^{-1} (aliphatic C−H stretching), 2334 cm^{-1} (CO_2), 1608 and 1378 cm^{-1} (COO$^-$ carboxylate stretching modes) [65, 221]. From AHA to PAHA, the intensity of carboxylate band at 1608 cm^{-1} was slightly decreased while the intensity of carboxylic band at 1718 cm^{-1} (C=O stretching) was significantly increased. This is expected since the carboxylate groups are protonated during purification [65]. Another noticeable increase of absorbance peak was at 1236 cm^{-1}, which was associated with a mixture of C−O stretching and C−O−H bending vibrations. Compared to SRHA, both AHA and PAHA showed absorbance bands centred around 3690−3620 cm^{-1} and 1000−1100 cm^{-1}. The former peaks correspond to absorption by aluminosilicates which are common in clays [222], while the latter are attributed to Si−O stretching of other silicate impurities [221]. The FT-IR spectra clearly show PAHA having an intermediate character between AHA and SRHA, though silicate impurities were not completely removed by purification.
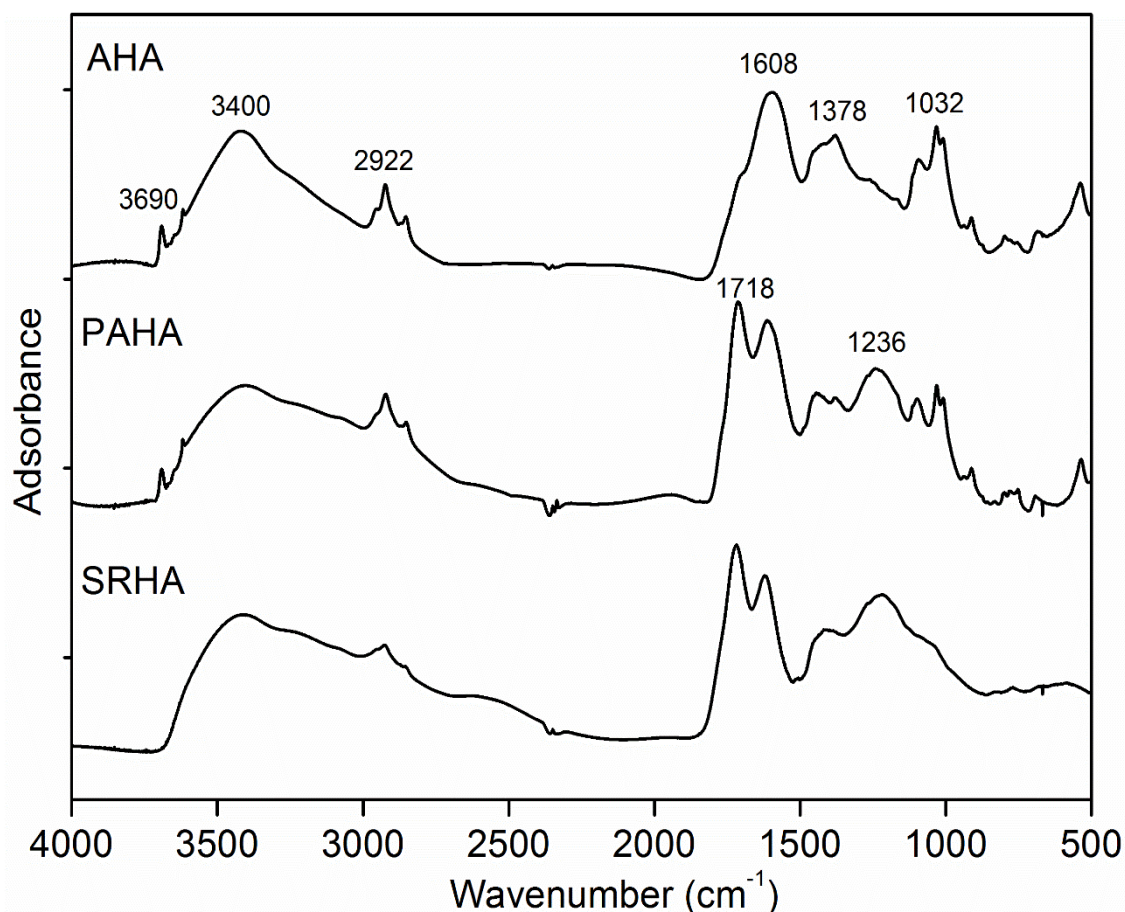
Figure 3.1: FT-IR spectra of AHA, PAHA and SRHA

As shown in **Table 3.2**, elemental analysis confirms that AHA has a very high ash content of more than 30%, which, as shown by the FT-IR spectra, can be attributed to the presence of silicate minerals. Previous studies demonstrated that AHA had highly variable ash contents from batch to batch, with a reported maximum of 31.21% [177]. After purification, the ash content was decreased to 9.60%, and this change was accompanied by an increase in the content of carbon, hydrogen, nitrogen and oxygen. SRHA, as the standard HS, had the lowest ash content and the highest content of major elements. It is believed that different origins (terrestrial and aquatic) as well as isolation and purification procedures contribute to the presence of different functional groups and affect the compositions of the three HS types. Furthermore, the availability of these HS samples makes it possible to study their behaviour as a function of HS composition and the corresponding effect on fluoride determination.

Table 3.2: Elemental analysis of AHA, PAHA and SRHA

	C (%)	**H (%)**	**N (%)**	**O (%)**	**Ash (%)**
AHA	41.51	3.08	0.68	24.37	30.36
PAHA	49.42	3.63	0.91	36.44	9.60
SRHA	52.63	4.28	1.17	42.04	1.04

Table 3.3 displays the major components of the natural water sample and shows that this sample was very alkaline and brackish. It had both high F^- concentration (53.8 mg L^{-1}) and high DOC value (196.5 mg L^{-1}) which was due to the local geology. The water was identified as sodium-bicarbonate (Na-HCO$_3$) type, which is a typical occurrence in East Africa [223]. The Na-HCO$_3$ water limits Ca^{2+} concentration by CaCO$_3$ precipitation, and consequently facilitates F^- accumulation as the insoluble CaF$_2$ is no longer a restricting factor [223]. On the other hand, the alkaline *pH* increases the dissolution of NOM from peat soils. SUVA values above 4 indicate the abundance of highly aromatic and hydrophobic HS in NOM [224]. The SUVA value of this natural water was 6.26, revealing that HS were the predominant NOM fractions. The unique water characteristics made this sample extremely interesting for our study.

Table 3.3: Water quality parameters in the natural sample collected in Tanzania

Parameter	Unit	Value
pH (20 °C)	–	8.57
Conductivity (20 °C)	$\mu S\ cm^{-1}$	3374
Turbidity	NTU	2.4
DOC	mg L^{-1}	196.5
SUVA	L mg^{-1} m^{-1}	6.26
F^-	mg L^{-1}	53.8
Cl^-	mg L^{-1}	199.0
HCO_3^-	mg L^{-1}	1666.1
SO_4^{2-}	mg L^{-1}	230.4
CO_3^{2-}	mg L^{-1}	33.9
Na^+	mg L^{-1}	885.5
K^+	mg L^{-1}	185.7
Ca^{2+}	mg L^{-1}	11.5
Mg^{2+}	mg L^{-1}	2.5

3.4   Effect of *pH*

As discussed in Chapter 1, HS are abundant of *pH*-dependent carboxylic and phenolic groups. Therefore the HS structure is expected to be affected by a change of solution *pH*. The size of HS was quantified as the Z-average diameter which was measured by DLS. Although the Z-average diameter cannot describe the polymodal distribution of HS, it is sufficient to represent the difference in relative sizes between HS molecules.

Figure 3.2A shows the dependence of Z-average diameter on *pH* in the presence of background electrolyte. At higher *pH* values (> 5), the Z-average diameters for both synthetic HS solutions and the natural water sample placed them in the colloidal range (1 nm to 1 µm) [225]. Specifically, the Z-average diameters for AHA were in the range of 221–238 (20 mM NaCl) and 255–293 nm (100 mM NaCl); for PAHA were 218–230 nm (20 mM NaCl) and 237–249 (100 mM NaCl); for SRHA were 192–220 (20 mM NaCl) and 226–239 (100 mM NaCl); and for NNHS values ranged from 111 to 128 nm. Given that small HS molecules (or basic units) are less than 10 nm [226, 227], our results indicate that HS exist in solution as association of small molecules, which agrees with the supramolecular model [51].

The size sequence among synthetic HS solutions was AHA > PAHA > SRHA. These results are in agreement with previous studies indicating that terrestrial HS are larger than their aquatic counterparts [228]. At similar *pH* values, Esfahani *et al.* [211] found values of Z-average diameter for AHA ranging from 263 to 332 nm, while Palmer and von Wandruszka [229] found a comparable diameter of 210–280 nm for SRHA. The Z-average diameters of NNHS were approximately 50% lower than those of synthetic HS solutions. These results must be interpreted with caution given that natural water contains both organic and inorganic colloids. Major inorganic colloids found in surface water include clays, oxides, silica, calcite and several other minerals [230]. Inorganic colloids are usually associated with and stabilized by NOM, particularly by HS [225, 230]. Therefore the measured Z-average diameters of NNHS include contributions from both inorganic and organic colloids which are difficult to separate from each other. In addition to inorganic colloids, the non-humic fractions of NOM also affect the Z-average diameter. These fractions, containing low molecular-weight acids and low molecular-weight neutral molecules, are much smaller in size compared to HS [21].

At lower *pH* values (< 5), all synthetic HS solutions exhibited a sharp rise in size (**Figure 3.2**A). The same trend was also observed for NNHS. At *pH* 2, the Z-average diameters of AHA (20 and 100 mM NaCl), PAHA (100 mM NaCl) and NNHS were beyond 1 µm, showing the formation of larger particles. Similar results were previously reported by other authors, though the extent of size increase varied from case to case, depending on HS origins, sample preparation, and characterization methods [46, 227, 231]. The increase in HS size under acidic conditions suggests aggregation of HS colloids. This is attributed to the attenuation of the negative charges through protonation and the consequent enhancement of intermolecular hydrogen bonds [49, 231]. The original colloidal states that were stabilized by hydrophobic dispersive forces and electrostatic repulsions are thus disrupted. At *pH* 2, HS aggregates grew progressively until precipitation was observed. At higher *pH* values, on the contrary, the dissociation of functional groups eliminated protons that were able to participate in hydrogen bonding, increasing intramolecular and intermolecular electrostatic repulsions [46, 56]. As a result, the aggregation process was hindered.

Some researchers reported a size increase at alkaline *pH* and attributed it to electrostatically-driven molecular expansion and swelling [232, 233]. In our study, no distinct size increase was observed under alkaline conditions. AHA and NNHS exhibited the highest size increase whereas SRHA displays negligible size change (particularly with 20 mM NaCl background).

Figure 3.2B shows a general trend towards increased (more negative) zeta potential with increasing *pH*. This is primarily due to dissociation of carboxylic groups (*pKa* = 0.2–6.2) under acidic conditions (the extremely low *pKa* values are associated with haloacetic acids such as trifluoroacetic acid) [42, 56]. The zeta potential of synthetic HS solutions (20 mM NaCl) increased further under alkaline conditions until to -60 mV, indicating the dissociation of phenolic groups (*pKa* = 4–10) [46, 56, 61]. However, the zeta potential values of HS solutions (100 mM NaCl) and NNHS remained relatively stable between -30 and -40 mV, regardless of increasing *pH*. This is likely due to the high ionic strength of the background electrolytes effectively shielding the increased surface charge from dissociation of functional groups.
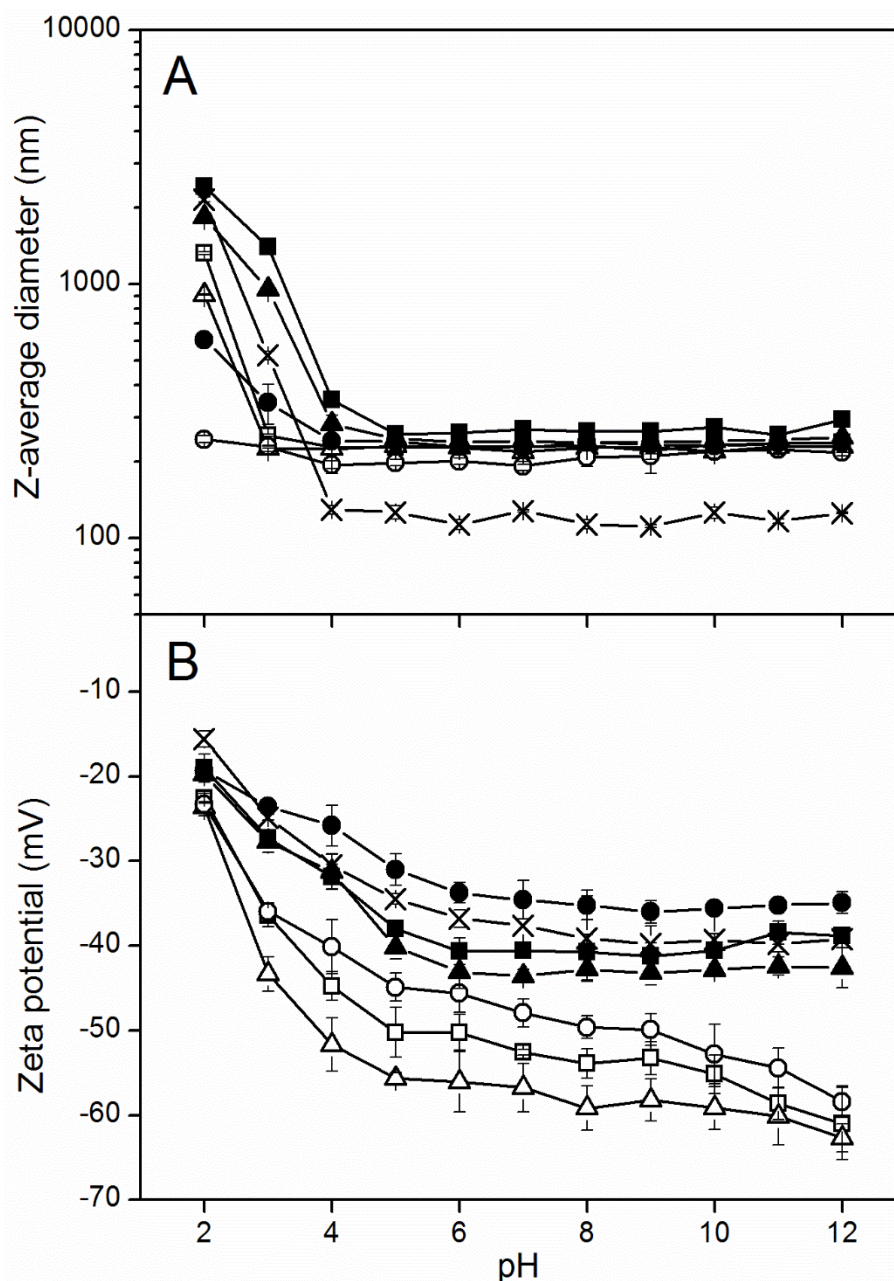
Figure 3.2: (A) Size and (B) zeta potential of AHA, PAHA, SRHA and NNHS as a function of *pH* with 20 mM NaCl (empty symbols) and 100 mM NaCl (full symbols) backgrounds (□/■ AHA, △/▲ PAHA, ○/● SRHA), NNHS symbolized as ×.

The zeta potential of a particle indicates its colloidal stability. The general dividing line between stable and unstable particles is at either +30 mV or −30 mV [234]. Our results suggest a clear dependence of HS size on colloidal stability. As shown in **Figure 3.2**, HS particles with zeta potential less negative than −30 mV had a strong tendency towards aggregation. As the zeta potential became increasingly negative, intermolecular electrostatic repulsions increased and the system became more stable and dispersed in solution [56].

3.5   Effect of ionic strength

The ionic strength of a solution significantly influences the charge properties of molecules. **Figure 3.3** shows that ionic strength affected the size of HS molecules but the effect differed from the one observed as a function of *pH*. To investigate the effect of ionic strength, solutions with *pH* fixed at either 7 or 3 were studied. For synthetic HS solutions, the Z-average diameters initially decreased with increasing ionic strength from 0 to 20 mM NaCl, and then rose continuously from 20 to 500 mM NaCl (**Figure 3.3**A). The size variations (both increase and decrease) were significantly greater at *pH* 3. The maximum Z-average diameters observed for each HS type were: 3211 nm (AHA), 2552 nm (PAHA), and 1916 nm (SRHA). For NNHS, however, the Z-average diameters remained in the narrow range of 114–119 nm regardless of ionic strength. The original ionic strength of NNHS, as calculated from electrical conductivity [235], was equal to 54 mM NaCl. It seems that the complex components of the natural water (*e.g.* carbonate species) minimized the influence of external NaCl on the size of HS.

The initial decrease in HS size was previously observed by Palmer and von Wandruszka [229] and Pinheiro *et al.* [231], and explained in terms of intramolecular contraction. Specifically, it was argued that the intramolecular electrostatic repulsions are screened by cations through charge neutralization, leading to a more compact HS configuration until a minimum size is reached [229]. The proposed charge screening effect by ionic strength is consistent with the decrease (less negative) of zeta potential observed in **Figure 3.3**B. However, further ionic strength increase results in intermolecular association and eventually aggregation, which were linked to intermolecular hydrophobic interactions [229]. The colloidal system is no longer electrically stable, as can be seen from **Figure 3.3**B. Wang *et al.* [61] reported that the aggregation rate of HS at high NaCl concentration fitted well with the DLCA regime within the DLVO theory since there was negligible repulsive force. They also reported that the divalent cation Mg^{2+} was far more effective than the monovalent cation Na^+ in enhancing the size of HS, which was attributed to the combined effects of charge repulsions, metal complexation and bridging [61, 226].
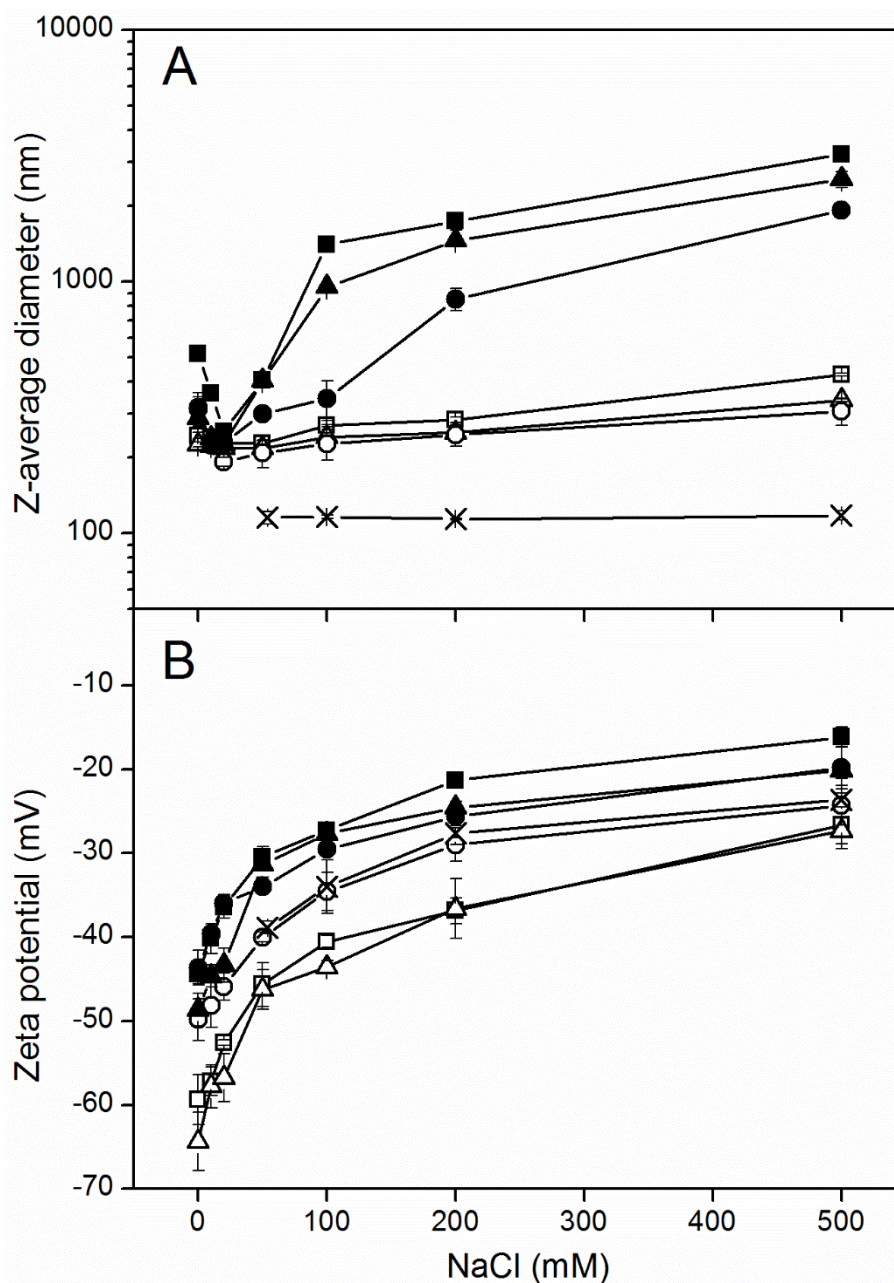
Figure 3.3: (A) Size and (B) zeta potential of AHA, PAHA, SRHA and NNHS as a function of ionic strength at *pH* = 7 (empty symbols) and *pH* = 3 (full symbols) (□/■ AHA, △/▲ PAHA, ○/● SRHA), NNHS symbolized as ✕.

3.6   Effect of fluoride and HS concentration

The effect of initial fluoride and HS concentration on HS structure was also investigated. AHA and PAHA were tested as they had a much higher tendency to aggregate than SRHA and NNHS. Given that acidic *pH* and high ionic strength promoted HS aggregation, the solution condition was set at *pH* 7 and 20 mM NaCl where the effect of *pH* and ionic

strength was negligible. The results are shown in **Figure 3.4** and **Figure 3.5,** for fluoride concentration and HS concentration, respectively.
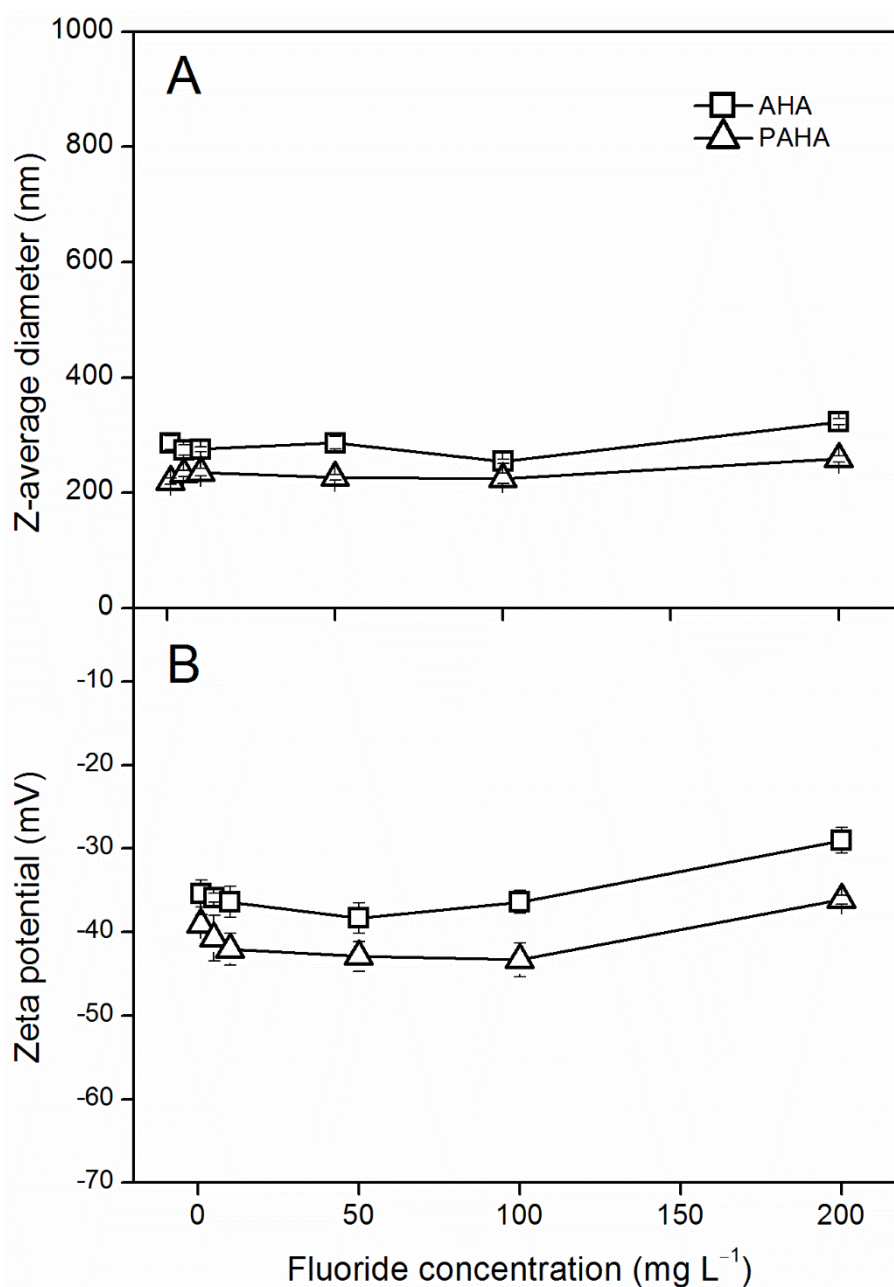
Figure 3.4: (A) Size and (B) zeta potential of AHA and PAHA as a function of fluoride concentration (250 mg L^{-1} HS, 20 mM NaCl, *pH* 7)

The Z-average diameters of HS were observed to vary within a narrow range (220–300 nm) by either increasing fluoride concentration from 1 to 200 mg L^{-1}, or changing HS concentration from 50 to 1000 mg L^{-1}. One should note that the slight increase of zeta potential with increasing fluoride concentration was due to the increase of ionic strength (**Figures 3.4**B and **3.5**B). These results indicate that fluoride and HS concentrations have

little effect on HS structure compared to *pH* and ionic strength. It is worth mentioning that at *pH* 3, an increase of HS concentration led to a drastic increase of HS size (data not shown), but this was attributed to the *pH* effect rather than the concentration effect.
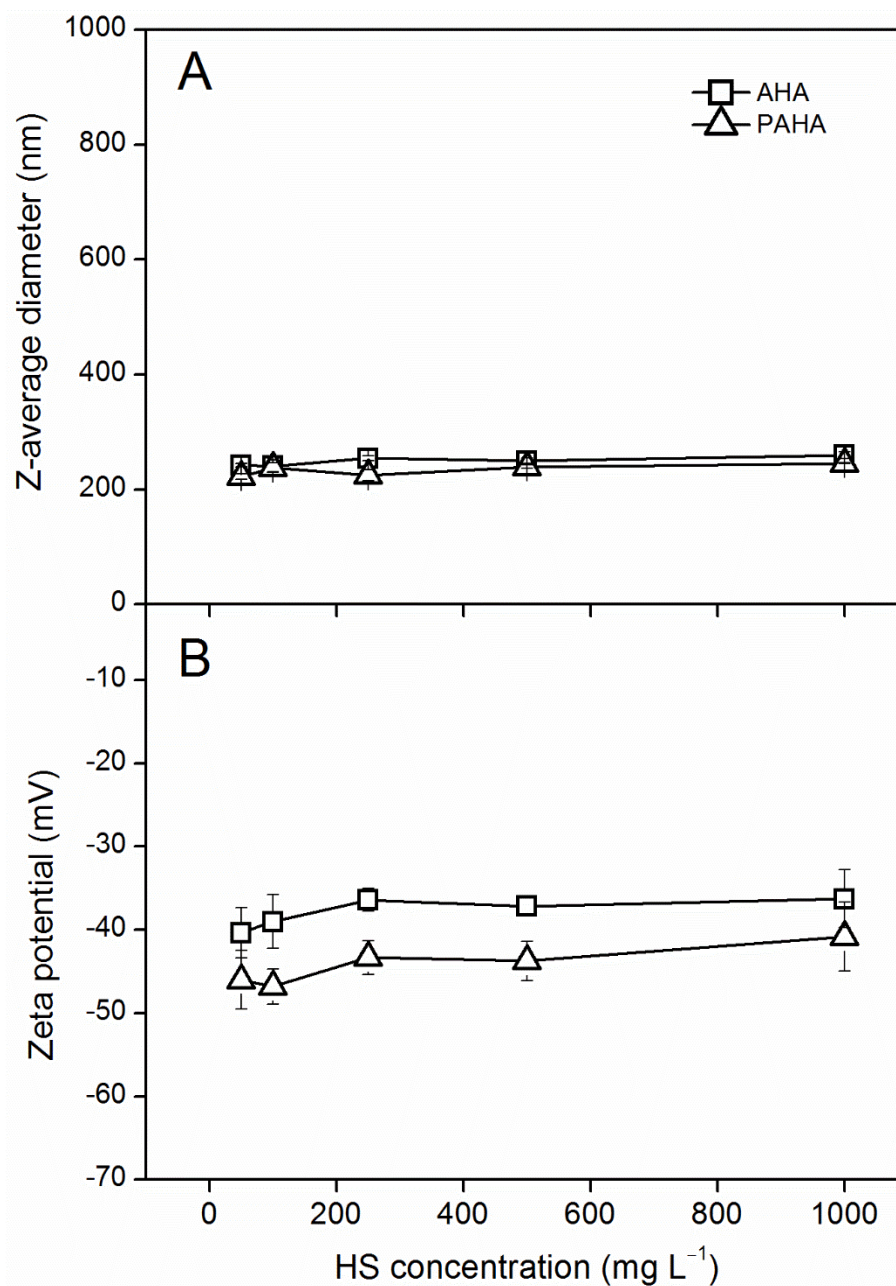
Figure 3.5: (A) Size and (B) zeta potential of AHA and PAHA as a function of HS concentration (100 mg L^{-1} F$^-$, 20 mM NaCl, *pH* 7)

3.7 Influence on fluoride measurement

After observing the change of HS structure under different conditions, the next step was to relate such change to the variation of fluoride concentration. **Figure 3.6** shows that a

clear relationship exists between the variation in fluoride concentration and HS size. For Z-average diameters of HS smaller than 300 nm, *i.e.* predominantly under high *pH* and low ionic strength conditions, the fluoride concentration measured after 24 hr was identical to its initial value. However, when the Z-average diameter exceeded 300 nm, the fluoride concentration after 24 hr was found to be lower than the initial value. As shown in **Figure 3.6**, the ratio of final and initial fluoride concentrations decreased almost linearly with increasing HS size. These results suggest that aggregation of HS colloids results in "apparent" values that differ from the expected fluoride concentration, causing an error in the measurements. At a fixed initial fluoride concentration, the ratios by different HS types followed the same trend, indicating that the type of HS was an insignificant factor.

When the initial fluoride concentration was 2 mg L^{-1}, the lowest fluoride concentration measured after 24 hr was 1.62 mg L^{-1}, in the presence of the largest AHA particles (Z-average diameter 3010 nm). This represents a 19% decrease with respect to the initial value (and corresponds to a 0.81 ratio in **Figure 3.6**). Given that the WHO guideline value for fluoride in drinking water is 1.5 mg L^{-1}, measurement errors of this magnitude need to be considered in water quality monitoring and the associated defluoridation practices. Remarkably, solutions with higher fluoride concentrations were less affected. For NNHS, with 54 mg L^{-1} F$^-$, the lowest ratio was 0.94 (corresponding Z-average diameter = 2154 nm); for 100 mg L^{-1} F$^-$ synthetic solutions, the lowest ratio further increased to 0.95 (which corresponds to a Z-average diameter of 3211 nm).

Based on the supramolecular model proposed by Piccolo [49], HS aggregation occurs as a result of intermolecular hydrogen bonds. One can imagine that fluoride ions may enter the internal structure of HS aggregates but not necessarily site bind to any functional groups. A new "open cage" concept was thus proposed to describe such spatial interaction between fluoride and HS. The "open cage" concept assumes that the heterogeneous HS system of aggregates has a cage-like framework with very weak internal electric field. Free ions move in and out of the framework, without the restriction of electrostatic attraction, site binding or territorial binding. The amount of fluoride ions retained by the framework is merely dependent on the size and conformation of the framework. For similar degrees of HS aggregation, the solution with lower fluoride concentration experiences higher fluoride retention, as shown in **Figure 3.6**. The "open

cage" concept differs from territorial binding since, in this case, the effect of electric field is minimum due to the protonation of acidic groups, while the latter was maintained by the overlapping electric field of spatially-distributed functional groups [71]. Previous studies reported that HS can immobilize hydrophobic molecules within its hydrophobic domains under acidic conditions [48, 236]. However, the temporary trapping of free ions such as fluoride was not been previously reported. Alternatively, one could argue that organic molecules could first bind cations and then attract anions *via* cation−anion interactions [77]. However, in this study, potential interactions between fluoride and cations were eliminated by the use of TISAB solution.
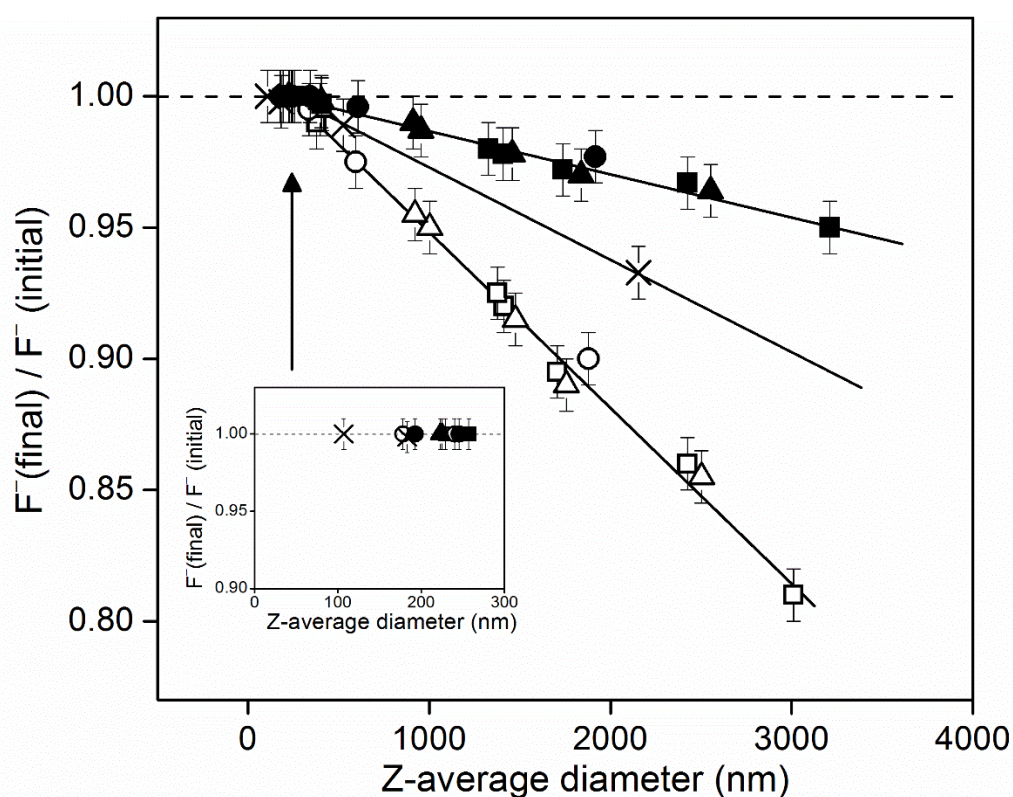
Figure 3.6: Fluoride measurement error in 2 mg L^{-1} F^{-} (empty symbols) and 100 mg L^{-1} F^{-} (full symbols) solutions as a function of HS size ($\square$/$\blacksquare$ AHA, $\triangle$/$\blacktriangle$ PAHA, $\bigcirc$/$\bullet$ SRHA, NNHS symbolized as $\times$, the solid lines are guides to the eye)

3.8   Effect of pretreatment methods

The effect of two sample pretreatment methods, centrifugation and membrane filtration, were investigated to establish whether these could affect the fluoride measurements. As **Figure 3.7** shows, after centrifugation, solutions with severe HS aggregation are clear with HS aggregates present as sediment in the solid residue. The fluoride concentrations

after centrifugation were found to be identical to the initial values, showing a 100% recovery. It is believed that during the centrifugation process, fluoride ions are released from the HS structure and free to enter the supernatant solution. These results demonstrate the reversibility of the proposed "open cage" model.
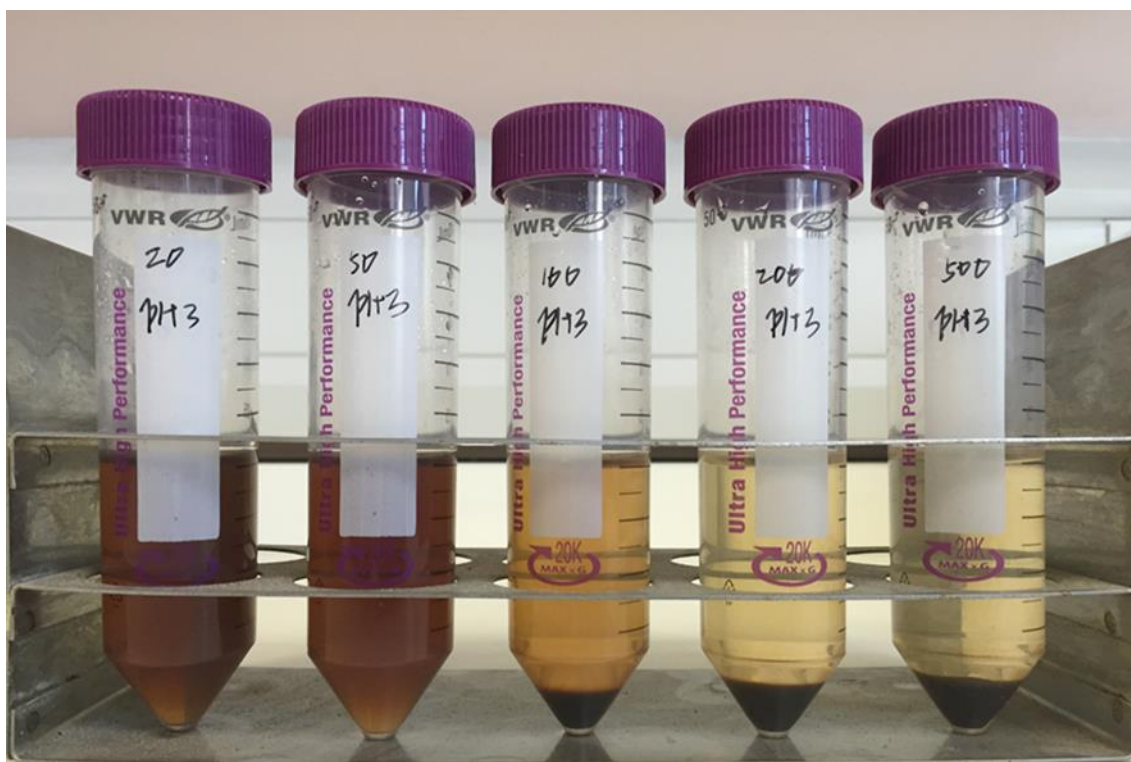
Figure 3.7: PAHA solutions (*pH* 3) after centrifugation. Ionic strength increased from 20 mM to 500 mM from left to right as indicated on the bottle labels

HS solutions were also filtered. The membrane material used for the filtration process was PTFE and the pore size was 1 μm. Each syringe filter was used only once. Because the size of HS aggregates could reach up to several μm, the filters were easily fouled after filtration (**Figure 3.8**). The fluoride concentration measured after filtration was even lower than before (data not shown). This is because HS aggregates of various sizes readily cause membrane fouling by pore blocking (small molecules) and cake deposition (large particles) [147]. As a result fluoride ions cannot permeate the fouled membrane due to size exclusion [103]. The effects of HS on fluoride under different conditions (*i.e.* in solution, centrifugation and filtration) are illustrated in **Figure 3.9.** In the absence of HS aggregation, both centrifugation and filtration had no effect on fluoride measurements.

Figure 3.8: Comparison between a new, unused filter and the HS-fouled filter after filtration.
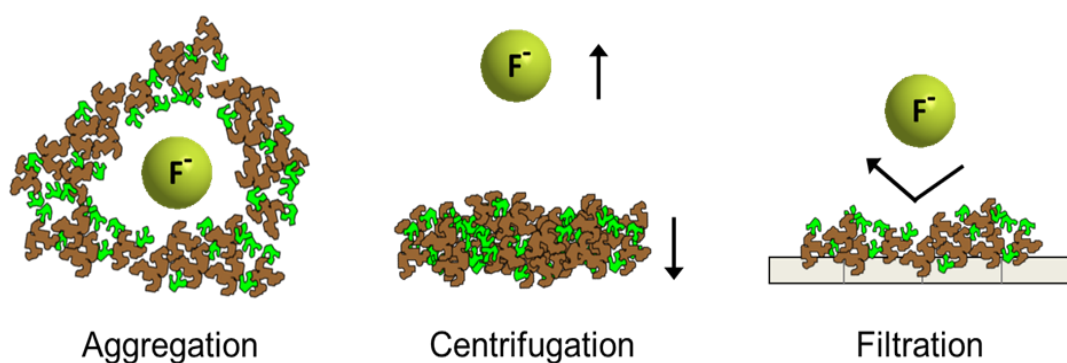
Figure 3.9: Schematic showing the effect of HS on fluoride

3.9 Conclusions

In this chapter, a study of the territorial effect of HS on measurements of fluoride concentration was carried out to establish a relationship between HS structure and fluoride ISE measurements. The size and zeta potential results show that the extent of HS aggregation was dependent on HS sources (*e.g.* terrestrial or aquatic) and water environment (*e.g. pH* and ionic strength). The extent of HS aggregation under variable

pH and ionic strength conditions can be explained by using the supramolecular model. At a fixed ionic strength, lower *pH* values promote HS aggregation due to protonation of functional groups and development of intermolecular hydrogen bonds. At a fixed *pH*, increased ionic strength facilitates HS aggregation by neutralizing surface charges and inducing intramolecular contraction and intermolecular associations.

The fluoride concentration measured by ISE was found to decrease in the presence of HS aggregation. In the worst scenario, the fluoride concentration was 19% lower than its initial value. This phenomenon was explained by adopting an "open cage" concept in which fluoride ions are temporarily trapped in the framework of HS aggregates. The "open cage" concept has features of reversibility.

The results presented in this chapter also highlighted the importance of pretreatment in fluoride ISE measurements for water samples. Centrifugation proved to be effective in separating fluoride ions from the HS aggregates. Future research is needed to characterize the internal structure of these HS aggregates, and to determine the effect of HS aggregation on other anions.

Chapter 4: Removal of Fluoride and NOM by Nanofiltration/Reverse Osmosis

4.1 Introduction

As mentioned in Chapter 1, high fluoride concentrations in drinking water are known to cause severe health risks to humans [12, 16]. WHO recommends a guideline value of fluoride to be 1.5 mg L^{-1} at which the harmful effect should be minimal. However, drinking water with fluoride concentrations above the guideline value is consumed by more than 200 million people in over 20 developed and developing countries [10, 12]. In the East African Rift Valley which is a naturally high fluoride zone, over 80 million people exhibit varying degrees of fluorosis symptoms [11, 237]. Tanzania, located in east Africa, is projected to face serious water stress (defined as average water resources below 1500 m^3 per capita per year) by 2025 due to population growth [238]. The increased fluoride guideline of 4 mg L^{-1} in Tanzania reflects the difficult situation of water quality that is worsened by water scarcity [239].

NF and RO are very promising defluoridation methods due to their high fluoride retention compared to conventional methods such as adsorption and precipitation [81]. In NF/RO processes, fluoride transport through the membrane consists of three mechanisms: diffusion, convention, and electromigration [84, 106, 240]. Fluoride retention by NF/RO is generally governed by steric (size exclusion) and electrical effects (charge repulsion, Donnan exclusion and dielectric exclusion) [103]. A variety of parameters, including feed compositions, membrane characteristics and operational conditions, lead conditions to be more conducive to one mechanism over the other [103, 104, 241, 242].

The simultaneous occurrence of fluoride and NOM in natural waters, as those commonly found in Tanzania, sets a significant challenge for water engineers. NOM has been found to compete with fluoride ions in adsorptive processes, particularly adsorption onto activated carbon [243] and bone char [244]. Chapter 3 studied the potential interaction between fluoride and HS. The results showed that fluoride ions can be sterically trapped in the structure of HS aggregates. However, the importance of NOM in fluoride removal by NF/RO processes is not understood to date.

The aim of the work presented in this chapter was to fill this knowledge gap. This was achieved by treating a number of natural water samples containing of both high fluoride and NOM content with a selection of NF/RO membranes. The effect of NOM and other parameters on fluoride retention by NF/RO were investigated systematically by (1) examining the chemical composition of high fluoride waters in Tanzania; (2) determining the mechanisms by which fluoride and tropical NOM are removed by NF/RO, and (3) exploring the impact of NOM on fluoride removal by NF/RO.

The experimental work reported in this chapter was conducted during a field trip in Tanzania. University of Dar es Salaam (UDSM) hosted the PhD candidate from November 2012 to April 2013, and Nelson Mandela African Institution of Science and Technology (NM-AIST) hosted the PhD candidate from May 2013 to April 2014.

4.2 Experimental summary

4.2.1 Water sampling

The northern regions of Tanzania, which are part of the major East African Rift system, have the most extensive areas of fluoride-rich waters and possibly the highest reported fluoride concentrations in the world. For this reason this area was identified as an excellent choice for this study. In order to assess local water quality, and therefore choose the most interesting water samples for membrane filtration, samples were collected from surface water (rivers, springs, freshwater lakes), groundwater (boreholes and wells), and soda lakes. Soda lakes are not suitable for drinking water applications, but were studied as an important part of the local geology and the local water cycle.

The sampling work was conducted by Professor Andrea Schäfer, Professor Bryce Richards and the PhD candidate with help from local guides. There were in total 166 natural water samples being collected from 120 sites over 16 months, including 105 surface water samples, 45 groundwater samples, and 16 soda lake samples. The precise location of sites was determined in the field using a hand-held GPS device (Garmin GPSmap 60csx, USA). The sampling sites are shown in **Figure 4.1**. Some photos taken during water sampling are shown in **Figure 4.2**. The sites were selected in a manner

aimed to identify the variation of water quality over different water types with the overall aim to identify worst case water supply scenarios and subsequent treatment challenges.
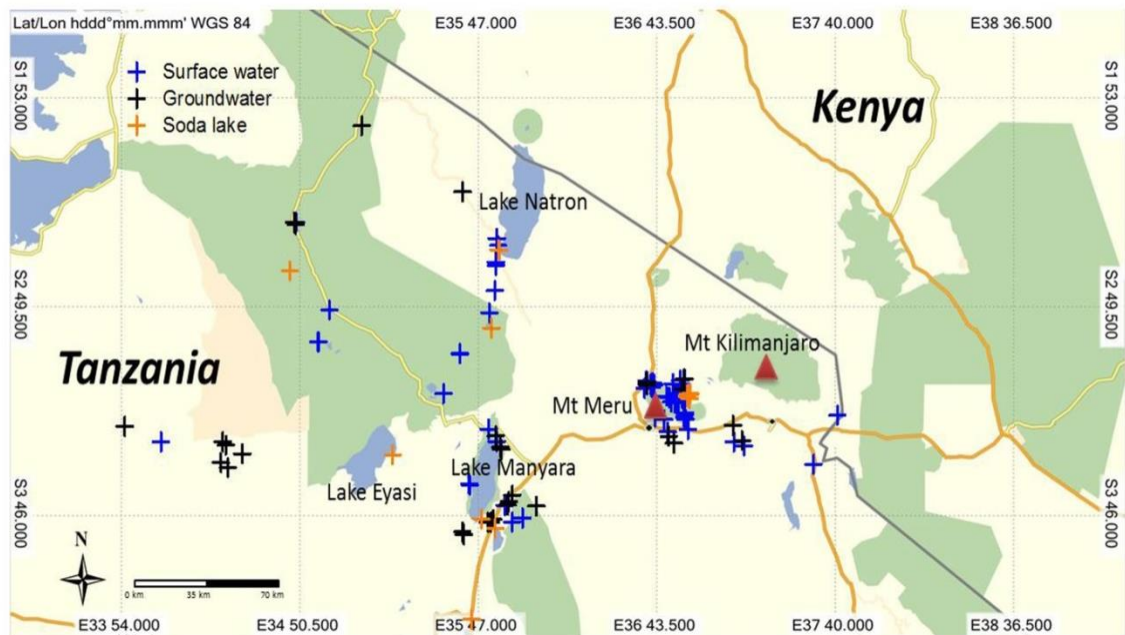
Figure 4.1: Map of northern Tanzania with sampling sites (adapted from Tracks4Africa)

Before detecting any contaminant in the samples, some safety risks at the sampling sites were identified. Most boreholes were lacking protection covers, posing a high risk of falling down when collecting water. Moreover, the water quality of the unprotected source was easily affected by rainfall and contaminated by animals. One extreme sample was an open water tank in a remote community. People collected water for cooking and drinking from the inner tank while livestock could reach water from the edge (which was lower). Inner and outer were connected directly. Such unprotected (but possibly classified as 'improved') water sources were inevitably contaminated by microbiological contaminants (bacteria, viruses) from animal excreta. In some protected facilities, such as the hand pump of borehole and the tap of standpipe, flying insects like bees became a major source of contamination as they preferred to live near the water outlet. In order to investigate the original water quality, the effects of such terminal contamination are undesirable and should be avoided to the greatest extent. Samples were collected in 5 L or 12 L plastic containers (washed thoroughly with the sample water prior to collection) and stored at 20 °C in the laboratory at UDSM or at room temperature in the laboratory at NM-AIST (**Figure 4.3**). Parameter including fluoride, *pH*, EC, turbidity, TOC, IC, and

SUVA were measured at UDSM or NM-AIST. Then the samples were shipped to KIT for ICP-OES and ion chromatography analysis.

Figure 4.2: Photos taken during water sampling: (top left) collecting water from a fast river; (top right) sampling from a well secured hand pump; (bottom left) uncapped well with high risk of drowning; (bottom middle) sampling from a black water; (bottom right) cows drinking water near a hand pump

Figure 4.3: Water samples stored in the laboratory at NM-AIST

4.2.2   Filtration protocol

Bench-scale filtration experiments were conducted using a stainless steel stirred cell. Although 166 water samples were collected, only 22 samples were treated in NF/RO experiments.   The selection criteria included: (1) fluoride concentration above WHO guideline of 1.5 mg L^{-1}; (2) osmotic pressure lower than the applied pressure of 10 bar; (3) representative samples (*e.g.* black water). Osmotic pressure was calculated from ionic concentrations using the van't Hoff formula [245].

$$\pi = \sum C_i \, RT \tag{7}$$

where π is the osmotic pressure (bar), C_i is concentration of each solute (mol L^{-1}), R is the universal gas constant (0.083145 L bar mol^{-1} K^{-1}), and T is the absolute temperature (K). Only solutes with concentrations >1 mg L^{-1} were taken account in the calculation.

Prior to each experiment, a new membrane was rinsed with clean water and then compacted for one hour at 10 bar. Pure water flux was subsequently determined at 10 bar for 30 min. For each batch experiment, the feed solution volume was 400 mL. Eight consecutive permeate samples (25 mL each for a total filtrate of 200 mL) were collected.

After the experiment, the pure water flux was measured again as an indicator for membrane fouling.

Some key terms used for the analysis of the experimental are defined below. Recovery is defined as the ratio of permeate to feed volume. Maximum recovery in these bench-scale experiments was set at 50%, which is within the practical range of full-scale systems (30–90%) [246]. Retention is the percentage of solute removed from the feed and to calculate retention in the stirred cell the retentate concentration (C_R) is required. C_R was calculated as a function of permeate volume from mass balance, where:

$$C_R = \frac{C_F V_F - \sum C_{Pi} V_{Pi}}{V_R} \tag{8}$$

where C_F and C_{Pi} are the initial feed and permeate concentrations of the solute of interest (mg L^{-1}), V_F and V_{Pi} are the feed and permeate volume (mL), while V_R is the retentate volume remaining in the cell (mL). The observed retention (R) was thus calculated as below:

$$R = \left(1 - \frac{C_{Pi}}{C_R}\right) \times 100\% \tag{9}$$

and was not corrected for real retention based on boundary layer concentration [247].

4.3 Drinking water guidelines

Before assessing natural water quality in Tanzania, the guidelines of various water quality parameters made by different authorities were carefully reviewed. According to WHO, the fluoride concentration in drinking water should not exceed 1.5 mg L^{-1} [12]. The same is true for EU Drinking water guidelines [248, 249]. High fluoride concentrations above 1.5 mg L^{-1} may cause dental fluorosis (1.5–4 mg L^{-1}), skeletal fluorosis (4–10 mg L^{-1}) and crippling fluorosis (>10 mg L^{-1}) [12]. The guideline value is based on an average per capita daily water consumption of 2 liters. For countries with a hot and dry climate, the daily intake of water is much higher than the WHO proposed level. For this reason, Brouwer *et al.* [250] suggested that fluoride levels in Senegal should be below 0.6 mg L^{-1} in order to prevent the mildest form of dental fluorosis. In contrast, other countries, such

as Ethiopia [251] and Tanzania [239], have other types of fluoride guidelines set on the basis of economical, practical and technical considerations. Tanzania has temporarily allowed consumption of drinking water with fluoride concentrations up to 8 mg L^{-1} in areas with no alternative water sources within acceptable walking distances [252]. This value has been reduced to 4 mg L^{-1} in 2008 [239], as a result of raising public awareness on fluoride issues and the development of defluoridation methods that promise alleviation of the problem such as bone char filters [253].

Although *pH* usually has no direct impact on human health, it is one of the most important parameters for water quality. WHO recommends *pH* of 6.5–8.5, based on aesthetic considerations such as taste and colour and corrosion of materials (metals and cement based materials) [254]. Exposure to *pH* values greater than 11 results in eye irritation and exacerbation of skin disorders. In addition, waters with *pH* 10–12.5 have been reported to cause hair fibers to swell [255].

There is no health-based guideline value set for EC but it is an indicator parameter in the drinking water ordinance (EU: 2500 µS cm^{-1} at 20°C [248], Germany: 2790 µS cm^{-1} at 25°C [249]). Typically drinking water has a conductivity of 50–500 µS cm^{-1}, while seawater EC is about 50 mS cm^{-1}.

Turbidity can be initially noticed by the naked eye above approximately 4.0 NTU. However, to ensure effectiveness of disinfection, turbidity should be no more than 1 NTU and preferably much lower [254].

TOC is used to quantify NOM which has been emphasized as the precursor to disinfection by-products including THMs [256]. United States Environmental Protection Agency (USEPA) indicates that water with TOC above 2 mg L^{-1} requires treatment to avoid THMs formation [257] and, as a consequence, this is a target value for this case study as chlorination is often performed in an uncontrolled manner in Tanzania [258]. Environmental Protection Agency Ireland [224] reports that THM formation can occur at TOC >2.0 mg L^{-1}, and THM levels will likely exceed 100 µg L^{-1} at TOC >4.0 mg L^{-1}. In the European guideline for drinking water, TOC is related to the indicator parameters, and it should not show abnormal change. The parameter oxidisability should not exceed 5 mg L^{-1} O_2. This parameter need not be measured if the TOC is analyzed [248].

SUVA provides a measure of the aromaticity and hydrophobicity of NOM and hence the potential to form THMs [256, 259]. SUVA values lower than 2 represent a high fraction of non-humic, non-hydrophobic NOM with low UV absorbance, which has low THM formation potential. SUVA values between 2 and 4 indicate a mixture of hydrophobic humic and hydrophilic non-humic NOM. SUVA values above 4 are indicative of the presence of highly aromatic, hydrophobic, and humic NOM with a high THM formation potential [224].

In order to evaluate water quality in Tanzania, a classification scheme was proposed, applicable within Tanzanian context (**Table 4.1**). The concept of the classification scheme for water quality was firstly raised by Sargaonkar and Deshpande [260]. The Tanzanian scheme was based on the above mentioned drinking water guidelines. Parameters including turbidity, EC, fluoride, TOC and specific UV SUVA were considered as important indicators for this scheme.

Table 4.1: Proposed water classification in Tanzanian context

Parameter	Excellent	Acceptable	Slightly contaminated	Moderately contaminated	Heavily contaminated
pH	6.5–8.5	8.5–9.5	9.5–10.5	10.5–12.5	>12.5
Turbidity (NTU)	<0.5	0.5–2	2–4	4–10	>10
EC (μS cm^{-1})	<500	500–1000	1000–2500	2500–10000	>10000
F$^-$ (mg L^{-1})	<0.5	0.5–1.5	1.5–4	4–10	>10
TOC (mg L^{-1})	<1	1–2	2–4	4–10	>10
SUVA	<0.5	0.5–1	1–2	2–4	>4

4.4   Water quality assessment

By comparing the water quality datasheet in the Appendix with the classification scheme proposed above, an overall picture of Tanzanian water quality was obtained. **Figure 4.4** summarizes the contamination levels of 166 natural water samples. Among the five water quality indicators, fluoride and NOM were found to be largely responsible for most of the heavy contamination.
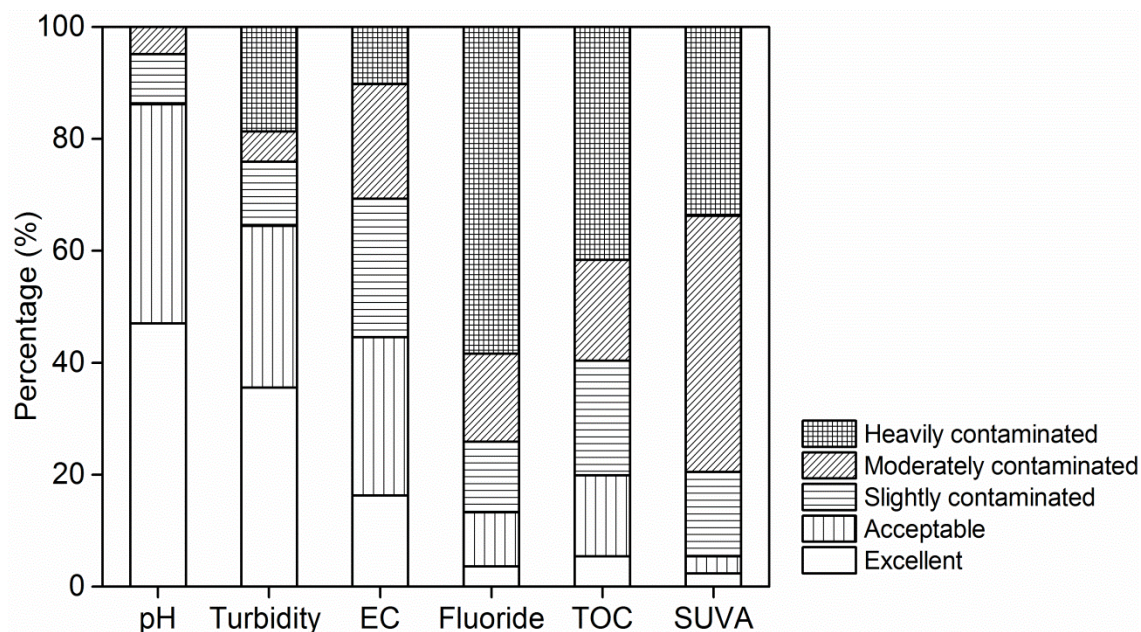
Figure 4.4: Percentage of contamination levels in 166 Tanzanian samples

In terms of fluoride concentration, the majority of samples (86%) contained fluoride exceeding the WHO guideline (1.5 mg L^{-1}), whereas 74% were above the Tanzanian guideline (4 mg L^{-1}). Soda lakes had much higher fluoride concentrations than surface water and groundwater, with the highest occurring in S82 (Lake Big Momella, 1391 mg L^{-1}). Fluoride concentrations up to 88 mg L^{-1} were observed in a surface river (S129, Pagasi River) which was flowing into Lake Natron. As for groundwater, the highest fluoride concentration (62 mg L^{-1}) was found for S54 (Mdori Borehole) which was a borehole near Lake Manyara. Fluorides are naturally released into water by the dissolution of fluoride-containing rocks and soils [7]. The volcanic rocks of East Africa are richer in fluoride than analogous rocks in other parts of the world [261]. The dissolution process is affected by various factors including rock composition, groundwater age, residence time, and pathway conditions [8].

The TOC results suggest that NOM existed as a major component in some of the Tanzanian waters. SUVA results indicate that HS were the dominant NOM fractions in these samples. Over 80% of the water samples have NOM concentrations exceeding the EPA guideline (2 mg L^{-1} TOC). In some cases very high concentrations were observed, for example up to 260 mg L^{-1} in S147 (Ngare Nanyuki Swamp, which means "red water" in Masai) and 35 mg L^{-1} in S40 (Maji ya Chai River, which means "tea river" in Swahili). Such tropical black water owes the black colour to NOM. This was also reported elsewhere, for example, in the Siak river in Indonesia [262] and the Rio Negro in Brazil

[263]. However, for some alkaline soda lakes, it was claimed that ferrous sulfide is the major reason for the blackness and the abundance of NOM whilst relatively high temperatures account for the high rate of sulfide production [264]. Excessive iron and sulfate concentrations were also found in some samples collected during this study (see the Appendices).

Contamination related to *pH*, turbidity and EC is also noticeable, though not as significant as fluoride and TOC. According to the classification scheme, 14% of the samples have unacceptable *pH*, 36% of the samples have undesirable turbidity, and 55% of them have excessive EC.

Cation and anion data from ICP-OES and ion chromatography shed light on the chemical composition of the samples. Major cations were Na^+, K^+, Ca^{2+}, and Mg^{2+}. Major anions were Cl^-, HCO_3^-, and SO_4^{2-}. A ternary diagram was constructed to summarise data based on the major cations and anions of 166 water samples (**Figure 4.5**). Analysis of the ternary diagram identifies a unique bicarbonate-alkaline water type for most samples, especially for surface water samples. Typically, alkaline lava and ash have high contents of silicate minerals and glass. Natural water sources, particularly those containing dissolved CO_2, react readily with alkaline silicates to release sodium and bicarbonate ions [265]. The presence of bicarbonate and sodium ions exerts a positive influence over fluoride and NOM concentration. This is because fluoride concentration in water is heavily controlled by calcium ions as these two species can form the insoluble calcium fluorite [9]. In bicarbonate-alkaline water, calcium is limited by precipitation. Consequently there is not enough calcium to fix fluoride ions, resulting in high fluoride concentration. The results confirm previous findings that fluoride concentration was positively correlated with salinity, sodium, and bicarbonate [266]. Evaporation processes further favors fluoride accumulation, which explains the extraordinarily high salinity and fluoride concentration in those closed-basin soda lakes.

Some groundwater samples, on the other hand, are of the sulfate-alkaline-earth type (**Figure 4.5**). Similar to fluoride, sulfate in groundwater is generated from the dissolution of minerals, such as gypsum and anhydrite. Since levels of dissolved oxygen are typically low in groundwater, dissolved hydrogen sulfide (H_2S) is the common form of sulfur [267]. This is because sulfate-reducing bacteria, which live in oxygen-deficient

environments such as deep wells, chemically change sulfate into hydrogen sulfide [268]. These sulfate-reducing bacteria flourish in hot water. A good example is sample S54 which was taken from a capped hot spring. When the groundwater was pumped to the surface, the rotten egg odor of hydrogen sulfide was detected. The smell problem still existed even after membrane filtration, as will be discussed in Chapter 5.6. The sulfate-alkaline-earth type of water is not favorable for fluoride accumulation due to the high contents of alkaline earth metals such as calcium, magnesium and strontium.

Soda lakes in the East African Rift Valley are considered as one of the most extreme aquatic environments on earth [269]. The results show that they are typically characterized by high *pH* and high concentrations of carbonate salts, associated with low concentrations of calcium and magnesium. Examples are S14 (Lake Natron), S36 (Lake Manyara) and S82 (Lake Big Momella). These lakes are found in arid and semi-arid areas where hot and dry weather leads to evaporation of the lake water. The high alkalinity and salinity arise when the rapid evaporation exceeds any inflow. The absence of calcium and magnesium is also critical for the formation of a soda lake, because dissolved calcium and magnesium can easily immobilize the carbonate ions and the resultant precipitates (*e.g.* calcite, dolomite, magnesite) will further neutralize the *pH* of the alkaline lake water [269]. Meanwhile the absence of soluble calcium facilitates accumulation of fluoride, as explained earlier. Among 166 Tanzanian water samples, S82 (Lake Big Momella) contained the highest fluoride concentration of 1391 mg L^{-1}. Comparably, Gaciri and Davies [270] reported fluoride concentration up to 2170 mg L^{-1} in Lake Magadi in Kenya. The name "Magadi" is locally used to refer to a natural mineral trona ($Na_2CO_3 \cdot NaHCO_3 \cdot 2H_2O$) which significantly contributes to the prevalence of fluorosis in East Africa [271].

Noticeably, some soda lakes also contain high concentrations of sodium chloride, making them saline- or hypersaline lakes as well. An extreme example is sample S49 (from Lake Eyasi) which has a chloride concentration of 15770 mg L^{-1} and a sodium concentration of 9286 mg L^{-1}. This soda lake sample is as saline as seawater (chloride around 19000 mg L^{-1} and sodium around 10000 mg L^{-1}).
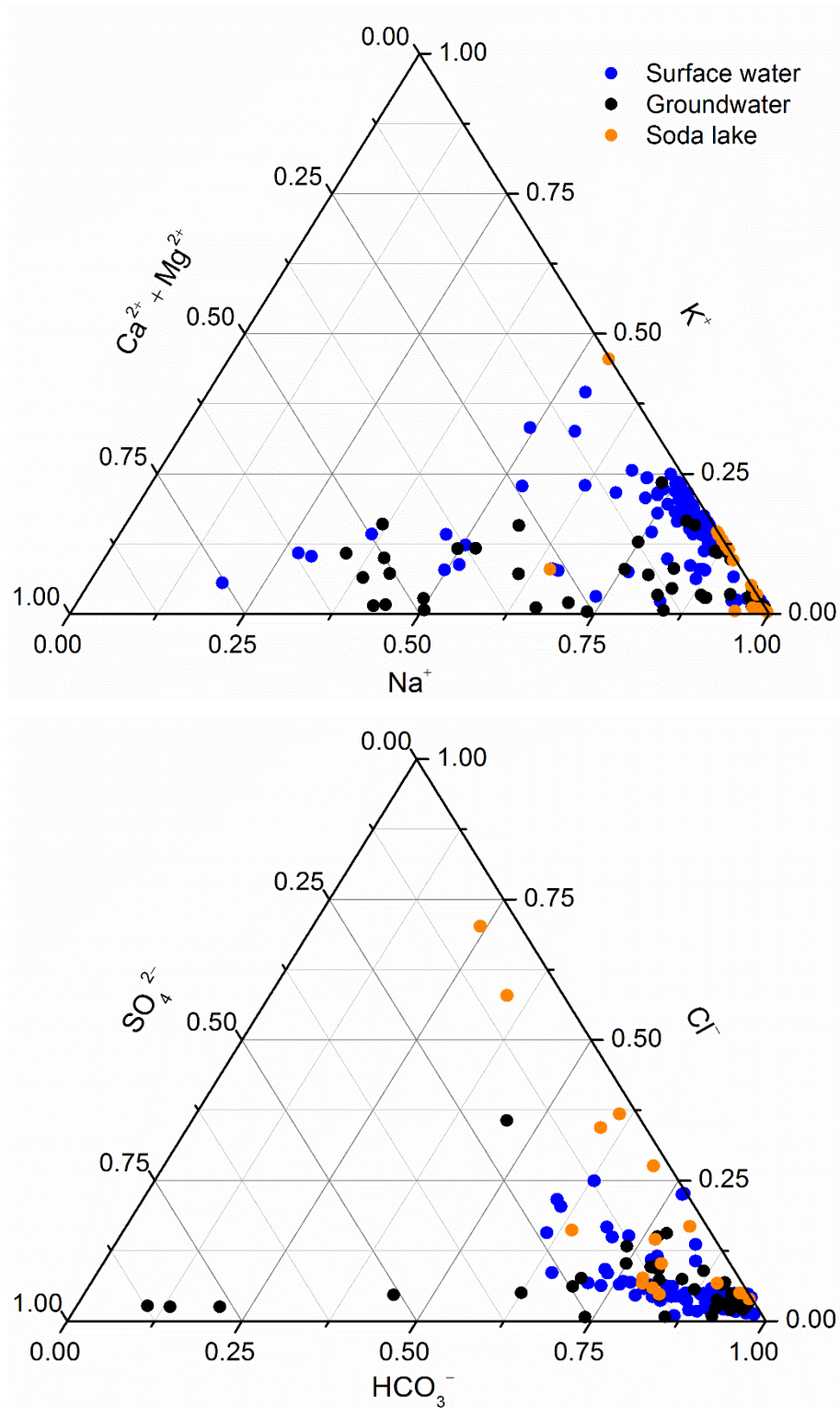
Figure 4.5: Ternary plots showing the water composition of 166 samples. The Na-K-(Ca+Mg) ternary plot is shown on the top, and the HCO_3-SO_4-Cl one on the bottom.

4.5   Membrane screening

After thoroughly analysing 166 natural water samples, 22 of them were selected for NF/RO tests. These samples covered surface water, groundwater and soda lakes. Some

of these were important drinking water supply for local community, while some others had unique geographical characteristics (*e.g.* high alkaline or high TOC). The major water parameters of the 22 samples are provided in **Table 4.2**. The compositions of these samples varied considerably, but they all had a fluoride concentration above the WHO guideline of 1.5 mg L^{-1}.

There were at least two reasons for conducting the bench-scale NF/RO experiments. Firstly, it was vital to investigate the performances of different NF/RO membranes in order to select the most suitable membrane type for future pilot-scale applications. Secondly, although fluoride removal by NF/RO in synthetic solutions was extensively studied, no previous work had treated such a wide variety of natural waters with very different compositions. There was a considerable need to understand the effect of raw water characteristics on membrane performance in fluoride removal, in order to effectively test NF/RO procedures in real environment conditions.

The first step of a series of bench-scale experiments was treating one water sample with six different NF/RO membranes: two RO membranes (BW30, BW30-LE) and four NF membranes (NF90, NF270, TFC-SR2, TFC-SR3). Sample S8 was selected as the testing sample. It contained both high fluoride (42.4 mg L^{-1}) and high TOC (243 mg L^{-1}) concentrations. Meanwhile it had a moderate salinity with an osmotic pressure of approximately 1.2 bar. Therefore the performance of different membranes could be compared without requiring a pressure higher than 10 bar.

Based on the design of the stainless steel stirred cell, the feed solution was pressurized to pass through the membrane and the permeate solution was discharged from the closed system, which led to an increasingly concentrated solution in the cell. The degree of filtration process can thus be represented by the recovery *i.e.* the ratio of permeate to feed volume. The recovery for all bench-scale experiments was fixed in the range between 6.25% and 50% for comparable purposes.

Table 4.2: Water quality of the NF/RO treated samples (uncertainty is ± 1% for *pH*, EC, turbidity and F⁻, ± 7% for TOC)

ID	Type[a]	*pH*	EC (µS cm⁻¹)	Turbidity (NTU)	TOC (mg L⁻¹)	F⁻ (mg L⁻¹)	NF/RO membrane[b]
1	SL	9.46	9230	5.31	32.8	212.0	1, 6
3	SL	9.53	8710	14.23	39.8	239.9	1, 6
6	SW	8.92	1545	12.84	3.9	19.4	1
8	SW	8.29	2270	9.20	243.0	42.4	1–6
9	SW	8.76	922	3.73	2.3	22.8	1–6
10	SW	8.75	908	2.15	3.5	10.2	1
11	SW	8.35	314	5.79	3.5	3.3	1
12	GW	8.33	548	0.12	0.9	10.9	1, 4
13	GW	8.00	504	0.90	2.4	12.8	1, 4
15	SW	8.65	1097	0.65	0.8	4.8	1
20	SW	9.62	3020	3.91	1.7	22.9	1
21	SW	8.38	4720	21.75	270.0	33.1	1, 6
23	SL	8.99	16150	38.96	58.2	56.6	1, 6
25	SW	9.05	1535	497.8	25.7	3.6	1
26	SW	8.34	472	10.13	7.2	2.6	1
28	SW	8.43	907	0.31	1.3	20.2	1–6
30	SW	8.67	609	0.40	2.1	17.1	1
36	SL	9.6	14800	69.2	124.0	40.7	1, 6
39	SW	7.53	443	0.45	10.1	13.4	1, 4
80	GW	8.78	3930	0.04	11.4	50.5	1, 3
98	GW	9.44	5310	0.78	12.5	57.6	1–6
117	SW	8.92	3340	1.03	114.0	59.7	1–6

[a]SW refers to surface water, GW refers to groundwater, and SL refers to soda lake

[b]Each number refers to a membrane type. 1 is BW30, 2 is BW30-LE, 3 is NF90, 4 is NF270, 5 is TFC-SR2, 6 is TFC-SR3.

Figure 4.6 shows the sequence of permeate water flux is: BW30 < BW30-LE < TFC-SR3 < NF90 < TFC-SR2 < NF270. This agrees with the permeability data of different membranes (**Table 2.1**). The permeate water flux decreased gradually with increasing recovery. This is attributed to an increase of osmotic pressure and therefore a decrease of the net driving pressure which refers to the difference between the applied pressure and the osmotic pressure [272, 273].
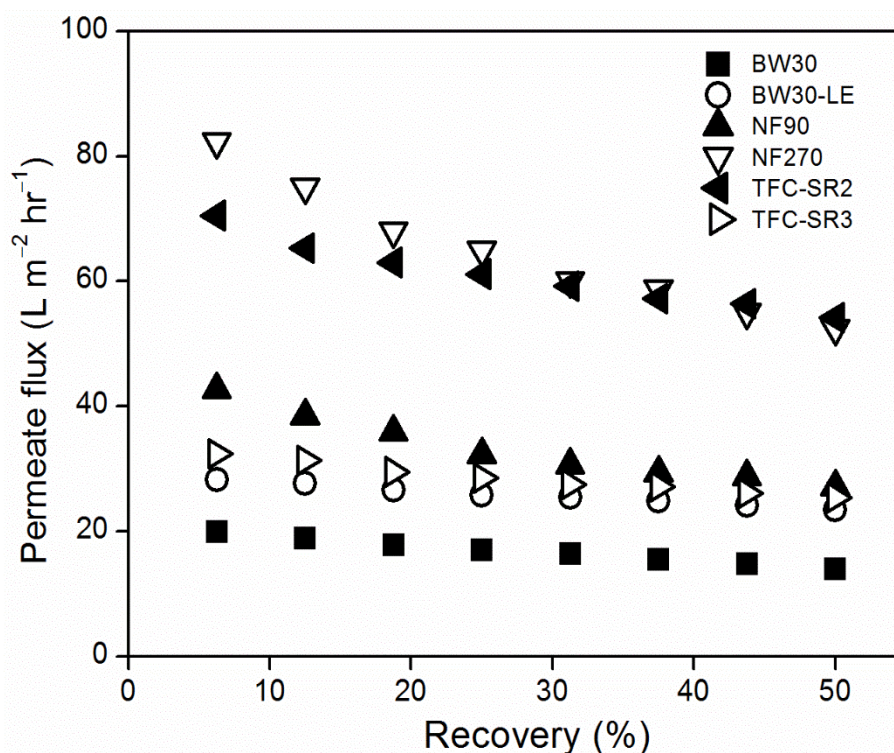
Figure 4.6: Permeate water flux of sample S8 by different membranes as a function of recovery (uncertainty is ± 1% for flux)

4.5.1 Fluoride and TOC removal

Figure 4.7 shows the permeate fluoride concentration and fluoride retention of sample S8 as a function of recovery for the six NF/RO membranes. Overall, an increasing trend of permeate fluoride concentration with increasing recovery was observed. This was primarily attributed to the increase of retentate fluoride concentration.

The permeate fluoride concentration varied significantly with membrane types. The most open NF membrane TFC-SR2 experiences the largest increase of permeate fluoride concentration, followed by the NF270 membrane. The permeate fluoride concentration by these two membranes were always above the WHO guideline of 1.5 mg L^{-1}, even at the lowest recovery of 6.25%. The results indicate that TFC-SR2 and NF270 membranes were incapable of defluoridation for this certain water sample (fluoride 42.4 mg L^{-1}), though they might be able to treat some low-fluoride samples (details will be discussed in Chapter 4.6).

The other two NF membranes, namely NF90 and TFC-SR3, could successfully reduce permeate fluoride concentration below the WHO guideline of 1.5 mg L^{-1} in the low

recovery range. Indeed, the permeate fluoride concentration obtained using NF90 exceeded 1.5 mg L^{-1} at recovery above 25%, and the permeate fluoride concentration of TFC-SR3 was more than 1.5 mg L^{-1} at recovery above 12.5%. This highlights the importance of selecting the right recovery range for NF membranes in treating high-fluoride water.

The two RO membranes, BW30 and BW30-LE, always removed fluoride ions to levels that met the WHO guideline, despite the change of recovery. At the highest recovery of 50%, the permeate fluoride concentration by BW30 was 1.2 mg L^{-1}, and that by BW30-LE was 0.7 mg L^{-1}. The results confirms the expected superior capability of RO membranes towards defluoridation.

Fluoride retention decreased when recovery went up, which was opposite to the trend of permeate fluoride concentration. As explained earlier, fluoride retention was calculated from the permeate concentration and the retentate concentration. Given that both permeate and retentate concentrations increased with recovery, a decreased retention arose when the increase of permeate concentration was faster than that of retentate concentration (Equation 9). This is probably because fluorides accumulate more rapidly in the boundary layer than in the bulk solution.

Unlike fluoride, permeate TOC concentration firstly decreased with increasing recovery and then remained stable at high recoveries (**Figure 4.8**). It is well understood that size exclusion is the dominant removal mechanism for NOM. While larger NOM particles are rejected by the membrane, LMW fractions may pass through the membrane *via* convection [144]. In convective transport, the solutes are carried in the solvent stream through the membrane. Therefore, convection is directly related to permeate flux.

The convective transport of NOM thus changed with the permeate water flux. The increased TOC retention is the result of decreased permeate concentration and increased retentate concentration. The six NF and RO membranes exhibited very similar TOC retention (> 99.8%) at the highest recovery of 50%, showing that NOM can be almost completely removed by NF/RO processes.
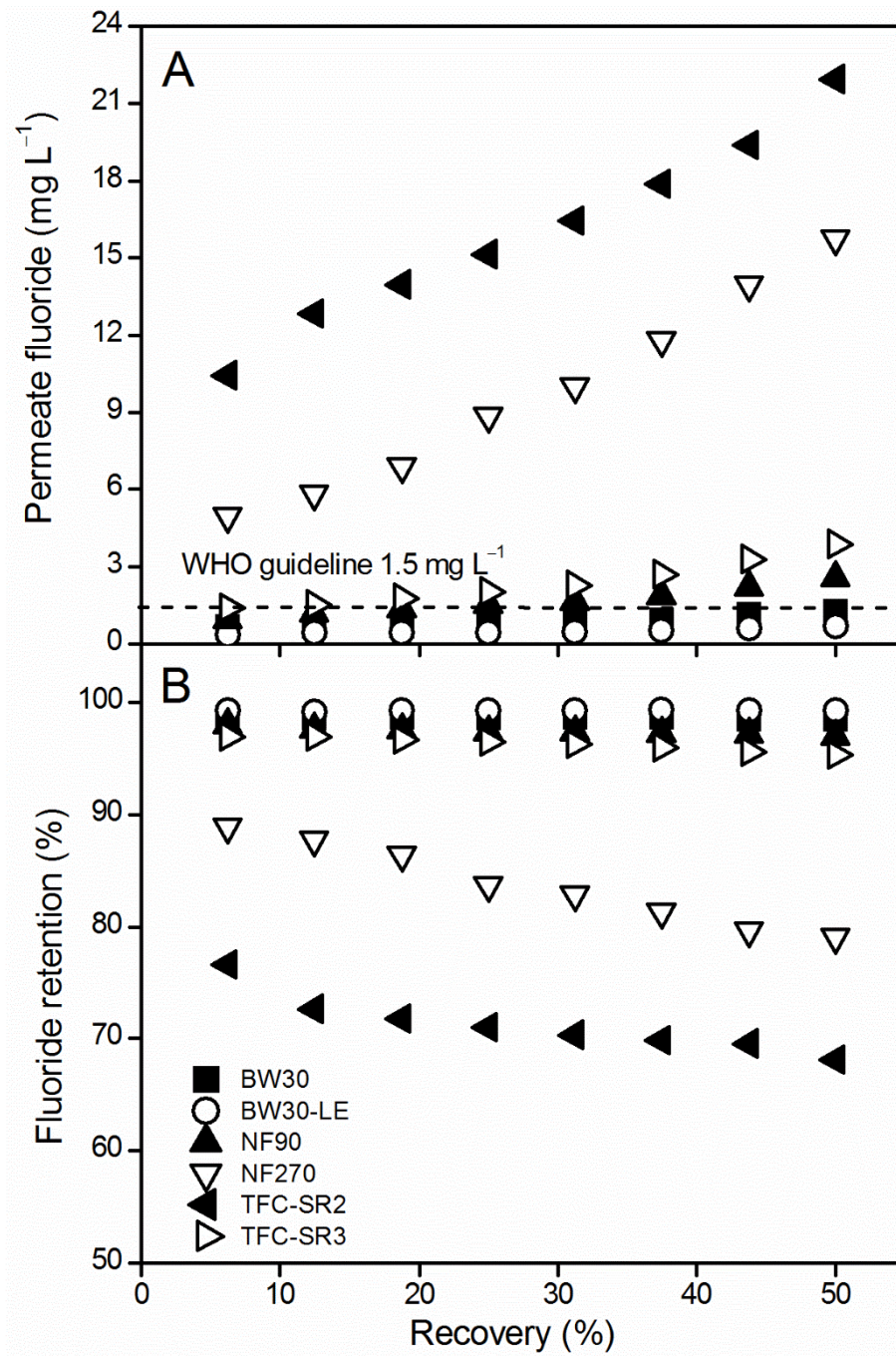
Figure 4.7: (A) Permeate fluoride and (B) fluoride retention of sample S8 by different membranes as a function of recovery (uncertainty is ± 1% for permeate fluoride, approximately ± 2% for fluoride retention)
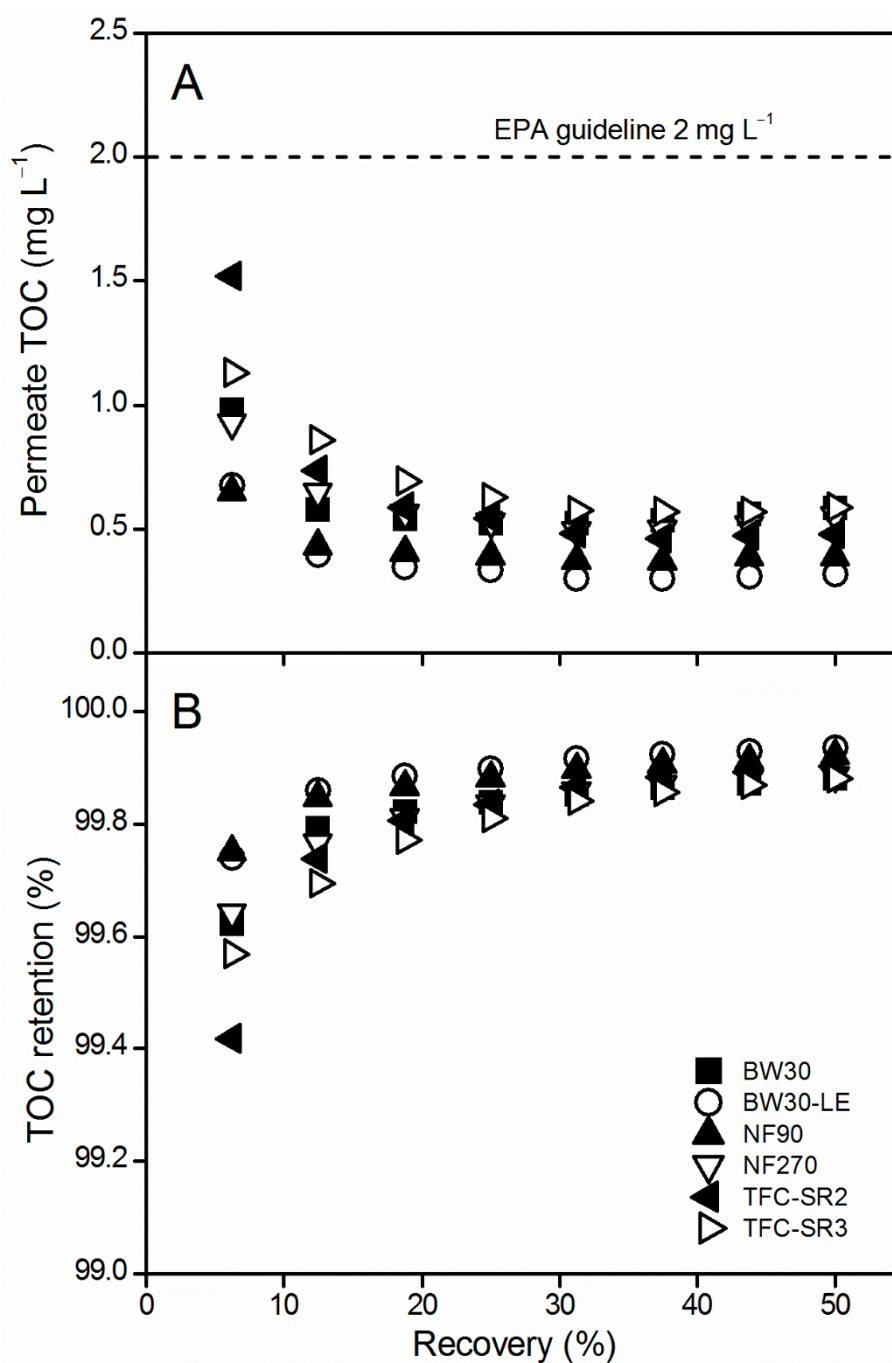
Figure 4.8: (A) Permeate TOC and (B) TOC retention of sample S8 by different membranes as a function of recovery (uncertainty is ± 7% for permeate TOC, approximately ± 10% for TOC retention)

In summary, six NF and RO membranes exhibited very different fluoride removal capacities but similar NOM removal capacity. Membrane characteristics were the major reason for the differences in fluoride removal capacities. The conceptual model shown in **Figure 4.9** illustrates three membrane regimes for fluoride removal with regard to membrane pore *versus* ion size [274]:

    (1) the hydrated ion fits completely inside the pore;

    (2) the pore size is between the size of the bare ion and the hydrated ion;

(3) the bare ion does not fit inside the pore.
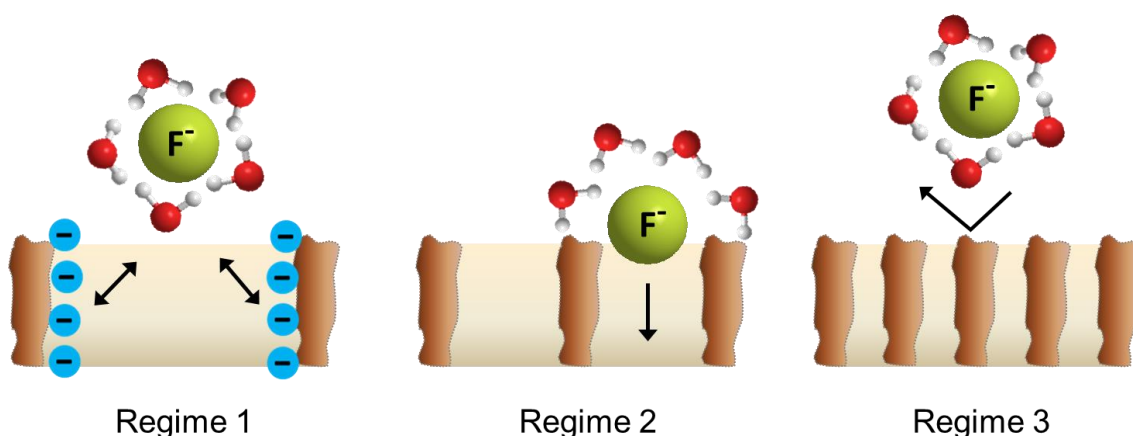
Figure 4.9: Schematic of the three regimes for fluoride with regard to membrane pore size (1) the hydrated ion fits completely inside the pore; (2) the pore size is between the size of the bare ion and the hydrated ion; (3) the bare ion does not fit inside the pore

As mentioned previously, the fluoride ion has an ionic radius of 0.13 nm and a hydrated radius of 0.34 nm. Based on pore size data from **Table 2.1,** three NF membranes (NF270, TFC-SR2, TFC-SR3) had pore radii larger than the fluoride hydrated radius. Regime 1 applies to these membranes, and charge repulsion becomes the dominant mechanism instead of size exclusion. The other three membranes (BW30-LE, BW30 and NF90) had pore radii between the fluoride ionic radius and hydrated radius, and therefore they belong to Regime 2. Their high fluoride retention is a result of size exclusion due to hydration, and energy barriers caused by partial dehydration [112].

Fluoride and TOC retention as a function of membrane size (MWCO) and zeta potential is plotted in **Figure 4.10**. Fluoride retention decreased steadily with increasing MWCO, indicating the importance of size exclusion. Regime 1 membranes (NF270 and TFC-SR3) had identical pore radius (0.38 nm) and very similar MWCO (180 and 167 Da, respectively) but different surface charge densities (**Table 2.1**). The more negatively charged TFC-SR3 membrane had higher fluoride retention than the NF270 as a result of charge repulsion effects.

In contrast, TOC retention is consistently high independent of membrane type. This is because the molecular size of NOM is significantly larger compared to the membrane

pore size [181]. Only small amounts of LMW fractions are able to permeate the membrane [144] .
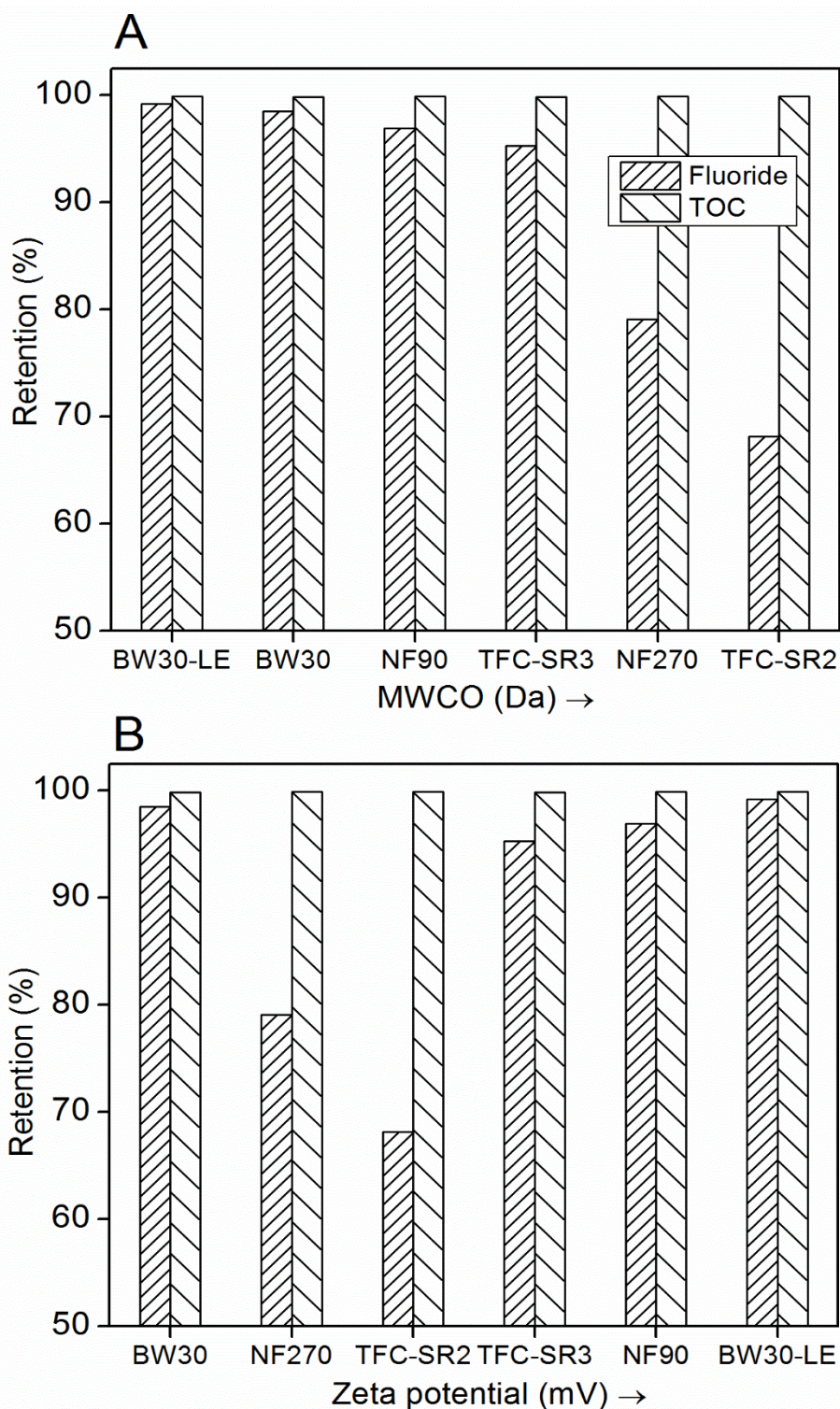
Figure 4.10: Fluoride and TOC retention of sample S8 as a function of membrane type with increasing (A) MWCO and (B) zeta potential at 50% recovery (uncertainty is approximately ± 2% for fluoride retention, ± 10% for TOC retention)

Referring to **Figure 4.6**, Regime 1 membranes TFC-SR2 and NF270 had the largest decline in retention with increasing recovery. This is presumably due to the fact that higher permeability facilitates concentration polarization at the membrane surface and thus the diffusion rate of fluoride [129, 275]. In contrast, Regime 2 membranes BW30 and BW30-LE had the smallest retention decline with recovery, and can effectively remove fluoride to below the WHO guideline almost independent of concentration, which highlights a size exclusion mechanism. The results confirm that the hydration of fluoride cannot be neglected in NF/RO when the membrane pore size is similar to the dimension of the hydrated ion [223].

4.5.2   Other ion removal

The removal of other ions by NF/RO membranes was also worth investigating. **Figure 4.11** shows the permeate IC and IC retention as a function of recovery. The rising of permeate IC with increasing recovery was very similar to fluoride. The sequence of permeate IC was BW30-LE < BW30 < NF90 < TFC-SR3 < NF270 < TFC-SR2, which was also the same as that of fluoride. The dominant carbonate species in sample S8 was the monovalent bicarbonate. The bicarbonate ion has a Stokes radius of 0.15 nm [110] and a hydrated radius of 0.36 nm [276], while the fluoride has a Stokes radius of 0.13 nm and a hydrated radius of 0.34 nm as mentioned before. In addition, the bicarbonate ion has the same charge and very similar size to the fluoride ion. This can explain why bicarbonate ions exhibited a fluoride-like behaviour in NF/RO processes. Moreover, the plot of permeate EC with recovery shows the same trend as that of permeate IC (**Figure 4.12**). Sample S8 is a bicarbonate-alkaline type of water, therefore its ionic strength (as measured by EC) is closely dependent on IC.

The permeate samples of S8 were further sent to KIT for ICP-OES and ion chromatograph analysis. Unfortunately the plastic vials containing these samples were damaged during the delivery from Tanzania to Germany. Instead another water sample (S39) was tested using the same experimental procedure but with only the BW30 and the NF270 membranes. Detailed water compositions can be found in **Table 4.2** and in the Appendix. Ion retention values calculated from ICP-OES and ion chromatograph data are presented in **Figure 4.13.** The results demonstrate the typical difference between RO and NF. The BW30 membrane retained all ions (both monovalent and multivalent) and NOM to more

than 90%, while the relatively open NF270 membrane was more effective in removing multivalent ions (Ca^{2+}, Mg^{2+}, SO_4^{2-}) than monovalent ions (K^+, Na^+, F^-, HCO_3^-). Both the NF and RO membranes achieved very high TOC retention as a result of size exclusion effect for large NOM molecules [146].
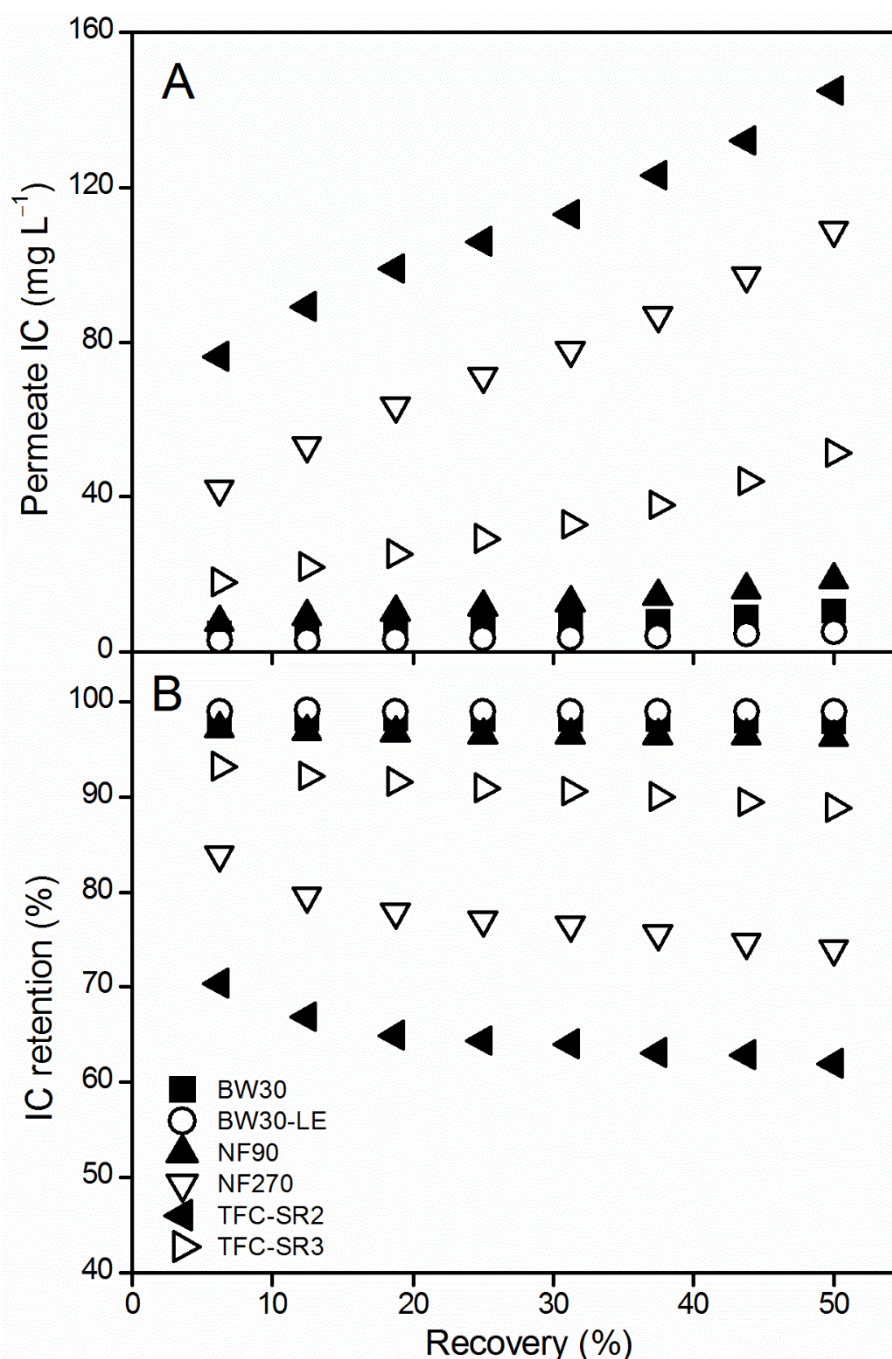
Figure 4.11: (A) Permeate IC and (B) IC retention of sample S8 by different membranes as a function of recovery (uncertainty is ± 5% for permeate IC, approximately ± 7% for IC retention)
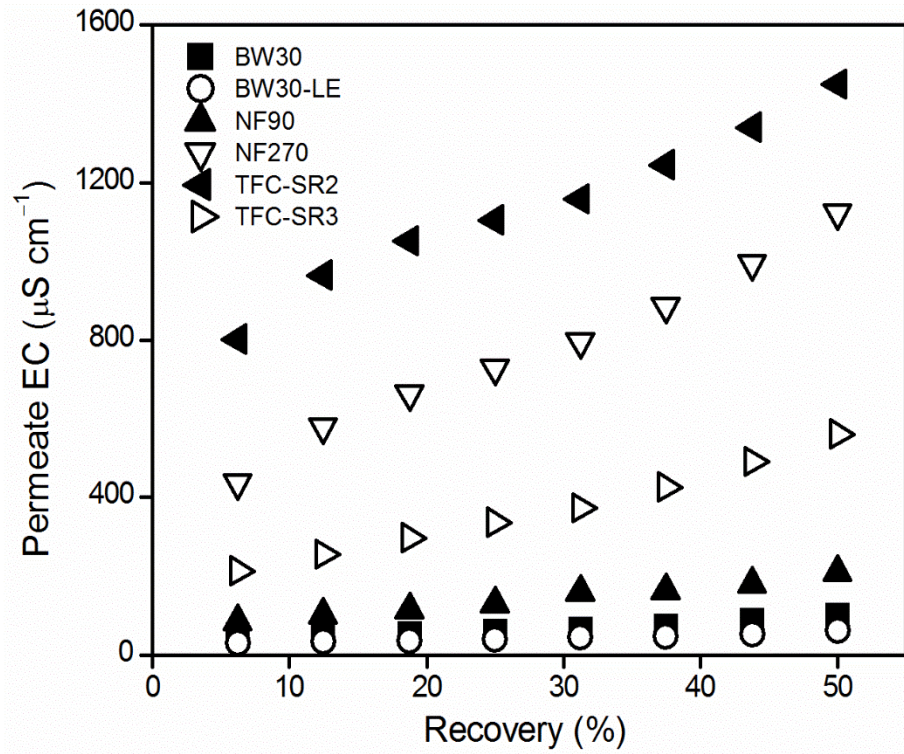
Figure 4.12: Permeate EC of sample S8 by different membranes as a function of recovery (uncertainty is ± 1% for permeate EC)
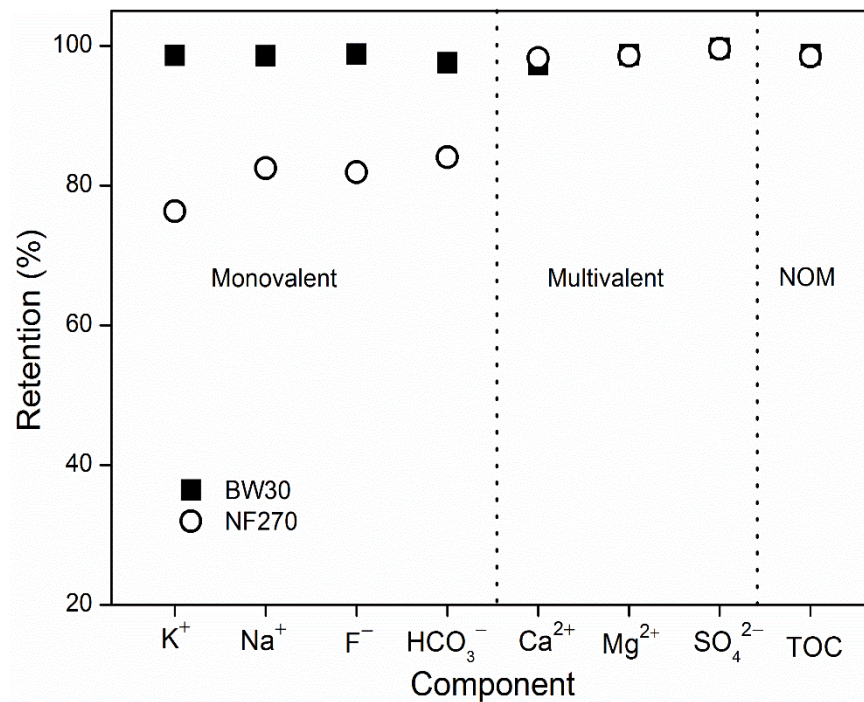
Figure 4.13: Ion retention of sample S39 by BW30 and NF270 membranes at 50% recovery (uncertainty is approximately ± 3% for ion retention, and ± 10% for TOC retention)

4.6 Impact of raw water characteristics

Membrane screening using the same water sample (S8) showed that RO membranes had much higher fluoride retention than NF membranes while both NF and RO had similarly high TOC retention. It should be noted that the tested water sample (S8) was an extreme example with unusually high fluoride (42.4 mg L^{-1}) and high TOC (243 mg L^{-1}) concentrations, which may not be representative of common real situations. It would be unnecessary to apply RO to the situation where NF can handle. Therefore it was useful to study the treatability of different water samples by different membrane types in order to make tailored and case-dependent treatment plans.

4.6.1 Ionic strength

The ionic strength determines the osmotic pressure of the solution. In this work, a measure of ionic strength was obtained *via* EC measurements. The influence of ionic strength on fluoride and TOC retention was studied by treating 22 samples using the Regime 2 membrane BW30. The EC of these 22 samples ranges from 0.3 to 16.1 mS cm^{-1}. It should be noted that the osmotic pressure used here was calculated from feed ionic concentrations and during the experiments the osmotic pressure increased with recovery. This increase was not considered in the calculation of the net driving pressure. At the constant applied pressure of 10 bar the net driving pressure decreased proportionally with initial EC (**Figure 4.14**A), resulting in the decrease of permeate water flux.

The extremely low permeate flux at high initial EC (*e.g.* soda lake samples) was attributed to osmotic pressure effects, which then resulted in the very low fluoride retention of about 70% due to diffusion (**Figure 4.14**B). The overall effect of initial EC on fluoride retention was also contributed by charge screening, particularly for Regime 1 membranes where charge repulsion is the dominant mechanism [277-279]. Indeed at high ionic strength, cations such as sodium and calcium neutralize partially the negative charges of the membrane, and consequently decrease the charge repulsion between fluoride and the membrane [280].
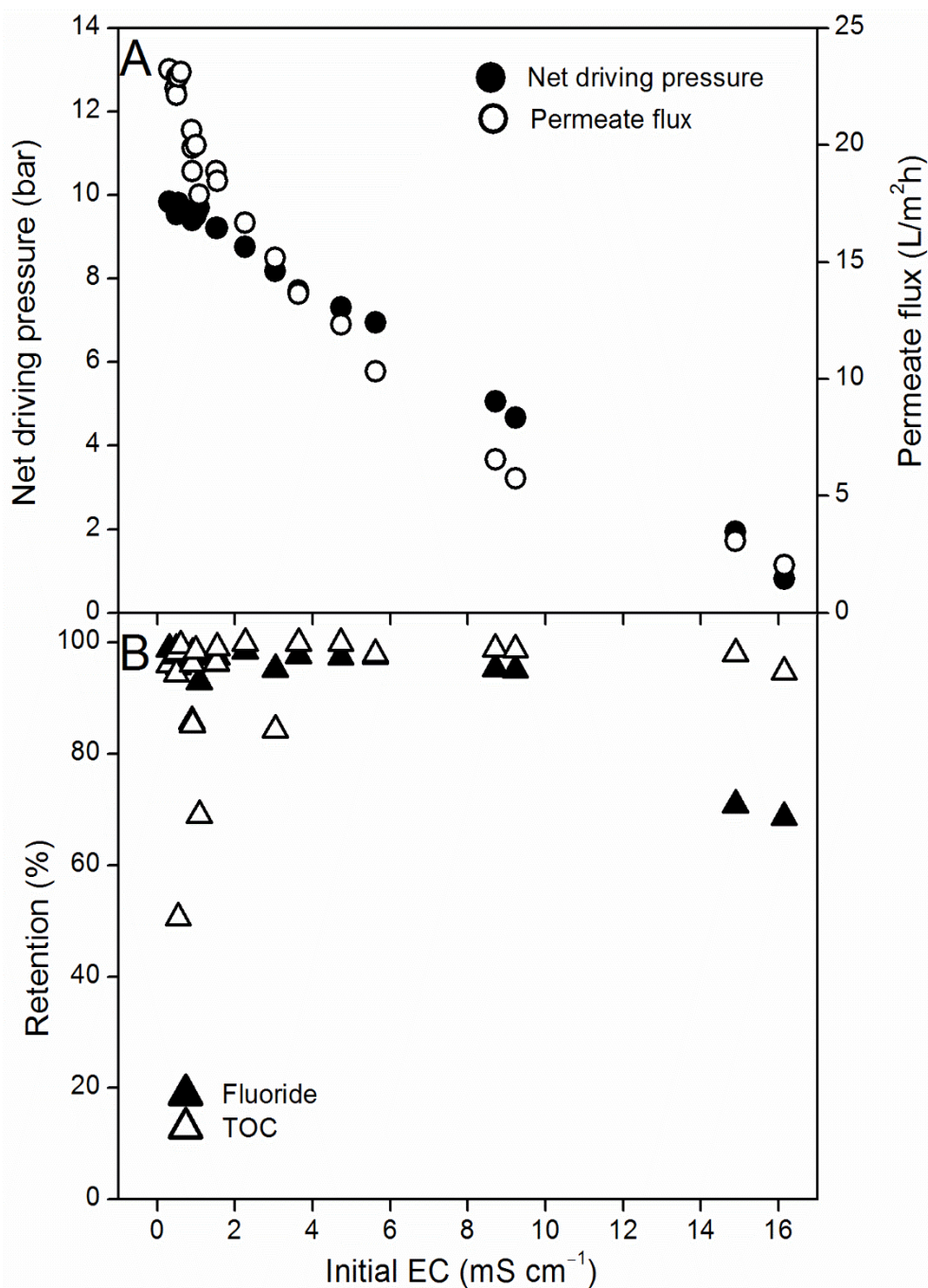
Figure 4.14: (A) Net driving pressure and permeate flux and (B) fluoride and TOC retention of 22 natural water samples by the BW30 membrane as a function of initial EC at 50% recovery (uncertainty is approximately $\pm 2\%$ for fluoride retention, $\pm 10\%$ for TOC retention)

In contrast, TOC retention was independent of initial EC. As mentioned above, only LMW fractions can permeate the membrane while other fractions are rejected by size exclusion. Initial EC affected the permeate water flux but its effect on TOC retention was not measurable most likely because the LMW organic fraction was only a small fraction of the TOC and hence of low concentration [223]. A few points of deviation in TOC retention at low EC ranges were in fact due to the detection limit of the TOC analyzer.

4.6.2   Fluoride concentration

To understand the impact of initial fluoride and TOC concentrations on membrane performance, the results of the 22 samples tested above with the BW30 membrane were plotted. Selected water samples were further treated with the other membranes to better understand retention mechanisms. **Table 4.2** shows the type of membranes used for each water sample.

Figure 4.15 shows permeate fluoride concentration and fluoride retention by six NF/RO membranes as a function of initial fluoride concentration. Despite the different membrane types, it is evident that increased initial fluoride concentration led to increased permeate concentration and decreased retention, which confirms the diffusive transport mechanism of fluoride [240].   The trendlines of permeate fluoride concentration had a linear relationships for all membranes, though some scatter was inevitable as each data point represented a very different water composition. The permeate fluoride concentrations of soda lake samples were exceptionally high as a result of the extreme ionic strength. These results were included to highlight the complexity and variation of these natural waters. The intersection of the trend line and the WHO guideline indicates the treatability limit in terms of initial fluoride concentration for a certain membrane. At 50% recovery, the limit for Regime 2 membranes BW30-LE, BW30 and NF90 is $30-40$ mg L^{-1} (except for soda lakes); for Regime 1 membranes TFC-SR3 it is about 20 mg L^{-1}, NF270 and TFC-SR2 it is $5-10$ mg L^{-1}. The treatability limit figures offer valuable information for system design and membrane selection [223].
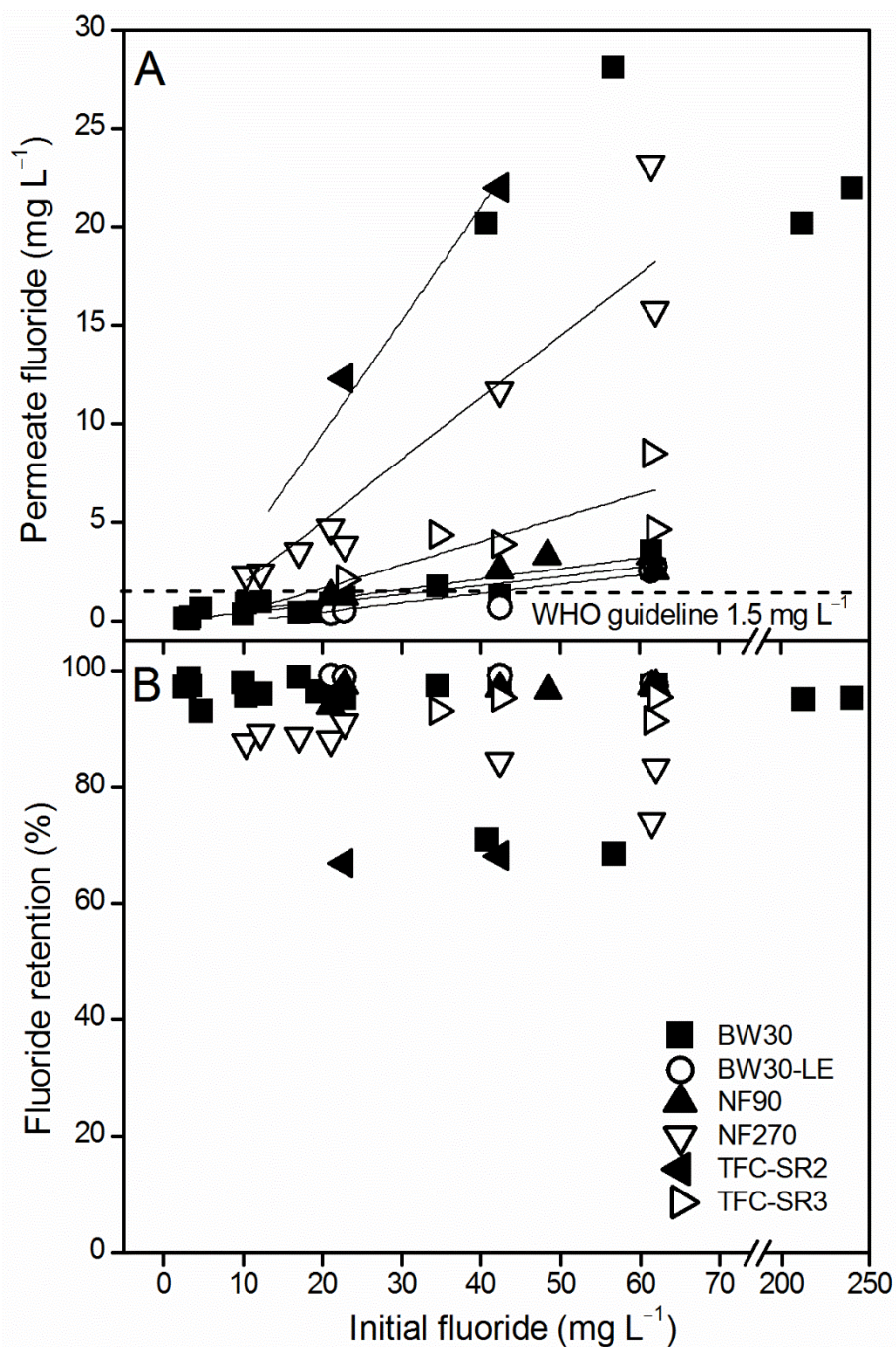
Figure 4.15: (A) Permeate fluoride and (B) fluoride retention of 22 natural water samples by different membranes as a function of initial fluoride concentration at 50% recovery (uncertainty is ± 1% for permeate fluoride, approximately ± 2% for fluoride retention, the solid lines are guides to the eye)

4.6.3   TOC concentration

The impact of initial TOC concentration on TOC retention is demonstrated in **Figure 4.16**. All membranes removed TOC consistently below the EPA guideline of 2 mg L^{-1} for all water samples except for two soda lake samples (S23, S36). This is likely due to extremely ionic strength of soda lake samples which caused very low permeate fluxes. In

fact it took more than 24 hr for S23 and S37 to reach 50% recovery. The extremely long filtration time caused severe concentration polarization phenomena.
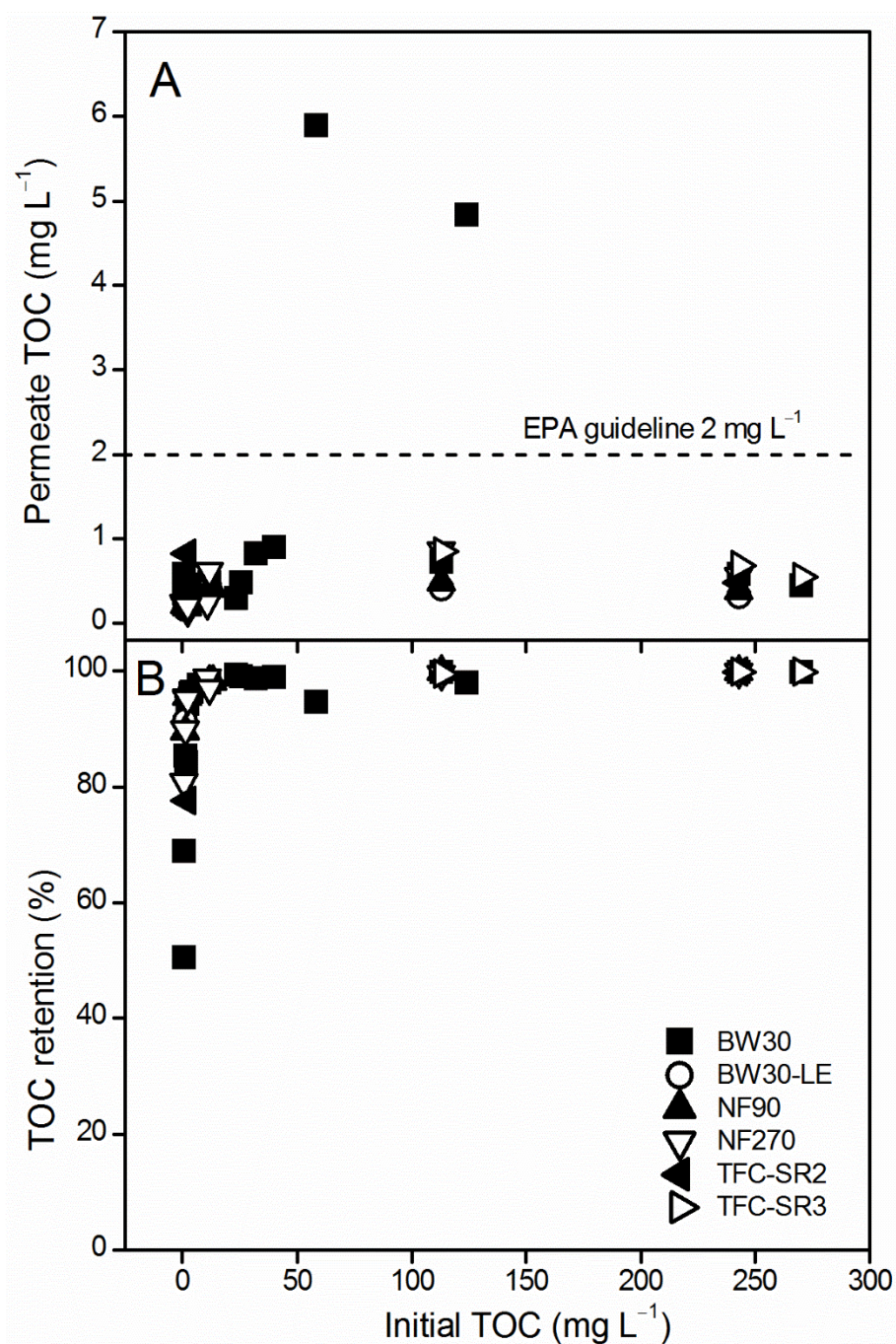
Figure 4.16: (A) Permeate TOC and (B) TOC retention of 22 natural water samples by different membranes as a function of initial TOC concentration at 50% recovery (uncertainty is ± 7% for permeate TOC, approximately ± 10% for TOC retention)

For all other water samples, the permeate TOC concentrations remained within a narrow range of 0.2−0.9 mg L^{-1} and were independent of the initial TOC. As explained before, this was because size exclusion is the dominant removal mechanism for NOM. The TOC

retention increased with initial TOC concentration, since the permeate concentration did not change with initial TOC concentration. Large errors arose when treating samples that had extremely low initial TOC concentration, because the permeate TOC concentration was close to the detection limit of the instrument. TOC retention of these samples must be interpreted with caution.

When plotting the permeate fluoride concentration against initial TOC concentration, an interesting trend was observed (**Figure 4.17**). It appears that the initial TOC concentration had a negative effect on permeate fluoride concentration. The trend was particularly obvious for three water samples (S8, S98 and S117) which had comparable EC and fluoride contents but had very different TOC concentrations. The trend was most evident for Regime 1 membranes (NF270 and TFC-SR3).

Given that Regime 1 membranes reject fluoride based on charge repulsion rather than size exclusion, there are two possible ways that NOM could improve fluoride retention. Firstly, NOM may increase charge repulsion between fluoride and the membrane. Possible mechanisms include (1) increase of membrane surface charge due to the adsorption of negatively charged NOM on the membrane [114, 281]; (2) charge repulsion between fluoride ions and NOM [282].

Secondly, NOM may create conditions for size exclusion effect, *i.e.* to increase the size of fluoride ions or to reduce the pore size of the membrane. Possible mechanisms for NOM could be: (1) membrane pore size restriction and blocking due to NOM fouling [143, 283]; (2) trapping of fluoride inside NOM structure [72].
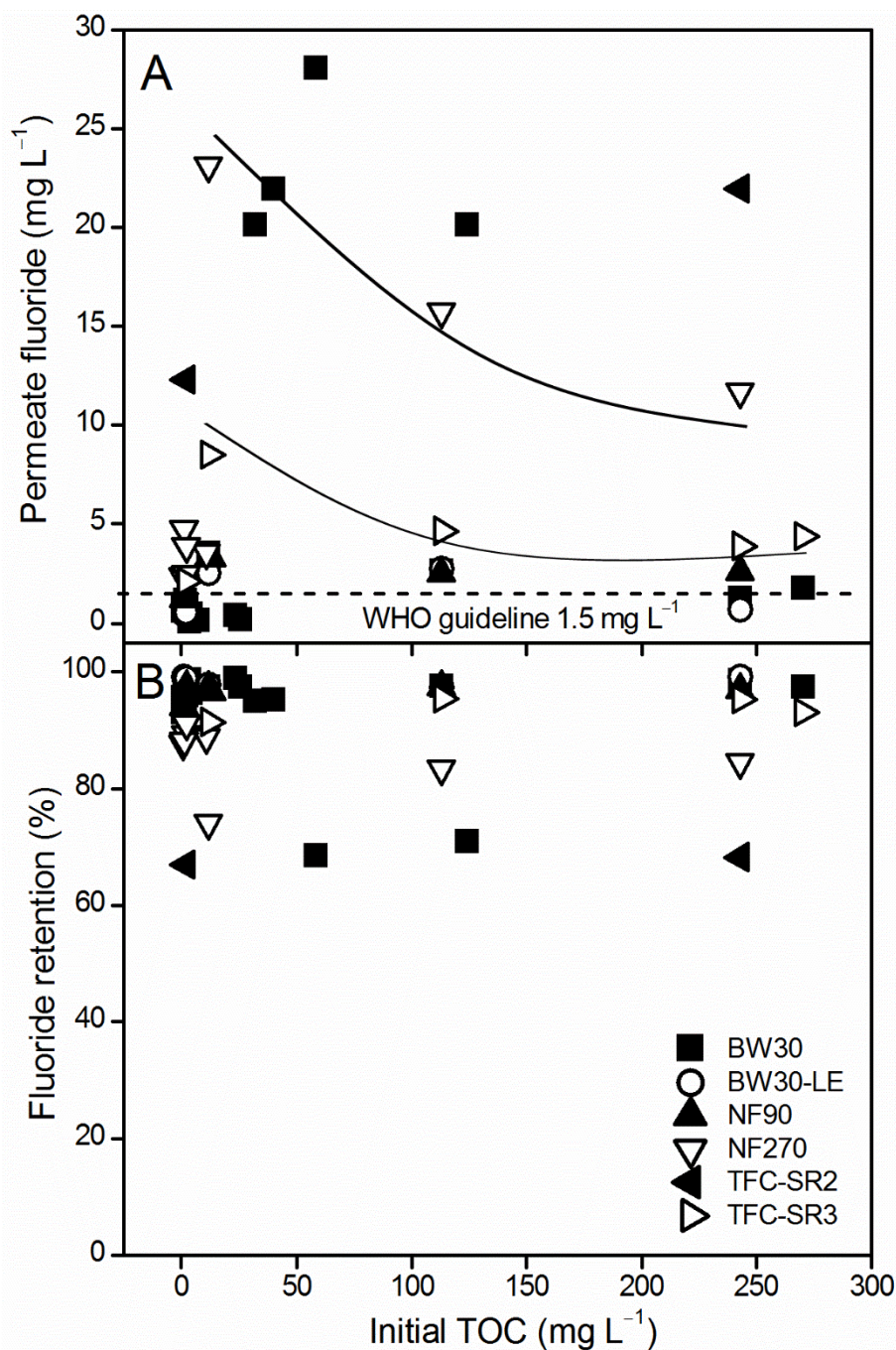
Figure 4.17: (A) Permeate fluoride and (B) fluoride retention of 22 natural water samples by different membranes as a function of initial TOC concentration at 50% recovery (uncertainty is ± 1% for permeate fluoride, approximately ± 2% for fluoride retention, the solid lines are guides to the eye)

With natural water being used as the feed solution, caution must be applied as the effect of NOM on fluoride ions might be linked to other parameters, *e.g.* ionic strength. To better investigate the potential mechanisms, synthetic solutions containing only TOC and fluoride were tested using the same experimental procedure (**Figure 4.18**). Regime 1 membrane NF270 was used. The initial TOC concentration of the synthetic solution was adjusted to 20 and 50 mg L^{-1} by dissolving appropriate amounts of AHA. The initial

fluoride concentration was fixed at 50 mg L^{-1} by adding NaF. The *pH* of the synthetic solutions was adjusted to either 3 or 8.

As discussed in Chapter 1 and Chapter 3, both fluoride and NOM species are heavily affected by the *pH*. At *pH* 3, fluoride exists in the form of uncharged hydrofluoric acid, meanwhile NOM tends to form large aggregates. As **Figure 4.18** illustrates, the permeate fluoride concentration at *pH* 3 was much higher than that at *pH* 8, and did not change with initial TOC concentration. This can be explained by the absence of charge repulsion as fluoride becomes neutral. Results from Chapter 3 indicate that fluoride ions can be sterically trapped inside the structure of NOM aggregates. Clearly this temporarily "trapping" phenomenon had no influence on the transport of fluoride through NF/RO membranes.

At *pH* 8, on the contrary, the permeate fluoride concentration decreased with increasing initial TOC concentration, as previously observed in the natural water experiments. No significant flux change was observed between solutions with and without HS. At *pH* 8, fluoride is negatively charged and NOM molecules are stable and well dispersed in solution. Combining the above observations, enhancement of membrane surface charge by NOM would be the most reasonable explanation for the negative effect of NOM on fluoride transport.

Indeed, more studies on membrane characterization (especially surface charge analysis) are needed before any of the above mentioned mechanisms can be confirmed. This study did not attempt to measure the surface charge of the used membranes due to limitations in experimental equipment. However, we aimed in the first instance to show the influence of NOM on fluoride transport and retention in not only synthetic solutions but also in such natural waters where NOM and fluoride occur sometimes in very high concentrations.
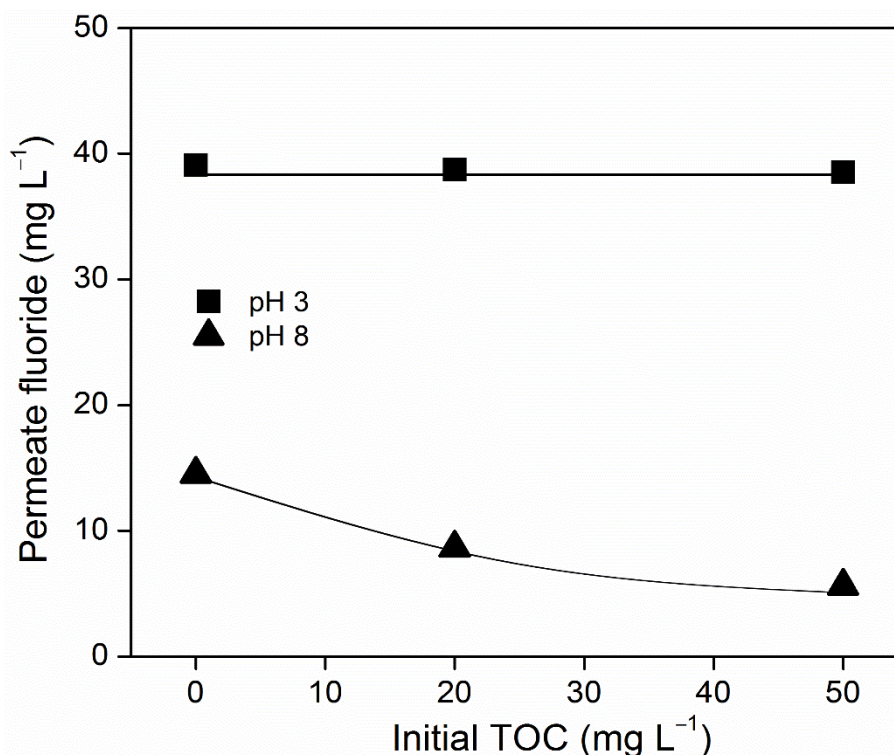
Figure 4.18: Permeate fluoride concentration of synthetic solutions by the NF270 membrane as a function of initial TOC at 50% recovery at two *pH* conditions (uncertainty is ± 1% for permeate fluoride, the solid lines are guides to the eye)

4.7   Conclusions

This chapter summarized the first stage of the field work in Tanzania, which included water sampling, water analysis and bench-scale NF/RO experiments. In total 166 natural water samples were collected from 120 sites over 16 months, including 105 surface water samples, 45 groundwater samples, and 16 soda lake samples.

Fluoride and NOM were identified as two major natural contaminants in these water samples. Specifically, 86% of samples had fluoride concentrations above the WHO guideline of 1.5 mg L^{-1}, and 80% of samples had TOC concentrations exceeding the EPA guideline of 2 mg L^{-1}. The abundance of fluoride and NOM was attributed to the dominance of sodium and bicarbonate in these water samples, because the combination of sodium and bicarbonate restricts the dissolution of calcium and increases the solution *pH*. A typical example was the tropical black water found in fluoride-rich areas.

Bench-scale experiments indicate that fluoride ions transfer through NF/RO predominantly by diffusion while NOM transfers by convection. Fluoride retention was

significantly influenced by recovery and raw water composition, particularly by ionic strength and fluoride and to some degree TOC concentration. High ionic strength resulted in reduction of the effective driving force and thus facilitated fluoride ions to permeate the membrane. The initial fluoride concentration determined the treatability of the raw water in terms of the WHO guideline.

TOC retention was mostly controlled by the size exclusion mechanism. TOC concentration was found to have a positive effect on fluoride removal, in both synthetic solutions and natural water samples. Several possible mechanisms were proposed, among which membrane surface charge modification by NOM was the most plausible. More research on water surface characterization is required before a solid conclusion can be drawn.

Chapter 5: Application of Renewable Energy Powered Membrane Technology

5.1   Introduction

The ideal defluoridation method for rural and remote areas should be reliable, cost effective, and easily implementable [284]. One great advantage of membrane processes is that it can be used in decentralized units, either at household or community level [237]. However, a primary concern of applying membrane units is the requirement for electricity as this is either not available or unreliable in remote areas. In this project, this problem was resolved by using a membrane system that is directly powered by photovoltaics. It has been suggested that the use of batteries in membrane systems should be avoided to increase robustness and efficiency, as well as reduce investment cost and simplify maintenance requirements [285, 286]. By directly coupling the renewable energy power supply to the pump, this naturally subjects the NF/RO system to widely varying energy availability which impacts on its performance. In particular, the subsequent fluctuation in pressure and flow rate inevitably affects permeate water quality, posing a considerable challenge to the implementation of such system in the field [190].

Another challenge is the availability of water sources. In many regions of Tanzania that suffer from freshwater scarcity, brackish water should be considered as an alternative water supply [287]. Brackish water is typically more saline than freshwater, but less saline than seawater. In terms of total dissolved solids (TDS), brackish water is defined as water containing TDS between 1000 and 10000 mg L^{-1}. Therefore, it is less expensive and energy intensive to treat than seawater, given the reduced osmotic pressure that needs to be overcome and the amount of salts that need to be retained [82].

A further concern is the integration of such advanced technology in a rural development context. The management and operation of such systems requires regular monitoring, maintenance procedures and accessibility to spare parts for repairs. The required infrastructure is typically not yet in place for supporting such technology in sub-Saharan African countries [288].

This study evaluated the performance of a solar-powered NF/RO system in treating fresh and brackish waters from several sources in northern Tanzania. The impact of energy fluctuation on system's performance was examined. The aims were (1) to understand the impact of energy fluctuations on retention; (2) to determine the short- and long-term performance of the decentralized membrane system under varying weather conditions; and (3) to assess the potential of implementation and likely challenges to membrane systems in rural areas.

5.2 Experimental summary

5.2.1 Water sources

Several raw water samples were collected from different places in northern Tanzania and transported by water tankers to NDRS where they were treated by ROSI. **Table 5.1** is a summary of sampling sites and their water types. Fresh waters in NDRS and Oldonyosambu are important drinking water sources for local communities but excessive fluoride becomes a major health issue. Brackish waters in Ngare Nanyuki, Mdori and St. Dorcas are not used for drinking purposes due to their high salinity and undesirable colour (Ngare Nanyuki) or unpleasant sulfur smell (Mdori). Instead local people rely on water tankers or hand dug wells (which often dry out in dry seasons) for drinking water. It is thus important to explore the feasibility of ROSI in treating these alternative water sources.

Table 5.1: Summary of water quality for ROSI experiments at NDRS (uncertainty is $\pm$ 1% for *pH*, EC, TDS and F$^-$, $\pm$ 5% for IC and $\pm$ 7% for TOC)

Source	Water type	*pH*	EC (μS cm^{-1})	TDS (mg L^{-1})	F$^-$ (mg L^{-1})	TOC (mg L^{-1})	IC (mg L^{-1})
NDRS	Fresh	8.43	907	726	20.2	1.3	80.3
Mareu	Fresh	8.18	441	353	17.9	2.8	42.9
St. Dorcas	Brackish	8.76	3940	3152	47.6	4.4	328.0
Mdori	Brackish	9.70	4940	3952	56.2	5.3	430.1
Ngare Nanyuki	Brackish	8.92	3340	2672	59.7	114.0	353.3

Figure 5.1: Photos of sampling sites: (top left) Mareu; (top right) St. Dorcas; (bottom left) Mdori; (bottom right) Ngare Nanyuki

5.2.2 *Membrane set-point determination*

The performances (*e.g.* salt retention and permeate flux) of different membranes in treating the same water are only comparable at consistent operational conditions. Therefore an operational set-point was required for each water sample, where different membranes were under the same transmembrane pressure (TMP) and feed flow conditions. TMP was calculated by the following equation:

$$TMP = \left(\frac{P_2 + P_3}{2}\right) - P_{permeate} \tag{10}$$

where P_2 and P_3 are the pressures measured on the feed and concentrate sides of the NF/RO module (as shown on **Figure 2.4**).

As for ROSI, there are essentially two variables that can alter TMP and feed flow, namely the input power and the regulating valve on the concentrate stream. An SAS was used to

power the pump to ensure reproducible solar power quality for the experiments. With the same input power, membranes of different pore sizes have different TMP. Various combinations of input power and valve position were tested in order to find the set-point. Here is a brief description of the experimental procedure:

(1) Open an input power file with the required value (*e.g.* 240 W or 300 W) in the LabVIEW interface so that the solar simulator can generate the required power.

(2) Adjust carefully the position of regulating valve and record the resultant TMP and feed flow values (normally adjust 3−4 times for one input power file).

(3) Open another input power file and repeat Step (2).

As shown in **Figure 5.2**, for the NDRS tap water, all membranes reached a TMP of 5 bar and a feed flow around 510 L hr^{-1} with an input power of 180 W, so the set-point was selected at TMP 5 bar and feed flow 510 L hr^{-1}. For the Oldonyosambu sample, the set-point was at TMP 4 bar and feed flow 530 L hr^{-1} with an input power of 180 W. For the Mdori and St Dorcas samples, the set-point was at TMP 5 bar and feed flow 530 L hr^{-1} with an input power of 200 W. For the Ngare Nanyuki sample, the set-point was at TMP 5 bar and feed flow 575 L hr^{-1} with an input power of 240 W. It also shows that the pump could not maintain high flow rates at high input power, especially for samples whose salinity is relatively low (*e.g.* the NDRS tap sample).

5.2.3 *Simulated solar experiments at NDRS*

Simulated solar experiments at NDRS were conducted in batch mode, *i.e.* the permeate and concentrate were recycled into the feed tank to maintain a constant feed concentration. Prior to each experiment, ROSI was adjusted to the required set-point based on the type of water sample. All experiments were done with the same simulated solar energy. Specifically, ten hours solar irradiance data were collected throughout a sunny day of the dry season at NDRS and modified to suit experimental requirements (**Figure 5.3**A). The solar irradiance varied with the rising and setting of the sun and also fluctuated due to cloud cover. This can be seen in **Figure 5.3**A where the light passing cloud at 08:42 had a slight effect on the power generated by the photovoltaic panels, while the two lots of heavier clouds (13:36 and 13:46, and 14:02 and 14:12) drastically reduced the amount of power available. Regular sampling of feed, permeate and concentrate occurred at 0.25 to 1 hr intervals throughout the experiments for water analysis.
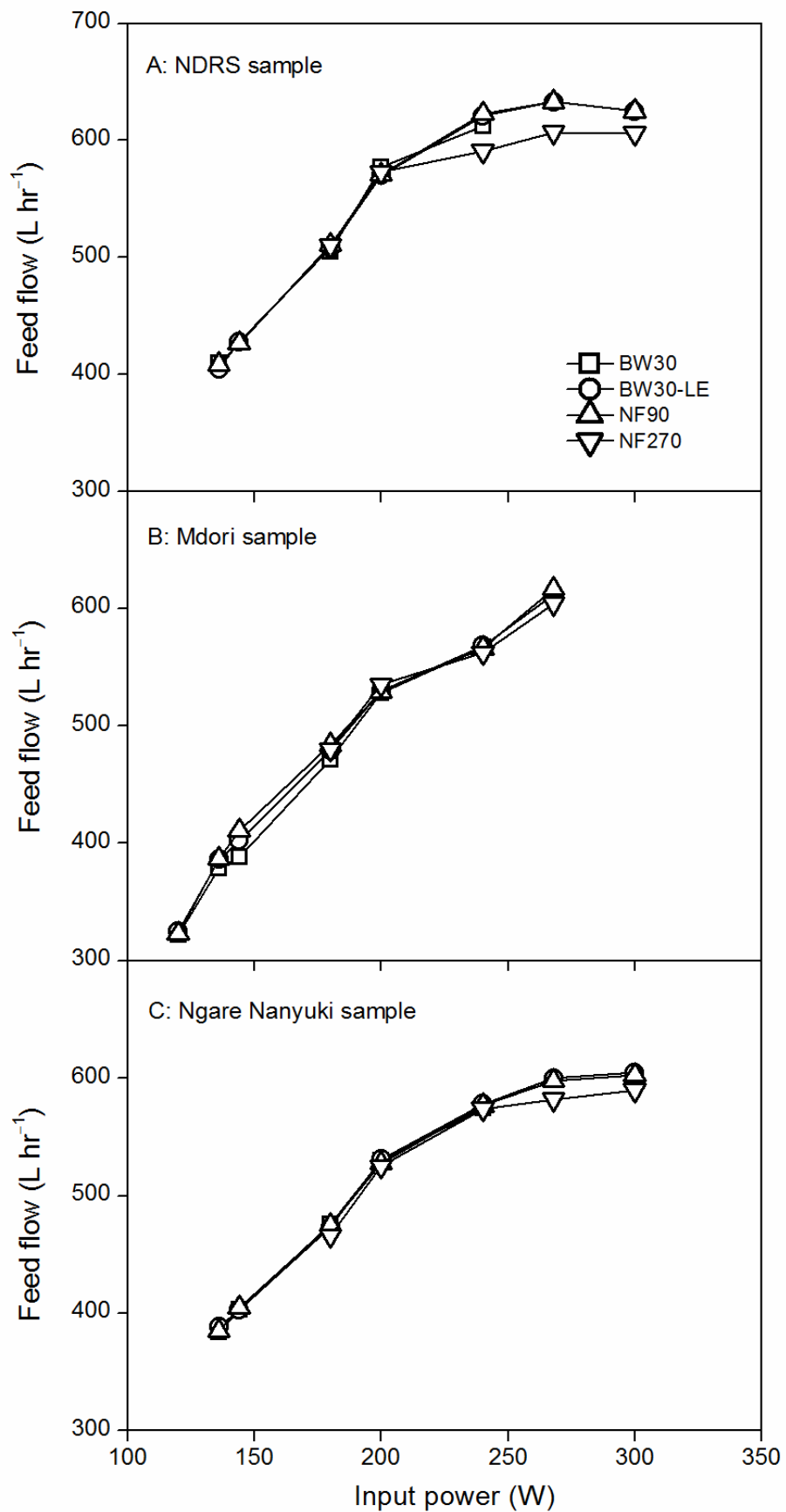
Figure 5.2: Feed flow of different membranes as a function of input power at a TMP of 5 bar
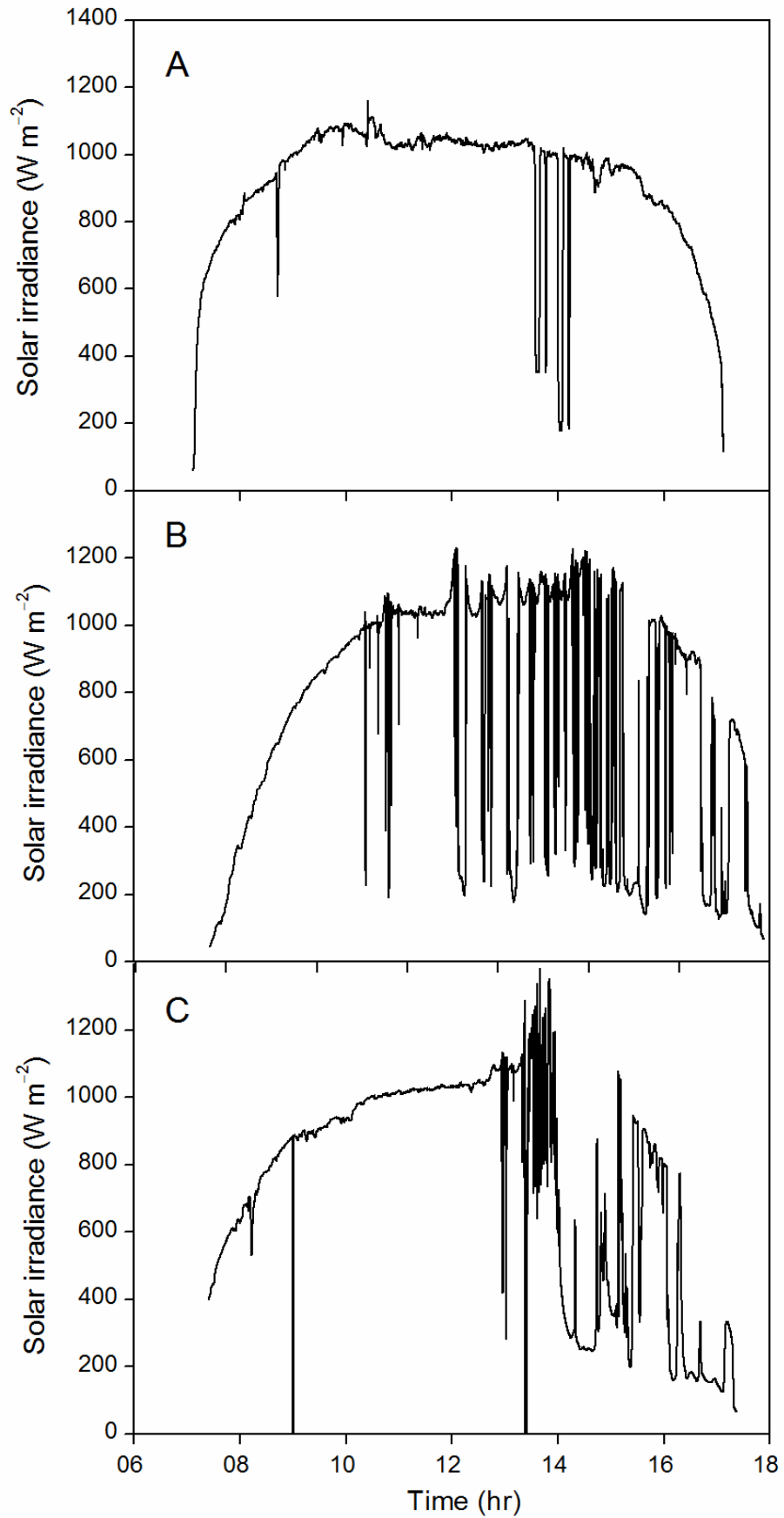
Figure 5.3: Solar irradiance of (A) a typical sunny day at NDRS; (B) a cloudy day at Mdori; and (C) a cloudy day at Ngare Nanyuki

5.2.4 Field experiments at Mdori and Ngare Nanyuki

In addition to conducting solar experiments at NDRS, ROSI's performance in treating water sources was evaluated at Mdori and Ngare Nanyuki during field experiments. The aims of the field experiments were (1) to test the performance of ROSI when powered directly by the sun and (2) to assess community acceptance for such advanced technology. The NF90 membrane was used and its operational set-point was adjusted using the solar array simulator prior to the field experiments. Then the ROSI pump was connected to solar panels. Field experiments were conducted in continuous mode. A Grundfos pump was used to transfer water from the source to the feed tank and was also powered by solar panels. Each field experiment started at sunrise and stopped at sunset. The solar irradiance data on the days of field experiments are shown in **Figure 5.3**B and **Figure 5.3C**. On these two days, the sky was very cloudy and cloud movements led to drastic energy fluctuations from noon untill sunset. Samples of feed, concentrate and permeate were taken at 0.5 hr interval.

Table 5.2: Summary of water quality for field experiments (uncertainty is ± 1% for *pH*, EC, TDS and F⁻, ± 5% for IC and ± 7% for TOC)

Source	Date	*pH*	EC (μS cm⁻¹)	TDS (mg L⁻¹)	F⁻ (mg L⁻¹)	TOC (mg L⁻¹)	IC (mg L⁻¹)
Mdori	2014/2/28	9.63	5150	4120	55.4	5.6	470
Ngare Nanyuki	2014/3/1	8.38	3580	2864	59.8	246	450

5.3 Impact of membrane types

The performance of different NF/RO membranes in treating five water samples is summarized in **Table 5.3**. Note that the values shown are average values calculated from numerous measurements throughout the solar day. The three key performance parameters are the permeate flux, salt retention and specific energy consumption (SEC). SEC (kWh m⁻³) was calculated using the following equation:

$$SEC = \frac{I_{pump} \times U_{pump}}{Q_{permeate}}$$

(11)

where I_{pump} is current (A) and U_{pump} is voltage (V), and $Q_{permeate}$ is the flow of the permeate (L hr⁻¹)

The first two parameters determine the water productivity and quality, while SEC values provide a measure of the energy efficiency of the process and are hence a major determining factor in capital costs (solar panels). Given that the solar irradiance was the same for all experiments, the water production and SEC of the system changed significantly with the membrane type.

As expected, the NF membranes had higher water productivity and energy efficiency but lower water quality than the RO membranes. The NF270 was the most energy-efficient membrane, but its permeate F^- concentration always failed to meet the WHO guideline. By contrast, the BW30 membrane produced very pure permeate water but with very small productivity and high energy cost. In between were the BW30-LE and NF90 membranes which had advantages of both high retention (RO) and high permeability (NF). The permeate F^- concentration by the BW30, BW30-LE, and NF90 membranes were below the WHO guideline of 1.5 mg L^{-1} for all the water samples, including the most challenging Mdori (F^- 56.2 mg L^{-1}) and Ngare Nanyuki (F^- 59.7 mg L^{-1}) brackish waters. Assuming a generous potable (drinking and cooking only) water consumption of 5 L per person, this system (equipped with either the BW30-LE or NF90 membrane) is in principle able to supply a remote community of almost 300 people with drinking water.

It is worth noting that the permeate EC by these tight membranes could be extremely low for fresh water samples (*e.g.* 10 and 12 µS cm^{-1} by BW30 and NF90 for the Mareu water). As a consequence, the treated water may lack the essential composition of minerals and result in an unpleasant taste. Some health experts believe that mineral-free water may be harmful to human health, leading to demineralization of the body [289] and in the case of malnourishment this may further aggravate the situation. Hence the RO treated water may require remineralisation post-treatment. This problem should however be considered as secondary compared to the health effects of fluoride and considered together with nutritional strategies. The NF270 membrane, on the other hand, allowed more ions to pass through due to its pore size. This reveals a major NF advantage over RO that NF removes salts selectively without requiring remineralisation. Clearly, choices exist regarding specific membranes with regard to the desired degree of purification and should be selected on a case by case basis.

Table 5.3: Comparison of average performance of NF/RO membranes for different water samples (Perm: Permeate; Ret: Retention. Uncertainty is ± 1% for EC, and F⁻, approximately ± 2% for EC and F⁻ retention and SEC)

Water	Membrane	Daily production (L)	Perm flux (L hr⁻¹ m⁻²)	TMP (bar)	Perm EC (µS cm⁻¹)	EC ret. (%)	Perm F⁻ (mg L⁻¹)	F⁻ ret. (%)	SEC (kWh m⁻³)
NDRS	BW30	1129	15.8	5.1	22	97.6	0.5	97.5	2.2
	BW30-LE	2136	29.7	5.6	12	98.7	0.3	98.5	1.0
	NF90	2773	36.5	5.8	16	98.2	0.4	98.0	0.9
	NF270	3033	39.9	5.3	276	69.6	5.7	71.8	0.8
Mareu	BW30	1000	13.8	4.5	10	97.7	0.6	96.6	2.2
	NF90	2444	32.3	4.4	12	97.3	0.4	97.8	0.9
	NF270	2656	34.9	4.3	120	72.8	3.7	79.3	0.8
St. Dorcas	BW30	735	10.2	5.0	79	98.0	0.6	98.7	3.4
	BW30-LE	1274	17.7	4.8	108	97.3	0.5	98.9	1.9
	NF90	1582	20.8	4.8	135	96.6	0.9	98.2	1.6
	NF270	2263	29.8	4.8	1415	64.0	14.2	71.9	1.1
Mdori	BW30	678	9.4	5.6	129	97.4	0.6	98.9	3.6
	BW30-LE	1146	16.0	5.5	167	96.6	0.8	98.5	2.2
	NF90	1416	18.6	5.4	237	95.2	1.1	98.0	1.7
	NF270	2369	31.2	5.2	2280	53.8	27.1	51.9	1.0
Ngare Nanyuki	BW30	707	9.9	5.0	62	98.1	0.5	99.1	3.4
	BW30-LE	1263	17.5	5.0	75	97.7	0.6	99.0	1.9
	NF90	1546	20.4	5.0	90	97.3	0.7	98.8	1.5
	NF270	2423	31.9	4.9	1161	65.2	18.0	69.8	0.9

Our results are comparable to many previous studies. Ghermandi and Messalem [290] applied a PV-powered NF system (equipped with two 4" NF90 membranes in one pressure vessel) to treat a brackish water of 2420 µS cm⁻¹. Under an operating pressure of 5 bar, the SEC of NF90 for that water was 0.89 kWh m⁻³ while the SEC of NF90 for brackish waters in our study was between 1.5 and 1.7 kWh m⁻³. Previous results from field trials in Australia treating brackish water of 8290 µS cm⁻¹ achieved a SEC of 1.5 kWh m⁻³ when using one NF90 membrane [190]. The SEC in the present work could be expected to be significantly lower given the lower salinity. The key difference in the experiments here is the use of set-point where a similar feed flow was achieved with each different membrane at roughly the same TMP. Indeed, it can be seen from other more controlled experiments in the past that treating the same 8290 µS cm⁻¹ feed water with a 4040 NF90 membrane at a similar set-point (TMP 5 bar, feed flow 500 L hr⁻¹) resulted in a SEC of 3.5 kWh m⁻³ [189]. This highlights the importance of choosing the correct membrane for treating each water source and then optimizing the system performance, in order to achieve the best safe operating window [291]. For a batteryless system with

multiple pumps, Schies *et al.* [292] emphasized that the power must be distributed according to the optimum operating point of each pump under every irradiation condition. In this way energy-efficient operation of the entire system can be achieved.

5.4   Impact of energy fluctuations on fresh water

The ROSI system used in this study had no batteries for energy storage and hence the power delivered to the pump fluctuated with solar irradiance. This section will discuss the impact of energy fluctuations on the performance of ROSI in treating fresh water from Mareu. The solar irradiance varies with the rising and setting of the sun and also fluctuates due to cloud cover. During periods of high solar irradiance – from 8:00 through to 15:30 (except for the noted passing clouds), the input power for the pump was high. The power stayed relatively constant during this time due to the use of a solar tracker, which mechanically tracked the path of the sun such that the panels were always normally incident and thus producing maximum power. It is worth noting that additional solar irradiance after 8:00 am did not result in an increase in system performance. This also relates to the relatively low set-point of the back-pressure valve. Due to the use of the open NF270 module in the set of experiments, the set-point was at a low TMP and for a high feed flow rate. Providing more power than this did not translate directly into a higher feed flow since the helical cavity pump had reached its limitation in terms of the number of revolutions per minute [191].

A step in the data can be seen in BW30 experiment (**Figure 5.4**A, B, C, D, F). This was due to corrosion of the bearings in the flow meter on the feed stream (Omega model FTB9512) which resulted in a jammed paddlewheel [191]. The decreased resistance across the feed flow meter caused a pressure drop of about 0.3 bar. The altered load of the system caused the maximum power point tracker to adjust the current and voltage to better match the output from the SAS. As a result, the permeate flux and SEC changed correspondingly. Recovery, which was calculated as the ratio of permeate to feed volume, was less affected compared to other parameters.

Power fluctuations affect the TMP (**Figure 5.4**B) and feed flow (**Figure 5.4**C), and hence other performance parameters such as permeate flux (**Figure 5.4**D). Permeate flux reduced when the solar power (and hence TMP) decreased. The immediate nature of the

response of permeate flux towards solar irradiance is due to the directly solar-powered pump which provides the driving force of the filtration process. Just after 14:00, when solar irradiance dropped from 1000 to 200 W m^{-2}, the permeate flux reduced significantly. In particular, the permeate flux of the BW30 module reduced from 15 L hr^{-1} m^{-2} to zero, highlighting the intermittent nature of the system. In previous work, Richards *et al.* [192] have investigated the effects of including energy buffering components to overcome such short term fluctuations.

Similar to flux, the recovery (**Figure 5.4**E) depends on the amount of power available to the system. The BW30 recovery (17%) was significantly less than the values for NF90 and NF270 (40% and 45%, respectively).

The SEC (**Figure 5.4**F) is directly affected by the changes of input power and the permeate flux. Due to the low salinity of the raw water sample the SEC value is very low and the observed increase of SEC during low power periods can be attributed to the small amount of water produced.

It is important to note that the feed water temperature increased by about 30% throughout a typical day (**Figure 5.4**G). The experiment was in batch mode, where the permeate and concentrate were recycled back into the feed tank. Therefore a significant amount of waste heat generated by the pump was transferred to the feed flow. In addition, the actual weather conditions, especially ambient temperature, naturally affected the water temperature in the system [191]. It is important to note that on the day when experiment NF90 was conducted a large thunderstorm started just before 15:00 and within the next hour the ambient temperature had dropped from 27.1 °C to 19.6 °C (**Figure 5.4**H). This led to the drop in the feed water temperature over the same period. In contrast, the ambient temperature on the day when the NF270 experiment was conducted was significantly higher, peaking at 31.6 °C just after midday before cooling down in the afternoon. Both of these factors contribute to the increased feed water temperature and affect the gradual increase of permeate flux over time. Such factors will of course alter performance of the system under real conditions.
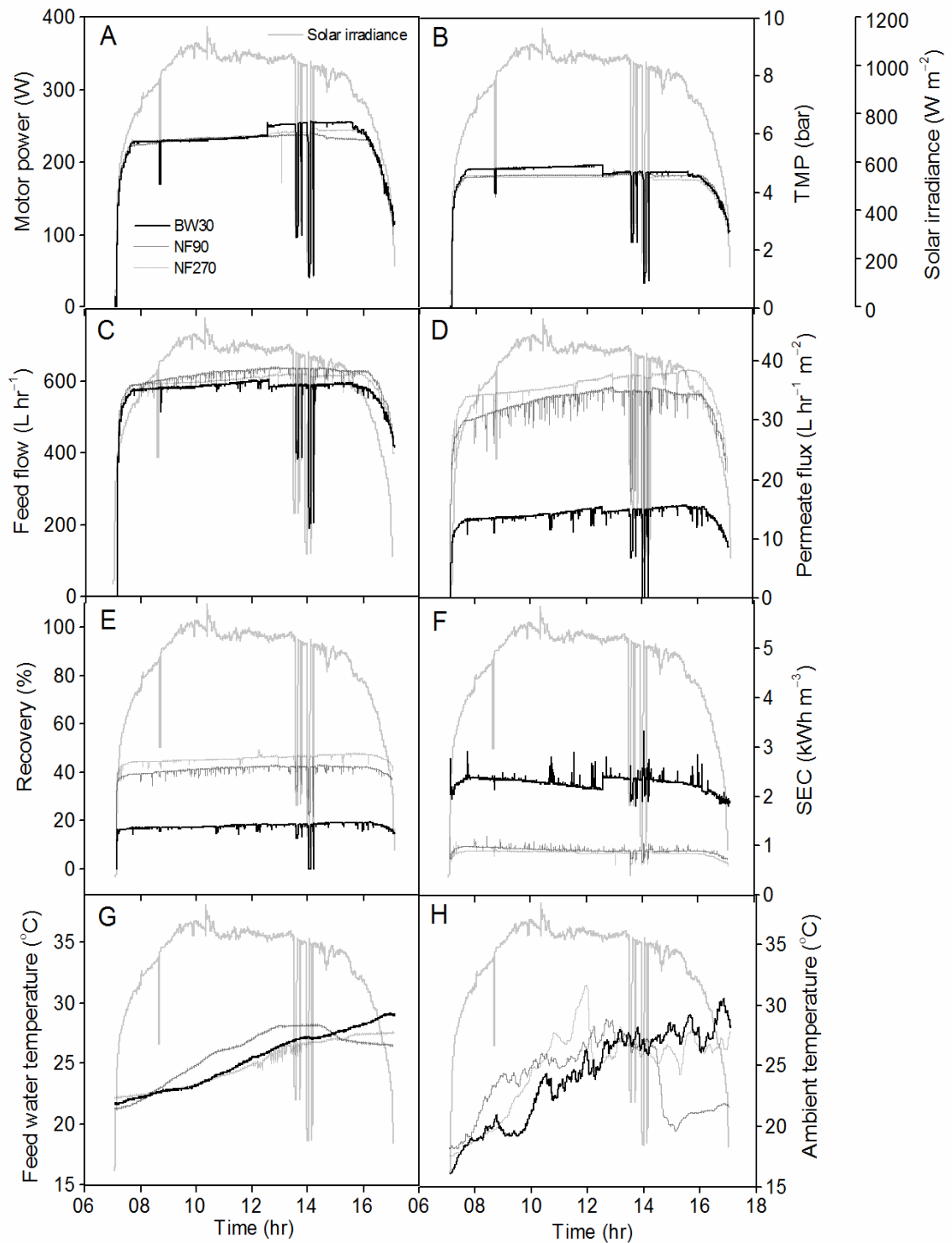
Figure 5.4: System performance throughout the solar day for Mareu water: (A) input power, (B) TMP, (C) feed flow, (D) permeate flux, (E) recovery, (F) SEC, (G) feed water temperature, and (H) ambient temperature

Despite slight energy fluctuations, average permeate fluoride remained well below the WHO guidelines throughout the day. **Figure 5.5** demonstrates the quality of permeate water produced by ROSI under a fluctuating weather condition. The last points in the

BW30 and NF90 curves in **Figure 5.5**A, as well as the ones just after 14:00 (large cloud passing) show that the permeate fluoride concentration increased with decreasing solar irradiance. Decreased solar power resulted in reduced crossflow velocity and thus increased fluoride diffusion due to concentration polarization [190].

For the BW30 experiment, the permeate flux dropped to zero for a short time after 14:00, where the permeate fluoride concentration experienced a dramatic increase (**Figure 5.5**A). The permeate fluoride concentration for the NF90 experiment remained well below the WHO guideline throughout the day despite slight changes with energy fluctuations. The permeate fluoride concentration for the NF270 experiment increased throughout the day. This is hypothesized to be related to the temperature change. Increasing water temperature can cause structural and morphological changes in the polymeric skin layer by increasing pore sizes while decreasing pore density [293]. The NF270 membrane is significantly more open than the other two and does not retain monovalent ions like fluoride well. Hence, any change in the membrane pore size and solute diffusivity caused by increased feed water temperatures will impact strongly on the retention. The effect is smaller for the tighter BW30 and NF90 membranes. The permeate EC and IC followed the same pattern as fluoride concentration changes (**Figure 5.5**B, C) throughout the solar day.

Figure 5.5D shows permeate TOC. The residual water in the system, energy fluctuations at 14:00, and the gradual increase of feed water temperature together affected the permeate TOC concentration, which is particularly evident in the NF270 experiment. By contrast, the tight BW30 and NF90 membranes showed high reliability to produce good-quality drinking water under such a fluctuating weather condition. Given the relatively low raw water TOC that will contribute to analytical errors, the collection and transport of a large volume for pilot studies at the NDRS in plastic tanks that may have resulted in contamination, this data should be treated with care.
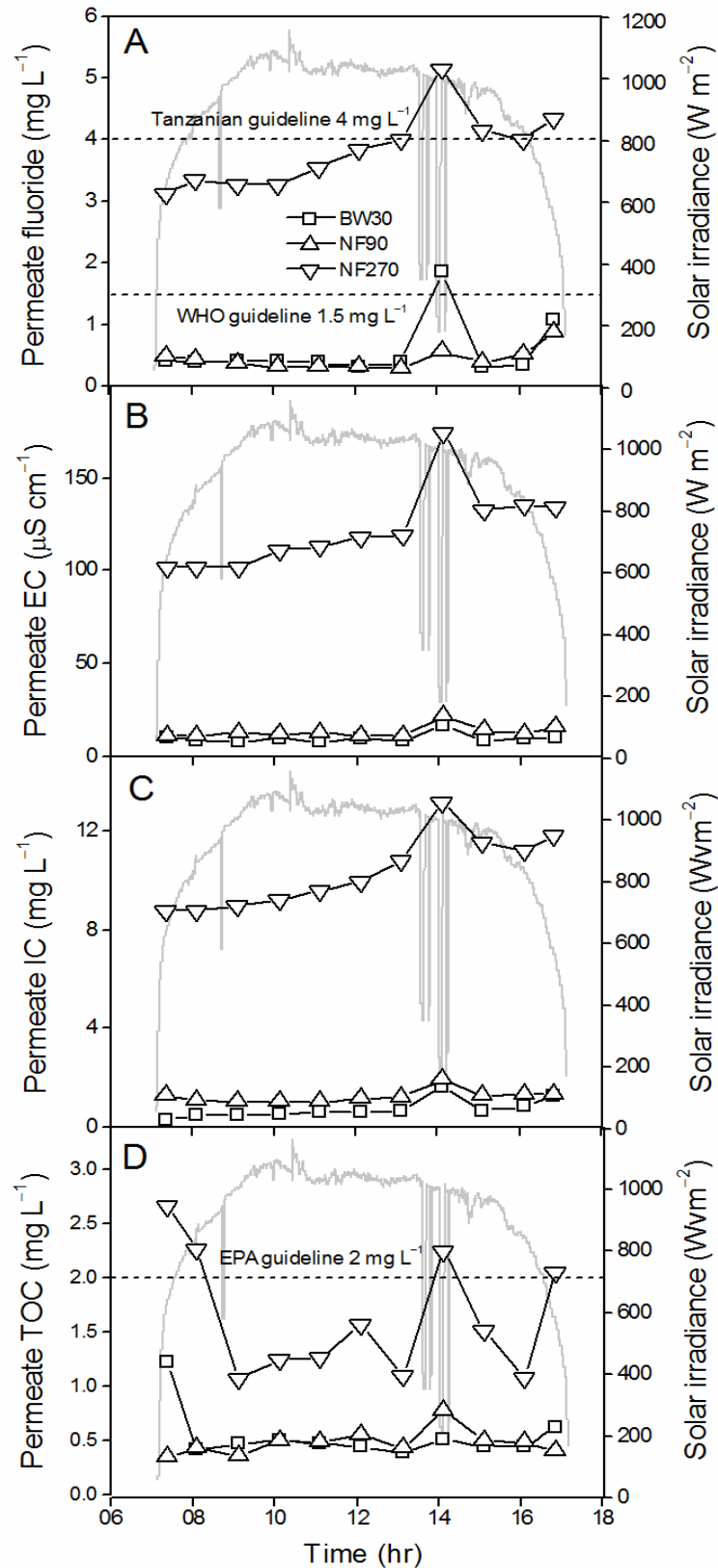
Figure 5.5: Permeate quality throughout the solar day for Mareu water: (A) permeate fluoride (B) permeate EC (C) permeate IC and (D) permeate TOC (uncertainty is ± 1% for permeate fluoride and EC, ± 5% for permeate IC and ± 7% for permeate TOC)

5.5   Impact of energy fluctuations on brackish water

Brackish waters have higher salinity and fluoride content than fresh waters and thus are more difficult to treat. St. Dorcas water was selected as representative brackish water. The performance of ROSI in treating St. Dorcas water under fluctuating solar conditions is shown in **Figure 5.6**. The general trend is similar to that observed for fresh water.

During periods of high solar irradiance (between 8:00 and 15:30), the input power (**Figure 5.6**A), TMP (**Figure 5.6**B), feed flow (**Figure 5.6**C), and therefore the permeate flux (**Figure 5.6**D) remain high. The movements of heavier clouds (at 13:36 and 13:46, and 14:02 and 14:12) drastically reduced the amount of power available. During the cloudy periods, the TMP and feed flow decreased and the pump would shut down if the power threshold was no longer met [294] (**Figure 5.6**B and **Figure 5.6**C). As for the BW30 membrane, when solar irradiance started dropping from 1000 to 200 W m^{-2} at 14:00, its feed flow reduced from 590 to 180 L hr^{-1}, and the TMP reduced from 6 to 0.8 bar. Permeate flux decreased from 12 L hr^{-1} m^{-2} to zero as a result of inadequate power (**Figure 5.6**D).

Over the whole solar day, the system only spent 9 min and 48 s in a state of temporary shutdown, however such intermittent operation had profound influence on the permeate water quality [295]. The recovery and SEC values depend on the hydrodynamic conditions and thus corresponded to the variations in pump power (**Figure 5.6**E and **Figure 5.6**F). The gradual increase of several parameters – feed flow, flux, recovery – as well as a decrease in SEC over time was driven by the increasing feed water temperature over the day (**Figure 5.6**G). This has also been observed in the above experiment using Mareu water and the primary reasons for this were: (1) waste heat generated by the pump that is transferred to the feed tank *via* permeate and concentrate flows, and (2) the increase in ambient temperature throughout the day (**Figure 5.6**H). Apart from the effects of energy fluctuation and temperature variation, the system did not show a decreased productivity over time, indicating the absence of membrane fouling, scaling or degradation.
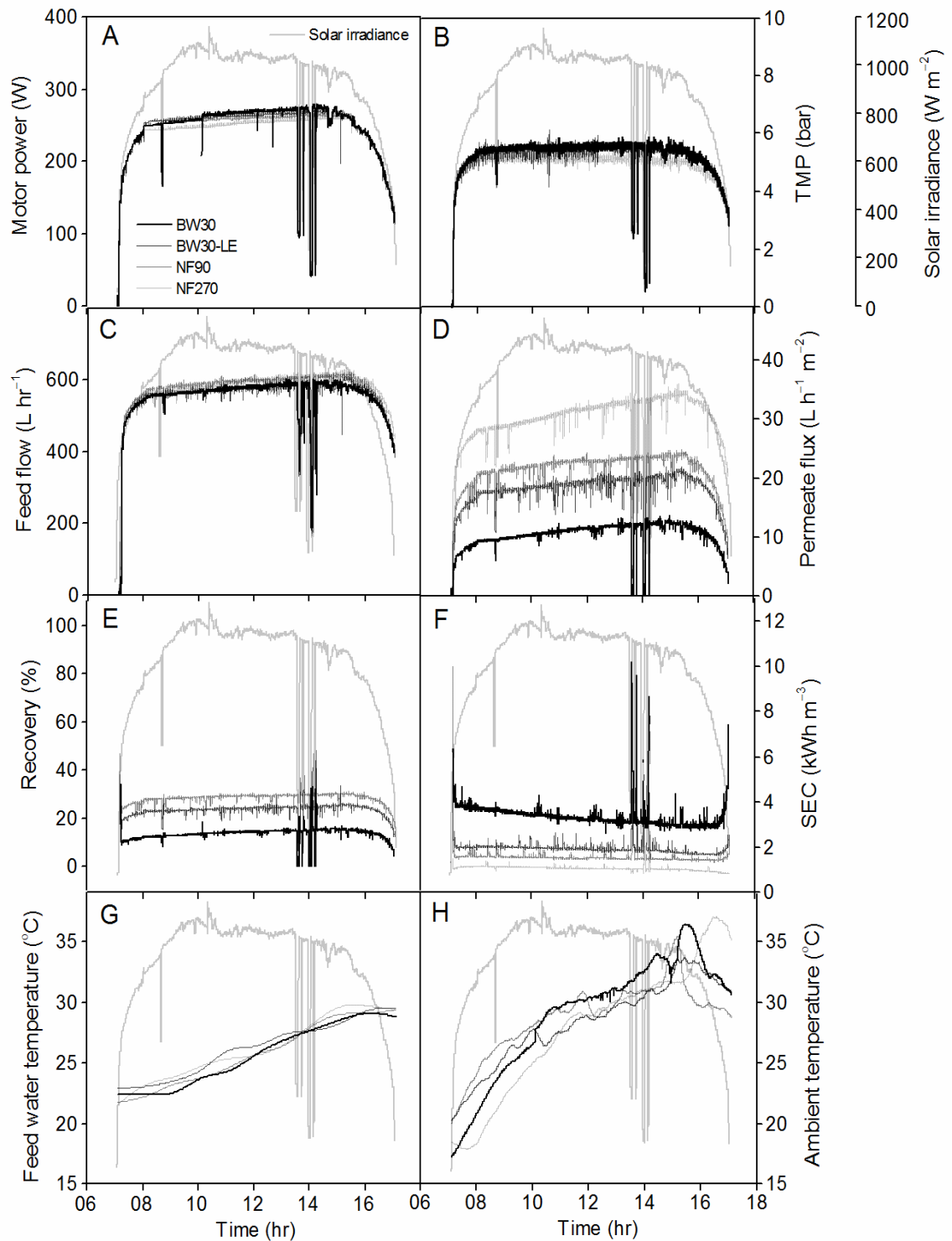
Figure 5.6: System performance throughout the solar day for St. Dorcas water: (A) input power, (B) TMP, (C) feed flow, (D) permeate flux, (E) recovery, (F) SEC, (G) feed water temperature , and (H) ambient temperature

Inevitably the variation of hydrodynamic parameters affects the retention of solutes. As seen from **Figure 5.7**, the permeate fluoride, EC, TOC and IC corresponded to solar irradiance in a similar manner, showing an abrupt peak during the period of largest energy

fluctuation in the afternoon. This is attributed to convection/diffusion mechanisms [294]. The decrease of solar irradiance resulted in the decline of feed flow, which reduced the crossflow velocity on the membrane surface and thus increased the thickness of the boundary layer [190]. As a result salt diffusion across the membrane was enhanced. The TMP and permeate flux also varied with solar irradiance. Permeate water flux dropped sharply at the lowest solar irradiance, which further concentrated the diffusing salts by reducing water permeation. The initial high values were due to the washing away of the solution which was remained in the system before the experiments. Despite the sudden increase during energy fluctuation, permeate concentrations (particularly for NF270) showed a slightly rising trend over time. As mentioned previously, this was attributed to an increasing feed water temperature, which resulted in a higher diffusion rate for salt through the membrane and also an increase in the effective pore radius of the membrane [296].

All the NF/RO membranes except for NF270, gave permeate fluoride concentration below the guideline most of the time. The instantaneous water quality exceeded the fluoride guideline only during the very brief energy fluctuation periods, which was found to have negligible effect on the average water quality because the volume of water produced during that period was extremely low. All the four membranes were able to meet the TOC guideline. These results demonstrate the short term robustness of the NF/RO system coupled with renewable energy to produce high-quality drinking water from brackish water under a fluctuating weather condition.
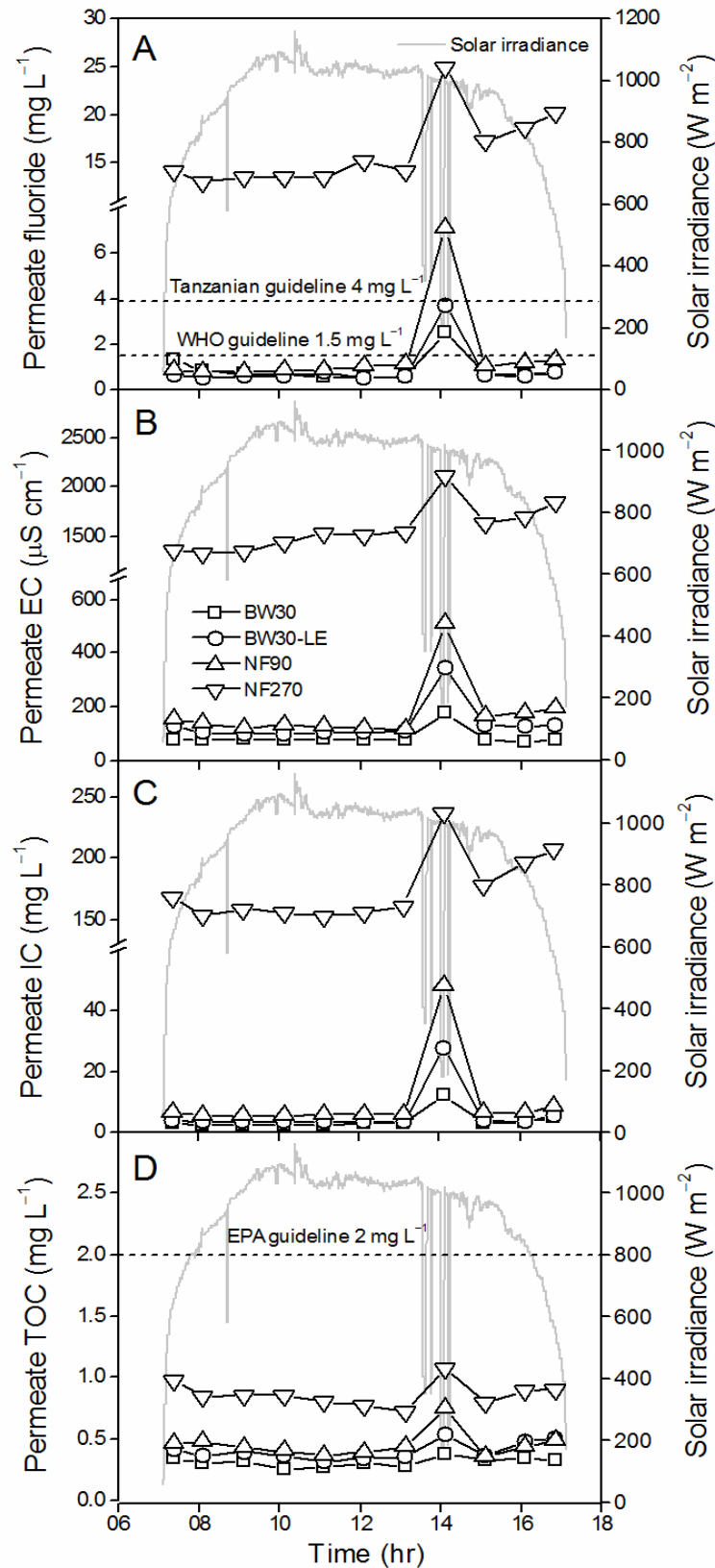
Figure 5.7: Permeate quality throughout the solar day for St. Dorcas water: (A) permeate fluoride (B) permeate EC (C) permeate IC and (D) permeate TOC (uncertainty is ± 1% for permeate fluoride and EC, ± 5% for permeate IC and ± 7% for permeate TOC)

5.6   Field experiments

Mdori, a remote village near Lake Manyara, was selected for field experiments. The weather is hot and dry and water sources are rare. Several years ago the Anglican Church paid money to drill a borehole for villagers. However, it turned out that the water overflowing from the bore was very salty with high fluoride concentration (nearly 60 mg L^{-1}). Therefore villagers used this water for washing purpose only, in fact the water is soapy due to high IC level.

The field experiment at Mdori was conducted on a cloudy day (**Figure 5.3**). ROSI was installed in the morning, before sunrise, near the borehole. As the sun rose, the system started to work. The permeate was collected into a 1000 L tank and the F^- concentration was frequently monitored. The concentrate was discarded back to the puddle around the borehole.

The performance of ROSI is summarized in **Table 5.4**. Because of the cloudy weather, the solar irradiance received at Mdori was significantly lower than that at NDRS. This led to a lower TMP and thus a lower permeate flux. The permeate quality was not as good as the one at NDRS as a result of huge energy fluctuations. However, fluoride concentration in the product tank was always below the WHO guideline of 1.5 mg L^{-1}, making the water safe for drinking. A practical problem that still needed solving was the unpleasant smell of the water due to hydrogen sulfide gas, which could not be removed by ROSI. A post-treatment method that employs a degasifier was recommended for future practice.

Table 5.4: Summary of ROSI performance in treating natural waters in the field (Perm: Permeate; Ret: Retention. Uncertainty is ± 1% for EC, and F^-, approximately ± 2% for EC and F^- retention and SEC)

Water	Daily production (L)	Perm flux (L hr^{-1} m^{-2})	TMP (bar)	Perm EC (µS cm^{-1})	EC ret. (%)	Perm F^- (mg L^{-1})	F^- ret. (%)	SEC (kWh m^{-3})
Mdori	1226	15.5	4.1	314	94.0	1.3	97.6	1.4
Ngare Nanyuki	1156	15.3	4.2	92	97.4	0.7	98.8	1.6

The other field site, Ngare Nanyuki, is located at the source of Maji ya Chai River. The water has a brownish colour due to abundant NOM content. On the day of the experiment, the TOC concentration in the water was found to be 246 mg L^{-1} and the fluoride concentration was 59.8 mg L^{-1}. The weather was overcast, especially in the afternoon.

Therefore the TMP and permeate flux in this field experiment were both lower than those recorded in previous experiments at NDRS. Overall, the permeate quality was still satisfactory with fluoride concentration of 0.7 mg L^{-1}, meeting the WHO guideline.

An interesting observation in this field experiment was NOM fouling on the UF membrane. Just 1.5 hr after ROSI started, the suction pressure at the UF membrane decreased from −0.3 to −0.7 bar, and the permeate flux decreased from 19.7 to 16.8 L hr^{-1} m^{-2}. In order to reduce NOM fouling on the UF membrane, an air bubbler was used to increase aeration in the UF tank. The air bubbler was powered by a standalone petrol generator, which was turned on at 9:23 am. The generated bubbles agitated water in the feed tank and facilitated the removal of deposits from the UF membrane. Consequently, the suction pressure went back to −0.3 bar and the permeate flux increased to 19.7 L hr^{-1} m^{-2}. TOC in the UF permeate (which was also the feed for NF) reduced from 208 to 131 mg L^{-1} (**Figure 5.8**). As the air bubbler was on, TOC in the feed increased drastically attributed to the continuous filling of raw water, while TOC in the UF permeate remained stable. Then at 12:24 pm when the air bubbler stopped because the generator was overheating, NOM quickly accumulated on the UF membrane, resulting in a sudden drop of TOC in the feed and a sharp increase in the UF permeate. The air bubbler was turned on again and the fouling on the UF membrane was soon eliminated.

Unlike the UF permeate, the NF permeate was not affected by NOM fouling. TOC in the NF permeate remained in the narrow range of 0.2−0.4 mg L^{-1} most of the time. The only increase of TOC in the NF permeate was at the end of experiment when weak solar irradiance led to low TMP and feed flow and therefore intensive concentration polarization on the NF membrane surface.
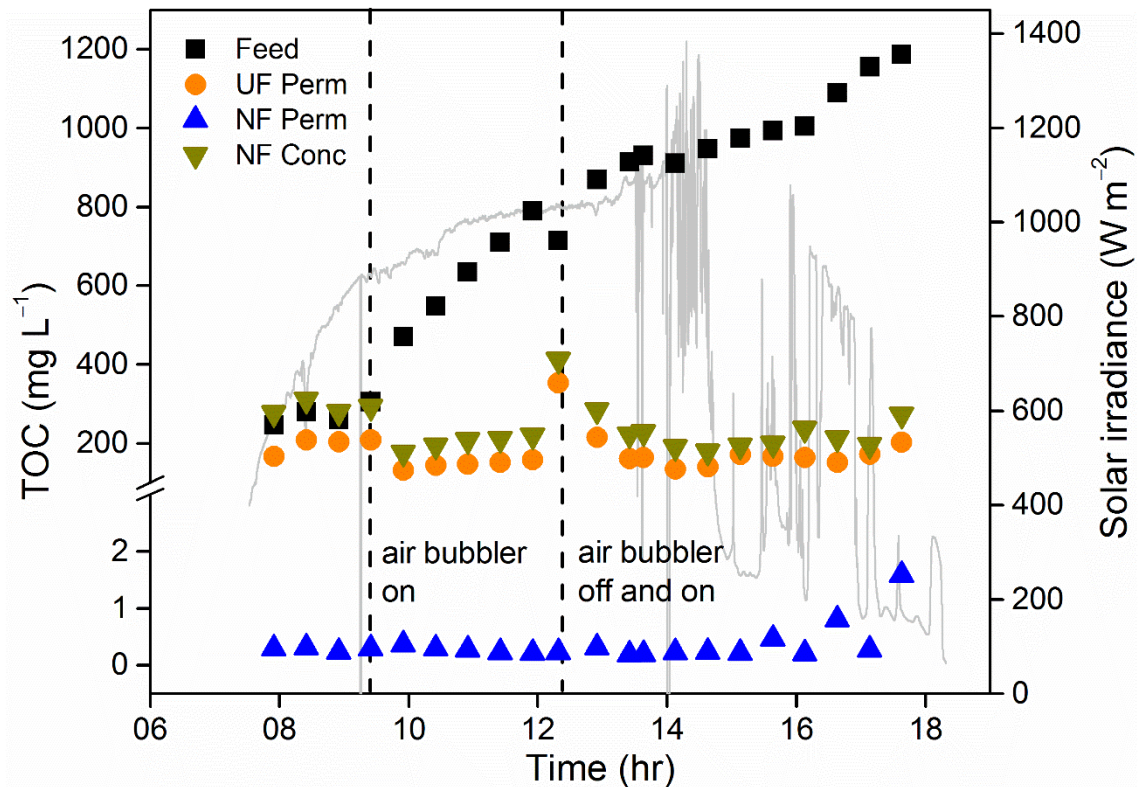
Figure 5.8: Variation of TOC in the feed, concentrate and permeate with time in the field experiment at Ngare Nanyuki (Perm: Permeate; Conc: Concentrate) (uncertainty is ± 7% for TOC)

Our field experiments at Mdori and Ngare Nanyuki attracted many visitors (**Figure 5.9**). We offered the treated water to curious villagers for tasting. People were surprised to see the "untreatable" water became potable. They called our water "Maji Safi", which means safe water in Swahili. News traveled fast and more and more people came to take the water. There were children and women with buckets on their heads, and men carrying containers on their bicycles and motorbikes. They were thrilled to get such good quality drinking water near home, whereas collecting drinking water from outdoor sources could normally cost them several hours.

We also received students from local primary and secondary schools. We explained them the basic mechanisms of membrane filtration and demonstrated the operation of ROSI system. We were impressed by the scientific questions the students asked and more importantly, by their strong interest on learning new technology.

Figure 5.9: Photos taken during the field experiments: students from Mdori Primary School watching ROSI and trying the treated water (left); children drinking the treated water at Ngare Nanyuki (right)

5.7   System sustainability

In the last five decades, different research teams have visited villages in northern Tanzania with the goal to alleviate health problems associated with insufficient water supply and poor water qualities [192, 297-299]. So far, only the technique of bone char adsorption columns has been adopted but its implementation is found to be far from satisfactory [300]. This indicates the need to ensure that the communities are fully aware of the problem and actively engage in the solution – most importantly *via* committing some of their own resources – to ensure that systems are sustainable in long term operation.

Montgomery *et al*. [284] identified three components of sustainability for water supplies in developing countries as (1) effective community demand; (2) local financing and cost recovery; and (3) dynamic operation and maintenance. Membrane technologies are superior to meet community water demands as modular membrane systems can be easily sized to different scales, and can be coupled with hybrid power systems. Costs of such advanced membrane systems have always been regarded as the main limitation for rural areas [301]. However, considering the cost of unsuccessful boreholes, it could be worthwhile for the government and NGOs to invest in the capital costs of water treatment systems instead [301]. In addition, previous studies indicated that in developing countries, the general costs estimated for decentralized membrane systems are within the range of some untreated water costs such as tanker trucks and water vendors, and well below infrastructure costs of centralized systems with medium range distribution [288,

301]. Setting the optimum price for the treated water is of crucial importance for cost recovery as many villagers prefer to use free untreated water sources when the prices are too high. Charging high-quality (drinking) water and low-quality (washing) water at different prices seems to be a logical solution and this is indeed already practiced by many villages.

Operation and maintenance is probably the most significant obstacle for adopting defluoridation systems in remote locations [300]. While training of local technicians should be a mid- to long-term goal, technical support from the suppliers must accompany the early adopters of such technologies and this support has to be included in the system cost to ensure feasibility and sustainability [191]. The long-term integration of such RE-membrane systems requires comprehensive assessment from a techno-socio-economic perspective and solid strategies at a local level. Research into suitable business plans, operation and maintenance regimes is currently under way to develop creative and responsible solutions.

5.8   Conclusions

This chapter evaluated the performance of a pilot-scale solar-powered membrane system in treating high-fluoride fresh and brackish waters in northern Tanzania. In rural areas with limited fresh water supply but abundant brackish water resources, brackish water desalination may be considered as a sustainable solution. The BW30, BW30-LE and NF90 membranes were efficient for removal of fluoride, salinity and TOC from both the fresh and brackish waters. Among these, the NF90 membrane achieved the optimum balance between water quality and energy efficiency. Throughout a typical solar day, the system equipped with NF90 could produce about 2500 L drinking water meeting the WHO guideline for fluoride from a high-fluoride fresh water source, or 1500 L drinking water from a high-fluoride brackish water source.

The fluctuations of solar irradiance resulted in variations in feed flow and TMP, which caused the water quality exceeding the guidelines on occasion as a result of concentration polarization. However, over the daily operation, the average water quality was invulnerable to energy fluctuations given the produced volume, indicating the high reliability of the system.

In summary, RE-membrane technology provides a promising solution for safe drinking water supply in small communities in rural areas. Both technology and methodology in this study are transferable to any remote location in the world where dissolved contaminants are of concern. This study is intending to encourage further work to adapt such decentralised and advanced technologies for those rural locations where water quality is posing particularly difficult challenges. Future research on long-term performance, operating and maintenance strategies, economic feasibility and social acceptance is needed.

Chapter 6: Photocatalytic Polymers for Decontamination and Disinfection

6.1 Introduction

Chapter 4 and Chapter 5 investigated the feasibility of membrane technologies in producing drinking water, with an emphasis on the removal of natural contaminants, particularly fluoride ions and NOM. The work presented in this Chapter extends the research scope to wastewater treatment which needs very different strategies and methods compared to drinking water production. Due to the diversity of wastewater sources (domestic, industrial, and agricultural), the contaminants found in wastewater are varied and numerous. They include, but are not limited to, heavy metals, ammonia, pathogens, and a variety of emerging contaminants such as pharmaceuticals, pesticides, and EDCs. Unlike natural contaminants which have relatively low environmental hazards, wastewater contaminants are harmful to both humans and the environment. Therefore wastewater effluents require high levels of decontamination and disinfection. Furthermore, wastewater effluents often have a wide range of *pH* values (from 2 to 12), and elevated temperatures (up to 90°C in the dyeing wastewater) [302]. Suitable treatment methods should be chemically and thermally stable.

As discussed in Chapter 1, photosensitization is a promising tool for wastewater treatment. $^1O_2$ generated from photosensitization can degrade organic compounds and inactive microorganisms at the same time. A major issue limiting photosensitization is the recovery of the photosensitizer from water. This problem can be solved by immobilizing the photosensitizer onto a solid support which allows it to be easily recovered and reused [150]. Many common photosensitizers, such as Rose Bengal, 5,10,15,20-tetrakis(*p*-hydroxyphenyl)porphyrin, and C$_{60}$ aminofullerene, have been immobilized on different solid supports, including silica nanoparticles [303], silica gels [304], chitosan [305], and some hydrophilic polymers [306]. Immobilization can also increase the photostability because the matrix constitutes an efficient oxygen diffusion barrier that inhibits photobleaching [307]. For similar reasons, the quantum yield and thus the photocatalysis efficiency of the photosensitizer might be reduced after

immobilization [150]. Nevertheless the benefits of having a heterogeneous and stable photosensitising system outweigh the lower photocatalysis efficiency.

This chapter reports the synthesis of an organic photosensitizer and its incorporation into polymers. The $^1O_2$ productivity and stability of these materials were assessed in both organic and aqueous media under visible light irradiation. Two emerging contaminants, *i.e.* BPA and cimetidine, and one microorganism *Cryptosporidium* were treated by the photocatalytic polymers. At the end of the chapter, the potential configurations of photocatalytic membrane reactors are discussed.

6.2   Experimental summary

6.2.1   *Suzuki coupling*

The photosensitizer monomer was synthesized through Suzuki-Miyaura reaction, which is also referred to as the "Suzuki coupling". This reaction was named after its first reporter Akira Suzuki who shared the 2010 Nobel Prize in Chemistry with other two chemists for their contributions in developing palladium-catalysed cross couplings in organic synthesis. The prevailing mechanism is shown in **Figure 6.1**, where a carbon-carbon single bond (R_1-R_2) is formed by coupling an organoboron compound (R_2-BY_n) with an organic halide (R_1-X) using a palladium catalyst (Pd) and a base (NaZ). The letters X, Y, and Z refer to different ligands.

The Suzuki coupling reaction consists of three steps [308]. The first step is the oxidative addition of palladium to the halide where the palladium catalyst is oxidized from Pd(0) to Pd(II) (The numbers in bracket indicate the oxidation states). The oxidation addition step breaks the carbon-halogen bond to form organopalladium species ($R_1-Pd(II)-X$). The second step is a transmetalation. The base NaZ is believed to facilitate the formation of $R_1-Pd(II)-Z$ from $R_1-Pd(II)-X$, and also activate R_2-BY_n. The ligand R_2 is then transferred from the activated R_2-BY_n-Z to $R_1-Pd(II)-Z$ to form the new $R_1-Pd(II)-R_2$ complex. The exact mechanism of transmetalation in Suzuki coupling is still unclear [309]. The final step is the reductive elimination step where the product R_1-R_2 is eliminated from the $R_1-Pd(II)-R_2$ complex and the Pd(0) catalyst is regenerated.

Suzuki coupling is one of the most efficient methods for the construction of carbon-carbon single bonds [308]. Compared to other similar reactions, Suzuki coupling utilizes boronic acids and esters which are relatively cheap and less toxic compared to organostannane and organozinc compounds. Water can be used as a solvent in Suzuki coupling, allowing the use of a variety of water-soluble reagents for making many different organic molecules [310].
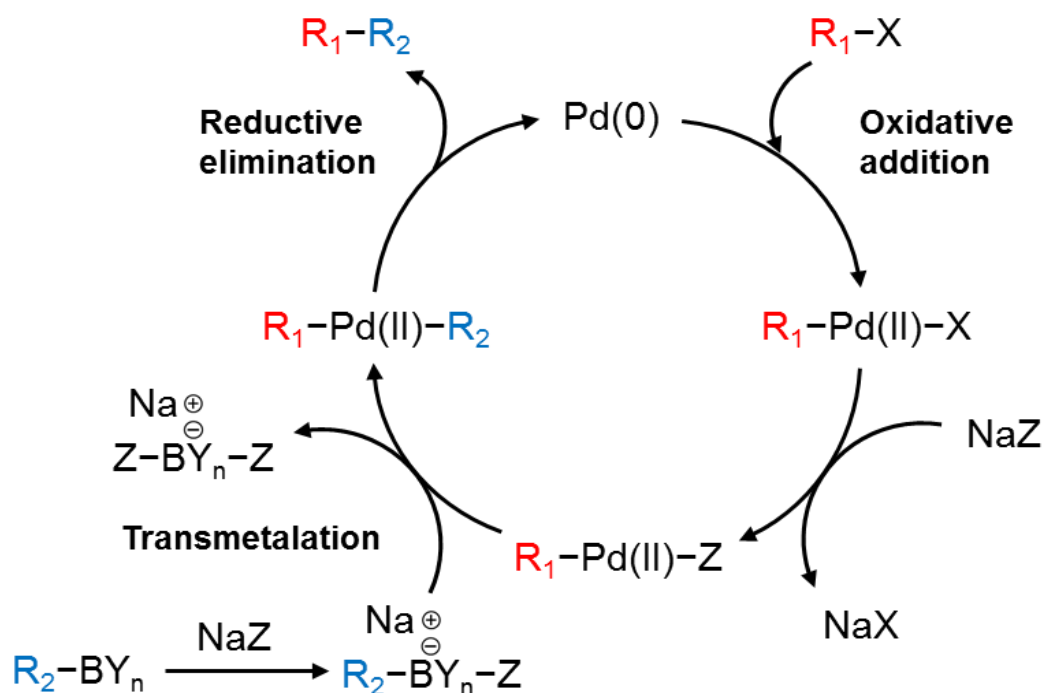
Figure 6.1: Schematic of Suzuki coupling

6.2.2 *Synthesis of the photocatalytic polymers*

The photosensitizer monomer ABT was synthesized through Suzuki coupling of 4-bromoaniline with 4,7-bis(boronic pinacol ester)-2,1,3-benzothiadiazole in the presence of a Pd(0) catalyst (**Scheme 1**). Benzothiadiazole (BT) is a strong electron-accepting moiety due to its small electronic band-gap and high absorption coefficient [311]. The combination of BT with weak electron-donors increases the yield of intersystem crossing to the triplet state, leading to the formation of an efficient photosensitizer [311]. Details of the synthesis are included in Chapter 2.1.
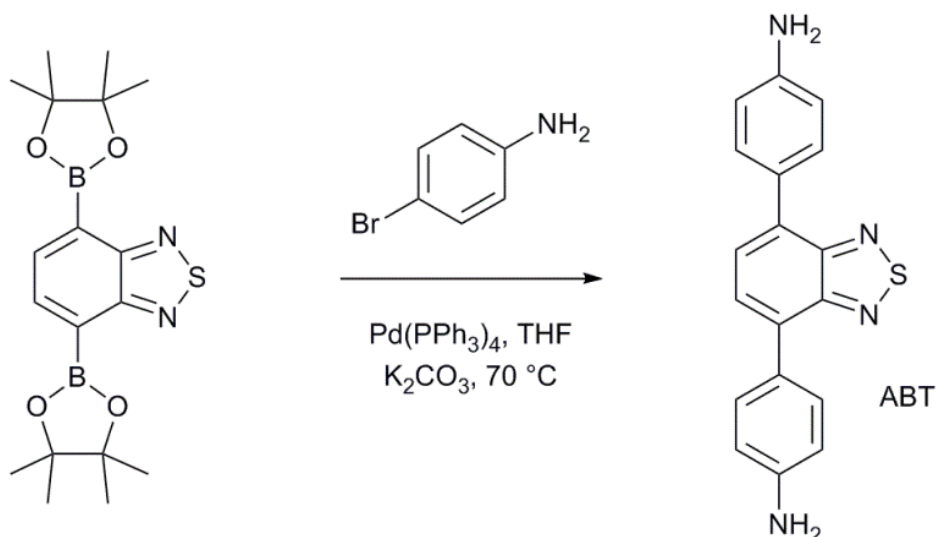
Scheme 1: Synthetic scheme of the photosensitizer monomer

As a reference to the photocatalytic polyamides, the non-photocatalytic polyamide was prepared *via* a metal-free polymerization reaction of trimesoylchloride (TMC) and m-phenylendiamine (MPD) (**Scheme 2**) [87]. The mole ratio of TMC and MPD in the polymerization reaction was fixed at a 2 to 3 ratio. MPD was dissolved in deionized water, and TMC was dissolved in dichloromethane (CH_2Cl_2). The solution of TMC was stirred at 750 rpm and MPD were quickly added. The reaction mixture was stirred at room temperature for 16 hr and then heated to 50 °C for 30 min. A precipitate formed which was filtered and washed with deionized water and methylene chloride. The solids were dried in vacuum at 98 °C to remove water.

The photocatalytic polyamides were synthesized *via* the same metal-free polymerization method but using certain amount of ABT to replace MPD (**Scheme 3**). Similar to MPD, ABT also contains diamine groups and can thus undergo polymerization reaction with TMC. ABT was dissolved in THF and added into the MPD solution together with the TMC solution. The subsequent steps were the same as mentioned above. In this way the photosensitizer monomer was introduced into the polyamide backbone during the polymer synthesis. Specific quantities for ABT and MPD can be found in **Table 6.1**. For each polymerization, the product was named as PA-ABT (x%). For example, PA-ABT (25%) indicated that 25% of MPD (mole fraction) was replaced by ABT. Please note that this number did not represent the percentage of ABT in PA.

Table 6.1: Composition of synthesized polyamides

	ABT		MPD	
% of ABT	**Mass (mg)**	**mmol**	**Mass (mg)**	**mmol**
0	–	–	18.8	0.174
3	1.7	0.005	18	0.167
5	2.7	0.009	17.6	0.163
10	5.5	0.017	16.7	0.155
15	8.2	0.026	15.8	0.146
25	13.7	0.043	13.9	0.129
50	27.3	0.086	9.3	0.086
75	41.0	0.129	4.6	0.043
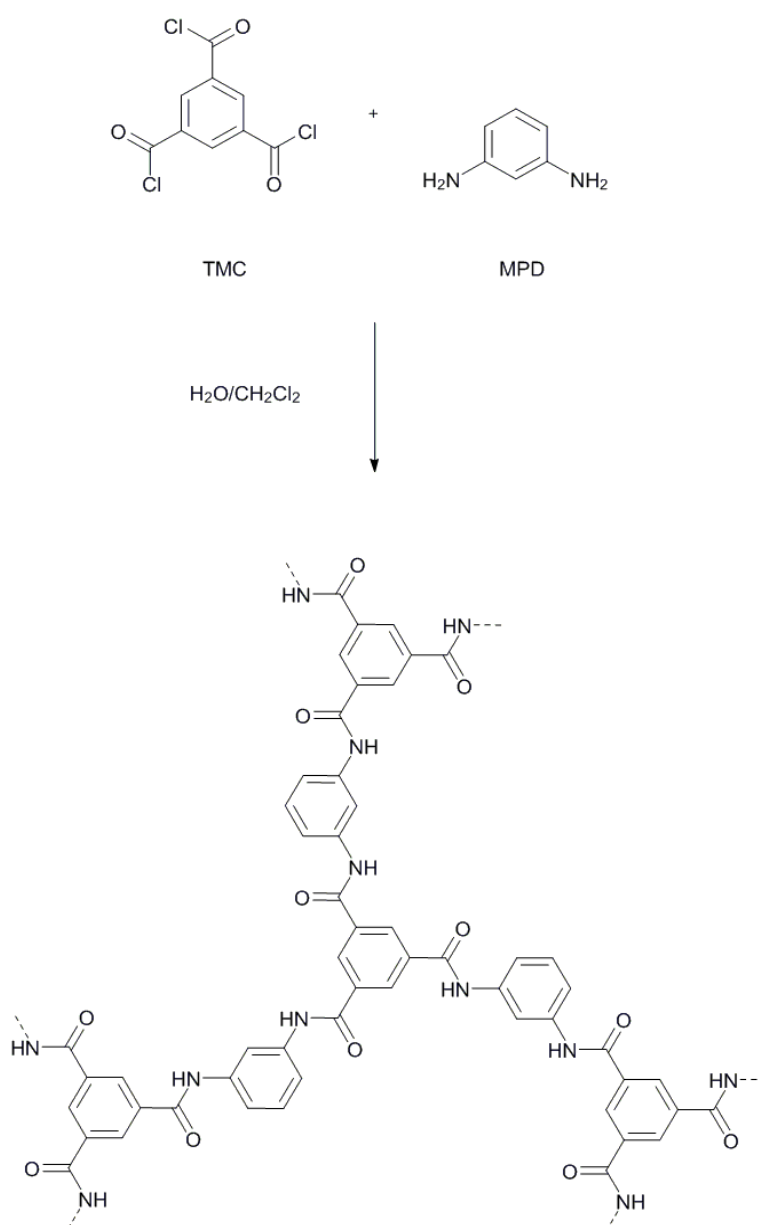
Scheme 2: Synthesis of non-photocatalytic polymer *via* polymerization
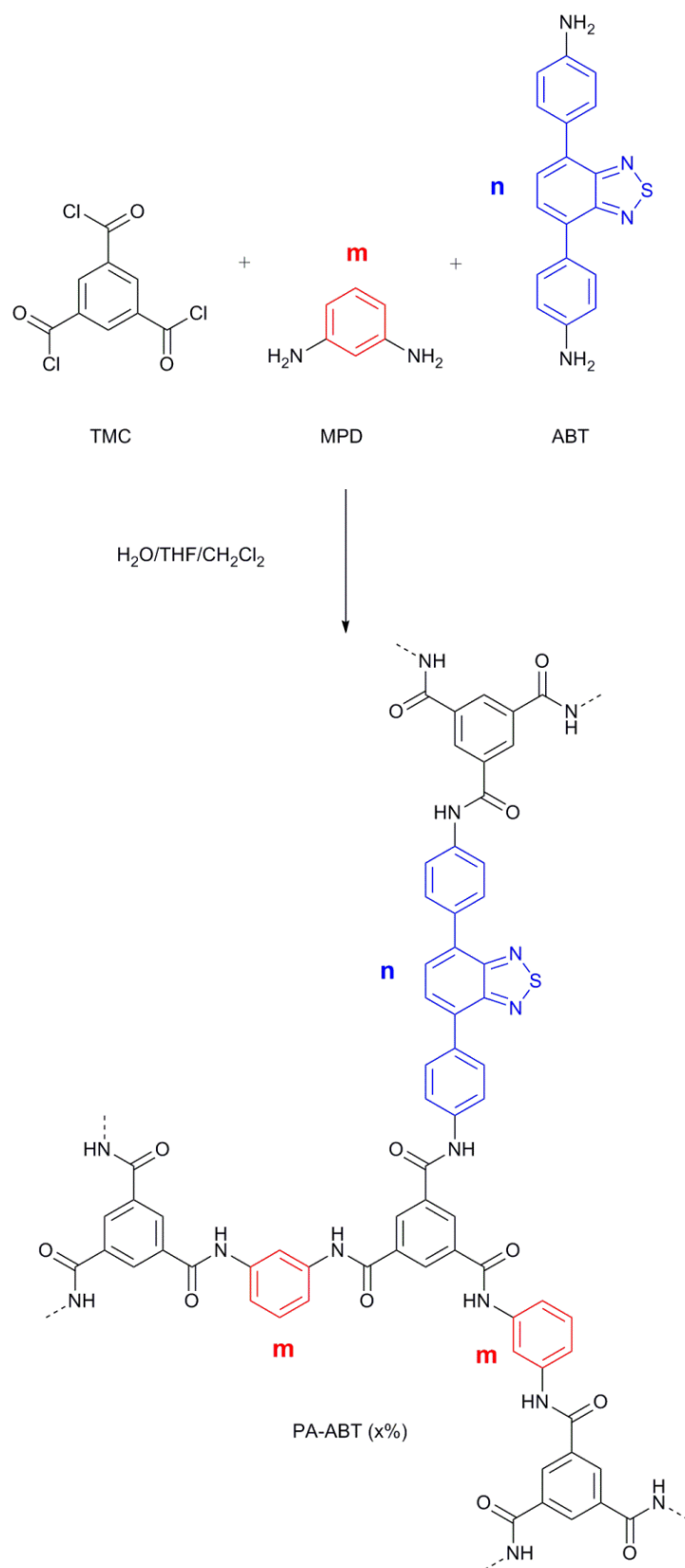
Scheme 3: Synthesis of the photocatalytic polymer and representation of a possible fragment of the polymer network

6.2.3 *Decontamination and disinfection experiments*

Decontamination experiments were conducted in a commercial flow reactor (as described in Chapter 2). Compared to conventional batch systems this offers consistent light penetration and controlled exposure times, which leads to more efficient $^1O_2$ generation. ABT monomer or PA-ABT (x%) were added into a 20 mL solution containing target molecules (α-terpinene, FFA, BPA or cimetidine). FFA conversion by PA-ABT (25%) was repeated over five cycles in order to test the photostability of the polymers. After one cycle of photoreaction, PA-ABT (25%) was separated through centrifugation and washed with water before being used in the next cycle. Negative control experiments were performed using the same procedure in the absence of photosensitizer or light, or oxygen.

The disinfection capacity of PA-ABT (25%) was assessed through a *Cryptosporidium* inactivation experiment. Four samples were prepared and each sample contained 1 million oocysts in 200 µL phosphate-buffered saline solution (**Table 6.5**). Sample 1 and 2 had no PA-ABT (25%) while Sample 3 and 4 each contained 50 mg L^{-1} PA-ABT (25%). Sample 2 and 4 were exposed to visible light at 420 nm wavelength for one hour. To ensure adequate oxygen mixing, the samples were vortexed every 10 min.

6.3 Characterization of ABT monomer and polymers

In order to check whether the ABT monomer was successfully incorporated into the polymer, both the ABT monomer and polymers were characterized by UV/Vis, FT-IR and NMR.

The ABT monomer was obtained as a light orange powder while the polymers were yellow powders. The solid-state UV/Vis absorption spectrum (**Figure 6.2**) of ABT shows a broad absorption band between 350 and 500 nm with maximum at 435 nm (Soret band), which is assigned to the transition from the electron-donating moiety to the electron-accepting BT moiety [312]. This absorption band was scarcely shifted after ABT was incorporated into polyamide, indicating that no electronic interactions occur between the ABT and TMC monomers. The pure PA, on the other hand, had no adsorption peak at 435 nm. The fluctuations observed at low wavelength (300−400nm) in **Figure 6.2** are due to aromatic groups.
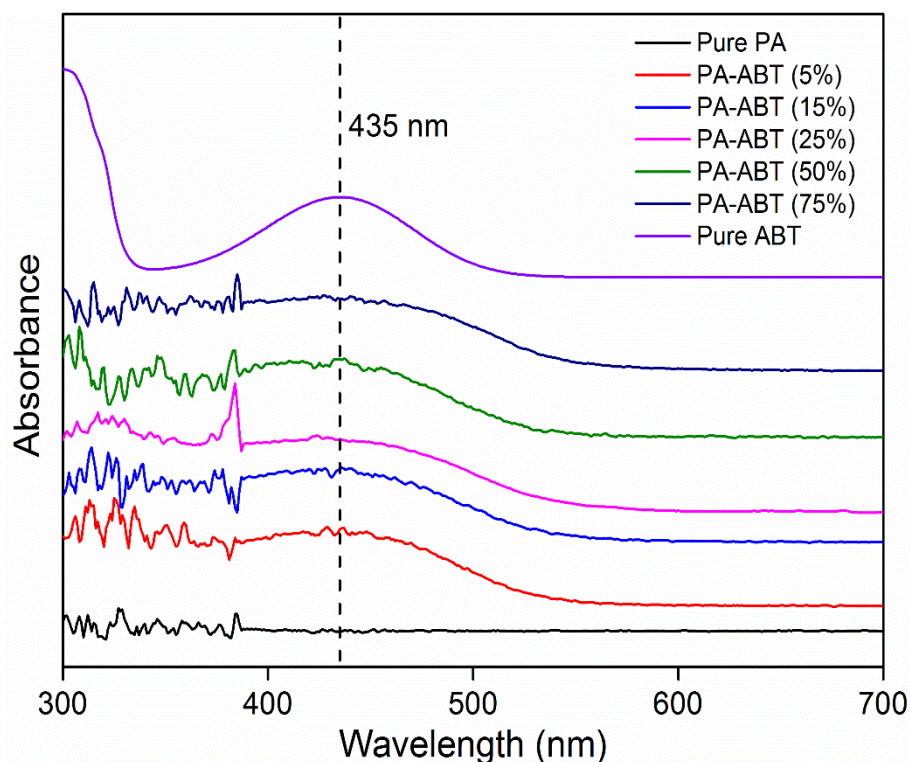
Figure 6.2: UV/Vis spectra of ABT monomer, PA-ABT and PA

Figure 6.3 presents the FT-IR spectra of the ABT monomer, PA-ABT and pure PA. Peaks at 1470–1520 cm^{-1} and 1517–1618 cm^{-1} were observed in all samples and attributed to C=C stretching of the aromatic rings and to N–H bending of the amide group, respectively. The peaks at 1658 cm^{-1} that appeared in PA and PA-ABT but not in the ABT monomer were attributed to C=O stretching of amide groups. On the other hand, the peaks at 824 cm^{-1} and 892 cm^{-1} were the characteristic peaks for the BT moiety, as they were observed for ABT and PA-ABT but not for the pure PA. The intensity of the BT peaks increased with increasing amount of ABT in PA-ABT, which indicated the successful incorporation of ABT in PA.
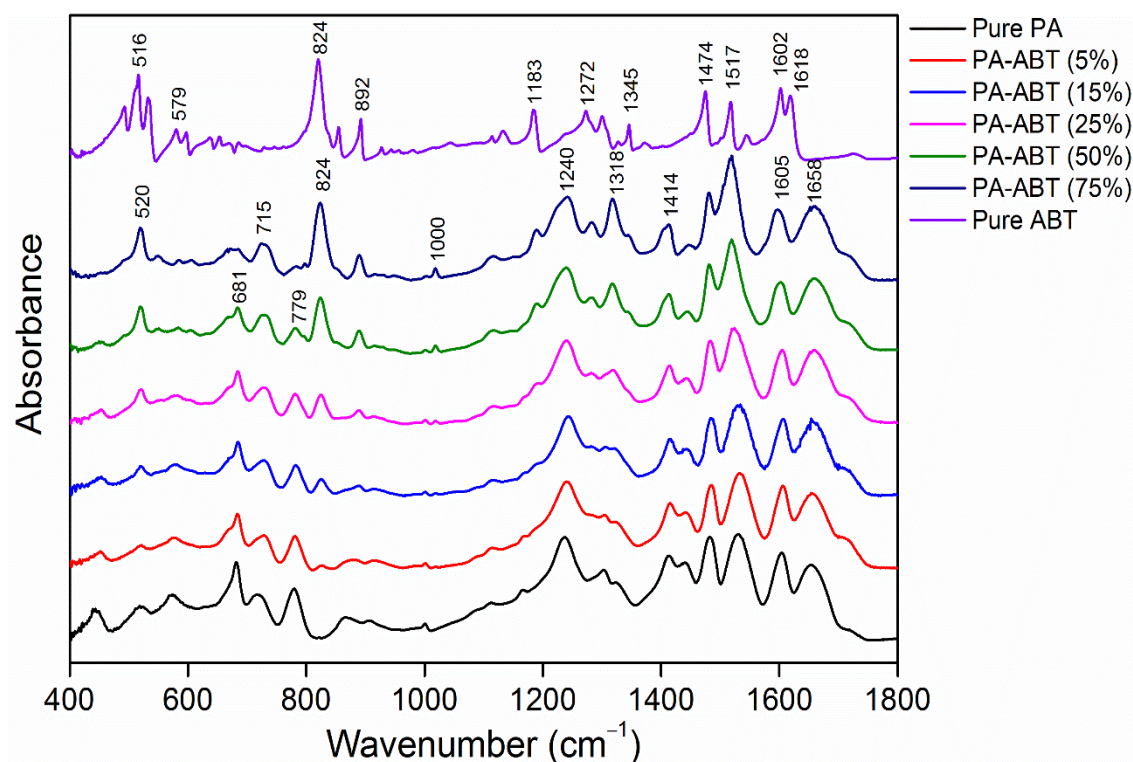
Figure 6.3: FT-IR spectra of ABT monomer, PA-ABT and PA

The ^{1}H and ^{13}C NMR spectra of the ABT monomer are shown in **Figure 6.4** and **Figure 6.5**. Due to the symmetric structure of the molecule, a mirror plane could be placed at the center of the BT core where both halves were equivalent. The unsplit (singlet) peaks at 7.71 and 3.87 ppm in the ^{1}H-NMR spectrum represent H_1 and H_4 (as labelled in **Figure 6.4**), respectively. The peaks at 7.84 and 6.88 ppm were both split into two sub-peaks due to spin-spin coupling. The sub-peaks were referred to as a doublet. The doublet at 7.84 ppm corresponds to H_2 and the doublet at 6.88 ppm to H_3. The intense peak at 7.29 ppm is due to the solvent ($CDCl_3$).

The ^{13}C-NMR spectrum presented seven distinct peaks and assignments to the corresponding carbon atoms in **Figure 6.5.** In fact, it became more difficult at this point to assign the peaks to specific atoms as they were within aromatic rings. Similarly to ^{1}H-NMR, the symmetry of the molecule allowed for both halves to have equal shifts with respect to the carbon atoms.
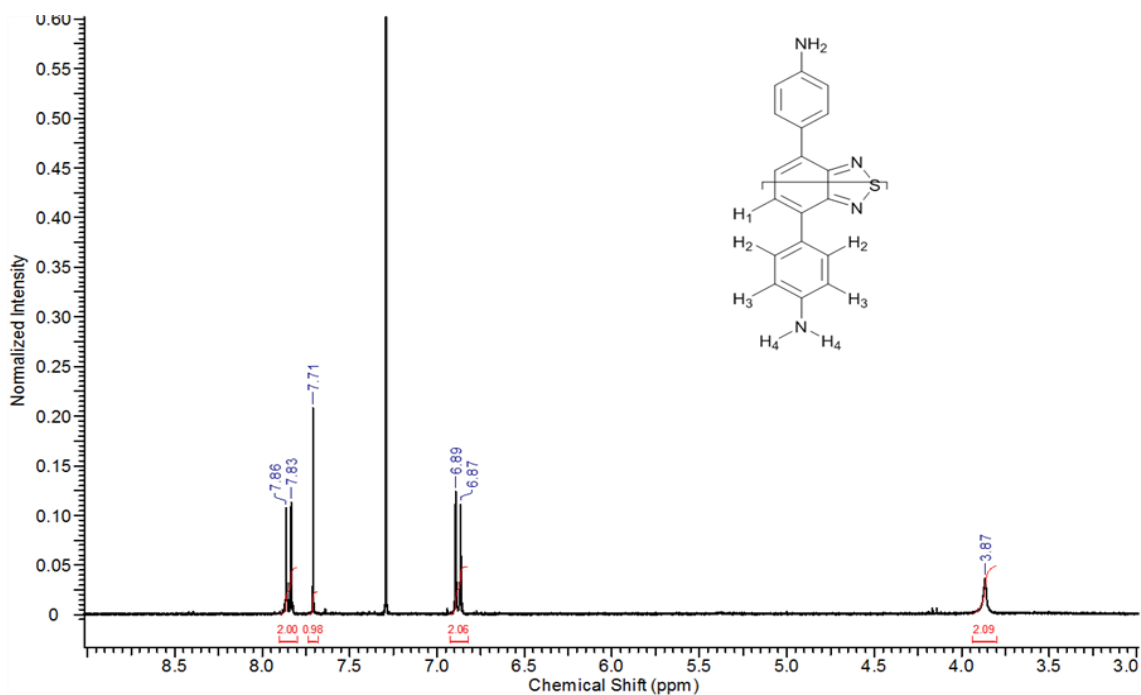
Figure 6.4: ^{1}H NMR of ABT monomer (300 MHz, 30 °C, CDCl$_3$), δ = 3.87 (s, 2 H, H$_4$), 6.88 (d, 2 H, H$_3$), 7.71 (s, 1 H, H$_1$), 7.84 (d, 2 H, H$_2$).
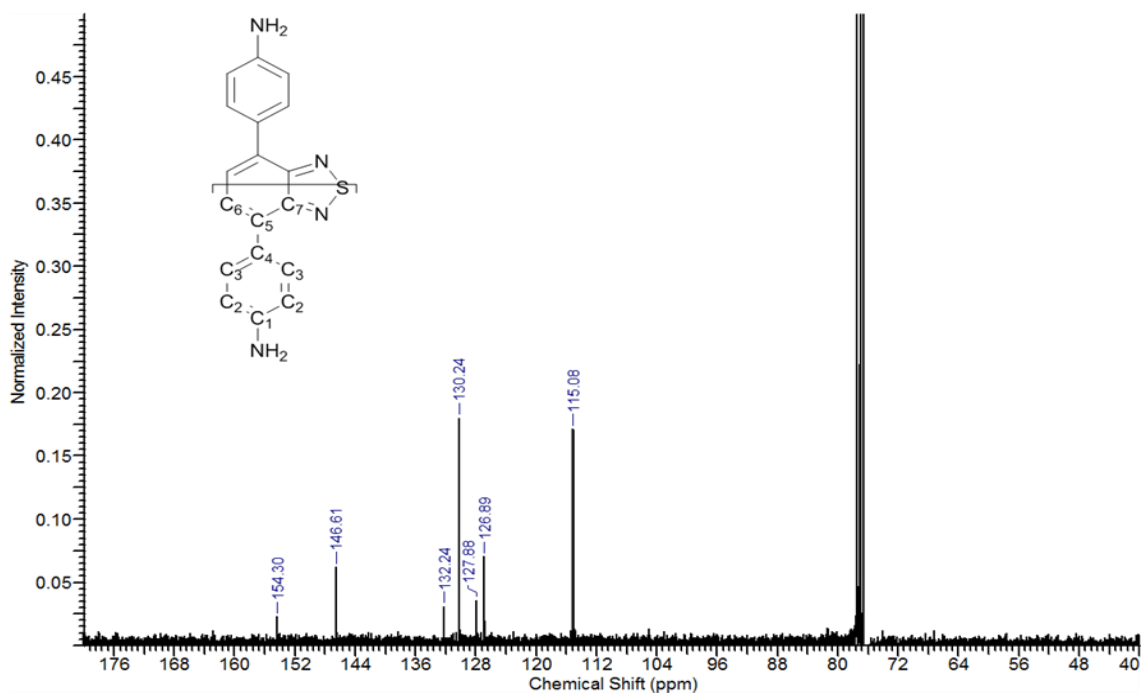
Figure 6.5: ^{13}C NMR of ABT monomer (400 MHz, 30 °C, CDCl$_3$), δ = 115.08 (C$_1$), 126.69 (C$_7$), 127.68 (C$_6$) 130.24 (C$_2$), 132.24 (C$_3$), 146.61 (C$_4$), 154.30 (C$_5$).

Unlike the monomer, the photocatalytic polymer did not dissolve in CDCl$_3$ and hence could not be analyzed by classical liquid-state NMR. Instead, solid state NMR was used to analyse PA-ABT (25%). The peak at 167.8 ppm was assigned to the carbon atom in

the amide functional group (O=C–N). The peaks at 153.4 and 144.7 ppm correspond to carbon atoms bound to nitrogen atoms (C–N). The other peaks, at 138.4, 132.6, 118.7 ppm, were attributed to other aromatic carbon atoms but the accurate assignment was not possible due to the poor resolution of the solid-state NMR spectrum. Overall, the UV/Vis, FT-IR and NMR spectra demonstrate the successful incorporation of the ABT monomer within the PA backbone.
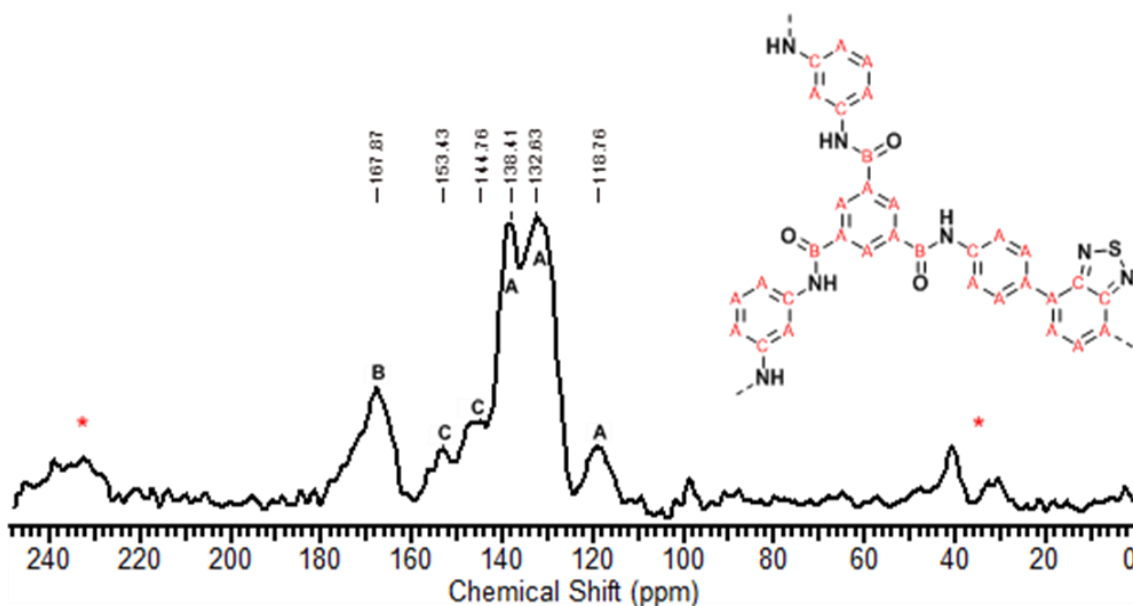
Figure 6.6: Solid state ^{13}C-NMR of PA-ABT (25%), δ = 167.8 (O=C–N, labelled as B in the formula), 153.4, 144.7 (C–N, labelled as C), 138.4, 132.6, 118.7 (other aromatic C, labelled as A). Peaks denoted by (*) indicate the presence of side bands.

6.4 Production of singlet oxygen in chloroform

The photoactivity of the ABT monomer and the PA-ABT polymers as $^1O_2$ photosensitizers was initially tested by employing the conversion of α-terpinene to ascaridole in chloroform (**Scheme 4**). Chloroform was chosen as the solvent because the lifetime of $^1O_2$ in chloroform (~250 μs) is considerably longer than in water (~2 μs) [313-315]. It is well-known that α-terpinene is extremely susceptible to photosensitized $^1O_2$ oxidation whilst being rather stable against other oxygen-rich oxidants such as OH·, ozone (O_3), and hydrogen peroxide (H_2O_2) [316, 317]. The conversion of α-terpinene to ascaridole was quantified by ^{1}H-NMR (**Figure 6.7**). The α-terpinene peaks were observed at 5.56–5.70 ppm while the ascaridole peaks were at 6.40–6.57 ppm. The concentrations of α-terpinene to ascaridole were obtained from the peak areas.
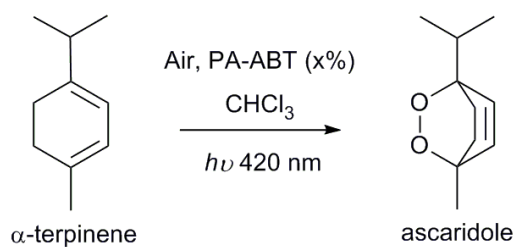
Scheme 4: Conversion of α-terpinene to ascaridole in chloroform
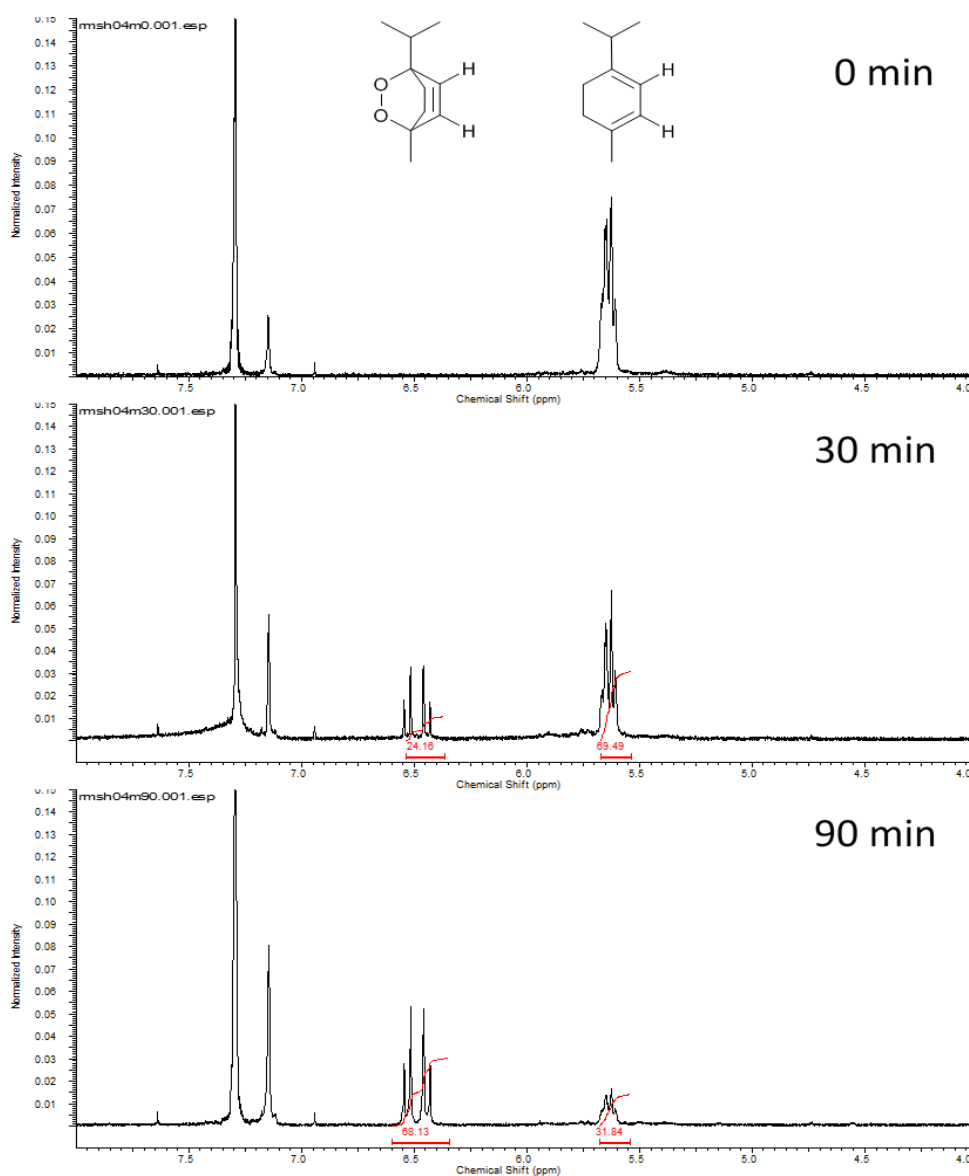
Figure 6.7: ^{1}H NMR of conversion of α-terpinene to ascaridole in chloroform (0.1 M α-terpinene, 500 mg L^{-1} PA-ABT (75%), reaction time 90 min)

When irradiated with blue light at 420 nm, the ABT monomer and the PA-ABT samples were able to convert α-terpinene into ascaridole, at different rates, whereas the pure PA had no effect on α-terpinene (**Figure 6.8**). This confirms that the conversion of α-terpinene was due to the photochemical generation of $^1O_2$. The photoreaction between

$^1O_2$ and the target molecule is essentially a second-order reaction, which means the rate of the reaction depends on the concentrations of both reactants. However, in practice, most studies conducted the photoreactions in a batch mode where the concentration of the target molecule was much greater than the concentration of $^1O_2$. Therefore the kinetics of photoreactions between $^1O_2$ and the target molecule can be simplified by the pseudo-first-order model [168, 169, 304]. The pseudo-first-order model is expressed in the differential rate law:

$$-\frac{dC}{dt} = kC \tag{12}$$

where C is the concentration of the target molecule and k is the pseudo-first-order rate constant. If the initial concentration of the target molecule is C_0, the differential rate law can be integrated as follow:

$$\ln C - \ln C_0 = -kt \tag{13}$$

Equation (13) can be further presented in exponential form as follow:

$$C/C_0 = e^{-kt} \tag{14}$$

The kinetics of α-terpinene conversion were fitted to the pseudo-first-order model by non-linear regression of concentration *versus* time data and the pseudo-first-order rate constants k and correlation coefficients R^2 were determined (**Table 6.2**). The conversion of α-terpinene generally followed the pseudo-first-order decay. However, the actual conversion at the later stage of the reaction was considerably faster than the expected conversion by the pseudo-first-order model. This is probably due to the fact that a continuous flow of air (and hence oxygen) was supplied into the flow reactor, which led to continuous $^1O_2$ generation. Increased concentration of $^1O_2$ and decreased concentration of α-terpinene did not fulfil the condition for the pseudo-first-order model any more. Therefore both the degree of conversion and the conversion rate were higher than those estimated by the pseudo-first-order model, which highlights a major advantage of the continuous-flow reaction over the batch reaction.
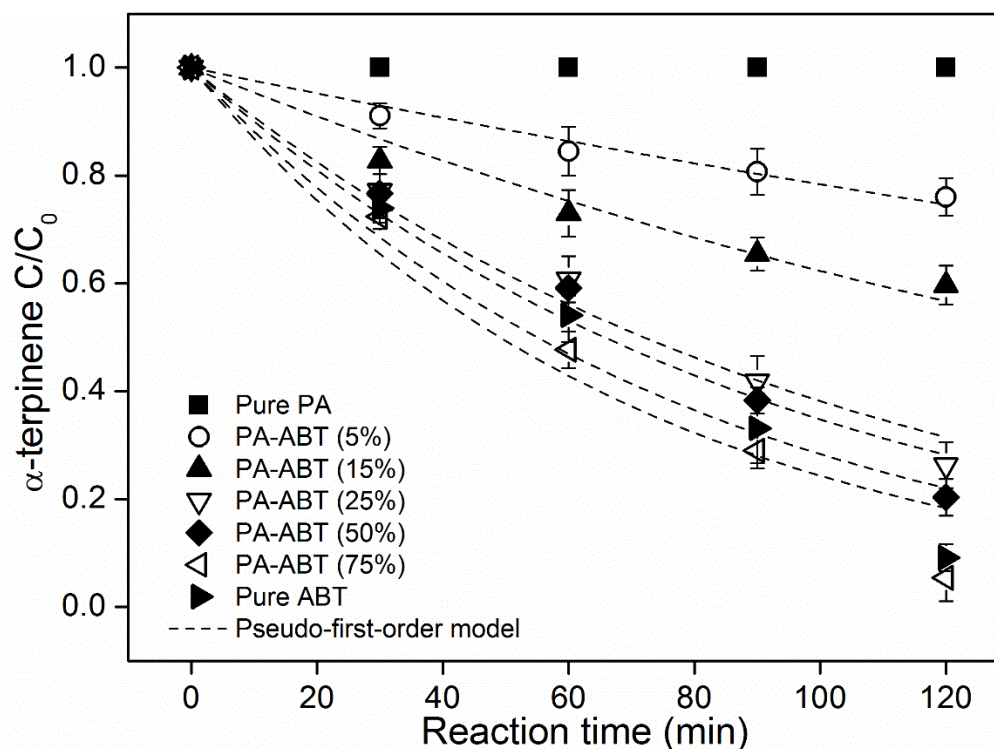
Figure 6.8: Conversion of α-terpinene to ascaridole by ABT monomer, PA-ABT and PA in chloroform under visible light irradiation (λ = 420 nm) as a function of ABT content (0.1 M α-terpinene, 500 mg L^{-1} ABT/PA-ABT/PA)

Table 6.2: Pseudo-first-order kinetics parameters of α-terpinene conversion by PA-ABT (x%) and pure ABT (0.1 M α-terpinene, 500 mg L^{-1} ABT/PA-ABT/PA)

Photocatalyst	k (hr^{-1})	R^2
PA-ABT (5%)	0.146 ± 0.007	0.974
PA-ABT (15%)	0.284 ± 0.016	0.970
PA-ABT (25%)	0.578 ± 0.033	0.984
PA-ABT (50%)	0.634 ± 0.052	0.971
PA-ABT (75%)	0.848 ± 0.100	0.956
Pure ABT	0.756 ± 0.091	0.950

It should be noted that the actual amount of photosensitized $^1O_2$ includes (i) $^1O_2$ interacting with the target molecule, (ii) $^1O_2$ quenched by the target molecule without reaction and (iii) $^1O_2$ decaying in solution [318]. Given that α-terpinene is not a physical quencher and it has a reaction rate much greater than the natural decay rate of $^1O_2$ in chloroform [318], the generation of $^1O_2$ was inferred from the conversion of α-terpinene into ascaridole. As shown in **Figure 6.8**, the conversion of α-terpinene increased with increasing percentage of ABT in PA-ABT. This is expected since greater amount of ABT generates more $^1O_2$. A noticeable result is that PA-ABT (75%) had a comparable α-terpinene conversion than the ABT monomer. This is somewhat surprising given that the

ABT monomer acted as a homogeneous photosensitizer (i.e. the target molecules and the photosensitizer exist in the same phase) whereas PA-ABT produced $^1O_2$ in a heterogeneous fashion (i.e. the photosensitizer exists in a different phase from the target molecules). These results suggest that immobilization within the PA network improves the efficacy of ABT in $^1O_2$ generation. Previously, Lee *et al*. [304] reported that immobilization of C_{60} aminofullerene on silica support accelerated $^1O_2$ production. They attributed such improved photocatalysis efficiency to decreased C_{60} aggregation in aqueous solution [304]. This was not the case here since ABT was soluble in chloroform and dispersible in water [319]. However, a colour change from light yellow to dark brown was observed in the solution during the photoreaction (**Figure 6.9**). The photobleaching phenomenon indicates that although the ABT monomer is an efficient photosensitizer, it is also a sensitive quencher and reacts with the $^1O_2$ once formed [150]. On the other hand, the PA-ABT did not experience photobleaching owing to the highly cross-linked character of the polymer network structure. The improved photostability by immobilization enables long-term use of ABT without significant loss of activity, leading to enhanced $^1O_2$ production. In control experiments, negligible conversion of α-terpinene occurred in the absence of ABT/PA-ABT under light; in the presence of ABT/PA-ABT under light in a N_2-saturated environment; and in the presence of ABT/PA-ABT in dark. Negative control experiments verify that the photosensitizer, light and O_2 are the three essential elements for initiating a photoreaction.
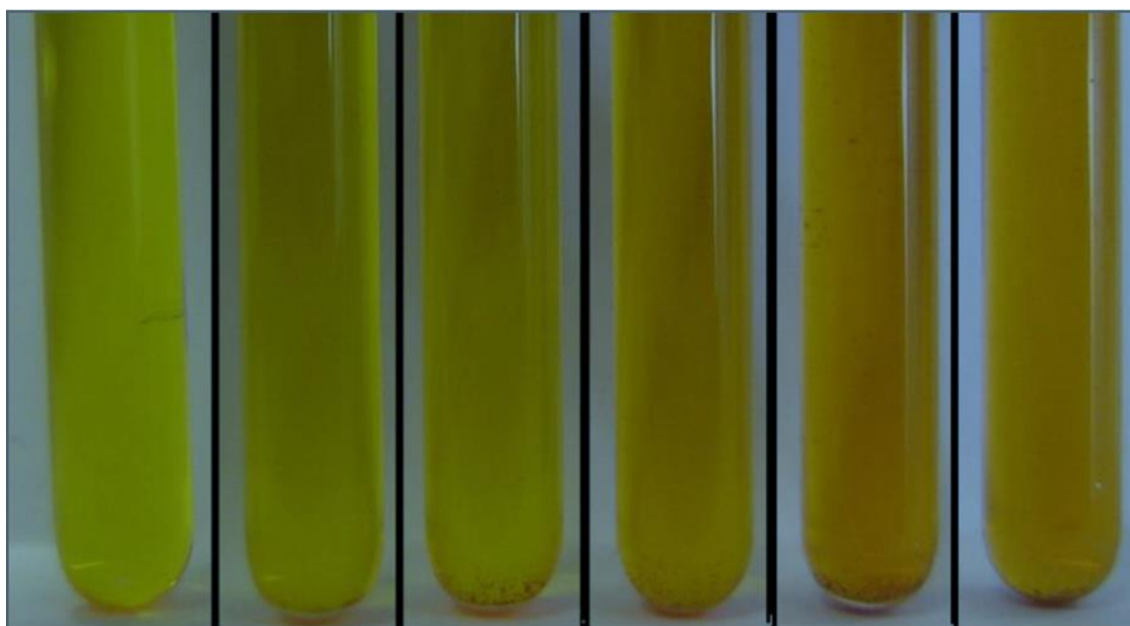
Figure 6.9: Colour change of the dissolved ABT monomer in chloroform (on the leftmost side is the fresh prepared solution and on the rightmost side is the solution after 90 min)

6.5   Production of singlet oxygen in water

PA-ABT (25%) was selected for subsequent experiments because it achieved comparatively high conversion of α-terpinene at relatively moderate ABT content. Experiments in aqueous solutions were carried out to test the suitability of PA-ABT (25%) for water treatment. FFA, which is water soluble and does not quench the excited states of various sensitizers, was used as the $^1O_2$ specific indicator in water. It has been reported that the influence of other oxidants such as OH$^\cdot$ and H_2O_2 on FFA is insignificant [320]. The major reaction products of FFA and $^1O_2$ are 6-hydroxy-2H-pyran-3(6H)-one and H_2O_2, with the produced H_2O_2 having negligible effect on the reaction [320] (**Scheme 5**). The $^1O_2$ production was measured via the consumption of FFA using HPLC (**Figure 6.10**). The retention time for the FFA peak was 1.75 min, and the retention time for the product peak was 1.35 min.
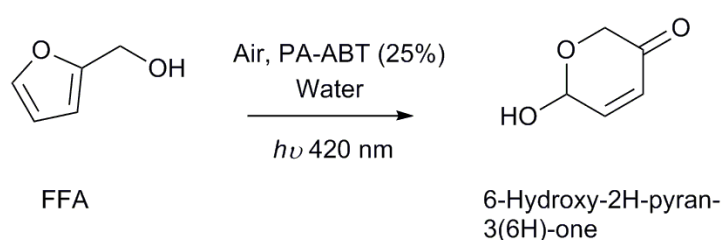
Scheme 5: Conversion of FFA to 6-hydroxy-2H-pyran-3(6H)-one in water
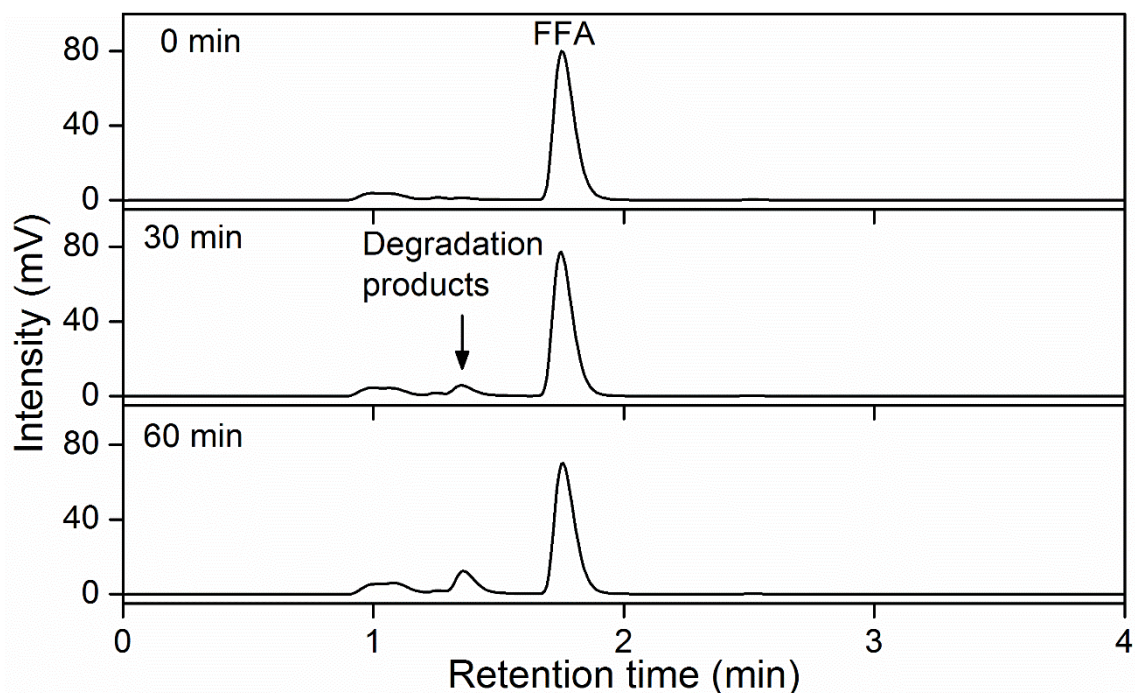
Figure 6.10: HPLC spectra of FFA conversion by PA-ABT (25%) (0.1 mM FFA, 50 mg L^{-1} PA-ABT (25%), *pH* 7, reaction time 60 min)

Figure 6.11 shows that approximately 14% of FFA was converted within the first 1 hr by PA-ABT (25%). The reaction was stopped after 1 hr. The photosensitizer was recovered from the suspension by centrifugation and reused for another 1 hr experiment run, treating the same amount of FFA as the initial run. In total, the process was repeated 5 times using the same photosensitizer. As can be seen from **Figure 6.11** and **Table 6.3**, the conversion of FFA by PA-ABT (25%) fits the pseudo-first-order model very well. Despite loss of photosensitizer during centrifugation, the reduction in conversion of FFA over the 5 repeated runs was very small, which implies good photostability of PA-ABT (25%) as a photosensitizer. In the future, when used in a larger amount, the photosensitizer can be more completely recovered from suspension by advanced separation techniques such as membrane filtration and solid phase extraction.
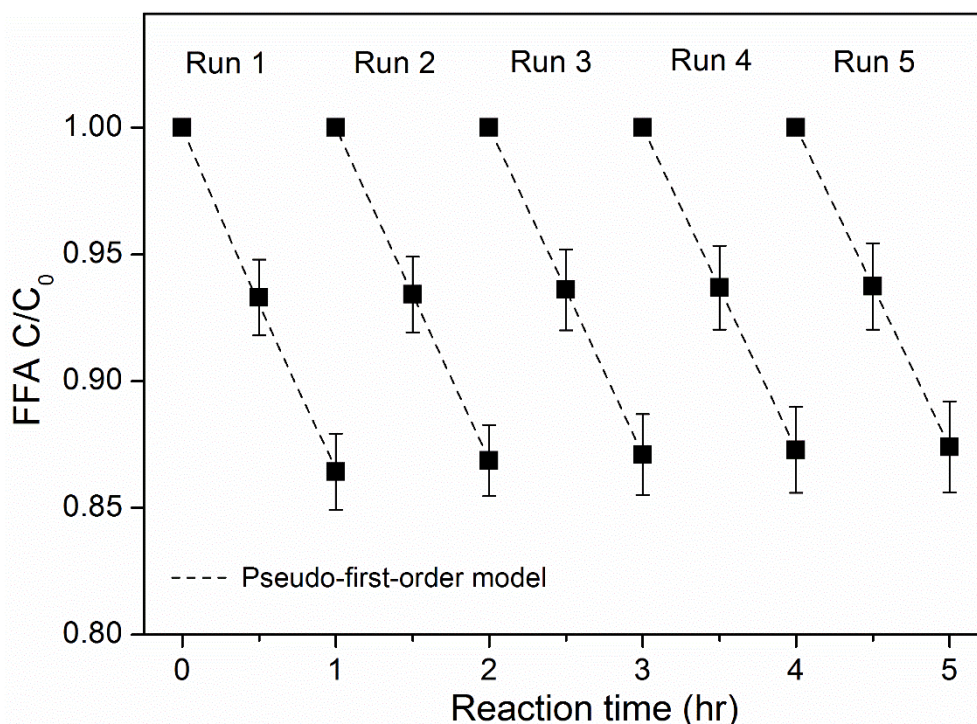
Figure 6.11: Repeated conversion of FFA by PA-ABT (25%) in water under visible light irradiation ($\lambda =$ 420 nm) (0.1 mM FFA, 50 mg L^{-1} PA-ABT (25%), *pH* 7)

Table 6.3: Pseudo-first-order kinetics parameters of FFA conversion by PA-ABT (24%) (0.1 mM FFA, 50 mg L^{-1} PA-ABT (25%), *pH* 7)

Run	k (hr^{-1})	R^2
1	0.144 ± 0.002	0.999
2	0.139 ± 0.002	0.999
3	0.137 ± 0.002	0.999
4	0.136 ± 0.002	0.999
5	0.135 ± 0.002	0.999

6.6   Degradation of emerging contaminants

Two emerging contaminants, BPA and cimetidine, were selected as typical wastewater contaminants to be treated by the photocatalytic polymer [28] (**Scheme 6**). BPA belongs to EDCs and cimetidine is a pharmaceutical compound. Previously, both of them were used as target molecules in photochemical reactions, such as with TiO$_2$ [321], C$_{60}$ fullerene [168], and NaBiO$_3$ [169]. The major advantage of using BPA and cimetidine in photochemical reactions is that the degradation mechanisms are well understood.

Scheme 6: Structure of BPA and cimetidine

The concentrations of BPA and cimetidine were quantified by HPLC analysis (**Figure 6.12** and **Figure 6.13**). The retention time for the BPA peak was 7.74 min and retention times for degradation products were shorter than that of BPA. The cimetidine peak was very broad with the centre at about 5.60 min. The broad peak reveals that the current combination of column and mobile phase did not fit cimetidine best, though it was sufficient to quantify the concentration of cimetidine, which was the main purpose of the HPLC analysis.
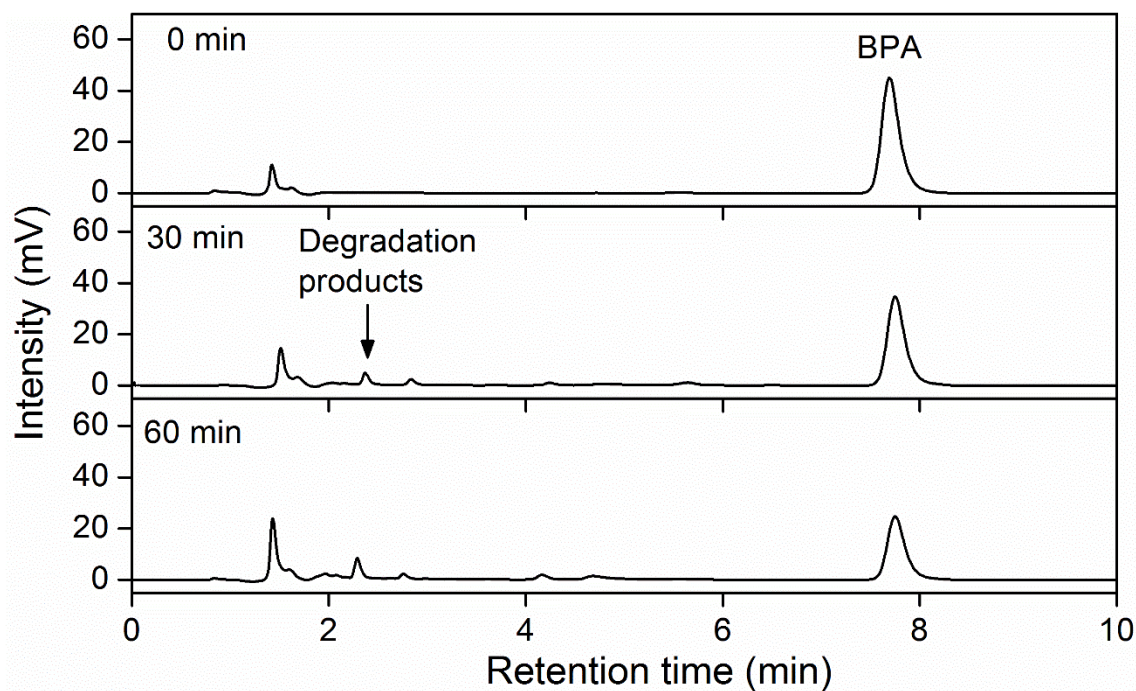
Figure 6.12: HPLC spectra of BPA degradation by PA-ABT (25%) (0.1 mM BPA, 50 mg L^{-1} PA-ABT (25%), *pH* 7, reaction time 60 min)
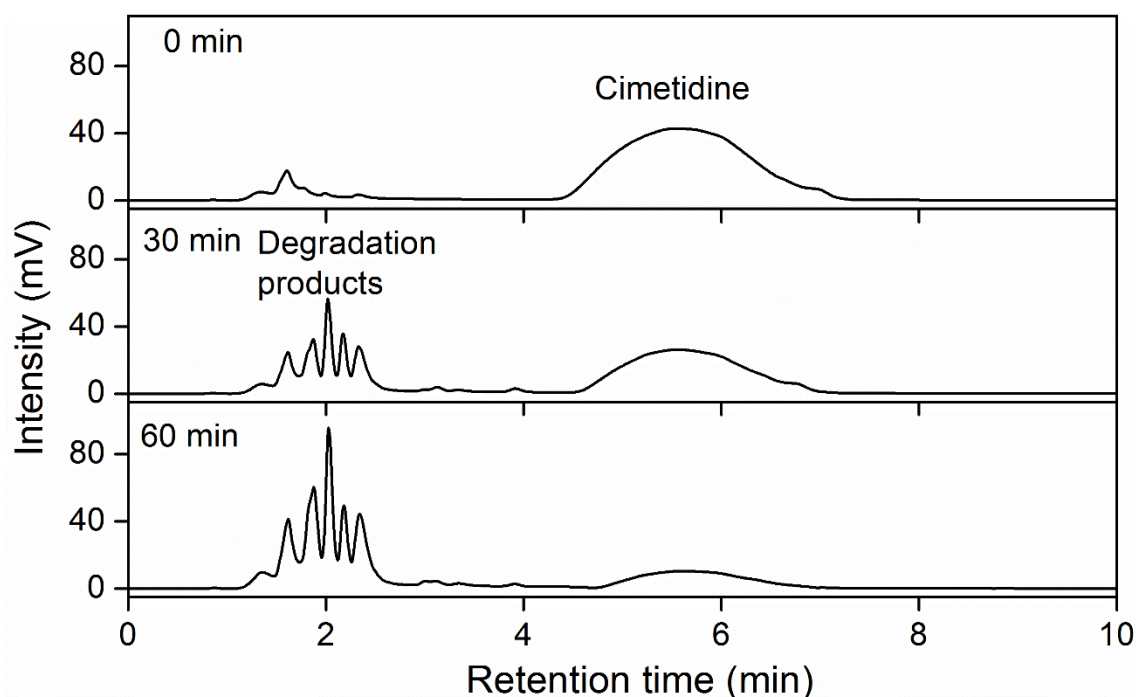
Figure 6.13: HPLC spectra of cimetidine degradation by PA-ABT (25%) (0.1 mM cimetidine, 50 mg L^{-1} PA-ABT (25%), *pH* 7, reaction time 60 min)

Based on the HPLC results, PA-ABT (25%) was shown to achieve efficient conversion of BPA and cimetidine under visible light of 420 nm (**Figure 6.14** and **Table 6.4**). The conversion of BPA and cimetidine also followed the pseudo-first-order model while some deviations at later stage were due to the excessive amount of $^1O_2$. The degradation pathway for the photoreaction between $^1O_2$ and BPA has been extensively studied [169, 322-324]. On the one hand, $^1O_2$ directly attacks the aromatic ring of BPA, leading to the formation of BPA catechol [323]. On the other hand, $^1O_2$ readily cleaves the bond between two aromatic rings, producing phenol, 4-isopropylphenol, and hydroquinone [169, 322, 324]. Toxicological studies showed that BPA catechol has a weak estrogenic activity, which is approximately three times lower than that of BPA [325]. Phenol, 4-isopropylphenol, and hydroquinone have negligible hazardous effects in humans. These less-toxic intermediates can be further biodegraded by microorganisms under environmental conditions [326]. As for cimetidine, Latch *et al.* [30] investigated its degradation pathway by using model compounds. They found that the imidazole model compound reacted 12 times faster with $^1O_2$ than the sulfide model system and 500 times faster than the cyanoguanidine model compound, indicating that the imidazole ring is the dominant reactive group [30]. The interaction of imidazole derivatives with $^1O_2$ leads to the formation of endoperoxides which eventually decompose to form CO_2 [327].
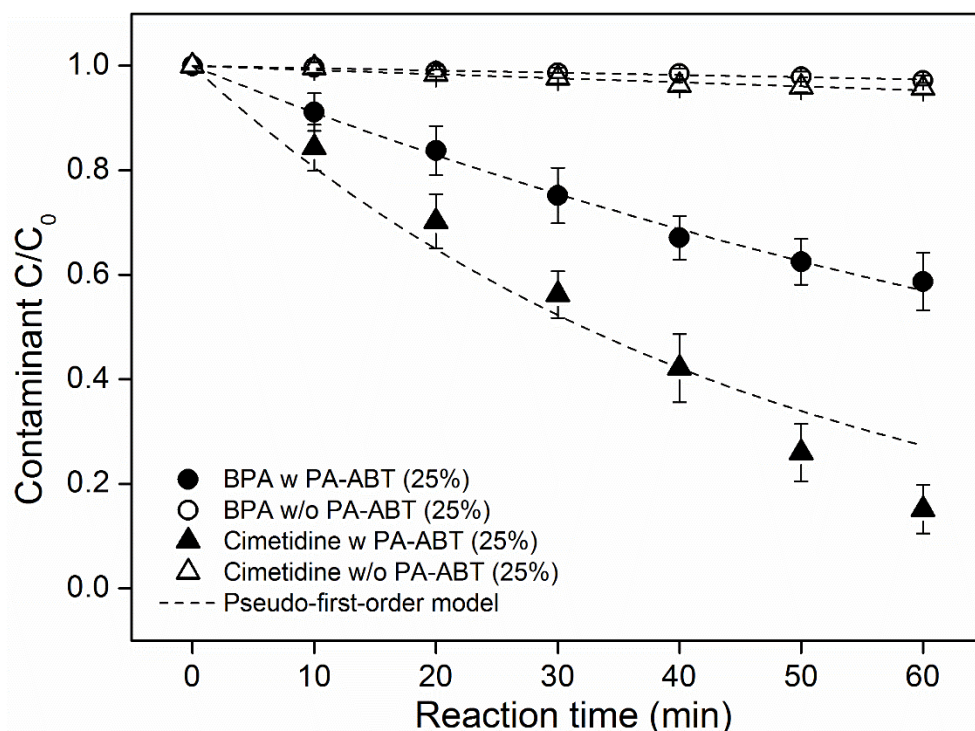
Figure 6.14: Conversion of BPA and cimetidine by PA-ABT (25%) in water under visible light irradiation ($\lambda = 420$ nm) (0.1 mM BPA/cimetidine, 50 mg L^{-1} PA-ABT (25%), *pH* 7)

Table 6.4: Pseudo-first-order kinetics parameters of BPA and cimetidine conversion by PA-ABT (24%) (0.1 mM BPA/cimetidine, 50 mg L^{-1} PA-ABT (25%), *pH* 7)

Condition	k (hr^{-1})	R^2
BPA w PA-ABT (25%)	0.562 ± 0.010	0.998
BPA w/o PA-ABT (25%)	0.026 ± 0.001	0.972
Cimetidine w PA-ABT (25%)	1.297 ± 0.106	0.981
Cimetidine w/o PA-ABT (25%)	0.048 ± 0.002	0.962

Direct photolysis experiments showed minor degradation of BPA (2%) and cimetidine (4%) in the first 1 hr. The photostability of these compounds can be rationalized by the fact that they lack chromophores capable of absorbing light at 420 nm wavelength (UV/Vis. spectra in **Figure 6.15**). It is worth mentioning that BPA and cimetidine both undergo spontaneous photoreactions upon irradiation in the presence of NOM (especially HS), which absorbs light and produces ^{1}O$_2$ and other reactive oxygen species [30, 328]. However, the quantum yields of ^{1}O$_2$ production for NOM are much lower compared to artificial photocatalysts and photosensitizers [329]. No direct dark transformation of BPA and cimetidine occurred in the presence of PA-ABT (25%) alone.
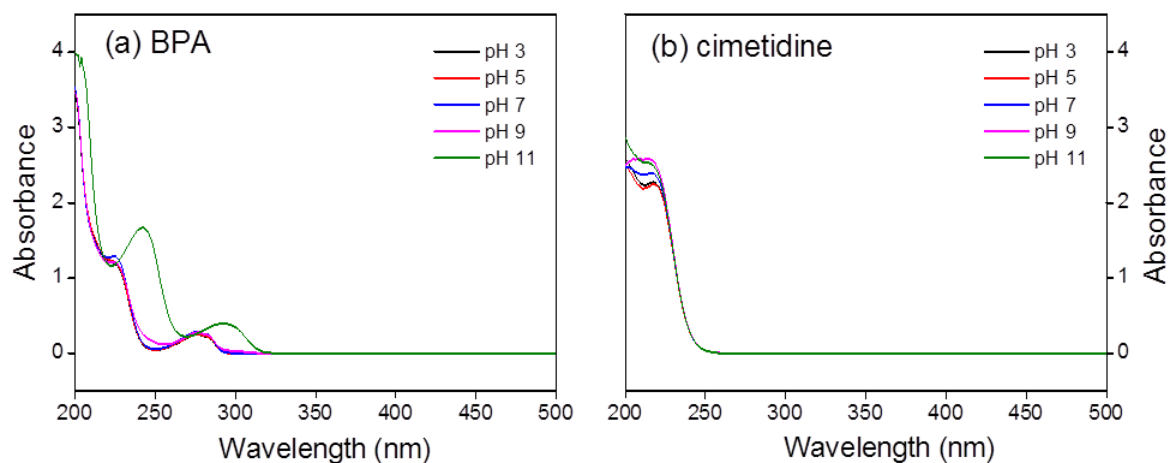
Figure 6.15: UV/Vis absorption spectra of (a) BPA and (b) cimetidine in aqueous solution at different *pH* values (0.1 mM BPA/cimetidine)

Since the *pH* of wastewater may vary significantly depending on the source and environment, the photocatalytic performance of PA-ABT (25%) at different *pH* conditions was studied. **Figure 6.16** shows the degree of conversion (defined as the concentration reduction after 1 hr photoreaction) of FFA, BPA and cimetidine by PA-ABT (25%) as a function of initial *pH*.

The degree of conversion of FFA was constant (~13.5%) despite of *pH* variation. It has been shown that the reaction of FFA with $^1O_2$ is independent of *pH* in the range 5 to 12 [330]. Therefore, the constant FFA conversion reported here over a wider *pH* range demonstrates the superior chemical stability of PA-ABT (25%). This is promising for water and wastewater treatment because it means the *pH* can be adjusted to control the speciation of target contaminants without losing the functionality of the photosensitizer. As a result the treatability of water and wastewater that contain *pH*-dependent contaminants can be maximized.

Both BPA and cimetidine showed *pH*-dependent degradation by PA-ABT (25%). The degree of conversion of BPA increased from 35% to 44% at *pH* below 9, and rose steeply to 90% at *pH* 11. This is consistent with the *pKa* of BPA which was reported to be between 9.6 and 10.2 [331]. At *pH > pKa*, BPA became negatively charged by the deprotonation of phenol to the phenolate anion. The phenolate anion is more electrophilic than the neutral phenol and reacts more readily with photosensitized $^1O_2$. This leads to a drastic enhancement in the degree of conversion of BPA under alkaline *pH* [170, 322].

Similarly, the *pH* dependence of cimetidine conversion can be explained considering its *pKa* which varies from 6.8 to 7 [30]. As shown in **Figure 6.16**, the degradation rate varied from 27% at *pH* 3, where cimetidine was primarily in its protonated form, to 96% at *pH* 11, where the unprotonated cimetidine dominated the speciation. Given that imidazole is the reactive site, the unprotonated imidazole ring has increased electron density and is thus more reactive towards $^1O_2$ [30]. Complete degradation of BPA and cimetidine by PA-ABT (25%) could be obtained at *pH* values above their *pKa*. These studies ultimately demonstrate that the polymeric photosensitizer is active within a wide-range of *pH* values.
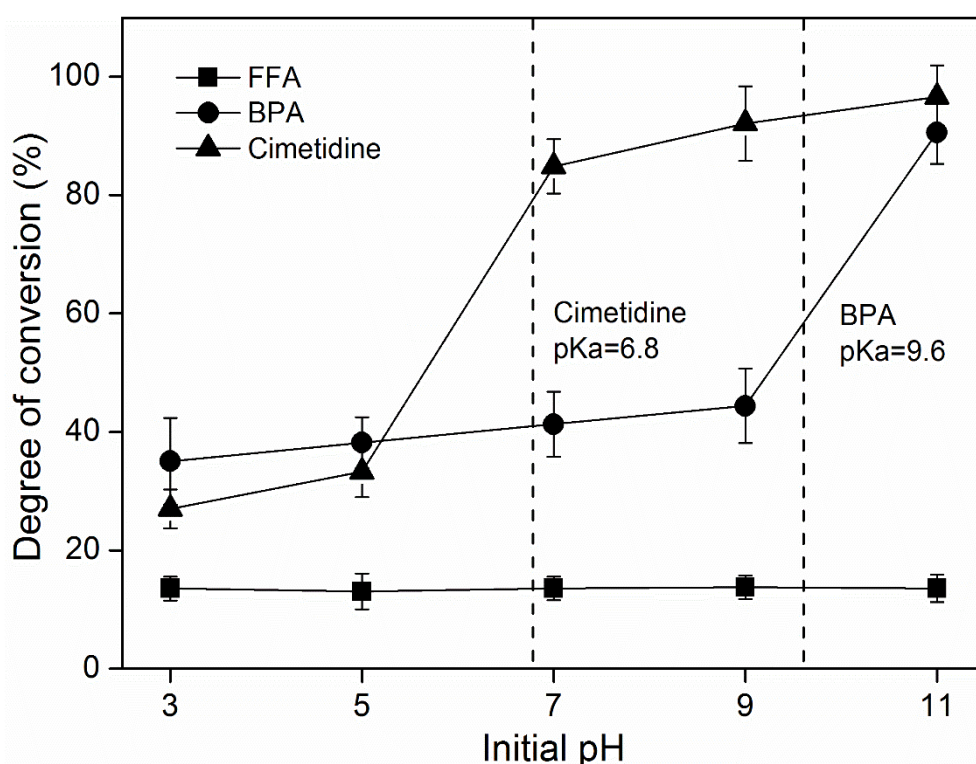
Figure 6.16: Degree of conversion of FFA, BPA, and cimetidine by PA-ABT (25%) in water as a function of initial *pH* under 1 hr of visible light irradiation (λ = 420 nm) (0.1 mM FFA/BPA/cimetidine, 50 mg L^{-1} PA-ABT (25%))

6.7 Inactivation of *Cryptosporidium*

Cryptosporidium is of significant public health concern in drinking water because it causes a disease called cryptosporidiosis. This concern is worsened by the resistance of *Cryptosporidium* to commonly used disinfection practices such as chlorination.

Results of the excystation assay showed that exposure of *Cryptosporidium* to PA-ABT (25%) in combination with visible light irradiation at 420 nm caused a substantial reduction in viability. Excystation percentage decreased from 90% to 65% (**Table 6.5**). UV irradiation is the most commonly used method of inactivating *Cryptosporidium.* The photosensitizer showed a comparable inactivation capability to a moderate UV dose of 137 mWs cm^{-2} but not as significant as a higher UV dose of 167 mWs cm^{-2} [332, 333]. Greater levels of inactivation could potentially be achieved by longer exposure times and/or higher photosensitizer doses.

However, exposure to either PA-ABT (25%) or 420 nm irradiation alone caused a reduced excystation of around 80%. This indicates that the inactivated photosensitizer might have potential intrinsic acute toxicity. The detailed mechanism is unknown.

To the best of our knowledge, this is the first example of protozoan disinfection using a photocatalytic polymer and is particularly interesting given the resistance of this protozoan parasite to chlorine disinfection. The effectiveness of the photocatalytic polymer on bacteria (*e.g. E.coli*) and virus will be explored in future work.

Table 6.5: Inactivation of *Cryptosporidium* with and without PA-ABT (25%)

Sample	Description	Excystation (%)
1	Live control	90
2	Light only	82
3	PA-ABT (25%) only	80
4	Light + PA-ABT (25%)	65

6.8   Photocatalytic membrane reactors

Photocatalytic membrane reactors (PMR) conduct hybrid photocatalysis-membrane processes. PMR have a large diversity of designs, depending on the operation mode (batch or continuous flow), filtration mode (dead-end or cross-flow), membrane module (flat sheet, hollow fibre), membrane type (*e.g.* MF, UF, NF) and light source type (UV or visible) [334]. Nevertheless, PMR can be divided generally into two main configurations: the first one with the photocatalyst suspended in the feed solution and the second one with the photocatalyst immobilized on the membrane [334]. The photocatalytic polymer can be applied in both configurations.

In the first configuration, the membrane acts as a single-step barrier for the photocatalyst. The light source can be positioned above the feed tank or inside the tank when immersed lamps are used. Immersed lamps can be coupled with either submerged membranes [335] or separate membrane modules [336]. The light source can also be placed above the membrane module. In this case the module is fabricated with transparent materials (such as glass and quartz) to allow the light to enter [337]. The major disadvantage of this configuration is membrane fouling due to photocatalyst particles, which results in low water productivity. Previous studies suggested that aeration and intermittent permeation could prevent accumulation of photocatalyst on the membrane [338]. Other strategies to prevent fouling include coagulation/sedimentation pretreatment prior to the membrane filtration [339].

The second configuration, *i.e.* photocatalytic membranes with immobilized photocatalyst, has low risk of membrane fouling because of the generation of ROS on the membrane surface. In this configuration, contaminants in the feed solution are decomposed and inactivated on the membrane surface or within the pores of the membrane when exposed to light [334]. The final products and by-products of photoreaction may permeate the membrane or be rejected, depending on the separation characteristics of the membrane. One group of the most often applied photocatalytic membranes is polymeric membranes containing TiO_2 particles. Based on the fabrication methods, these membranes can accommodate TiO_2 on the active layer or entrap TiO_2 within the structure [334]. A main disadvantage of these membranes is the risk of membrane damage caused by the UV light or ROS. Obviously this is not a problem for the photocatalytic polymer because it functions under visible light and more importantly, it has good photostability and chemical stability due to the cross-linked structure. However in the long run, it may be worth considering the necessity of membrane replacement when the photocatalytic polymer loses its activity.

6.9   Conclusions

A series of novel photocatalytic metal-free polymers (PA-ABT) were synthesized by incorporating a photosensitizer monomer (ABT) into a polyamide structure. Photochemical experiments were conducted in a commercial flow reactor with continuous air injection and visible light illumination. The conversion of α-terpinene to

ascaridole in chloroform was used to compare the efficiency of the ABT monomer to that of heterogeneous polymers with varying ABT content. Interestingly, PA-ABT (75%) had a higher α-terpinene conversion rate than the ABT monomer, suggesting that immobilization within the PA network improves the efficacy of ABT in $^1O_2$ generation. PA-ABT (25%) was used in aqueous solution experiments to assess the feasibility of PA-ABT in water and wastewater treatment. PA-ABT (25%) achieved 14% FFA conversion in 1 hr; repeated experiments demonstrated the photostability of the polymers. Despite its relatively low photosensitizer content and short exposure time to light, PA-ABT (25%) showed high efficiency in degradation of BPA and cimetidine, and inactivation of *Cryptosporidium*. The water *pH* can be adjusted to achieve the highest degradation based on the speciation of target contaminants.

PA-ABT polymers offer several advantages compared to conventional photocatalysts. Firstly, the metal-free synthesis is cost-effective and eco-friendly. Secondly, they function readily under visible light, eliminating the requirement for UV irradiation. Thirdly, their cross-linked structure prevents photobleaching and enables easy separation from water. Therefore, these new materials are very suitable candidates in the use of water and wastewater treatment.

A natural progression of this work is to develop photocatalytic polymeric membranes using these materials. Design of associated PMR for pilot-scale applications is also required.

Chapter 7: Conclusions

When it comes to reducing the impact that we, as a society, have on our environment it is important that water treatment is at the top of our list of priorities. Water is probably our most valuable natural resource and it is absolutely vital to sustain populations, industries and the environment. With a wide range of uses, a comprehensive water management plan can be applied to not only lessen the stress placed on the environment, but also protect public health. Water and wastewater treatment is therefore essential to prepare this valuable resource for human use.

Membrane technologies, especially NF and RO, are very promising water purification techniques compared with conventional methods. NF/RO can achieve high contaminant removal as they involve a mixture of separation mechanisms including solution diffusion, size exclusion, charge repulsion and adsorption. Suitable membrane characteristics can be selected to match particular water qualities. Membrane systems are modular in design and flexible in implementation, making them a suitable choice for remote communities. High energy consumption can be compensated by introducing renewable energy technologies. Furthermore, natural contaminants in water are often accompanied by bacteria, viruses and emerging contaminants such as EDCs and pharmaceuticals. Membrane filtration combined with advanced oxidation technologies can simultaneously degrade and separate those contaminants in one single process.

The first experimental chapter, Chapter 3, investigated the solute-solute interactions between two natural contaminants, namely fluoride and HS in solution. The ultimate aim was to understand the influence of solute-solute interactions on membrane filtration. The approach was to first study the aggregation behaviour of HS and then to determine the variation of fluoride concentration measured by ISE in the presence of HS aggregation. DLS techniques were used to characterize the size and charge properties of HS under a wide range of water chemistry conditions. HS tend to aggregate at low *pH* and high ionic strength conditions as a result of hydrogen bonding and charge interactions. The behaviour of the HS aggregates was well explained by the supramolecular model and the DLVO theory. The fluoride concentration measured by ISE was found to decrease in the presence of HS aggregation. A new "open cage" concept was proposed where fluoride ions are physically trapped in the framework of the HS aggregates. The "open cage"

effect can be eliminated by separation pretreatment such as centrifugation. Future research is recommended on the characterization of the inner structure, heterogeneity and hydrophobicity of HS aggregates and the verification of similar solute-solute interaction for other anions such as chloride and carbonate ions.

Following experimental evidence for solute-solute interactions between fluoride and HS found in Chapter 3, Chapter 4 reported bench-scale NF/RO experiments treating a diverse collection of natural water samples from Tanzania, where fluoride and NOM were identified as two major contaminants in drinking water sources. Comprehensive water quality analysis revealed that the typical water type in Tanzania was bicarbonate-alkaline type. The dominance of sodium and bicarbonate ions facilitates accumulation of fluoride by restricting the dissolution of calcium, and increases the solubility of NOM due to the alkaline *pH* conditions. Filtration results showed that fluoride and NOM transferred through the membrane *via* different mechanisms. Removal of fluoride was governed by a solution-diffusion mechanism and thus affected by parameters that relate to the concentration gradient, such as recovery, initial fluoride concentration and ionic strength. Removal of NOM, on the other hand, was controlled by a size exclusion mechanism and did not vary significantly due to the much larger size of NOM than the pore size of NF/RO membranes. A position effect of TOC concentration on fluoride removal was observed in both synthetic solutions and natural water samples. The involvement of solute-solute interactions was ruled out because of the absence of NOM aggregation at alkaline conditions. Several possible mechanisms were proposed, including the modification of membrane surface charge. This observation brought to light the complexity of membrane filtration processes due to feed water characteristics. Further research should focus on the surface characterization of the used membranes. A combination of various characterization techniques such as scanning electron microscopy (SEM), atomic force microscope (AFM), contact angle measurement and zeta potential measurement is highly recommended.

From laboratory to field, Chapter 5 evaluated the performance of a pilot-scale solar-powered membrane system in treating some challenging water sources in Tanzania. The selection of membrane types and water sources was based on the membrane screening and water quality analysis conducted in Chapter 4. In remote areas where electricity and infrastructure are not always available, decentralized RE-membrane system can be

considered as a sustainable solution. The RE-membrane system used in this chapter contained no batteries in order to save capital cost and reduce environmental impact. Without energy storage, the fluctuations of solar irradiance resulted in variations in system performance. Specifically, drop of solar irradiance led to decrease of feed flow and TMP, and hence caused abnormally high fluoride and TOC concentrations due to concentration polarization. However, the system restored from energy fluctuations very quickly. Given the small amount of water produced during the energy fluctuation periods, the impact of these energy fluctuations on the quality of water collected over one-day operation was insignificant. The RE-membrane system was tested in several rural and remote places in Tanzania where water quality, especially high fluoride concentrations, was a major health concern. The field demonstration received very positive feedback from local authorities and residents. Future research is required to monitor the long-term performance of the RE-membrane system and to develop sustainable operating and maintenance strategies. Different development strategies should be considered for different places with different sets of water requirements and socioeconomic realities.

Chapter 6 expanded the research scope from drinking water purification to wastewater treatment. Unlike natural contaminants which are environmentally compatible, emerging and biological contaminants from wastewater effluents pose a risk to both human health and the environment. The idea behind the work presented in this chapter was to first reduce the toxicity of these contaminants by photocatalysis and then separate the degradation products from water by membrane filtration. In order to achieve this, a novel visible light-responsive photosensitizer was synthesised *via* Suzuki coupling and was incorporated into a polyamide matrix through polymerization. The resulting photocatalytic polymer PA-ABT (25%) showed efficient $^1O_2$ production in both organic solvent and water. Two organic compounds, α-terpinene and FFA, were selected as the specific $^1O_2$ indicators in chloroform and in water, respectively. BPA and cimetidine were selected as typical emerging contaminants and *Cryptosporidium* as the representative pathogen. PA-ABT (25%) achieved rapid degradation of BPA and cimetidine as well as inactivation *Cryptosporidium* within a short time of light irradiation. The photoreactions can be optimized by adjusting photosensitizer amount, exposure time and solution *pH*. The major advantages of the new photocatalytic polymers compared to conventional photocatalysts are their inexpensive synthetic method, visible light photosensitization and most importantly, the intrinsic convenience of turning these polymers into polymeric

membranes. There is abundant room for further progress in developing photocatalytic membranes and membrane reactors based on these materials.

In conclusion, this thesis investigated the removal of several important and diverse contaminants by membrane technologies. The results obtained from each chapter provided new insights into solute-solute interactions, solute transport mechanisms, decentralized membrane system and novel membrane materials. It is hoped that this work will serve as a stepping stone to solving the most pressing problem facing the world in the upcoming decades: water.

Appendix

A.1 Health implications of fluoride: A case study in northern Tanzania

A.1.1 Location

The Oldonyosambu Ward is located in the Arumeru District of northern Tanzania and in the north-western sector of the Mount Meru natural system. The Oldonyosambu Ward includes three villages which are Oldonyowas, Lemongo and Losinoni. According to the 2012 national census, Oldonyosambu Ward had a total population of about 22000 [340]. The dominant ethnic groups are Warusha, Maasai and Wameru [341]. The Warusha and Maasai live in polygamous communal settlements called *boma* (**Figure A.1**).

(A) Oldonyosambu *boma* 1   (B) Oldonyosambu *boma* 2

(C) Oldonyosambu *boma* 3   (D) Oldonyowas
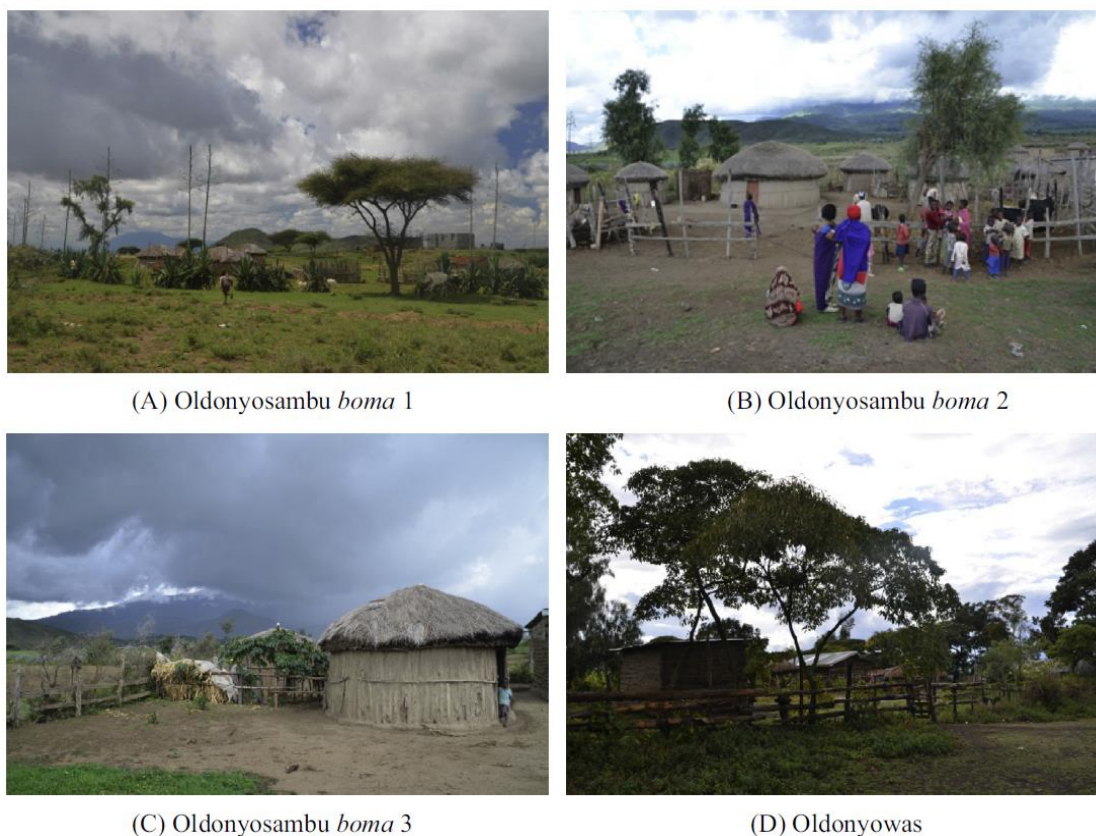
Figure A.1: Different *bomas* studied in Oldonyosambu Ward, villages of Lemongo and Oldonyowas with GPS coordinates (A) S03º07.692' E036º41.123', (B) S03º08.104' E036º40.844', (C) S03º08.379' E036º41.163', (D) S03º10.135' E036º41.779' (photos from [191])

A.1.2 *Water demand and alternative sources*

Oldonyosambu Ward has a limited number of permanent water sources and those available are known to suffer from high levels of fluoride concentrations. The water demands in Oldonyosambu Ward were estimated (per person per day) at a minimum of 5 L for cooking and drinking water and 30 L of water that does not need to be free of fluoride for domestic use (**Table A.1**).

Table A.1: Population and estimated water demands in the Oldonyosambu Ward

Village	Household number	Total population	Drinking water demand (L per day)	Non-drinking water demand (L per day)
Lemongo	2200	14000	70000	420000
Oldonyowas	457	2650	13250	79500
Losinoni	600	6000	30000	180000

The obvious alternative water to fluoride contaminated sources is rainwater harvesting. In 2010, Instituto Oikos and Oikos East Africa installed, in the framework of a European Union and Intervita Onlus funded project, a total of 315000 L water storage tanks fed by rainwater harvesting systems in primary schools of Oldonyosambu Ward [342]. In the Oldonyosambu Primary School, where more than 1100 students had no access to water whether safe or unsafe, a colonial water pipeline was restored to feed two of the 10000 L rainwater tanks together with 185000 L of rainwater storage. The rainwater harvesting supplies the school with a good back-up for personal hygiene and irrigating the school vegetable gardens. The major limiting factors of rainwater harvesting are (1) erratic and seasonal rainfall patterns [343] and (2) the costs to install suitable roofs, gutters and storage systems. Despite those constraints rainwater harvesting ought to be considered to supplement supply and in some case may be the most viable solution.

In June 2012, Istituto Oikos facilitated the installation of two bone char defluoridation filters in the Oldonyosambu Primary School, and the Kimosonu Primary School in the neighbouring Ngare Nanyuki Ward. This intervention was coupled with the distribution of approximately 60 domestic fluoride filters of 20 L capacity among households in Ngare Nanyuki Ward. Monitoring data inform that both interventions had a relatively low success, mostly due to a lack of commitment and understanding of the importance of replacing the exhausted bone char. In both schools, in fact, 36 months after the installation of the filters and continue utilization, neither of the filters had the bone char

replaced, in spite of a signed Memorandum of Understanding between the donor and the beneficiaries where it was stated that the bone char had to be replaced on an annual basis. The same problem occurred at household level [300]. This highlights the importance of either being able to measure the fluoride concentration regularly on-site, or choosing a technology that guarantees a fluoride-free water supply as long as water is being treated. The community was not able to successfully maintain this relatively simple bone char technology.

A.1.3 Health implications of fluoride

Oldonyowas and Lemongo are the most fluoride-affected villages. In early April 2013, a number of *boma*s were visited in Mareu and Lemanda sub-villages in order to ascertain the prevalence and severity of fluorosis in this area. Observation of teeth and body impairments for the interviewed villagers was carried out informally by a team of visitors, village executives and Ministry of Water representatives. This was combined with an informal assessment of awareness and need. Such visits have been carried out for some decades, which have resulted in an increased awareness about fluoride issues. To reduce such fluoride exposure, many villagers who are financially able to send their children away for their education have done so.

Chronic ingestion of excess fluoride can cause fluorosis which affects teeth and bones [12]. Moderate amounts lead to dental fluorosis, and long-term ingestion of large amounts can lead to severe skeletal fluorosis. The clinical appearance of milder forms of dental fluorosis is characterized by narrow white lines following the perikymata and brown or yellowish stains in the opaque areas of the tooth. The more severe forms are subject to loss of outermost enamel and mechanical breakdown of the surface [344]. In skeletal fluorosis, fluoride accumulates in the bone progressively over a long time. The early symptoms of skeletal fluorosis include bone pains and stiffness in the joints. In severe cases, the bone structure may change and ligaments may calcify, resulting in progressive kyphosis and restricted movement [12, 345].

Brown teeth are generally a very common sight in northern Tanzania. Many of the children aged between 5 and 15 years, as well as adults, were found to have serious dental fluorosis (**Figure A.2**). Similarly, Kaseva [271] reported that in the Maji ya Chai Ward

on the south-eastern side of Arusha National Park, all the 2217 children examined aged between 12 and 16 years had dental fluorosis while 74 percent of children in Ngurdoto Ward exhibited a severe degree. Dental fluorosis affects children more than adults because fluorosis is formed during the early stages of enamel development [344]. Dental fluorosis in an adult is likely be the result of high fluoride exposure when the adult was a child or adolescent [12]. **Figure A.2**B shows a baby born with four toes and deformed legs. Some studies found that the human placenta does not prevent the passage of fluoride from a pregnant mother's bloodstream to the fetus and may in fact increase exposure [346, 347]. As a result, a fetus can be harmed by fluoride ingested by the mother during pregnancy. **Figure A.2**C shows a five-year-old girl who underwent surgery to straighten her legs. Her legs are now less deformed but her condition is still not normal. She suffers like many others by inhibited growth and she is still drinking water from the local contaminated source. Adults above 40 years were observed to suffer from premature aging and were unable to walk straight due to serious backache. Severe kyphosis and mobility disability became apparent. **Figure A.2**D shows a woman who could no longer stand up straight and was using water containers as 'extended legs'. While families with sufficient means are sending children to school outside the ward to avoid this water exposure, others seemed somewhat oblivious to the problem or do not have the means and/or family connections to realize such an option.

Although agreement exists regarding the endemic fluorosis in the area, fluoride may not be the only cause of the observed endemic diseases and it is very obvious that not all those exposed show similar symptoms. Enamel opacities similar to dental fluorosis are associated with other conditions, such as malnutrition with deficiency of calories, proteins or vitamins [348]. Lifestyle and diet will almost certainly play an important role and may offer important remediation strategies. Malnutrition is an important issue in the area. Oikos East Africa led a four-year biometric campaign (2010−2013) targeting 5-19 year old children in the Arusha Region. It was found that among the students of the Primary Schools in Oldonyosambu Ward, specifically Oldonyosambu, Leminyor, Losinoni and Engutukoit Primary Schools, the total prevalence of malnutrition measured was 32 of malnourished and 35 of severely malnourished (n = 10668) [349]. Far greater studies are thus needed to relate life style, dietary pattern, and other possible contributing factors to the observed health effects. This will naturally lead to opportunities to correct the problem.

(A) Adult with dental fluorosis

(B) Baby born with four toes and deformed leg

(C) Child with deformed and scarred legs

(D) Skeletal fluorosis of the aged

Figure A.2: Evidence of dental and skeletal fluorosis in the villagers within Oldonyosambu Ward (photos from [191])

A.2 Datasheet of Tanzanian water samples

Table A.2: Datasheet of Tanzanian water samples

ID	pH	EC	Turbidity	IC	TOC	SUVA	F⁻	Cl⁻	SO₄²⁻	Si	Na	K	Mg	Ca	Sr	Al	B	Ba	Fe	Mo	Zn
	–	µS cm	NTU	mg L⁻¹	mg L⁻¹	–	mg L⁻¹	mg L⁻¹	mg L⁻¹	mg L⁻¹	mg L⁻¹	mg L⁻¹	mg L⁻¹	mg L⁻¹	mg L⁻¹	µg L⁻¹	µg L⁻¹	µg L⁻¹	µg L⁻¹	µg L⁻¹	µg L⁻¹
1	9.46	9230	5.3	749.0	32.8	2.16	212.0	323.2	689.9	1.8	2469.7	261.7	6.3	2.7	0.1	928.0	626.3	7.3	38.7	443.2	18.0
2	9.89	31400	16.9	2310.0	60.2	4.25	974.9	1494.5	1444.0	12.2	9921.0	1507.5	6.2	7.0	0.7	14.4	2944.4	26.1	13.6	2063.2	11.0
3	9.53	8710	14.2	736.0	39.8	1.69	239.9	215.4	585.0	4.2	2184.9	358.8	3.3	0.9	0.1	222.6	479.9	< 5	20.9	388.2	< 5
4	9.95	28900	15.0	2540.0	74.2	2.99	897.7	966.9	514.1	18.4	8911.5	1476.0	3.5	6.6	0.5	67.6	2269.7	33.4	15.7	1351.0	< 5
5	9.88	38000	9.5	3120.0	106.0	1.64	1173.7	1548.4	2772.8	16.4	11800.1	2024.1	8.2	7.6	0.5	< 10	3045.4	34.5	107.6	2167.1	5.0
6	8.92	1545	12.8	123.0	3.9	4.17	19.4	43.9	104.5	15.8	320.5	72.7	1.8	7.0	0.2	59.8	141.5	< 5	84.6	120.2	< 5
7	8.34	921	3.5	83.2	2.3	2.18	21.9	21.3	31.5	11.0	199.4	25.9	0.5	3.2	0.1	< 10	67.3	< 5	< 10	44.8	< 5
8	8.29	2270	9.2	245.0	243.0	4.69	42.4	46.6	15.5	9.1	539.4	71.1	2.5	21.0	0.7	933.5	203.8	14.6	4468.4	60.1	9.0
9	8.76	922	3.7	83.2	2.3	3.25	22.8	21.4	31.0	9.8	197.5	25.6	0.5	3.2	0.1	25.5	52.4	< 5	13.6	41.8	< 5
10	8.75	908	2.1	79.4	3.5	3.80	10.2	21.8	51.5	15.5	178.2	31.0	1.3	6.9	0.1	23.3	61.3	< 5	16.7	46.9	< 5
11	8.35	314	5.8	32.3	3.5	4.24	3.3	5.5	3.9	20.2	53.4	16.1	0.5	2.4	0.0	25.5	21.8	< 5	12.5	< 20	17.0
12	8.33	548	0.1	52.5	0.9	2.38	10.9	5.6	11.4	20.8	112.3	23.2	0.6	4.4	0.1	< 10	21.8	< 5	< 10	< 20	15.0
13	8	504	0.9	47.0	2.4	4.68	12.8	6.4	10.0	20.6	94.1	30.2	0.7	4.0	0.1	28.8	16.8	5.2	39.7	< 20	5.0
14	9.67	105500	317.8	9030.0	367.0	6.00	672.6	27857.2	1895.6	103.2	48955.5	2605.9	0.3	3.8	0.3	< 10	44077.6	801.5	755.5	1645.4	14.0
15	8.65	1097	0.7	81.1	0.8	2.23	4.8	48.3	103.7	18.2	225.0	16.2	2.1	2.3	0.1	< 10	135.5	< 5	< 10	40.8	< 5
16	7.87	255	1.7	53.6	1.9	2.36	0.6	11.8	8.3	18.3	29.9	6.7	5.5	15.2	0.3	6.2	20.0	152.1	< 10	< 20	20.0
17	7.89	262	12.5	16.8	1.6	2.08	0.3	6.8	44.4	12.6	21.4	9.3	4.1	23.4	0.2	8.3	19.0	86.3	< 10	< 20	20.0
18	10.1	30800	30.4	2280.0	98.8	0.75	158.8	2188.5	1289.2	27.5	9679.1	1249.1	0.2	3.3	0.4	< 10	2663.5	174.5	< 10	524.7	< 5
19	7.44	381	123.4	40.8	2.7	2.95	1.0	8.6	7.5	25.3	39.8	9.7	9.9	19.6	0.3	34.3	21.0	18.5	26.0	< 20	< 5
20	9.62	3020	3.9	160.0	1.7	1.23	22.9	197.3	169.6	67.1	698.5	17.0	0.0	0.4	0.0	19.9	726.2	17.8	11.5	< 20	< 5
21	8.38	4720	21.8	463.0	270.0	5.30	33.1	297.4	130.8	22.1	1290.0	14.2	1.0	7.9	0.1	17.7	1526.6	95.1	1463.0	< 20	5.0
22	8.27	348	2.0	39.6	0.5	0.40	0.5	4.4	3.3	23.4	19.8	6.9	15.9	24.7	0.3	< 5	13.0	17.5	< 10	< 20	< 5
23	8.99	16150	39.0	908.0	58.2	2.63	56.6	486.1	5291.5	10.6	4730.9	91.9	8.0	10.1	1.2	< 10	5159.7	160.9	11.5	183.4	9.0
24	7.5	604	15.9	70.6	13.1	3.47	0.7	16.1	10.3	12.7	66.7	15.6	8.9	43.2	2.9	< 10	85.1	295.7	11.5	43.8	< 5
25	9.05	1535	497.8	119.0	25.7	3.71	3.6	177.1	5.4	28.0	348.8	9.1	7.1	5.2	0.1	4476.0	228.6	43.9	5068.3	< 20	12.0
26	8.34	472	10.1	50.3	7.2	0.65	2.6	11.2	0.0	40.0	55.4	23.7	10.0	14.9	0.2	< 10	34.6	13.6	< 10	< 20	< 5

27	7.87	995	1.2	95.4	10.4	4.30	18.6	24.1	25.2	13.5	212.7	38.1	1.1	5.1	0.2	48.7	49.5	< 5	76.3	37.7	< 5
28	8.43	907	0.3	80.3	1.3	1.78	20.2	22.2	32.2	11.4	184.4	23.7	0.7	4.1	0.1	< 10	44.5	< 5	< 10	42.8	10.0
29	8.77	930	1.1	82.2	3.2	2.32	21.9	22.0	30.8	10.3	193.3	26.1	0.6	3.7	0.1	11.1	39.6	< 5	14.6	42.8	< 5
30	8.67	609	0.4	53.5	2.1	3.22	17.1	17.7	14.7	15.7	108.8	31.5	0.5	3.1	0.1	12.2	50.5	< 5	< 10	37.7	17.0
31	7.73	120	0.4	10.7	0.4	1.49	0.1	0.7	0.6	11.7	3.4	1.0	3.3	10.3	0.1	8.3	< 10	3.1	< 10	< 20	32.0
32	7.38	487	0.1	55.4	0.4	3.70	0.8	8.3	9.0	32.6	40.7	10.1	25.3	25.5	0.3	< 5	18.0	10.3	< 10	< 20	158.0
33	7.54	1289	6.4	107.0	22.9	3.66	0.5	160.4	2.6	26.4	177.0	21.7	30.5	42.7	0.5	< 10	82.1	61.7	1360.6	< 20	< 5
34	8.23	868	0.7	76.7	4.2	3.76	21.0	21.8	28.3	8.5	180.9	25.2	0.6	3.6	0.1	16.6	42.5	< 5	37.6	36.7	< 5
35	7.51	1000	6.0	96.6	24.4	3.61	11.3	30.0	16.7	11.7	190.6	49.3	2.2	9.7	0.2	140.6	53.4	< 5	285.3	22.4	14.0
36	9.6	14800	69.2	856.0	124.0	2.15	40.7	2532.7	472.9	2.7	3893.0	27.8	7.4	7.9	0.3	35.4	2158.9	117.0	34.5	215.0	< 5
37	8.77	718	0.3	82.3	2.4	3.45	23.8	21.9	29.3	8.5	216.9	28.6	0.6	3.5	0.1	5.1	39.2	< 5	17.4	34.8	< 5
38	8.86	757	0.1	84.5	0.6	2.53	3.3	14.4	3.8	18.9	145.1	24.8	7.5	16.3	0.2	< 5	21.5	< 5	< 10	< 20	15.0
39	7.53	443	0.5	35.6	10.1	5.60	13.4	7.2	12.6	20.3	86.1	22.8	0.5	2.6	0.1	37.0	23.5	5.1	48.1	< 20	133.0
40	8.28	816	2.3	69.7	35.6	4.43	10.9	20.6	36.8	10.4	172.9	38.2	1.2	5.6	0.2	600.8	39.2	< 5	566.0	27.1	5.0
41	7.97	775	16.8	59.5	35.8	5.41	12.3	17.6	62.6	12.8	162.1	30.4	1.1	6.5	0.2	611.1	36.2	< 5	751.3	24.2	< 5
42	6.99	1489	0.1	151.0	2.1	3.41	3.6	34.6	36.8	37.1	241.3	29.9	55.3	46.1	0.9	< 5	92.1	14.4	< 10	< 20	< 5
43	7.85	308	0.4	30.1	16.4	5.40	3.9	6.3	10.2	18.8	54.0	15.5	1.0	4.5	0.1	92.5	22.0	< 5	246.0	< 20	< 5
44	8.45	580	0.6	55.0	17.6	5.44	7.8	13.9	17.8	17.7	118.4	27.8	1.2	5.5	0.2	119.5	29.0	< 5	329.0	< 20	< 5
45	7.89	111	0.1	12.6	2.2	2.67	0.3	1.2	1.4	16.8	13.7	9.2	0.8	4.0	0.2	15.6	12.0	< 5	< 10	< 20	< 5
46	7.77	213	0.2	23.2	3.2	3.11	1.3	3.5	3.2	27.2	37.2	10.8	0.4	2.3	0.0	38.5	13.0	< 5	19.0	< 20	< 5
47	8.72	840	0.1	70.7	2.4	3.41	27.0	15.0	39.2	12.1	168.6	46.9	0.4	1.4	0.1	19.7	70.0	< 5	< 10	57.5	< 5
48	9.06	1350	0.3	110.0	1.9	3.26	29.3	29.9	80.9	11.9	298.1	79.9	0.9	3.7	0.2	26.0	107.0	< 5	< 10	92.7	< 5
49	9.95	54600	185.0	1820.0	77.2	3.74	239.9	15770.5	2197.6	2.4	9286.1	31.4	1.9	6.1	0.3	34.3	3144.0	106.9	143.0	552.1	< 5
50	8.7	1362	14.8	88.7	4.7	3.40	2.9	178.7	86.5	13.5	278.1	7.3	11.6	36.6	0.8	< 5	179.0	103.8	< 10	< 20	< 5
51	8.08	27100	14.6	420.2	57.2	2.28	9.2	569.0	18362.0	18.0	8472.5	272.0	605.4	128.3	8.2	< 5	5645.0	81.2	20.0	861.3	< 5
52	8.68	950	0.9	88.9	13.9	5.02	15.8	24.0	35.2	15.5	211.7	40.0	1.3	6.2	0.2	94.6	45.0	< 5	282.0	39.0	< 5
53	8.58	793	0.4	74.0	14.6	5.40	15.8	17.9	25.4	14.3	163.4	30.4	1.0	5.4	0.1	112.2	39.0	< 5	431.0	32.2	< 5
54	9.47	5190	0.8	444.4	11.4	1.10	61.5	276.9	332.8	15.8	1478.6	17.3	0.1	0.5	0.2	5.2	2036.0	131.5	< 10	25.4	< 5
55	8.63	1141	0.4	119.0	2.2	3.13	2.8	32.2	16.0	33.9	252.7	13.5	11.1	24.0	0.5	< 5	352.0	33.9	< 10	< 20	< 5

56	8.87	2210	61.5	212.3	23.8	2.17	3.4	225.4	32.7	12.3	575.9	6.6	3.2	7.5	0.2	1189.9	238.0	23.6	1018.0	< 20	< 5
57	9.28	3230	26.7	217.8	10.6	2.39	13.9	278.7	339.8	9.4	857.8	7.9	2.5	7.8	0.3	664.1	960.0	56.5	444.0	62.4	< 5
58	8.44	649	2.5	72.7	9.1	1.33	1.3	19.8	4.7	0.9	94.5	11.6	25.7	14.3	0.4	< 5	39.0	58.6	< 10	< 20	< 5
59	8.32	693	0.1	50.6	0.4	1.59	0.3	54.5	52.9	28.6	48.7	8.3	16.1	21.7	0.5	< 5	20.0	29.8	< 10	< 20	35.0
60	8.49	27600	1.1	580.8	46.6	2.36	8.9	554.0	18430.5	19.5	9012.5	288.5	638.9	122.8	8.0	< 5	6157.0	59.6	< 10	707.2	9.0
61	7.98	507	0.3	54.6	16.7	2.00	0.3	6.7	18.4	7.8	33.9	10.7	7.2	47.6	2.2	< 5	43.0	248.7	< 10	< 20	< 5
62	8.37	365	0.4	41.8	2.2	1.14	0.3	10.7	3.3	19.0	19.4	7.7	22.3	21.7	0.3	< 5	22.0	6.2	< 10	< 20	< 5
63	8.61	1064	0.8	97.2	10.6	4.42	16.4	27.3	29.4	15.0	240.5	45.5	1.5	6.1	0.0	< 5	< 10	< 5	< 10	< 20	< 5
64	8.52	807	0.8	74.3	10.8	5.13	17.9	18.1	24.5	12.6	169.4	28.9	0.8	4.5	0.1	118.5	38.0	< 5	351.0	34.1	< 5
65	8.2	128	0.2	14.8	1.5	3.49	0.8	1.8	1.3	17.5	18.9	6.9	1.0	3.5	0.1	19.7	10.0	< 5	11.0	< 20	16.0
66	8.28	441	0.5	42.9	0.9	3.40	17.9	4.9	11.8	23.8	89.2	18.7	0.3	1.7	0.0	22.9	19.0	< 5	12.0	22.4	< 5
67	8.55	540	0.8	67.6	4.5	3.63	3.3	5.0	7.5	24.7	96.1	36.4	2.0	7.6	0.4	34.3	16.0	7.2	38.0	< 20	136.0
68	7.68	433	0.0	42.9	1.1	2.20	13.4	5.0	9.7	21.9	86.1	23.4	0.2	1.5	0.1	22.9	15.0	< 5	< 10	< 20	< 5
69	7.8	430	0.0	42.2	1.2	2.87	13.9	5.0	9.8	21.9	86.8	23.4	0.2	1.4	0.0	17.7	15.0	< 5	< 10	< 20	< 5
70	8.64	498	3.3	41.6	1.3	2.04	13.9	5.1	9.7	22.0	87.9	24.0	0.2	1.3	0.0	55.1	15.0	< 5	20.0	< 20	< 5
71	8.31	202	0.6	21.3	2.1	2.88	0.9	1.8	2.2	11.2	24.4	14.2	0.4	4.5	0.2	28.1	< 10	< 5	< 10	< 20	48.0
72	8.68	544	0.8	48.4	1.9	3.70	14.5	4.6	9.5	20.9	95.8	23.9	0.5	2.8	0.1	23.9	18.0	6.2	21.0	< 20	< 5
73	8.46	527	0.7	51.7	2.4	4.27	15.1	5.5	11.5	23.3	109.7	26.5	0.4	2.2	0.0	15.6	19.0	< 5	42.0	< 20	< 5
74	8.57	502	0.4	47.8	1.9	4.04	17.1	5.3	11.5	21.1	101.4	25.8	0.5	2.8	0.1	23.9	19.0	5.1	28.0	< 20	29.0
75	8.79	705	1.0	79.2	1.8	3.83	5.2	7.1	14.6	21.5	142.0	27.3	3.1	14.7	0.5	15.6	20.0	7.2	11.0	< 20	< 5
76	8.77	800	2.9	76.8	9.2	4.62	18.6	18.3	25.3	12.8	171.6	28.7	0.7	4.2	0.1	75.9	37.0	< 5	284.0	33.2	< 5
77	8.66	1025	0.5	101.0	9.6	4.34	18.6	26.5	28.6	14.6	232.6	45.2	1.2	5.5	0.2	61.3	40.0	< 5	145.0	36.1	< 5
78	8.12	534	1.0	56.4	38.5	7.01	6.9	9.1	11.6	19.2	107.3	31.6	1.2	6.4	0.2	364.8	21.0	< 5	1454.0	< 20	< 5
79	8.66	2200	3.4	295.2	88.8	3.81	46.4	75.5	2.9	1.9	532.8	75.9	1.4	8.4	0.3	1181.1	733.0	5.0	1049.0	76.1	8.0
80	8.78	3930	0.0	413.5	11.4	3.94	50.5	186.7	745.0	3.4	920.0	116.4	1.9	3.8	0.2	639.5	902.0	< 5	< 10	492.6	5.0
81	8.35	787	0.6	93.6	14.5	5.25	15.0	18.3	24.7	12.9	167.9	30.4	0.8	4.5	0.1	254.5	805.0	< 5	386.0	29.3	6.0
82	10.24	35000	36.1	3500.0	113.6	1.13	1391.0	1295.4	2913.1	0.3	1769.2	1482.0	3.6	1.9	0.2	512.2	1967.0	< 5	120.0	1130.5	6.0
83	9.37	4480	0.8	525.0	16.0	0.88	65.0	175.3	365.1	14.6	1020.1	217.5	2.4	4.7	0.6	35.5	353.0	5.3	< 10	274.2	< 5
84	9.08	1493	0.4	247.0	1.9	3.83	28.1	56.6	140.6	15.7	287.0	89.0	1.5	5.2	0.3	< 5	1234.0	< 5	< 10	112.2	< 5

85	8.53	960	0.6	107.0	11.1	4.51	18.4	24.3	28.2	14.5	209.1	41.0	1.1	5.2	0.2	275.1	853.0	< 5	202.0	41.9	6.0
86	7.92	218	0.7	24.5	1.9	3.49	2.8	1.9	2.0	20.9	31.6	10.1	1.2	4.0	0.1	6.5	< 10	< 5	< 10	< 20	< 5
87	8.42	924	0.5	82.8	5.9	4.25	20.1	20.5	27.5	10.4	182.4	27.7	0.7	4.3	0.1	20.5	35.0	< 5	64.2	34.5	63.0
88	8.07	1242	0.4	117.0	9.7	4.03	18.4	29.9	28.4	15.3	259.5	50.4	1.3	5.7	0.2	23.7	39.0	< 5	56.9	36.6	< 5
89	9	1924	0.5	141.0	2.3	3.66	29.3	63.7	148.0	12.7	375.4	97.4	1.4	4.9	0.3	12.9	137.0	< 5	< 10	120.9	< 5
90	8.29	4430	3.3	492.5	77.5	6.84	40.9	132.9	431.4	8.5	996.5	338.5	3.3	18.8	1.3	210.1	189.0	7.5	1117.0	87.3	< 5
91	9.01	2110	40.1	199.0	26.1	3.04	29.3	81.7	170.1	8.6	477.7	116.5	1.9	5.4	0.3	11.8	155.0	< 5	20.7	135.1	< 5
92	8.37	3020	2.8	325.5	54.5	6.23	36.1	72.2	264.7	8.1	677.3	203.3	2.4	8.5	0.6	137.9	170.0	6.4	384.1	44.7	7.2
93	8.9	1858	0.9	132.0	2.8	3.53	30.5	62.1	148.7	12.8	391.2	105.0	1.4	4.7	0.3	17.2	137.0	< 5	< 10	121.9	< 5
94	8.22	810	2.9	77.5	1.6	3.72	7.3	17.2	24.7	23.6	159.2	33.4	2.1	7.8	0.2	12.9	29.0	< 5	< 10	28.4	< 5
95	8.12	879	0.4	90.0	1.3	2.84	7.6	16.7	35.5	52.8	168.6	40.3	3.5	12.3	0.4	< 5	37.0	< 5	< 10	30.5	31.0
96	8.88	994	1.2	82.6	5.2	4.85	23.7	21.0	28.3	10.4	191.0	28.8	0.5	3.5	0.1	30.2	34.0	< 5	80.7	35.5	< 5
97	8.91	1434	0.8	132.0	7.9	4.28	22.8	34.2	27.1	18.3	287.7	55.1	1.4	6.3	0.2	29.1	42.0	< 5	62.1	38.6	< 5
98	9.44	5310	0.8	441.0	12.5	1.25	57.6	272.2	329.0	16.0	1334.0	15.1	0.1	0.5	0.2	< 5	1751.0	116.0	< 10	22.3	7.2
99	8.51	590	3.3	57.0	1.4	3.55	4.1	2.5	47.9	27.5	80.2	1.3	3.4	36.5	0.6	< 5	113.0	83.0	< 10	188.9	< 5
100	8.41	1212	0.8	117.0	1.6	3.20	8.3	5.8	205.6	42.5	114.9	19.6	65.4	72.7	2.8	< 5	127.0	92.6	< 10	249.8	21.7
101	7.53	2890	1.2	462.0	7.3	3.06	11.2	66.4	34.6	42.7	686.6	67.4	47.0	32.6	6.6	< 5	1053.0	809.1	< 10	52.8	< 5
102	8.45	723	1.8	88.7	2.3	2.79	0.9	14.2	21.8	13.1	66.5	11.1	10.9	83.4	1.1	< 5	117.0	380.1	< 10	< 20	< 5
103	8.43	481	2.0	60.2	1.4	3.16	1.0	9.8	7.6	34.6	40.5	1.4	23.1	26.3	0.2	< 5	43.0	89.4	< 10	< 20	< 5
104	8.32	1098	1.5	111.0	1.7	3.16	1.4	49.7	55.4	39.8	98.5	3.3	69.5	59.5	0.7	< 5	94.0	178.9	< 10	< 20	< 5
105	9.54	2900	0.9	248.0	2.6	2.96	23.8	185.2	156.0	65.8	750.0	11.8	0.0	0.3	0.0	11.8	619.0	14.9	< 10	< 20	< 5
106	8.77	2600	2.3	378.0	11.0	4.63	8.3	39.7	45.5	32.9	726.3	20.7	5.3	2.5	0.2	< 5	367.0	38.3	< 10	< 20	< 5
107	7.55	2500	8.0	282.0	26.0	4.06	3.2	195.4	284.0	16.4	528.2	21.2	30.8	60.7	9.5	< 5	183.0	529.1	10.4	81.2	< 5
108	8.18	28500	15.8	960.0	107.0	3.43	4.6	593.1	18230.4	14.8	7256.7	271.0	505.2	155.6	10.4	< 5	4464.0	101.1	135.6	< 20	< 5
109	8.85	3850	3.5	415.0	29.4	4.02	19.9	190.2	302.4	29.8	1033.7	32.2	8.6	6.2	1.2	2601.4	842.0	233.1	6007.2	138.1	16.5
110	7.4	1237	7.8	171.0	19.1	2.57	1.0	56.2	74.1	16.6	178.0	20.9	29.0	65.7	7.9	< 5	85.0	588.7	< 10	20.3	< 5
111	8.56	3640	0.9	422.0	113.0	7.00	62.1	41.3	216.0	3.8	973.0	184.2	1.3	5.7	0.4	311.3	254.0	7.5	441.0	104.6	8.0
112	9.11	1306	0.4	161.0	0.9	1.42	24.8	62.0	21.8	5.7	324.9	15.1	0.1	0.5	0.0	115.3	61.0	< 5	< 10	61.9	< 5
113	8.78	878	0.4	84.1	3.4	3.65	22.6	21.7	29.5	8.9	202.8	29.6	0.6	3.6	0.1	14.0	36.0	< 5	21.0	38.0	< 5

114	8.62	921	0.6	89.5	4.9	4.09	21.5	22.7	27.8	9.8	207.0	34.1	0.7	4.2	0.1	29.0	37.0	< 5	40.0	38.0	< 5
115	8.53	1126	0.6	111.0	13.6	4.04	21.4	30.1	27.7	13.8	251.4	53.3	1.4	5.6	0.2	40.0	52.0	< 5	835.0	36.0	6.0
116	8.07	722	0.8	68.3	35.0	5.11	15.3	19.1	37.8	10.4	147.3	32.5	0.9	5.6	0.1	186.0	36.0	< 5	107.0	22.0	< 5
117	8.92	3340	1.0	353.0	114.0	5.64	59.7	40.6	204.8	4.1	868.1	171.1	1.1	5.3	0.3	256.0	248.0	8.0	408.0	123.0	44.0
118	8.28	2750	0.2	173.6	2.5	0.93	5.5	321.9	283.9	27.2	688.1	16.5	16.4	13.5	0.9	< 5	342.0	36.8	< 10	304.5	171.3
119	8.28	2790	0.2	176.4	3.0	0.74	5.5	301.9	283.4	27.1	655.0	16.1	16.0	13.6	0.9	< 5	317.7	36.8	< 10	309.7	160.8
120	9.67	4920	0.2	446.0	6.8	2.22	57.6	258.8	306.0	15.6	1334.8	13.9	0.1	0.4	0.2	< 5	1715.8	108.3	< 10	24.5	< 5
121	8.45	2910	0.9	413.0	2.3	3.47	13.4	20.5	165.1	42.7	796.2	29.5	22.3	10.7	2.0	< 5	1149.6	107.2	< 10	188.0	8.4
122	8.93	1037	0.2	94.5	10.7	4.92	18.4	26.1	23.1	14.9	235.0	43.2	1.2	5.2	0.2	61.6	47.4	< 5	138.0	32.7	6.3
123	9.09	832	0.3	73.0	8.9	5.69	20.0	20.0	26.6	10.8	37.4	27.4	0.6	3.8	0.1	83.5	33.5	< 5	229.3	33.7	< 5
124	9.7	4940	15.8	430.0	5.3	6.72	56.2	268.0	306.1	17.3	1358.1	16.3	0.5	1.6	0.1	150.2	1932.9	57.6	241.8	26.9	< 5
125	9.3	1054	0.5	81.5	4.2	1.03	2.0	12.5	6.1	21.2	90.3	14.2	13.3	63.9	1.7	< 5	13.1	224.7	< 10	< 20	< 5
126	8.58	283	28.0	23.75	34.5	1.49	2.0	1.7	1.5	14.4	27.3	10.7	5.6	32.0	0.9	< 5	13.1	130.0	< 10	< 20	< 5
127	12.25	21100	31.7	2220	167.0	1.24	175.8	460.2	51.4	67.1	7156.2	985.3	0.6	7.3	0.7	< 5	601.5	230.3	11.5	309.5	< 5
128	11.06	669	0.0	55	1.7	2.80	9.8	6.7	14.3	16.8	61.9	18.8	5.6	46.2	0.8	< 5	13.1	19.5	< 10	< 20	40.8
129	11.67	10420	0.3	1110	38.0	2.37	88.0	142.8	457.7	313.6	3184.3	459.3	1.9	7.6	1.0	< 5	337.0	274.8	39.0	331.1	< 5
130	10.86	2580	0.4	184.5	7.1	0.42	14.7	88.8	291.3	18.9	617.9	56.9	27.4	12.1	0.7	< 5	50.6	21.4	< 10	154.3	< 5
131	8.93	1048	0.0	70	1.3	0.12	4.5	46.9	143.7	23.2	227.6	23.2	11.3	7.3	0.3	< 5	49.8	< 5	12.4	35.9	6.1
132	11.26	60500	29.0	5580	564.0	5.68	596.0	11178.5	920.7	47.5	24010.1	865.1	0.3	4.4	0.5	< 5	17932.5	434.5	869.8	724.9	36.5
133	11.05	813	8.0	71.5	2.5	3.66	15.3	46.3	92.2	18.9	219.4	15.8	5.4	13.3	0.5	46.9	79.4	8.4	51.4	49.3	< 5
134	10.52	4160	48.6	625	265.0	6.10	58.6	167.4	70.7	17.3	1251.7	35.6	1.8	22.9	0.9	726.6	847.7	280.4	906.1	35.0	14.8
135	10.84	10720	138.0	1390	640.0	5.88	132.2	427.2	284.5	48.7	3639.7	115.7	0.5	11.6	1.0	264.7	1561.0	279.5	322.4	54.7	6.1
136	9.08	2450	0.2	177	8.5	1.08	27.0	187.8	148.3	42.0	604.0	55.6	18.3	23.2	3.9	< 5	312.5	127.2	< 10	32.3	69.0
137	9.32	1561	0.0	135	8.1	1.32	9.0	70.6	34.9	41.7	320.8	33.7	31.4	39.4	3.9	< 5	142.3	138.3	< 10	< 20	46.9
138	8.63	1576	0.2	133	5.5	1.60	7.1	94.6	94.3	27.8	338.1	33.2	31.2	41.6	1.7	< 5	129.2	76.1	< 10	< 20	8.7
139	8.38	2030	0.4	170	6.7	1.24	8.6	156.2	155.5	32.9	476.9	41.8	33.1	49.9	2.2	< 5	159.8	76.1	< 10	22.4	26.9
140	7.2	1031	0.3	20.3	6.3	2.46	1.1	81.7	44.1	29.3	122.2	34.2	23.8	36.6	0.5	19.7	23.6	1102.1	< 10	< 20	9.6
141	7.73	1326	0.3	176.0	8.6	3.12	14.7	10.0	130.8	62.4	248.6	29.2	49.0	50.0	1.5	< 5	438.3	354.7	< 10	226.1	24.3
142	9.3	27100	1.1	676.0	8.2	8.62	4.7	10049.5	823.0	1.1	6728.8	36.7	219.3	110.2	4.2	< 5	52.4	499.5	< 10	< 20	< 5

143	8.76	3940	0.4	328	4.4	3.18	47.6	182.2	540.5	4.7	1083.7	117.7	2.2	5.3	0.2	45.1	147.5	< 5	< 10	539.2	19.1
146	9.18	1835	2.8	155.0	3.0	5.29	32.6	57.1	143.4	13.3	397.8	112.7	1.5	5.5	0.3	33.8	145.8	< 5	19.5	130.1	< 5
147	8.68	4370	3.8	547.5	260.0	4.80	43.8	143.3	373.2	8.9	1079.7	334.8	2.9	15.2	1.0	310.7	179.8	18.6	1577.4	52.9	< 5
148	8.5	3990	3.2	485.0	233.0	4.68	38.5	134.6	327.6	8.9	980.3	306.4	2.8	14.4	0.9	411.2	196.4	18.6	1766.1	45.8	7.8
149	8.18	3130	2.0	367.5	218.8	4.65	49.7	137.9	230.0	10.4	834.3	149.3	2.0	9.8	0.5	499.4	187.7	12.1	1054.0	88.8	< 5
150	8.3	3530	1.5	395.0	255.0	4.70	53.2	152.0	267.7	10.1	948.3	177.5	2.5	11.9	0.6	519.1	201.7	13.0	1090.3	99.6	11.3
151	7.54	308	0.2	34.2	2.5	1.39	6.0	45.0	67.2	22.5	84.6	11.8	0.5	1.7	0.0	< 5	13.1	< 5	< 10	< 20	11.3
152	9.19	2120	2.8	257.5	46.5	4.33	34.0	67.6	160.9	12.7	511.9	120.0	1.8	7.0	0.4	92.9	176.4	5.6	186.9	126.5	< 5
153	7.79	167	1.0	19.5	2.1	3.72	2.4	3.3	2.8	8.4	35.3	12.1	0.4	2.2	0.1	< 5	11.3	< 5	< 10	< 20	806.8
154	7.76	166	0.7	19.5	1.9	6.32	1.8	3.4	2.7	8.6	36.1	12.5	0.5	2.3	0.1	< 5	13.1	< 5	< 10	< 20	615.7
155	8.4	2740	0.3	307.0	1.7	7.93	27.5	85.2	246.4	23.8	734.8	92.1	7.9	8.2	0.6	< 5	86.4	25.1	< 10	428.0	< 5
156	7.78	340	0.4	44.4	2.5	5.93	4.3	5.0	5.0	24.1	97.7	18.9	0.6	2.7	0.1	< 5	14.0	< 5	< 10	< 20	< 5
157	7.56	643	0.0	82.8	2.6	4.55	2.3	13.1	8.2	17.0	75.6	1.0	8.6	65.1	1.3	< 5	55.0	346.7	< 10	< 20	12.4
158	7.34	217	26.8	24.6	4.8	1.88	1.0	4.0	6.6	16.9	23.0	1.3	2.8	19.7	0.3	< 5	24.0	84.8	< 10	< 20	< 5
159	7.63	595	0.2	70.4	9.7	1.69	2.5	25.2	12.6	12.1	100.1	2.8	4.5	35.0	0.7	< 5	41.0	168.5	< 10	< 20	< 5
160	7.5	1571	0.0	149.5	22.3	3.26	3.5	148.5	79.0	16.5	289.6	2.0	12.4	38.3	1.5	< 5	94.0	223.2	< 10	< 20	< 5
161	8.33	537	2.2	50.5	9.9	1.86	1.8	42.0	10.0	7.6	92.9	3.9	3.4	25.8	0.7	< 5	35.0	129.9	< 10	< 20	< 5
162	9.05	2410	0.6	230.5	33.5	2.25	8.1	234.4	95.5	21.8	592.3	7.8	5.3	5.8	0.6	< 5	290.0	56.9	< 10	< 20	18.6
163	7.5	1184	0.0	151.0	15.1	1.61	3.5	32.0	42.0	13.3	183.8	1.0	9.9	54.5	1.6	< 5	80.0	301.6	< 10	< 20	< 5
164	8.11	3250	84.9	328.0	87.7	1.97	30.0	137.1	294.3	19.6	832.1	107.4	9.4	10.9	1.1	< 5	74.0	31.1	< 10	309.2	< 5
165	8.92	1524	0.1	134.0	4.8	3.81	4.2	58.6	189.7	21.5	299.5	36.4	20.3	15.5	0.9	< 5	32.0	6.4	< 10	92.1	< 5
166	9.07	2580	0.1	248.0	10.8	3.86	8.9	108.3	293.9	17.9	596.1	53.4	24.8	11.3	0.8	< 5	48.0	29.0	< 10	156.7	5.2

References

[1] World Health Organization, *UN-water global analysis and assessment of sanitation and drinking-water (GLAAS) 2014 report: investing in water and sanitation: increasing access, reducing inequalities*: Switzerland (2014)

[2] Sivakumar, B., *Water crisis: from conflict to cooperation – an overview.* Hydrological Sciences Journal, **56,** 531-552 (2011)

[3] Mbonile, M.J., *Migration and intensification of water conflicts in the Pangani Basin, Tanzania.* Habitat International, **29,** 41-67 (2005)

[4] Lee, A., Elam, J.W., and Darling, S.B., *Membrane materials for water purification: design, development, and application.* Environmental Science: Water Research & Technology, **2,** 17-42 (2016)

[5] Committee on Environment and Public Works, *The Safe Drinking Water Act*, in *Public law*: USA (1996)

[6] Ayoob, S. and Gupta, A.K., *Fluoride in drinking water: a review on the status and stress effects.* Critical Reviews in Environmental Science and Technology, **36,** 433-487 (2006)

[7] Edmunds, W.M. and Smedley, P., *Fluoride in natural waters*, in *Essentials of Medical Geology: Impacts of The Natural Environment on Public Health*, Selinus, O., Alloway, B., Centeno, J.A., Finkelman, R.B., Fuge, R., Lindh, U., and Smedley, P.L., Academic Press, US. 301-329 (2005)

[8] Kim, K. and Jeong, G.Y., *Factors influencing natural occurrence of fluoride-rich groundwaters: a case study in the southeastern part of the Korean Peninsula.* Chemosphere, **58,** 1399-1408 (2005)

[9] Kwasnik, W., *Fluorine Compounds*, in *Handbook of Preparative Inorganic Chemistry*, Brauer, G., Academic Press, New York, US (1963)

[10] Amini, M., Mueller, K., Abbaspour, K.C., Rosenberg, T., Afyuni, M., Møller, K.N., Sarr, M., and Johnson, C.A., *Statistical modeling of global geogenic fluoride contamination in groundwaters.* Environmental Science & Technology, **42,** 3662-3668 (2008)

[11] Smedley, P.L., Nkotagu, H., Pelig-Ba, K., MacDonald, A.M., Tyler-Whittle, R., Whitehead, E.J., and Kinniburgh, D.G., *Fluoride in groundwater from high-fluoride areas of Ghana and Tanzania.* British Geological Survey: Nottingham (2002)

[12] Fawell, J., Bailey, K., Chilton, J., Dahi, E., Fewtrell, L., and Magara, Y., *Fluoride in drinking water*. London World Health Organization (2006)

[13] Ndiaye, P.I., Moulin, P., Dominguez, L., Millet, J.C., and Charbit, F., *Removal of fluoride from electronic industrial effluentby RO membrane separation.* Desalination, **173,** 25-32 (2005)

[14] Dolar, D., Košutić, K., and Vučić, B., *RO/NF treatment of wastewater from fertilizer factory — removal of fluoride and phosphate.* Desalination, **265,** 237-241 (2011)

[15] Gouider, M., Feki, M., and Sayadi, S., *Separative recovery with lime of phosphate and fluoride from an acidic effluent containing H_3PO_4, HF and/or H_2SiF_6.* Journal of Hazardous materials, **170,** 962-968 (2009)

[16] Bhatnagar, A., Kumar, E., and Sillanpää, M., *Fluoride removal from water by adsorption—A review.* Chemical Engineering Journal, **171,** 811-840 (2011)

[17] Ozsvath, D., *Fluoride and environmental health: a review.* Reviews in Environmental Science and Bio/Technology, **8,** 59-79 (2009)

[18] Wang, S.X., Wang, Z.H., Cheng, X.T., Li, J., Sang, Z.P., Zhang, X.D., Han, L.L., Mao, X.Y., Wu, Z.M., and Wang, Z.Q., *Arsenic and fluoride exposure in drinking water: Children's IQ and growth in Shanyin county, Shanxi province, China.* Environmental Health Perspectives, **115,** 643-647 (2007)

[19] Schwarzenbach, R.P., Gschwend, P.M., and Imboden, D.M., *An Introduction to Environmental Organic Chemicals*, in *Environmental Organic Chemistry*Wiley. 13-54 (2005)

[20] Zumstein, J. and Buffle, J., *Circulation of pedogenic and aquagenic organic matter in an eutrophic lake.* Water Research, **23,** 229-239 (1989)

[21] Huber, S.A., Balz, A., Abert, M., and Pronk, W., *Characterisation of aquatic humic and non-humic matter with size-exclusion chromatography – organic carbon detection – organic nitrogen detection (LC-OCD-OND).* Water Research, **45,** 879-885 (2011)

[22] Aiken, G.R., McKnight, D.M., Thorn, K.A., and Thurman, E.M., *Isolation of hydrophilic organic acids from water using nonionic macroporous resins.* Organic Geochemistry, **18,** 567-573 (1992)

[23] Haberkamp, J., Ernst, M., Böckelmann, U., Szewzyk, U., and Jekel, M., *Complexity of ultrafiltration membrane fouling caused by macromolecular dissolved organic compounds in secondary effluents.* Water Research, **42,** 3153-3161 (2008)

[24] Fujioka, T., Khan, S.J., McDonald, J.A., Henderson, R.K., Poussade, Y., Drewes, J.E., and Nghiem, L.D., *Effects of membrane fouling on N-nitrosamine rejection by*

nanofiltration and reverse osmosis membranes. Journal of Membrane Science, **427,** 311-319 (2013)

[25] Aiken, G.R., McKnight, D.M., Wershaw, R.L., and MacCarthy, P., *Humic Substances in Soil, Sediment, and Water: Geochemistry, Isolation, and Characterization.* USA, Wiley (1985)

[26] Zularisam, A.W., Ismail, A.F., Salim, M.R., Sakinah, M., and Ozaki, H., *The effects of natural organic matter (NOM) fractions on fouling characteristics and flux recovery of ultrafiltration membranes.* Desalination, **212,** 191-208 (2007)

[27] Pal, A., Gin, K.Y.-H., Lin, A.Y.-C., and Reinhard, M., *Impacts of emerging organic contaminants on freshwater resources: Review of recent occurrences, sources, fate and effects.* Science of the Total Environment, **408,** 6062-6069 (2010)

[28] Petrie, B., Barden, R., and Kasprzyk-Hordern, B., *A review on emerging contaminants in wastewaters and the environment: Current knowledge, understudied areas and recommendations for future monitoring.* Water Research, **72,** 3-27 (2015)

[29] Vandenberg, L.N., Ehrlich, S., Belcher, S.M., Ben-Jonathan, N., Dolinoy, D.C., Hugo, E.R., Hunt, P.A., Newbold, R.R., Rubin, B.S., Saili, K.S., Soto, A.M., Wang, H.-S., and vom Saal, F.S., *Low dose effects of bisphenol A.* Endocrine Disruptors, **1,** 1-20 (2013)

[30] Latch, D.E., Stender, B.L., Packer, J.L., Arnold, W.A., and McNeill, K., *Photochemical fate of pharmaceuticals in the environment: cimetidine and ranitidine.* Environmental Science & Technology, **37,** 3342-3350 (2003)

[31] World Health Organization, *Guidelines for drinking-water quality, fourth edition,*: Malta (2011)

[32] Hunter, P.R. and Nichols, G., *Epidemiology and clinical features of cryptosporidium infection in immunocompromised patients.* Clinical Microbiology Reviews, **15,** 145-154 (2002)

[33] United States Environmental Protection Agency, *Cryptosporidium: Drinking Water Health Advisory*: USA (2001)

[34] Korich, D., Mead, J., Madore, M., Sinclair, N., and Sterling, C.R., *Effects of ozone, chlorine dioxide, chlorine, and monochloramine on Cryptosporidium parvum oocyst viability.* Applied and Environmental Microbiology, **56,** 1423-1428 (1990)

[35] Dalrymple, O.K., Stefanakos, E., Trotz, M.A., and Goswami, D.Y., *A review of the mechanisms and modeling of photocatalytic disinfection.* Applied Catalysis B: Environmental, **98,** 27-38 (2010)

[36] Kim, J.I., Buckau, G., Klenze, R., Rhee, D.S., and Wimmer, H., *Characterization and complexation of humic acids*. Germany, Commission of the European Communities (1990)

[37] Senesi, N., *Binding mechanisms of pesticides to soil humic substances.* Science of the Total Environment, **123–124,** 63-76 (1992)

[38] Laor, Y. and Rebhun, M., *Complexation-flocculation: A new method to determine binding coefficients of organic contaminants to dissolved humic substances.* Environmental Science & Technology, **31,** 3558-3564 (1997)

[39] Kohl, S.D. and Rice, J.A., *The binding of contaminants to humin: A mass balance.* Chemosphere, **36,** 251-261 (1998)

[40] Laor, Y. and Rebhun, M., *Evidence for nonlinear binding of PAHs to dissolved humic acids.* Environmental Science & Technology, **36,** 955-961 (2002)

[41] Christl, I., Milne, C.J., Kinniburgh, D.G., and Kretzschmar, R., *Relating ion binding by fulvic and humic acids to chemical composition and molecular size. 2. metal binding.* Environmental Science & Technology, **35,** 2512-2517 (2001)

[42] Haynes, W.M., *CRC Handbook of Chemistry and Physics*. USA, CRC Press (2014)

[43] Hayes, M.H.B., MacCarthy, P., Malcolm, R.L., and Swift, R.S., *Humic substances II. In search of structure*. Wiley (1989)

[44] Swift, R.S., *Macromolecular properties of soil humic substances: Fact, fiction, and opinion.* Soil science, **164,** 790-802 (1999)

[45] Ghosh, K. and Schnitzer, M., *Macromolecular structures of humic substances.* Soil Science, **129,** 266-276 (1980)

[46] Alvarez-Puebla, R.A. and Garrido, J.J., *Effect of pH on the aggregation of a gray humic acid in colloidal and solid states.* Chemosphere, **59,** 659-667 (2005)

[47] Chen, C., Wang, X., Jiang, H., and Hu, W., *Direct observation of macromolecular structures of humic acid by AFM and SEM.* Colloids and Surfaces A: Physicochemical and Engineering Aspects, **302,** 121-125 (2007)

[48] Sutton, R. and Sposito, G., *Molecular structure in soil humic substances: The new view.* Environmental Science & Technology, **39,** 9009-9015 (2005)

[49] Piccolo, A., *The supramolecular structure of humic substances: A novel understanding of humus chemistry and implications in soil science*, in *Advances in Agronomy*Academic Press. 57-134 (2002)

[50] Piccolo, A., Conte, P., and Cozzolino, A., *Chromatographic and spectrophotometric properties of dissolved humic substances compared with macromolecular polymers.* Soil Science, **166,** 174-185 (2001)

[51] Piccolo, A., *The supramolecular structure of humic substances.* Soil Science, **166,** 810-832 (2001)

[52] Peuravuori, J., Bursáková, P., and Pihlaja, K., *ESI-MS analyses of lake dissolved organic matter in light of supramolecular assembly.* Analytical and Bioanalytical Chemistry, **389,** 1559-1568 (2007)

[53] Šmejkalová, D. and Piccolo, A., *Aggregation and disaggregation of humic supramolecular assemblies by NMR diffusion ordered spectroscopy (DOSY-NMR).* Environmental Science & Technology, **42,** 699-706 (2008)

[54] Baalousha, M., Motelica-Heino, M., Galaup, S., and Le Coustumer, P., *Supramolecular structure of humic acids by TEM with improved sample preparation and staining.* Microscopy Research and Technique, **66,** 299-306 (2005)

[55] Colombo, C., Palumbo, G., Angelico, R., Cho, H.G., Francioso, O., Ertani, A., and Nardi, S., *Spontaneous aggregation of humic acid observed with AFM at different pH.* Chemosphere, **138,** 821-828 (2015)

[56] Tombacz, E. and Meleg, E., *A theoretical explanation of the aggregation of humic substances as a function of pH and electrolyte concentration.* Organic Geochemistry, **15,** 375-381 (1990)

[57] Jones, M.N. and Bryan, N.D., *Colloidal properties of humic substances.* Advances in Colloid and Interface Science, **78,** 1-48 (1998)

[58] Buffle, J., Wilkinson, K.J., Stoll, S., Filella, M., and Zhang, J., *A generalized description of aquatic colloidal interactions: The three-colloidal component approach.* Environmental Science & Technology, **32,** 2887-2899 (1998)

[59] Wall, N.A. and Choppin, G.R., *Humic acids coagulation: influence of divalent cations.* Applied Geochemistry, **18,** 1573-1582 (2003)

[60] Lin, M.Y., Lindsay, H.M., Weitz, D.A., Ball, R.C., Klein, R., and Meakin, P., *Universality in colloid aggregation.* Nature, **339,** 360-362 (1989)

[61] Wang, L.-F., Wang, L.-L., Ye, X.-D., Li, W.-W., Ren, X.-M., Sheng, G.-P., Yu, H.-Q., and Wang, X.-K., *Coagulation kinetics of humic aggregates in mono- and di-valent electrolyte solutions.* Environmental Science & Technology, **47,** 5042-5049 (2013)

[62] Grasso, D., Subramaniam, K., Butkus, M., Strevett, K., and Bergendahl, J., *A review of non-DLVO interactions in environmental colloidal systems.* Reviews in Environmental Science and Biotechnology, **1,** 17-38 (2002)

[63] Van Oss, C.J., *Energetics of cell-cell and cell-biopolymer interactions.* Cell Biophysics, **14,** 1-16 (1989)

[64] Zhou, Z., Wu, P., and Ma, C., *Hydrophobic interaction and stability of collidal silica.* Colloids and Surfaces, **50,** 177-188 (1990)

[65] Shin, H.-S., Monsallier, J.M., and Choppin, G.R., *Spectroscopic and chemical characterizations of molecular size fractionated humic acid.* Talanta, **50,** 641-647 (1999)

[66] Leenheer, J.A., Brown, P.A., and Noyes, T.I., *Implications of mixture characteristics on humic-substance chemistry*, in *Aquatic Humic Substances*American Chemical Society. 25-39 (1988)

[67] Kovács, A. and Varga, Z., *Halogen acceptors in hydrogen bonding.* Coordination Chemistry Reviews, **250,** 710-727 (2006)

[68] Craig, J.D.C. and Brooker, M.H., *On the nature of fluoride ion hydration.* Journal of Solution Chemistry, **29,** 879-888 (2000)

[69] Tansel, B., Sager, J., Rector, T., Garland, J., Strayer, R.F., Levine, L., Roberts, M., Hummerick, M., and Bauer, J., *Significance of hydrated radius and hydration shells on ionic permeability during nanofiltration in dead end and cross flow modes.* Separation and Purification Technology, **51,** 40-47 (2006)

[70] Schäfer, A.I., *Natural organics removal using membranes*, in *Chemical Engineering and Industrial Chemistry*. The University of New South Wales: Sydney (1999)

[71] Manning, G.S., *Counterion binding in polyelectrolyte theory.* Accounts of Chemical Research, **12,** 443-449 (1979)

[72] Hayes, D., Carter, J., and Manning, T., *Fluoride binding to humic acid.* Journal of Radioanalytical and Nuclear Chemistry, **201,** 135-141 (1995)

[73] McKnight, D.M. and Wershaw, R.L., *Complexation of copper by fulvic acid from the Suwannee River--effect of counter-ion concentration* in *Humic Substances in the Suwannee River, Georgia: Interactions, Properties, and Proposed Structures*, Averett, R.C., Leenheer, J.A., McKnight, D.M., and Thorn, K.A., U.S. Geological Survey. 59-80 (1989)

[74] Sivasamy, A., Singh, K.P., Mohan, D., and Maruthamuthu, M., *Studies on defluoridation of water by coal-based sorbents.* Journal of Chemical Technology & Biotechnology, **76,** 717-722 (2001)

[75] Abe, I., Iwasaki, S., Tokimoto, T., Kawasaki, N., Nakamura, T., and Tanada, S., *Adsorption of fluoride ions onto carbonaceous materials.* Journal of Colloid and Interface Science, **275,** 35-39 (2004)

[76] Pekař, M., *Fluoride anion binding by natural lignite (South Moravian Deposit of Vienna Basin).* Water, Air, and Soil Pollution, **197,** 303-312 (2009)

[77] Lund, M., Vacha, R., and Jungwirth, P., *Specific ion binding to macromolecules: effects of hydrophobicity and ion pairing.* Langmuir, **24,** 3387-3391 (2008)

[78] Tokunaga, S., Haron, M.J., Wasay, S.A., Wong, K.F., Laosangthum, K., and Uchiumi, A., *Removal of fluoride ions from aqueous solutions by multivalent metal compounds.* International Journal of Environmental Studies, **48,** 17-28 (1995)

[79] Jackson, P.J., Harvey, P.W., and Young, W.F., *Chemistry and bioavailability aspects of fluoride in drinking water* in *Report No: CO 5037.* WRc-NSF Ltd: Henley Road, Medmenham, Marlow, Bucks, SL7 2HD (2002)

[80] Farrah, H., Slavek, J., and Pickering, W., *Fluoride sorption by soil components: calcium carbonate, humic acid, manganese dioxide and ailica.* Soil Research, **23,** 429-439 (1985)

[81] Ayoob, S., Gupta, A.K., and Bhat, V.T., *A conceptual overview on sustainable technologies for the defluoridation of drinking water.* Critical Reviews in Environmental Science and Technology, **38,** 401-470 (2008)

[82] Greenlee, L.F., Lawler, D.F., Freeman, B.D., Marrot, B., and Moulin, P., *Reverse osmosis desalination: Water sources, technology, and today's challenges.* Water Research, **43,** 2317-2348 (2009)

[83] Nanda, D., Tung, K.-L., Hsiung, C.-C., Chuang, C.-J., Ruaan, R.-C., Chiang, Y.-C., Chen, C.-S., and Wu, T.-H., *Effect of solution chemistry on water softening using charged nanofiltration membranes.* Desalination, **234,** 344-353 (2008)

[84] Bowen, W.R. and Mukhtar, H., *Characterisation and prediction of separation performance of nanofiltration membranes.* Journal of Membrane Science, **112,** 263-274 (1996)

[85] Wijmans, J.G. and Baker, R.W., *The solution-diffusion model: a review.* Journal of Membrane Science, **107,** 1-21 (1995)

[86] Mulder, M.H.V., E. M. van Voorthuizen, and Peeters, J.M.M., *Membrane characterization*, in *Nanofiltration-Principles and Applications*, Schäfer, A.I., Fane, A.G., and Waite, T.D., Elsevier, Oxford, UK (2005)

[87] Ghosh, A.K., Jeong, B.-H., Huang, X., and Hoek, E.M.V., *Impacts of reaction and curing conditions on polyamide composite reverse osmosis membrane properties.* Journal of Membrane Science, **311,** 34-45 (2008)

[88] Guo, W., Ngo, H.-H., and Li, J., *A mini-review on membrane fouling.* Bioresource Technology, **122,** 27-34 (2012)

[89] DeFriend, K.A., Wiesner, M.R., and Barron, A.R., *Alumina and aluminate ultrafiltration membranes derived from alumina nanoparticles.* Journal of Membrane Science, **224,** 11-28 (2003)

[90] Verweij, H., *Inorganic membranes.* Current Opinion in Chemical Engineering, **1,** 156-162 (2012)

[91] Liu, H., Wang, H., and Zhang, X., *Facile fabrication of freestanding ultrathin reduced graphene oxide membranes for water purification.* Advanced Materials, **27,** 249-254 (2015)

[92] Brady-Estévez, A.S., Schnoor, M.H., Vecitis, C.D., Saleh, N.B., and Elimelech, M., *Multiwalled carbon nanotube filter: Improving viral removal at low pressure.* Langmuir, **26,** 14975-14982 (2010)

[93] Yin, J. and Deng, B., *Polymer-matrix nanocomposite membranes for water treatment.* Journal of Membrane Science, **479,** 256-275 (2015)

[94] Balta, S., Sotto, A., Luis, P., Benea, L., Van der Bruggen, B., and Kim, J., *A new outlook on membrane enhancement with nanoparticles: The alternative of ZnO.* Journal of Membrane Science, **389,** 155-161 (2012)

[95] Schäfer, A.I., Hughes, G., and Richards, B.S., *Renewable energy powered membrane technology: A leapfrog approach to rural water treatment in developing countries?* Renewable and Sustainable Energy Reviews, **40,** 542-556 (2014)

[96] Charcosset, C., *A review of membrane processes and renewable energies for desalination.* Desalination, **245,** 214-231 (2009)

[97] Robinson, R., Ho, G., and Mathew, K., *Development of a reliable low-cost reverse osmosis desalination unit for remote communities.* Desalination, **86,** 9-26 (1992)

[98] Alawaji, S., Smiai, M.S., Rafique, S., and Stafford, B., *PV-powered water pumping and desalination plant for remote areas in Saudi Arabia.* Applied Energy, **52,** 283-289 (1995)

[99] Herold, D. and Neskakis, A., *A small PV-driven reverse osmosis desalination plant on the island of Gran Canaria.* Desalination, **137,** 285-292 (2001)

[100]   Lhassani, A., Rumeau, M., Benjelloun, D., and Pontie, M., *Selective demineralization of water by nanofiltration Application to the defluorination of brackish water.* Water Research, **35,** 3260-3264 (2001)

[101] Pontie, M., Buisson, H., Diawara, C.K., and Essis-Tome, H., *Studies of halide ions mass transfer in nanofiltration – application to selective defluorination of brackish drinking water.* Desalination, **157,** 127-134 (2003)

[102] Pontie, M., Dach, H., Lhassani, A., and Diawara, C.K., *Water defluoridation using nanofiltration vs. reverse osmosis: the first world unit, Thiadiaye (Senegal).* Desalination and Water Treatment, **51,** 164-168 (2012)

[103] Shen, J. and Schäfer, A.I., *Removal of fluoride and uranium by nanofiltration and reverse osmosis: A review.* Chemosphere, **117,** 679-691 (2014)

[104] Richards, L.A., Vuachère, M., and Schäfer, A.I., *Impact of pH on the removal of fluoride, nitrate and boron by nanofiltration/reverse osmosis.* Desalination, **261,** 331-337 (2010)

[105] Mulder, M., *Basic Principles of Membrane Technology (second edition).* The Netherlands, Kluwer Academic Publishers (1996)

[106] Bowen, W.R. and Mohammad, A.W., *Characterization and prediction of nanofiltration membrane performance – a general assessment.* Chemical Engineering Research and Design, **76,** 885-893 (1998)

[107] Wang, X.-L., Tsuru, T., Togoh, M., Nakao, S.-i., and Kimura, S., *Evaluation of pore structure and electrical properties of nanofiltration membranes.* Journal of Chemical Engineering of Japan, **28,** 186-192 (1995)

[108] Bowen, W.R., Mohammad, A.W., and Hilal, N., *Characterisation of nanofiltration membranes for predictive purposes – use of salts, uncharged solutes and atomic force microscopy.* Journal of Membrane Science, **126,** 91-105 (1997)

[109] Hussain, A.A., Abashar, M.E.E., and Al-Mutaz, I.S., *Influence of ion size on the prediction of nanofiltration membrane systems.* Desalination, **214,** 150-166 (2007)

[110] Marcus, Y., *Thermodynamics of solvation of ions. Part 5.-Gibbs free energy of hydration at 298.15 K.* Journal of the Chemical Society, Faraday Transactions, **87,** 2995-2999 (1991)

[111] Richards, L.A., Schäfer, A.I., Richards, B.S., and Corry, B., *The importance of dehydration in determining ion transport in narrow pores.* Small, **8,** 1701-1709 (2012)

[112] Richards, L.A., Richards, B.S., Corry, B., and Schäfer, A.I., *Experimental energy barriers to anions transporting through nanofiltration membranes.* Environmental Science & Technology, **47,** 1968-1976 (2013)

[113] Morel, F.M.M. and Hering, J., *Principles and Applications of Aquatic Chemistry.* New York, Wiley (1993)

[114] Childress, A.E. and Elimelech, M., *Effect of solution chemistry on the surface charge of polymeric reverse osmosis and nanofiltration membranes.* Journal of Membrane Science, **119,** 253-268 (1996)

[115] Vankelecom, I.F.J., Smet, K.D., Gevers, L.E.M., and Jacobs, P.A., *Nanofiltration membrane materials and preparation*, in *Nanofiltration-Principles and Applications*, Schäfer, A.I., Fane, A.G., and Waite, T.D., Elsevier, Oxford, UK (2005)

[116] Hagmeyer, G. and Gimbel, R., *Modelling the rejection of nanofiltration membranes using zeta potential measurements.* Separation and Purification Technology, **15,** 19-30 (1999)

[117] Braghetta, DiGiano, F., and Ball, *Nanofiltration of natural organic matter: pH and ionic strength effects.* Journal of Environmental Engineering, **123,** 628-641 (1997)

[118] Childress, A.E. and Elimelech, M., *Relating nanofiltration membrane performance to membrane charge (electrokinetic) characteristics.* Environmental Science & Technology, **34,** 3710-3716 (2000)

[119] Schaep, J., Van der Bruggen, B., Vandecasteele, C., and Wilms, D., *Influence of ion size and charge in nanofiltration.* Separation and Purification Technology, **14,** 155-162 (1998)

[120] Teixeira, M.R., Rosa, M.J., and Nyström, M., *The role of membrane charge on nanofiltration performance.* Journal of Membrane Science, **265,** 160-166 (2005)

[121] Tsuru, T., Urairi, M., Nakao, S.-I., and Kimura, S., *Negative rejection of anions in the loose reverse osmosis separation of mono- and divalent ion mixtures.* Desalination, **81,** 219-227 (1991)

[122] Wang, X.-L., Tsuru, T., Nakao, S.-i., and Kimura, S., *The electrostatic and steric-hindrance model for the transport of charged solutes through nanofiltration membranes.* Journal of Membrane Science, **135,** 19-32 (1997)

[123] Nghiem, L.D., Schäfer, A.I., and Elimelech, M., *Role of electrostatic interactions in the retention of pharmaceutically active contaminants by a loose nanofiltration membrane.* Journal of Membrane Science, **286,** 52-59 (2006)

[124] Choi, S., Yun, Z., Hong, S., and Ahn, K., *The effect of co-existing ions and surface characteristics of nanomembranes on the removal of nitrate and fluoride.* Desalination, **133,** 53-64 (2001)

[125] Yaroshchuk, A.E., *Dielectric exclusion of ions from membranes.* Advances in Colloid and Interface Science, **85,** 193-230 (2000)

[126] Yaroshchuk, A.E., *Non-steric mechanisms of nanofiltration: superposition of Donnan and dielectric exclusion.* Separation and Purification Technology, **22–23,** 143-158 (2001)

[127] Bandini, S. and Vezzani, D., *Nanofiltration modeling: the role of dielectric exclusion in membrane characterization.* Chemical Engineering Science, **58,** 3303-3326 (2003)

[128] Oatley, D.L., Llenas, L., Pérez, R., Williams, P.M., Martínez-Lladó, X., and Rovira, M., *Review of the dielectric properties of nanofiltration membranes and verification of the single oriented layer approximation.* Advances in Colloid and Interface Science, **173,** 1-11 (2012)

[129] van de Lisdonk, C.A.C., Rietman, B.M., Heijman, S.G.J., Sterk, G.R., and Schippers, J.C., *Prediction of supersaturation and monitoring of scaling in reverse osmosis and nanofiltration membrane systems.* Desalination, **138,** 259-270 (2001)

[130] Bhattacharjee, S., Kim, A.S., and Elimelech, M., *Concentration Polarization of Interacting Solute Particles in Cross-Flow Membrane Filtration.* Journal of Colloid and Interface Science, **212,** 81-99 (1999)

[131] Koyuncu, I. and Topacik, D., *Effects of operating conditions on the salt rejection of nanofiltration membranes in reactive dye/salt mixtures.* Separation and Purification Technology, **33,** 283-294 (2003)

[132] Hu, K. and Dickson, J.M., *Nanofiltration membrane performance on fluoride removal from water.* Journal of Membrane Science, **279,** 529-538 (2006)

[133] Chakrabortty, S., Roy, M., and Pal, P., *Removal of fluoride from contaminated groundwater by cross flow nanofiltration: transport modeling and economic evaluation.* Desalination, **313,** 115-124 (2013)

[134] Tahaikt, M., Ait Haddou, A., El Habbani, R., Amor, Z., Elhannouni, F., Taky, M., Kharif, M., Boughriba, A., Hafsi, M., and Elmidaoui, A., *Comparison of the performances of three commercial membranes in fluoride removal by nanofiltration. Continuous operations.* Desalination, **225,** 209-219 (2008)

[135] Bellona, C. and Drewes, J.E., *The role of membrane surface charge and solute physico-chemical properties in the rejection of organic acids by NF membranes.* Journal of Membrane Science, **249,** 227-234 (2005)

[136] Schäfer, A.I., Andritsos, N., Karabelas, A.J., Hoek, E.M.V., Schneider, R., and Nyström, M., *Fouling in nanofiltration*, in *Nanofiltration: principles and applications*, Schäfer, A.I., Fane, A.G., and Waite, T.D., Elsevier (2004)

[137] Tu, K.L., Chivas, A.R., and Nghiem, L.D., *Effects of membrane fouling and scaling on boron rejection by nanofiltration and reverse osmosis membranes.* Desalination, **279,** 269-277 (2011)

[138] Hong, S. and Elimelech, M., *Chemical and physical aspects of natural organic matter (NOM) fouling of nanofiltration membranes.* Journal of Membrane Science, **132,** 159-181 (1997)

[139] Nghiem, L.D. and Hawkes, S., *Effects of membrane fouling on the nanofiltration of trace organic contaminants.* Desalination, **236,** 273-281 (2009)

[140] Tang, C.Y., Kwon, Y.-N., and Leckie, J.O., *Characterization of humic acid fouled reverse osmosis and nanofiltration membranes by transmission electron microscopy and streaming potential measurements.* Environmental Science & Technology, **41,** 942-949 (2006)

[141] Sehn, P., *Fluoride removal with extra low energy reverse osmosis membranes: three years of large scale field experience in Finland.* Desalination, **223,** 73-84 (2008)

[142] Sadiq, R. and Rodriguez, M.J., *Disinfection by-products (DBPs) in drinking water and predictive models for their occurrence: a review.* Science of the Total Environment, **321,** 21-46 (2004)

[143] Jarusutthirak, C., Mattaraj, S., and Jiraratananon, R., *Factors affecting nanofiltration performances in natural organic matter rejection and flux decline.* Separation and Purification Technology, **58,** 68-75 (2007)

[144] Schäfer, A.I., Pihlajamäki, A., Fane, A.G., Waite, T.D., and Nyström, M., *Natural organic matter removal by nanofiltration: effects of solution chemistry on retention of low molar mass acids versus bulk organic matter.* Journal of Membrane Science, **242,** 73-85 (2004)

[145] Meylan, S., Hammes, F., Traber, J., Salhi, E., von Gunten, U., and Pronk, W., *Permeability of low molecular weight organics through nanofiltration membranes.* Water Research, **41,** 3968-3976 (2007)

[146] Schäfer, A.I., Fane, A.G., and Waite, T.D., *Nanofiltration of natural organic matter: Removal, fouling and the influence of multivalent ions.* Desalination, **118,** 109-122 (1998)

[147] Zularisam, A.W., Ismail, A.F., and Salim, R., *Behaviours of natural organic matter in membrane filtration for surface water treatment – a review.* Desalination, **194,** 211-231 (2006)

[148] Tang, C.Y., Kwon, Y.-N., and Leckie, J.O., *Fouling of reverse osmosis and nanofiltration membranes by humic acid – Effects of solution composition and hydrodynamic conditions.* Journal of Membrane Science, **290,** 86-94 (2007)

[149] Braslavsky, S.E., Braun, A.M., Cassano, A.E., Emeline, A.V., Litter, M.I., Palmisano, L., Parmon, V.N., and Serpone, N., *Glossary of terms used in photocatalysis and radiation catalysis (IUPAC Recommendations 2011)* Pure and Applied Chemistry, **83,** 1215-1215 (2011)

[150] DeRosa, M.C. and Crutchley, R.J., *Photosensitized singlet oxygen and its applications.* Coordination Chemistry Reviews, **233–234,** 351-371 (2002)

[151] Ogilby, P.R., *Singlet oxygen: there is indeed something new under the sun.* Chemical Society Reviews, **39,** 3181-3209 (2010)

[152] Shankar, R., *Principles of Quantum Mechanics.* USA, Springer (2012)

[153] Debele, T.A., Peng, S., and Tsai, H.-C., *Drug carrier for photodynamic cancer therapy.* International journal of molecular sciences, **16,** 22094-22136 (2015)

[154] McQuarrie, D.A. and Simon, J.D., *Physical Chemistry: A Molecular Approach.* 1. USA, Sterling Publishing Company (1997)

[155] Braun, A.M., Maurette, M.T., and Oliveros, E., *Photochemical Technology.* USA, Wiley (1991)

[156] Wilkinson, F., Helman, W.P., and Ross, A.B., *Quantum yields for the photosensitized formation of the lowest electronically excited singlet state of molecular oxygen in solution.* Journal of Physical and Chemical Reference Data, **22,** 113-262 (1993)

[157] Hamano, T., Okuda, K., Mashino, T., Hirobe, M., Arakane, K., Ryu, A., Mashiko, S., and Nagano, T., *Singlet oxygen production from fullerene derivatives: effect of sequential functionalization of the fullerene core.* Chemical Communications, 21-22 (1997)

[158] Arakane, K., Ryu, A., Hayashi, C., Masunaga, T., Shinmoto, K., Mashiko, S., Nagano, T., and Hirobe, M., *Singlet Oxygen (1Δg) Generation from Coproporphyrin*

inPropionibacterium acneson Irradiation. Biochemical and Biophysical Research Communications, **223,** 578-582 (1996)

[159] Bonnett, R., *Photosensitizers of the porphyrin and phthalocyanine series for photodynamic therapy.* Chemical Society Reviews, **24,** 19-33 (1995)

[160] Lamberts, J.J.M. and Neckers, D.C., *Rose Bengal derivatives as singlet oxygen sensitizers.* Tetrahedron, **41,** 2183-2190 (1985)

[161] Prier, C.K., Rankic, D.A., and MacMillan, D.W.C., *Visible light photoredox catalysis with transition metal complexes: Applications in organic synthesis.* Chemical Reviews, **113,** 5322-5363 (2013)

[162] Galian, R.E. and Perez-Prieto, J., *Catalytic processes activated by light.* Energy & Environmental Science, **3,** 1488-1498 (2010)

[163] Villén, L., Manjón, F., García-Fresnadillo, D., and Orellana, G., *Solar water disinfection by photocatalytic singlet oxygen production in heterogeneous medium.* Applied Catalysis B: Environmental, **69,** 1-9 (2006)

[164] Krystynik, P., Kluson, P., Hejda, S., Buzek, D., Masin, P., and Tito, D.N., *Semi-pilot scale environment friendly photocatalytic degradation of 4-chlorophenol with singlet oxygen species – Direct comparison with H_2O_2/UV-C reaction system.* Applied Catalysis B: Environmental, **160–161,** 506-513 (2014)

[165] Schiff, L.J., Eisenberg, W.C., Dziuba, J., Taylor, K., and Moore, S.J., *Cytotoxic effects of singlet oxygen.* Environmental Health Perspectives, **76,** 199-203 (1987)

[166] Hernandez-Alonso, M.D., Fresno, F., Suarez, S., and Coronado, J.M., *Development of alternative photocatalysts to TiO_2: Challenges and opportunities.* Energy & Environmental Science, **2,** 1231-1257 (2009)

[167] Thandu, M., Comuzzi, C., and Goi, D., *Phototreatment of water by organic photosensitizers and comparison with inorganic semiconductors.* International Journal of Photoenergy, **2015,** 22 (2015)

[168] Kim, H., Kim, W., Mackeyev, Y., Lee, G.-S., Kim, H.-J., Tachikawa, T., Hong, S., Lee, S., Kim, J., Wilson, L.J., Majima, T., Alvarez, P.J.J., Choi, W., and Lee, J., *Selective oxidative degradation of organic pollutants by singlet oxygen-mediated photosensitization: tin porphyrin versus C60 aminofullerene systems.* Environmental Science & Technology, **46,** 9606-9613 (2012)

[169] Zhang, T., Ding, Y., and Tang, H., *Generation of singlet oxygen over Bi(V)/Bi(III) composite and its use for oxidative degradation of organic pollutants.* Chemical Engineering Journal, **264,** 681-689 (2015)

[170] Lee, J., Hong, S., Mackeyev, Y., Lee, C., Chung, E., Wilson, L.J., Kim, J.-H., and Alvarez, P.J.J., *Photosensitized oxidation of emerging organic pollutants by tetrakis C_{60} aminofullerene-derivatized silica under visible light irradiation.* Environmental Science & Technology, **45,** 10598-10604 (2011)

[171] Connick, W.B. and Gray, H.B., *Photooxidation of platinum (II) diimine dithiolates.* Journal of the American Chemical Society, **119,** 11620-11627 (1997)

[172] Abdel-Shafi, A.A., Beer, P.D., Mortimer, R.J., and Wilkinson, F., *Photosensitized generation of singlet oxygen from ruthenium (II)-substituted benzoaza-crown-bipyridine complexes.* Physical Chemistry Chemical Physics, **2,** 3137-3144 (2000)

[173] Abdel-Shafi, A.A., Beer, P.D., Mortimer, R.J., and Wilkinson, F., *Photosensitized generation of singlet oxygen from vinyl linked benzo-crown-ether-bipyridyl ruthenium (II) complexes.* Journal of Physical Chemistry A, **104,** 192-202 (2000)

[174] Goethals, A., Mugadza, T., Arslanoglu, Y., Zugle, R., Antunes, E., Hulle, S.W., Nyokong, T., and Clerck, K., *Polyamide nanofiber membranes functionalized with zinc phthalocyanines.* Journal of Applied Polymer Science, **131,** (2014)

[175] Gazi, S. and Ananthakrishnan, R., *Metal-free-photocatalytic reduction of 4-nitrophenol by resin-supported dye under the visible irradiation.* Applied Catalysis B: Environmental, **105,** 317-325 (2011)

[176] Nyokong, T. and Ahsen, V., *Photosensitizers in Medicine, Environment, and Security.* Springer Netherlands (2012)

[177] Malcolm, R.L. and MacCarthy, P., *Limitations in the use of commercial humic acids in water and soil research.* Environmental Science & Technology, **20,** 904-911 (1986)

[178] Kim, J.I., Buckau, G., Li, G.H., Duschner, H., and Psarros, N., *Characterization of humic and fulvic acids from Gorleben groundwater.* Fresenius Journal of Analytical Chemistry, **338,** 245-252 (1990)

[179] Pontié, M., Dach, H., Leparc, J., Hafsi, M., and Lhassani, A., *Novel approach combining physico-chemical characterizations and mass transfer modelling of nanofiltration and low pressure reverse osmosis membranes for brackish water desalination intensification.* Desalination, **221,** 174-191 (2008)

[180] Freger, V., Gilron, J., and Belfer, S., *TFC polyamide membranes modified by grafting of hydrophilic polymers: a FT-IR/AFM/TEM study.* Journal of Membrane Science, **209,** 283-292 (2002)

[181] Yoon, Y., Amy, G., Cho, J., and Her, N., *Effects of retained natural organic matter (NOM) on NOM rejection and membrane flux decline with nanofiltration and ultrafiltration.* Desalination, **173,** 209-221 (2005)

[182] Boussu, K., Zhang, Y., Cocquyt, J., Van der Meeren, P., Volodin, A., Van Haesendonck, C., Martens, J.A., and Van der Bruggen, B., *Characterization of polymeric nanofiltration membranes for systematic analysis of membrane performance.* Journal of Membrane Science, **278,** 418-427 (2006)

[183] Richards, L.A., *The removal of inorganic contaminants using nanofiltration and reverse osmosis*, in *School of Engineering and Physical Sciences*. Heriot-Watt University: Edinburgh, UK (2012)

[184] Johnson, J. and Busch, M., *Engineering aspects of reverse osmosis module design.* Desalination and Water Treatment, **15,** 236-248 (2010)

[185] Dow Chemical Company. *FILMTEC™ BW30-4040 Membranes FILMTEC Fiberglassed Elements for Light Industrial Systems*. [cited 2013 July]; Available from: http://www.dowwaterandprocess.com/en/products/f/filmtec_bw30_4040.

[186] Dow Chemical Company. *FILMTEC™ NF90-4040 Membranes FILMTEC NF90 Nanofiltration Elements for Commercial Systems*. [cited 2013 July]; Available from: http://www.dowwaterandprocess.com/en/products/f/filmtec-nf90_4040.

[187] Dow Chemical Company. *FILMTEC™ Membranes FILMTEC NF270 Nanofiltration Elements for Commercial Systems*. [cited 2013 July]; Available from: http://www.dowwaterandprocess.com/en/products/f/filmtec-nf270_4040.

[188] Neale, P.A., *Influence of solute-solute interactions on membrane filtration*, in *School of Engineering*. University of Edinburgh: Edinburgh, UK (2009)

[189] Schäfer, A.I., Broeckmann, A., and Richards, B.S., *Renewable energy powered membrane technology. 1. development and characterization of a photovoltaic hybrid membrane system.* Environmental Science & Technology, **41,** 998-1003 (2006)

[190] Richards, B.S., Capão, D.P.S., and Schäfer, A.I., *Renewable energy powered membrane technology. 2. the effect of energy fluctuations on performance of a photovoltaic hybrid membrane system.* Environmental Science & Technology, **42,** 4563-4569 (2008)

[191] Shen, J., Mkongo, G., Abbt-Braun, G., Ceppi, S.L., Richards, B.S., and Schäfer, A.I., *Renewable energy powered membrane technology: Fluoride removal in a rural community in northern Tanzania.* Separation and Purification Technology, **149,** 349-361 (2015)

[192]   Richards, B.S., Park, G.L., Pietzsch, T., and Schäfer, A.I., *Renewable energy powered membrane technology: Brackish water desalination system operated using real wind fluctuations and energy buffering.* Journal of Membrane Science, **468,** 224-232 (2014)

[193] Zhang, K., Vobecka, Z., Tauer, K., Antonietti, M., and Vilela, F., *π-Conjugated polyHIPEs as highly efficient and reusable heterogeneous photosensitizers.* Chemical Communications, **49,** 11158-11160 (2013)

[194]   Longsworth, L.G., *Determination of pH. Theory and practice.* Journal of the American Chemical Society, **86,** 3912-3912 (1964)

[195] NSW Public Works, *Brackish Groundwater: A Viable Community Water Supply Option?* National Water Commission: Australia (2011)

[196] Frant, M.S. and Ross, J.W., *Electrode for sensing fluoride ion activity in solution.* Science, **154,** 1553-1555 (1966)

[197] Harwood, J.E., *The use of an ion-selective electrode for routine fluoride analyses on water samples.* Water Research, **3,** 273-280 (1969)

[198]   United States Environmental Protection Agency, *Method 9214: Potentiometric determination of fluoride in aqueous samples with ion-selective electrode*: Washington DC, USA (1996)

[199]   Jackson, P.E., *Determination of inorganic ions in drinking water by ion chromatography.* Trends In Analytical Chemistry, **20,** 320-329 (2001)

[200]   Okamoto, Y., *Determination of fluorine in aqueous samples by electrothermal vaporisation inductively coupled plasma mass spectrometry (ETV-ICP-MS).* Journal of Analytical Atomic Spectrometry, **16,** 539-541 (2001)

[201]   Rodrigues, A., Brito, A., Janknecht, P., Proenca, M.F., and Nogueira, R., *Quantification of humic acids in surface water: effects of divalent cations, pH, and filtration.* Journal of Environmental Engineering, **11,** 377-82 (2009)

[202]   Yang, S., Liu, Y., and Feng, G., *Rapid and selective detection of fluoride in aqueous solution by a new hemicyanine-based colorimetric and fluorescent chemodosimeter.* RSC Advances, **3,** 20171-20178 (2013)

[203] Noh, J.-H. and Coetzee, P., *Evaluation of the potentiometric determination of trace fluoride in natural and drinking water with a fluoride ISE* Water SA, **33,** 519-529 (2007)

[204] Kauranen, P., *The use of buffers in the determination of fluoride by an ion-selective electrode at low concentrations and in the presence of aluminum.* Analytical Letters, **10,** 451-465 (1977)

[205] Liebman, J. and Ponikvar, M., *Ion selective electrode determination of free versus total fluoride ion in simple and fluoroligand coordinated hexafluoropnictate (PnF6 −, Pn = P, As, Sb, Bi) salts.* Structural Chemistry, **16,** 521-528 (2005)

[206] American Public Health Association, *Standard Methods for the Examination of Water and Wastewater 22nd Edition.* USA (2012)

[207] GE Analytical Instruments, *Sievers 900 Series Total Organic Carbon Analyzers Operation and Maintenance Manual*: USA (2011)

[208] Wolf-Gladrow, D.A., Zeebe, R.E., Klaas, C., Körtzinger, A., and Dickson, A.G., *Total alkalinity: The explicit conservative expression and its application to biogeochemical processes.* Marine Chemistry, **106,** 287-300 (2007)

[209] Goldburg, W.I., *Dynamic light scattering.* American Journal of Physics, **67,** 1152-1160 (1999)

[210] Edward, J.T., *Molecular volumes and the Stokes-Einstein equation.* Journal of Chemical Education, **47,** 261 (1970)

[211] Esfahani, M.R., Stretz, H.A., and Wells, M.J.M., *Abiotic reversible self-assembly of fulvic and humic acid aggregates in low electrolytic conductivity solutions by dynamic light scattering and zeta potential investigation.* Science of the Total Environment, **537,** 81-92 (2015)

[212] Goldberg, M.C. and Weiner, E.R., *Fluorescence measurements of the volume, shape, and fluorophore composition of fulvic acid from the Suwannee River*, in *Humic Substances in the Suwannee River, Georgia: Interactions, Properties, and Proposed Structures*, Averett, R.C., Leenheer, J.A., McKnight, D.M., and Thorn, K.A., United States Geological Survey, USA. 179-204 (1989)

[213] Hunter, R.J., *Zeta Potential in Colloid Science: Principles and Applications.* London, Academic Press (1981)

[214] Kaszuba, M., Corbett, J., Watson, F.M., and Jones, A., *High-concentration zeta potential measurements using light-scattering techniques.* Philosophical Transactions. Series A, Mathematical, Physical, and Engineering Sciences, **368,** 4439-4451 (2010)

[215] Griffiths, P.R. and De Haseth, J.A., *Fourier Transform Infrared Spectrometry.* USA, Wiley (2007)

[216] Olesik, J.W., *Elemental analysis using ICP-OES and ICP/MS.* Analytical Chemistry, **63,** 12A-21A (1991)

[217] Weiss, J., *Handbook of Ion Chromatography.* Germany, Wiley (2008)

[218] Brown, P. and Hartwick, R.A., *High Performance Liquid Chromatography*. USA, Wiley (1988)

[219] Hore, P., *Nuclear Magnetic Resonance*. UK, Oxford University Press (2015)

[220] Robertson, L.J. and Gjerde, B.K., *Cryptosporidium oocysts: challenging adversaries?* Trends in Parasitology, **23,** 344-347 (2007)

[221] Morra, M.J., Marshall, D.B., and Lee, C.M., *FT‑IR analysis of aldrich humic acid in water using cylindrical internal reflectance.* Communications in Soil Science and Plant Analysis, **20,** 851-867 (1989)

[222] Howe, K.J., Ishida, K.P., and Clark, M.M., *Use of ATR/FTIR spectrometry to study fouling of microfiltration membranes by natural waters.* Desalination, **147,** 251-255 (2002)

[223] Shen, J. and Schäfer, A.I., *Factors affecting fluoride and natural organic matter (NOM) removal from natural waters in Tanzania by nanofiltration/reverse osmosis.* Science of the Total Environment, **527–528,** 520-529 (2015)

[224] Environmental Protection Agency Ireland, *EPA Drinking Water Guidance on Disinfection By-Products Advice Note No. 4. Version 2. Disinfection By-Products in Drinking Water*: Ireland (2012)

[225] Buffle, J. and Leppard, G.G., *Characterization of aquatic colloids and macromolecules. 1. Structure and behavior of colloidal material.* Environmental Science & Technology, **29,** 2169-2175 (1995)

[226] Baalousha, M., Motelica-Heino, M., and Coustumer, P.L., *Conformation and size of humic substances: Effects of major cation concentration and type, pH, salinity, and residence time.* Colloids and Surfaces A: Physicochemical and Engineering Aspects, **272,** 48-55 (2006)

[227] Jovanović, U.D., Marković, M.M., Cupać, S.B., and Tomić, Z.P., *Soil humic acid aggregation by dynamic light scattering and laser Doppler electrophoresis.* Journal of Plant Nutrition and Soil Science, **176,** 674-679 (2013)

[228] Wagoner, D.B., Christman, R.F., Cauchon, G., and Paulson, R., *Molar mass and size of Suwannee River natural organic matter using multi-angle laser light scattering.* Environmental Science & Technology, **31,** 937-941 (1997)

[229] Palmer, N. and von Wandruszka, R., *Dynamic light scattering measurements of particle size development in aqueous humic materials.* Fresenius' Journal of Analytical Chemistry, **371,** 951-954 (2001)

[230] Gregory, J., *Particles in Water: Properties and Processes*. USA, CRC Press (2005)

[231] Pinheiro, J.P., Mota, A.M., d'Oliveira, J.M.R., and Martinho, J.M.G., *Dynamic properties of humic matter by dynamic light scattering and voltammetry.* Analytica Chimica Acta, **329,** 15-24 (1996)

[232] Orsetti, S., Andrade, E.M., and Molina, F.V., *Modeling ion binding to humic substances: elastic polyelectrolyte network model.* Langmuir, **26,** 3134-3144 (2010)

[233] Kipton, H., Powell, J., and Town, R.M., *Solubility and fractionation of humic acid: effect of pH and ionic medium.* Analytica Chimica Acta, **267,** 47-54 (1992)

[234] Duman, O. and Tunç, S., *Electrokinetic and rheological properties of Na-bentonite in some electrolyte solutions.* Microporous and Mesoporous Materials, **117,** 331-338 (2009)

[235] Chapra, S.C., *Surface Water-Quality Modeling.* USA, Waveland Press (2008)

[236] Ferreira, J.A., Nascimento, O.R., and Martin-Neto, L., *Hydrophobic interactions between spin-label 5-SASL and humic acid as revealed by ESR spectroscopy.* Environmental Science & Technology, **35,** 761-765 (2001)

[237] Frencken, J.E., ed. *Endemic fluorosis in developing countries: causes, effects and possible solutions*. 1990, NIPG-TNO: TNO Institute for Preventive Health Care.

[238] World Bank, *Water Resources in Tanzania*: Dar es Salaam (2006)

[239] Tanzania Bureau of Standards. *Tanzania Water Quality Standards*. 2008 [cited 2013 May]; Available from: http://frameweb.org/CommunityBrowser.aspx?id=4408.

[240] Mohammad, A.W., *A modified Donnan–steric-pore model for predicting flux and rejection of dye/NaCl mixture in nanofiltration membranes.* Separation Science and Technology, **37,** 1009-1029 (2002)

[241] Bejaoui, I., Mnif, A., and Hamrouni, B., *Influence of operating conditions on the retention of fluoride from water by nanofiltration.* Desalination and Water Treatment, **29,** 39-46 (2011)

[242] Mnif, A., Ben Sik Ali, M., and Hamrouni, B., *Effect of some physical and chemical parameters on fluoride removal by nanofiltration.* Ionics, **16,** 245-253 (2010)

[243] Newcombe, G., Drikas, M., Assemi, S., and Beckett, R., *Influence of characterised natural organic material on activated carbon adsorption: I. Characterisation of concentrated reservoir water.* Water Research, **31,** 965-972 (1997)

[244] Brunson, L.R. and Sabatini, D.A., *Practical considerations, column studies and natural organic material competition for fluoride removal with bone char and aluminum amended materials in the Main Ethiopian Rift Valley.* Science of the Total Environment, **488–489,** 580-587 (2014)

[245] van't Hoff, J.H., *The function of osmotic pressure in the analogy between solutions and gases.* Proceedings of the Physical Society of London, **9,** 307 (1887)

[246] DiGiano, F.A., Arweiler, S., and Riddick, J.A., *Alternative tests for evaluating NF fouling.* Journal American Water Works Association, **92,** 103-115 (2000)

[247] Jonsson, G., *Transport phenomena in ultrafiltration: membrane selectivity and boundary layer phenomena*, in *Pure and Applied Chemistry.* 1647 (1986)

[248] The Council of the European Union, *Council directive 98/83/EC of 3 November 1998 on the quality of water intended for human consumption.* Official Journal of the European Communities, **330,** 32-54 (1998)

[249] The Federal Ministry for Health, *Ordinance Amending the Drinking Water Ordinance*: Germany (2001)

[250] Brouwer, I.D., De Bruin, A., Dirks, O.B., and Hautvast, J.G.A.J., *Unsuitability of world health organization guidelines for fluoride concentrations in drinking water in Senegal.* The Lancet, **331,** 223-225 (1988)

[251] Ministry of Water Resources, *Ethiopian guidelines-specification for drinking water quality*: Addis Ababa, Ethiopia (2002)

[252] Parliament of the United Republic of Tanzania, *Water Utilization (Control and Regulation) Amendment Act*. Government Printers: Dar es Salaam, Tanzania (1981)

[253] Mjengera, H. and Mkongo, G., *Appropriate deflouridation technology for use in flourotic areas in Tanzania.* Physics and Chemistry of the Earth, **28,** 1097-1104 (2003)

[254] World Health Organization, *Guidelines for Drinking-Water Quality Fourth Edition*: Malta (2011)

[255] World Health Organization, *pH in drinking-water: Background document for development of WHO guidelines for drinking-water quality*: Geneva (2003)

[256] Chowdhury, S. and Champagne, P., *An investigation on parameters for modeling THMs formation.* Global NEST Journal, **10,** 80-91 (2008)

[257] United States Environmental Protection Agency, *Stage 1 Disinfectants and Disinfection Byproducts Rule*: USA (2001)

[258] Lantagne, D.S., Cardinali, F., and Blount, B.C., *Disinfection by-product formation and mitigation strategies in point-of-use chlorination with sodium dichloroisocyanurate in Tanzania.* The American Journal of Tropical Medicine and Hygiene, **83,** 135-143 (2010)

[259] Weishaar, J.L., Aiken, G.R., Bergamaschi, B.A., Fram, M.S., Fujii, R., and Mopper, K., *Evaluation of specific ultraviolet absorbance as an indicator of the chemical*

composition and reactivity of dissolved organic carbon. Environmental Science & Technology, **37,** 4702-4708 (2003)

[260] Sargaonkar, A. and Deshpande, V., *Development of an Overall Index of Pollution for Surface Water Based on a General Classification Scheme in Indian Context.* Environmental Monitoring and Assessment, **89,** 43-67 (2003)

[261] Gizaw, B., *The origin of high bicarbonate and fluoride concentrations in waters of the Main Ethiopian Rift Valley, East African Rift system.* Journal of African Earth Sciences, **22,** 391-402 (1996)

[262] Rixen, T., Baum, A., Sepryani, H., Pohlmann, T., Jose, C., and Samiaji, J., *Dissolved oxygen and its response to eutrophication in a tropical black water river.* Journal of Environmental Management, **91,** 1730-1737 (2010)

[263] Barbosa, A.C., de Souza, J., Dorea, J.G., Jardim, W.F., and Fadini, P.S., *Mercury biomagnification in a tropical black water, Rio Negro, Brazil.* Archives of Environmental Contamination and Toxicology, **45,** 235-246 (2003)

[264] Stahl, J.B., *Black water and two peculiar types of stratification in an organically loaded strip-mine lake.* Water Research, **13,** 467-471 (1979)

[265] Ghiglieri, G., Pittalis, D., Cerri, G., and Oggiano, G., *Hydrogeology and hydrogeochemistry of an alkaline volcanic area: the NE Mt. Meru slope (East African Rift – Northern Tanzania).* Hydrol Earth Syst Sci, **16,** 529-541 (2012)

[266] Rango, T., Kravchenko, J., Atlaw, B., McCornick, P.G., Jeuland, M., Merola, B., and Vengosh, A., *Groundwater quality and its health impact: An assessment of dental fluorosis in rural inhabitants of the Main Ethiopian Rift.* Environment International, **43,** 37-47 (2012)

[267] Moncaster, S.J., Bottrell, S.H., Tellam, J.H., Lloyd, J.W., and Konhauser, K.O., *Migration and attenuation of agrochemical pollutants: insights from isotopic analysis of groundwater sulphate.* Journal of Contaminant Hydrology, **43,** 147-163 (2000)

[268] Muyzer, G. and Stams, A.J.M., *The ecology and biotechnology of sulphate-reducing bacteria.* Nat Rev Micro, **6,** 441-454 (2008)

[269] Grant, W., *Alkaline environments and biodiversity.* Extremophiles; Encyclopedia of Life Support Systems (EOLSS). Oxford: EOLSS publishers, (2006)

[270] Gaciri, S.J. and Davies, T.C., *The occurrence and geochemistry of fluoride in some natural waters of Kenya.* Journal of Hydrology, **143,** 395-412 (1993)

[271] Kaseva, M.E., *Contribution of trona (magadi) into excessive fluorosis—a case study in Maji ya Chai ward, northern Tanzania.* Science of the Total Environment, **366,** 92-100 (2006)

[272] van den Berg, G.B. and Smolders, C.A., *Concentration polarization phenomena during dead-end ultrafiltration of protein mixtures. The influence of solute-solute interactions.* Journal of Membrane Science, **47,** 1-24 (1989)

[273] Wijmans, J.G., Nakao, S., van den Berg, J.W.A., Troelstra, F.R., and Smolders, C.A., *Hydrodynamic resistance of concentration polarization boundary layers in ultrafiltration.* Journal of Membrane Science, **22,** 117-135 (1985)

[274] Richards, L.A., Schafer, A.I., Richards, B.S., and Corry, B., *Quantifying barriers to monovalent anion transport in narrow non-polar pores.* Physical Chemistry Chemical Physics, **14,** 11633-11638 (2012c)

[275] Bowen, W.R. and Jenner, F., *Theoretical descriptions of membrane filtration of colloids and fine particles: An assessment and review.* Advances in Colloid and Interface Science, **56,** 141-200 (1995)

[276] Kiss, A.M., Myles, T.D., Grew, K.N., Peracchio, A.A., Nelson, G.J., and Chiu, W.K.S., *Carbonate and bicarbonate ion transport in alkaline anion exchange membranes.* Journal of the Electrochemical Society, **160,** F994-F999 (2013)

[277] Nasr, A.B., Charcosset, C., Amar, R.B., and Walha, K., *Defluoridation of water by nanofiltration.* Journal of Fluorine Chemistry, **150,** 92-97 (2013)

[278] Bejaoui, I., Mnif, A., and Hamrouni, B., *Performance of reverse osmosis and nanofiltration in the removal of fluoride from model water and metal packaging industrial effluent.* Separation Science and Technology, **49,** 1135-1145 (2014)

[279] Paugam, L., Taha, S., Dorange, G., Jaouen, P., and Quéméneur, F., *Mechanism of nitrate ions transfer in nanofiltration depending on pressure, pH, concentration and medium composition.* Journal of Membrane Science, **231,** 37-46 (2004)

[280] Szymczyk, A. and Fievet, P., *Ion transport through nanofiltration membranes: the steric, electric and dielectric exclusion model.* Desalination, **200,** 122-124 (2006)

[281] Shim, Y., Lee, H.-J., Lee, S., Moon, S.-H., and Cho, J., *Effects of natural organic matter and ionic species on membrane surface charge.* Environmental Science & Technology, **36,** 3864-3871 (2002)

[282] Kilduff, J.E., Mattaraj, S., and Belfort, G., *Flux decline during nanofiltration of naturally-occurring dissolved organic matter: effects of osmotic pressure, membrane permeability, and cake formation.* Journal of Membrane Science, **239,** 39-53 (2004)

[283] Comerton, A.M., Andrews, R.C., and Bagley, D.M., *The influence of natural organic matter and cations on fouled nanofiltration membrane effective molecular weight cut-off.* Journal of Membrane Science, **327,** 155-163 (2009)

[284] Montgomery, M.A., Bartram, J., and Elimelech, M., *Increasing Functional Sustainability of Water and Sanitation Supplies in Rural Sub-Saharan Africa.* Environmental Engineering Science, **26,** 1017-1023 (2009)

[285] Thomson, M. and Infield, D., *A photovoltaic-powered seawater reverse-osmosis system without batteries.* Desalination, **153,** 1-8 (2003)

[286] Mohamed, E.S., Papadakis, G., Mathioulakis, E., and Belessiotis, V., *A direct coupled photovoltaic seawater reverse osmosis desalination system toward battery based systems – A technical and economical experimental comparative study.* Desalination, **221,** 17-22 (2008)

[287] Makoye, K. *Pangani's coastal people forced to drink brackish water as sea levels continue rising*. 2013 [cited 2014 April]; Available from: http://www.theeastafrican.co.ke/news/Pangani-s-coastal-people-forced-to-drink-brackish-water/-/2558/2057476/-/10aeldz/-/index.html.

[288] Schäfer, A.I., Hughes, G., and Richards, B.S., *Renewable energy powered membrane technology: A leapfrog approach to rural water treatment in developing countries?* Renewable and Sustainable Energy Reviews, **40,** 542-556 (2014)

[289] Hibbard, P.L., *The significance of mineral matter in water.* Journal American Water Works Association, **26,** 884-890 (1934)

[290] Ghermandi, A. and Messalem, R., *The advantages of NF desalination of brackish water for sustainable irrigation: The case of the Arava Valley in Israel.* Desalination and Water Treatment, **10,** 101-107 (2009)

[291] Richards, B.S., Park, G.L., Pietzsch, T., and Schäfer, A.I., *Renewable energy powered membrane technology: Safe operating window of a brackish water desalination system.* Journal of Membrane Science, **468,** 400-409 (2014)

[292] Schies, A., Went, J., Heidtmann, C., Eisele, M., Kroemke, F., Schmoch, H., and Vetter, M., *Operating control strategies and dimensioning of photovoltaic powered reverse osmosis desalination plants without batteries.* Desalination and Water Treatment, **21,** 131-137 (2010)

[293] Sharma, R.R. and Chellam, S., *Temperature effects on the morphology of porous thin film composite nanofiltration membranes.* Environmental Science & Technology, **39,** 5022-5030 (2005)

[294]   Richards, L.A., Richards, B.S., and Schäfer, A.I., *Renewable energy powered membrane technology: salt and inorganic contaminant removal by nanofiltration/reverse osmosis.* Journal of Membrane Science, **369,** 188-195 (2011)

[295]   Park, G.L., Schäfer, A.I., and Richards, B.S., *Renewable energy powered membrane technology: The effect of wind speed fluctuations on the performance of a wind-powered membrane system for brackish water desalination.* Journal of Membrane Science, **370,** 34-44 (2011)

[296]   Dang, H.Q., Price, W.E., and Nghiem, L.D., *The effects of feed solution temperature on pore size and trace organic contaminant rejection by the nanofiltration membrane NF270.* Separation and Purification Technology, **125,** 43-51 (2014)

[297]   Ghiglieri, G., Balia, R., Oggiano, G., and Pittalis, D., *Prospecting for safe (low fluoride) groundwater in the eastern African Rift: a multidisciplinary approach in the Arumeru District (northern Tanzania).* Hydrology And Earth System Sciences, **6,** 7321-7348 (2009)

[298]   Ghiglieri, G., Pittalis, D., Cerri, G., and Oggiano, G., *Hydrogeology and hydrogeochemistry of an alkaline volcanic area: the NE Mt. Meru slope (East African Rift - Northern Tanzania).* Hydrology and Earth System Sciences, **16,** 529-541 (2012)

[299]   Fang, J. and Deng, B., *Rejection and modeling of arsenate by nanofiltration: Contributions of convection, diffusion and electromigration to arsenic transport.* Journal of Membrane Science, **453,** 42-51 (2014)

[300]   Holmgren, K.E., *Adsorbing for appropriateness: An interdisciplinary evaluation of the implementation of a defluoridation technique in rural Tanzania*, in *Graduate School*. Purdue University: Indiana, USA (2013)

[301]   Rossiter, H.M.A., Owusu, P.A., Awuah, E., MacDonald, A.M., and Schäfer, A.I., *Chemical drinking water quality in Ghana: Water costs and scope for advanced treatment.* Science of the Total Environment, **408,** 2378-2386 (2010)

[302]   Koparal, A.S., Yavuz, Y., Gürel, C., and Öğütveren, Ü.B., *Electrochemical degradation and toxicity reduction of C.I. Basic Red 29 solution and textile wastewater by using diamond anode.* Journal of Hazardous materials, **145,** 100-108 (2007)

[303] Yanyan, G., Snezna, R., and Peng, Z., *Rose Bengal-decorated silica nanoparticles as photosensitizers for inactivation of gram-positive bacteria.* Nanotechnology, **21,** 065102 (2010)

[304] Lee, J., Mackeyev, Y., Cho, M., Wilson, L.J., Kim, J.-H., and Alvarez, P.J.J., *C₆₀ aminofullerene immobilized on silica as a visible-light-activated photocatalyst.* Environmental Science & Technology, **44,** 9488-9495 (2010)

[305] Bonnett, R., Krysteva, M.A., Lalov, I.G., and Artarsky, S.V., *Water disinfection using photosensitizers immobilized on chitosan.* Water Research, **40,** 1269-1275 (2006)

[306] Schaap, A.P., Thayer, A.L., Zaklika, K.A., and Valenti, P.C., *Photooxygenations in aqueous solution with a hydrophilic polymer-immobilized photosensitizer.* Journal of the American Chemical Society, **101,** 4016-4017 (1979)

[307] Carpentier, R., Leblanc, R.M., and Mimeault, M., *Photoinhibition and chlorophyll photobleaching in immobilized thylakoid membranes.* Enzyme and Microbial Technology, **9,** 489-493 (1987)

[308] Miyaura, N. and Suzuki, A., *Palladium-catalyzed cross-coupling reactions of organoboron compounds.* Chemical Reviews, **95,** 2457-2483 (1995)

[309] Kurti, L. and Czakó, B., *Strategic Applications of Named Reactions in Organic Synthesis*. USA, Elsevier (2005)

[310] Casalnuovo, A.L. and Calabrese, J.C., *Palladium-catalyzed alkylations in aqueous media.* Journal of the American Chemical Society, **112,** 4324-4330 (1990)

[311] Zhang, K., Kopetzki, D., Seeberger, P.H., Antonietti, M., and Vilela, F., *Surface area control and photocatalytic activity of conjugated microporous poly(benzothiadiazole) networks.* Angewandte Chemie International Edition, **52,** 1432-1436 (2013)

[312] Kato, S.-i., Matsumoto, T., Shigeiwa, M., Gorohmaru, H., Maeda, S., Ishi-i, T., and Mataka, S., *Novel 2,1,3-benzothiadiazole-based red-fluorescent dyes with enhanced two-photon absorption cross-sections.* Chemistry – A European Journal, **12,** 2303-2317 (2006)

[313] Salokhiddinov, K.I., Byteva, I.M., and Gurinovich, G.P., *Lifetime of singlet oxygen in various solvents.* Journal of Applied Spectroscopy, **34,** 561-564 (1981)

[314] Schmidt, R., *Influence of heavy atoms on the deactivation of singlet oxygen (1.DELTA.g) in solution.* Journal of the American Chemical Society, **111,** 6983-6987 (1989)

[315] Wilkinson, F., Helman, W.P., and Ross, A.B., *Rate constants for the decay and reactions of the lowest electronically excited singlet state of molecular oxygen in solution-An expanded and revised compilation.* Journal of Physical and Chemical Reference Data, **24,** 663-677 (1995)

[316]   Ogawa, S., Fukui, S., Hanasaki, Y., Asano, K., Uegaki, H., Sumiko, F., and Ryosuke, S., *Determination method of singlet oxygen in the atmosphere by use of α - terpinene.* Chemosphere, **22,** 1211-1225 (1991)

[317]   Choi, D. and Jung, M., *Protective activities of catechins on singlet oxygen induced photooxidation of α-terpinene in methanol: structure and singlet oxygen quenching activity relationship.* Food Science and Biotechnology, **22,** 249-256 (2013)

[318]   Wilkinson, F. and Brummer, J.G., *Rate constants for the decay and reactions of the lowest electronically excited singlet state of molecular oxygen in solution.* Journal of Physical and Chemical Reference Data, **10,** 809-999 (1981)

[319]   Urakami, H., Zhang, K., and Vilela, F., *Modification of conjugated microporous poly-benzothiadiazole for photosensitized singlet oxygen generation in water.* Chemical Communications, **49,** 2353-2355 (2013)

[320]   Haag, W.R., Hoigne, J., Gassman, E., and Braun, A.M., *Singlet oxygen in surface waters – Part I: Furfuryl alcohol as a trapping agent.* Chemosphere, **13,** 631-640 (1984)

[321]   Ohko, Y., Ando, I., Niwa, C., Tatsuma, T., Yamamura, T., Nakashima, T., Kubota, Y., and Fujishima, A., *Degradation of Bisphenol A in water by TiO_2 photocatalyst.* Environmental Science & Technology, **35,** 2365-2368 (2001)

[322]   Tai, C., Jiang, G., Liu, J., Zhou, Q., and Liu, J., *Rapid degradation of bisphenol A using air as the oxidant catalyzed by polynuclear phthalocyanine complexes under visible light irradiation.* Journal of Photochemistry and Photobiology A: Chemistry, **172,** 275-282 (2005)

[323]   Barbieri, Y., Massad, W.A., Díaz, D.J., Sanz, J., Amat-Guerri, F., and García, N.A., *Photodegradation of bisphenol A and related compounds under natural-like conditions in the presence of riboflavin: Kinetics, mechanism and photoproducts.* Chemosphere, **73,** 564-571 (2008)

[324]   Díez-Mato, E., Cortezón-Tamarit, F.C., Bogialli, S., García-Fresnadillo, D., and Marazuela, M.D., *Phototransformation of model micropollutants in water samples by photocatalytic singlet oxygen production in heterogeneous medium.* Applied Catalysis B: Environmental, **160–161,** 445-455 (2014)

[325]   Ye, X., Zhou, X., Needham, L., and Calafat, A., *In-vitro oxidation of bisphenol A: Is bisphenol A catechol a suitable biomarker for human exposure to bisphenol A?* Analytical and Bioanalytical Chemistry, **399,** 1071-1079 (2011)

[326]   Halmann, M.M., *Photodegradation of Water Pollutants.* Taylor & Francis (1995)

[327] Kang, P. and Foote, C.S., *Photosensitized oxidation of ^{13}C, ^{15}N-labeled imidazole derivatives.* Journal of the American Chemical Society, **124,** 9629-9638 (2002)

[328] Chin, Y.-P., Miller, P.L., Zeng, L., Cawley, K., and Weavers, L.K., *Photosensitized degradation of bisphenol A by dissolved organic matter.* Environmental Science & Technology, **38,** 5888-5894 (2004)

[329] Haag, W.R., Hoigne, J., Gassman, E., and Braun, A.M., *Singlet oxygen in surface waters – Part II: Quantum yields of its production by some natural humic materials as a function of wavelength.* Chemosphere, **13,** 641-650 (1984)

[330] Tratnyek, P.G. and Hoigne, J., *Oxidation of substituted phenols in the environment: a QSAR analysis of rate constants for reaction with singlet oxygen.* Environmental Science & Technology, **25,** 1596-1604 (1991)

[331] Staples, C.A., Dome, P.B., Klecka, G.M., Oblock, S.T., and Harris, L.R., *A review of the environmental fate, effects, and exposures of bisphenol A.* Chemosphere, **36,** 2149-2173 (1998)

[332] Cotruvo, J., Craun, G.F., and Hearne, N., *Providing Safe Drinking Water in Small Systems: Technology, Operations, and Economics.* USA, CRC Press (1999)

[333] United States Environmental Protection Agency, *Inactivation of Cryptosporidium parvum oocysts in Drinking Water*: USA (1999)

[334] Mozia, S., *Photocatalytic membrane reactors (PMRs) in water and wastewater treatment. A review.* Separation and Purification Technology, **73,** 71-91 (2010)

[335] Fu, J., Ji, M., Wang, Z., Jin, L., and An, D., *A new submerged membrane photocatalysis reactor (SMPR) for fulvic acid removal using a nano-structured photocatalyst.* Journal of Hazardous materials, **131,** 238-242 (2006)

[336] Choo, K.-H., Chang, D.-I., Park, K.-W., and Kim, M.-H., *Use of an integrated photocatalysis/hollow fiber microfiltration system for the removal of trichloroethylene in water.* Journal of Hazardous materials, **152,** 183-190 (2008)

[337] Shon, H.K., Phuntsho, S., and Vigneswaran, S., *Effect of photocatalysis on the membrane hybrid system for wastewater treatment.* Desalination, **225,** 235-248 (2008)

[338] Chin, S.S., Lim, T.M., Chiang, K., and Fane, A.G., *Factors affecting the performance of a low-pressure submerged membrane photocatalytic reactor.* Chemical Engineering Journal, **130,** 53-63 (2007)

[339] Thiruvenkatachari, R., Ouk Kwon, T., and Shik Moon, I., *Application of slurry type photocatalytic oxidation‐submerged hollow fiber microfiltration hybrid system for*

the degradation of Bisphenol A (BPA). Separation Science and Technology, **40,** 2871-2888 (2005)

[340]   National Bureau of Statistics, *Population and Housing Census: Population Distribution by Administrative Areas.* Ministry of Finance: Dar es Salaam, Tanzania (2012)

[341]   Spear, T., *Mountain farmers: Moral economies of land and agricultural development in Arusha and Meru.* University of California Press (1997)

[342] Lazaro, H., *Oikos earns Tanzania global recognition*, in *The Arusha Times*: Arusha (2009)

[343] Istituto Oikos, *THE MOUNT MERU CHALLENGE Integrating conservation and development in Northern Tanzania*, Carugati, C., Rossi, R., and Tosi, G., Editors: Milano (2011)

[344] Aoba, T. and Fejerskov, O., *Dental fluorosis: chemistry and biology.* Critical Reviews in Oral Biology & Medicine, **13,** 155-170 (2002)

[345] Tekle-Haimanot, R., Fekadu, A., Bushera, B., and Mekonnen, Y. *Fluoride levels in water and endemic fluorosis in Ethiopian Rift Valley.* in *1st International Workshop on Fluorosis Prevention and Defluoridation of Water*. 1995. Ngurdoto, Tanzania: ISFR.

[346] Feltman, R. and Kosel, G., *Prenatal ingestion of fluorides and their transfer to the fetus.* Science, **122,** 560-561 (1955)

[347] Caldera R, Chavinie J, Fermanian J, Tortrat D, and AM., L., *Maternal-fetal transfer of fluoride in pregnant women.* Biology Of The Neonate, **54,** 263-269 (1988)

[348]   Rugg-Gunn, A.J., Al-Mohammadi, S.M., and Butler, T.J., *Malnutrition and developmental defects of enamel in 2- to 6 -year-old Saudi boys.* Caries Research, **32,** 181-192 (1998)

[349] Istituto Oikos, *Nutritional challenges in Tanzanian teenagers, a case study from Arusha Region*, (2013)